THE UNIVERISTY OF CHICAGO

NANOSCALE COORDINATION POLYMERS CO-DELIVER MULTIPLE THERAPEUTICS FOR COMBINATION THERAPY OF CANCER

A DISSERTATION SUBMITTED TO

THE FACULTY OF THE DIVISION OF THE PHYSICAL SCIENCES

IN CANDIDACY FOR THE DEGREE OF

DOCTOR OF PHILOSOPHY

DEPARTMENT OF CHEMISTRY

BY

CHRISTOPHER YAN HOI POON

CHICAGO, ILLINOIS

AUGUST 2016

TABLE OF CONTENTS

LIST OF TABLES xii

LIST OF FIGURES xiv

LIST OF SYMBOLS AND ABBREVIATIONS xxiv

ABSTRACT xxxiv

ACKNOWLEDGEMENTS xxxvi

CHAPTER I: INTRODUCTION AND BACKGROUND 1

1.1 Cancer is a World Epidemic 1

1.2 Combination Chemotherapy 5

1.3 Nanoparticles for Combination Therapy 8

1.3.1 Advantages of Anticancer Nanoparticles 9

1.3.2 FDA-Approved Anticancer Nanoparticles and Drawbacks of Ongoing Clinical Trials of Single-Agent Nanoplatforms 11

1.3.3 Recent Nanoplatforms for Combination Chemotherapy 13

1.4 Nanoscale Coordination Polymers 15

1.4.1 Advantages of Hybrid Nanoparticles 15

1.4.2 Synthesis of NCPs 17

1.4.3 NCPs as Drug Delivery Platforms 20

1.4.3.1 Nitrogen-Containing Bisphosphonate 21

1.4.3.2 Methotrexate 22

1.4.3.3 Doxorubicin 23

1.4.3.4 Pt-Based Drugs 23

1.5 Summary and Scope of Work 26

1.6 References 27

CHAPTER II: SELF-ASSEMBLED NANOSCALE COORDINATION POLYMERS CARRYING OXALIPLATIN AND GEMCITABINE FOR SYNERGISTIC COMBINATION THERAPY OF PANCREATIC CANCER....35
2.1 Introduction....35
2.2 Experimental Details....37
2.2.1 General Experimental....37
2.2.2 Synthesis of Prodrugs....38
2.2.2.1 Synthesis of dachPtBP....38
2.2.2.2 Synthesis of GMP....39
2.2.3 Preparation of DOPA-NCP particles....40
2.2.3.1 Preparation of NCP-Ox/GMP....40
2.2.3.2 Preparation of NCP-Ox....41
2.2.3.3 Preparation of NCP-GMP....41
2.2.3.4 Preparation of Zn Control....42
2.2.3.5 Preparation of Chlorin e6-Doped NCPs....42
2.2.4 General Procedure of Lipid Coating and PEGylation....43
2.2.5 Characterization of NCP Particles....43
2.2.6 *In Vitro* Stability Studies....44
2.2.7 *In Vitro* Drug Release....44
2.2.8 *In Vitro* Cytotoxicity Assays and Synergistic Effects of Drug Combinations....45
2.2.9 Intracelllular Uptake and Cell Apoptosis *In Vitro*....45
2.2.10 Cell Apoptosis by Flow Cytometry....46
2.2.11 Pharmacokinetics of NCP-Ox/GMP....46
2.2.12 Tumor Growth Inhibition....47
2.2.13 *In Vivo* Immunogenic Response, Hypersensitivity, and General Toxicity Evaluation of NCP-Ox/GMP....48

2.2.14 *In Vivo* Tumor Cell Apoptosis 49
2.2.15 Statistical Analysis 49
2.3 Results and Discussion 49
2.3.1 Synthesis of NCP-Ox/GMP 49
2.3.2 Characterization of NCP Particles 50
2.3.3 *In Vitro* Drug Release 57
2.3.4 *In Vitro* Cytotoxicity and Combination Index 58
2.3.5 Intracellular Uptake and Cell Apoptosis *In Vitro* 62
2.3.6 Pharmacokinetic Studies 68
2.3.7 Tumor Growth Inhibition Studies 70
2.3.8 *In Vivo* Tumor Cell Apoptosis 75
2.4 Conclusion 76
2.5 References 77
CHAPTER III: NANOSCALE COORDINATION POLYMERS WITH HIGH PAYLOADS OF CARBOPLATIN AND GEMCITABINE FOR SYNERGISTIC COMBINATION TREATMENT OF PLATINUM-RESISTANT OVARIAN CANCER 81
3.1 Introduction 81
3.2 Experimental Details 82
3.2.1 General Experimental 82
3.2.2 Synthesis of Carbo Prodrug 83
3.2.3 Particle Synthesis and Characterization 86
3.2.3.1 Preparation of NCP-Carbo/GMP 87
3.2.3.2 Preparation of NCP-Carbo 87
3.2.3.3 Preparation of Rhodamine B-Doped NCP-Carbo/GMP 87
3.2.3.4 Characterization of NCP Particles 88
3.2.3.5 General Procedures of Lipid Coating and PEGylation 88

3.2.4 *In Vitro* Stability Studies 89
3.2.5 *In Vitro* Drug Release 89
3.2.6 *In Vitro* Cytotoxicity and Synergistic Effect 89
3.2.7 Cell Apoptosis by Confocal Microscopy 90
3.2.8 Cell Apoptosis by Flow Cytometry 90
3.2.9 *In Vitro* Cellular Uptakes and Intercellular Distribution 91
3.2.10 *In Vivo* Pharmacokinetic and Biodistribution Studies 91
3.2.11 Antitumor Activity *In Vivo* 92
3.2.12 *In Vivo* Immunogenic Response, Hypersensitivity, and General Toxicity Evaluation of NCP 93
3.2.13 *In Vivo* Tumor Cell Apoptosis 93
3.2.14 Statistical Analysis 94
3.3 Results 94
3.3.1 Synthesis and Characterization of NCP-Carbo/GMP 94
3.3.2 *In Vitro* Drug Release 100
3.3.3 *In Vitro* Cytotoxicity and Synergistic Effect 101
3.3.4 *In Vitro* Cell Apoptosis 104
3.3.5 *In Vitro* Cellular Uptakes 108
3.3.6 Pharmacokinetics and Biodistribution 111
3.3.7 Antitumor Activity *In Vivo* 113
3.4 Discussion 117
3.5 Conclusion 119
3.6 References 119
CHAPTER IV: NANOSCALE COORDINATION POLYMERS CARRYING CISPLATIN AND GEMCITABINE FOR SYNERGISTIC COMBINATION TREATMENT OF LUNG CANCERS 123

4.1 Introduction 123

4.2 Experimental Details 125

4.2.1 General Experimental 125

4.2.2 Synthesis of Cisplatin Prodrug 125

4.2.3 Particle Synthesis and Characterization 126

4.2.3.1 Preparation of NCP-Cis/GMP 126

4.2.3.2 Preparation of NCP-Cis 127

4.2.3.3 Preparation of NCP-GMP 127

4.2.3.4 General Procedures of Lipid Coating and PEGylation 128

4.2.3.5 Characterization of NCP Particles 128

4.2.4 *In Vitro* Stability Studies 128

4.2.5 *In Vitro* Drug Release 129

4.2.6 *In Vitro* Cytotoxicity of NCP-Cis/GMP 129

4.2.7 Cell Apoptosis by Flow Cytometry 130

4.2.8 *In Vivo* Pharmacokinetic and Biodistribution Studies of NCP-Cis/GMP 130

4.2.9 *In Vivo* Pharmacokinetics of NCP in Red and White Blood Cell Layer and Plasma Layer 131

4.2.10 *In Vivo* Maximum Tolerated Dose 131

4.2.11 *In Vivo* Anticancer Efficacy of NCP-Cis/GMP in Subcutaneous Xenograft Mouse Models 132

4.2.12 Statistical Analysis 132

4.3 Results and Discussion 132

4.3.1 Synthesis and Characterization of NCP-Cis/GMP 132

4.3.2 *In Vitro* Drug Release 137

4.3.3 *In Vitro* Cytotoxicity and Synergistic Effect 138

4.3.4 *In Vitro* Cell Apoptosis 141

4.3.5 Pharmacokinetics and Biodistribution 145
4.3.6 Maximum Tolerated Dose for NCP-Cis/GMP 148
4.3.7 Antitumor Activity *In Vivo* 149
4.4 Conclusion 150
4.5 References 151
CHAPTER V: NANOSCALE COORDINATION POLYMERS CO-DELIVER CHEMOTHEREAPEUTICS AND SIRNAS TO ERADICATE TUMORS OF CISPLATIN-RESISTANT OVARIAN CANCER 153
5.1 Introduction 153
5.2 Experimental Details 155
5.2.1 General Experimental 155
5.2.2 Synthesis of DSPE-siRNA Conjugate 157
5.2.3 Mass spectroscopy analysis of DSPE-siRNA 157
5.2.4 Particle Synthesis and Characterization 157
5.2.4.1 Preparation of NCP-Cis/GMP 157
5.2.4.2 Preparation of NCP-Cis 158
5.2.4.3 Preparation of NCP-GMP 159
5.2.4.4 Preparation of Rhodamine B-Doped NCP-Cis/GMP 159
5.2.4.5 General Procedures of Lipid Coating and PEGylation of NCP-Cis/siRNAs 159
5.2.4.6 General Procedures of Lipid Coating and PEGylation of NCP-Cis/GMPsiRNAs 160
5.2.4.7 Characterization of NCP Particles 160
5.2.5 siRNA Protection and Release of NCP-Cis/siRNAs 161
5.2.6 Endosomal Escape Mechanism 161
5.2.7 *In Vitro* Transfection of NCP-Cis/GMP/siRNAs 162

5.2.8 *In Vitro* Cytotoxicity of NCP-Cis/GMP/siRNAs 163
5.2.9 Cell Apoptosis by Confocal Microscopy 163
5.2.10 Cell Apoptosis by Flow Cytometry 164
5.2.11 Gel Retardation Assay of NCP/siRNAs in Blood Serum 164
5.2.12 *In Vivo* Maximum Tolerated Dose 164
5.2.13 *In Vivo* Anticancer Efficacy of NCP-Cis/GMP/siRNAs in a SKOV-3 Subcutaneous Xenograft Mouse Model 165
5.2.14 *In Vivo* General Toxicity Evaluation of NCP in SKOV-3 Subcutaneous Xenograft Mouse Model 165
5.2.15 *In Vivo* Anticancer Efficacy of NCP-Cis/GMP/siRNAs in a A2780/CDDP Subcutaneous Xenograft Mouse Model 165
5.2.16 *In Vivo* Anticancer Efficacy of NCP-Cis/GMP/siRNAs in a SKOV-3 Subcutaneous Xenograft Mouse Model with Larger Tumors 166
5.2.17 Statistical Analysis 166
5.3 Results 167
5.3.1 Synthesis and Characterization of NCP-Cis/GMP/GMP 167
5.3.2 *In Vitro* Drug Release 172
5.3.3 Efficient Endosomal Escape 174
5.3.4 *In Vitro* Transfection Efficiency 177
5.3.5 *In Vitro* Cytotoxicity and Synergistic Effect 178
5.3.6 *In Vitro* Cell Apoptosis 182
5.3.7 Pharmacokinetics in Red and White Blood Cell Layer and Plasma Layer 186
5.3.8 Antitumor Activity *In Vivo* 188
5.4 Discussion 191
5.5 Conclusion 193
5.6 References 194

CHAPTER VI: NANOSCALE COORDINATION POLYMER CORE-SHELL NANOPARTICLES COMBINE CHEMOTHERAPY AND PHOTODYNAMIC THERAPY TO ELICIT POTENT ANTITUMOR IMMUNITY 198

6.1 Introduction 198

6.2 Experimental Details 200

6.2.1 General Experimental 200

6.2.2 Preparation and Characterization of NCP-Ox@pyrolipid 200

6.2.3 Singlet Oxygen Generation of NCP-Ox@pyrolipid 201

6.2.4 Cellular Uptake of NCP-Ox@pyrolipid 201

6.2.5 Cytotoxicity of NCP-Ox@pyrolipid in Colorectal Adenocarcinoma Cells 202

6.2.6 Cell Apoptosis by Flow Cytometry 202

6.2.7 *In Vitro* Immunogenic Cell Death 203

6.2.8 Pharmacokinetics and Tissue Distributions 204

6.2.9 *In Vivo* Anticancer Efficacy 204

6.2.10 Antitumor Vaccination 205

6.2.11 Abscopal Effect 206

6.2.12 Statistical Analysis 206

6.3 Results and Discussion 207

6.3.1 Self-Assembly and Characterization of NCP-Ox@pyrolipid 207

6.3.2 Cellular Uptake and Cytotoxicity 211

6.3.3 Immunogenic Cell Death Response 216

6.3.4 *In Vivo* Pharmacokinetic and Biodistribution Studies 218

6.3.5 Anticancer Activity in Colorectal Adenocarcinoma Mouse Models 219

6.3.6 *In Vivo* Antitumor-Immunity 224

6.3.7 Abscopal Effect 226

6.4 Conclusion 228

6.5 References 228

LIST OF TABLES

Table 2.1 Sizes, Polydispersities, and Zeta Potentials of NCP and Zn Control Particles 51

Table 2.2 Oxaliplatin IC_{50} Values of Oxaliplatin, GMP, Ox&GMP, NCP-Ox/GMP, NCP-Ox, and NCP-GMP Against AsPc-1 and BxPc-3 Cells 62

Table 2.3 Sizes, Polydispersities, and Zeta Potentials of Ce6-NCP Particles 63

Table 2.4 Pharmacokinetic Parameters of Pt Distribution for NCP-Ox/GMP in CT26 Bearing Nude Mice 70

Table 3.1 Sizes, Polydispersities, and Zeta Potentials of NCP Particles 99

Table 3.2 Carbo IC_{50} Values of Carbo, GMP, NCP-Carbo, NCP-GMP, NCP-Carbo/GMP against SKOV-3, and A2780/CDDP Cells 103

Table 3.3 Sizes, Polydispersities, and Zeta potentials of RhB-NCP-Carbo/GMP..... 104

Table 4.1 Sizes, Polydispersities, and Zeta Potentials of NCP Particles 134

Table 4.2 Cisplatin IC_{50} Values of Cisplatin, GMP, NCP-Cis, NCP-GMP, and NCP-Cis/GMP Against H82, H69, H460, and A549 Cells 141

Table 4.3 Percentages of Healthy, Apoptotic, and Necrotic H82, H69, H460 and A549 Cells After a 24-Hour Treatment of PBS, Cisplatin, GMP, Cisplatin/GMP, Zn control, NCP-Cis, NCP-GMP, and NCP-Cis/GMP 145

Table 5.1 Primer Sequences of β-actin, ERCC-1, Bcl-2, and Survivin for Real-Time PCR 162

Table 5.2 Sizes, Polydispersities, Zeta Potentials, and Drug Loadings of NCP-Cis/GMP Particles 168

Table 5.3 Cisplatin IC_{50} Values of Cisplatin, GMP, NCP-Cis, NCP-GMP, NCP-Cis/GMP, and NCP-Cis/GMP/siRNAs Against A2780/CDDP, SKOV-3, and A2780 Cells 181

Table 5.4 Cisplatin IC_{50} values of different formulation of NCP-Cis/GMP against A2780, A2780/CDDP, and SKOV-3 Cells 182

Table 5.5 Percentages of Healthy, Apoptotic, and Necrotic SKOV-3 and A2780/CDDP Cells After a 24-Hour Treatment of PBS, Cisplatin, GMP, Zn control, NCP-Cis, NCP-GMP, NCP-Cis/GMP, NCP-Cis/GMP/siRNAs 186

Table 6.1 Oxaliplatin and pyrolipid IC_{50} values in CT26 and HT29 cells treated with various formulations 214

Table 6.2 Apoptotic percentage of CT26 and HT29 cells treated with PBS, free oxaliplatin, NCP-Ox, NCP-Ox@pyrolipid, and porphysome under light and dark after 24 h incubation 216

LIST OF FIGURES

Figure 1.1 Estimated numbers of new cancer cases and deaths in 2016 based on American Cancer Society 2

Figure 1.2 Structures of the three FDA-approved Pt-based chemotherapeutics: cisplatin, oxaliplatin, and carboplatin 2

Figure 1.3 Different drug resistance mechanisms in cancer cells. 4

Figure 1.4 Signaling pathways that mediate cisplatin resistance 5

Figure 1.5 Progression-free survival of patients with platinum-resistant ovarian cancer treated with chemotherapy (CT) or chemotherapy with bevacizumab (BEV + CT) 8

Figure 1.6 Nanoparticles used in drug delivery consisted of dendrimers, micelle, emulsions, nanoparticulates, and liposomes for the delivery of small molecule drugs and therapeutic macromolecules like proteins, peptides, aptamers, and nucleic acid 9

Figure 1.7 Schematic showing enhanced permeability and retention (EPR) effect stemming from leaky neovasculatures and ineffective lymphatic drainage that are characteristic of tumors 10

Figure 1.8 Schematic of folate-targeted layer-by-layer liposome containing DOX in the aqueous core and erlotinib on the outer lipid shell for controlled sequential drug release 14

Figure 1.9 Schematic showing the synthesis and mechanistic action of PEG-Dox-Cur nanoparticle 15

Figure 1.10 Formation of nanoscale coordination polymers from metal-connecting points and organic bridging ligands 17

Figure 1.11 Surfactant-templated synthesis of NCPs by reverse microemulsion at room temperature or by surfactant-assisted solvothermal reactions at elevated temperature 18

Figure 1.12 Surfactant-free synthesis of NCPs and NMOFs by nanoprecipitation reaction at room temperature or by solvothermal reactions at elevated temperature 18

Figure 1.13 Synthesis and cell uptake mechanism of nitrogen-containing bisphosphate NCPs ..22

Figure 1.14 Schematic showing the surfactant-assisted solvothermal reaction of MTX-containing NCPs 23

Figure 1.15 Schematic showing the synthesis of Tb-DSCP NCP coated with a silica cell and conjugation with a cyclic peptide 24
Figure 1.16 Schematic and general procedure for self-assembly of NCP-Cis and NCP-Ox 25
Figure 2.1 Synthesis of bisphosphonic acid ligands based on dachPtBP prodrugs 39
Figure 2.2 Synthesis of gemcitabine monophosphate prodrug 40
Figure 2.3 Schematic representation of the synthesis, composition, and mechanism of NCP-Ox/GMP. 50
Figure 2.4 TEM micrographs of DOPA-NCP-Ox/GMP and NCP-Ox/GMP 51
Figure 2.5 Intensity-average and number-average size distribution of NCP-Ox/GMP particles .52
Figure 2.6 TEM micrographs of DOPA-NCP-Ox and NCP-Ox 52
Figure 2.7 Intensity-average and number-average size distribution of NCP-Ox particles. 53
Figure 2.8 TEM micrographs of DOPA-NCP-GMP and NCP-GMP 53
Figure 2.9 Intensity-average and number-average size distribution of NCP-GMP particles 54
Figure 2.10 TEM micrographs of DOPA-NCP-Zn Control and NCP-Zn Control 54
Figure 2.11 Intensity-average and number-average size distribution of NCP-Zn Control particles. 55
Figure 2.12 TGA analysis of DOPA-NCP-Ox/GMP to determine GMP wt% loading 56
Figure 2.13 UV-Vis analysis and standard curve of DOPA-NCP-Ox/GMP to determine GMP wt% loading 56
Figure 2.14 Stability test of NCP-Ox/GMP after PEGylation in PBS buffer with BSA at 37 ^{o}C 57
Figure 2.15 Pt and GMP release profiles of DOPA-NCP-Ox/GMP and NCP-Ox/GMP in 5 mM PBS buffer at 37 ^{o}C. 58
Figure 2.16 *In vitro* cytotoxicity plots and combination index of oxaliplatin and GMP combinations on AsPc-1 cells 60
Figure 2.17 *In vitro* cytotoxicity plots and combination index of oxaliplatin and GMP combinations on BxPc-3 cells 61
Figure 2.18 TEM micrographs of DOPA-Ce6-NCP-Ox/GMP and NCP-Ce6-Ox/GMP 63
Figure 2.19 TEM micrographs of DOPA-Ce6-NCP-Ox and Ce6-NCP-Ox..... 64
Figure 2.20 TEM micrographs of DOPA-Ce6-NCP-GMP and Ce6-NCP-GMP 64

Figure 2.21 CLSM images showing the apoptosis induced by saline, oxaliplatin, GMP, Ox&GMP, Ce6-Zn Control, Ce6-NCP-Ox/GMP, Ce6-NCP-Ox, and Ce6-NCP-GMP in AsPc-1 pancreatic cancer cells 65

Figure 2.22 CLSM images showing the apoptosis induced by saline, oxaliplatin, GMP, Ox&GMP, Ce6-Zn Control, Ce6-NCP-Ox/GMP, Ce6-NCP-Ox, and Ce6-NCP-GMP in AsPc-1 pancreatic cancer cells 66

Figure 2.23 Flow cytometry analysis of saline, oxaliplatin, GMP, Ox&GMP, Zn Control, NCP-Ox/GMP, NCP-Ox, and NCP-GMP in AsPc-1 pancreatic cancer cells. 67

Figure 2.24 Flow cytometry analysis of saline, oxaliplatin, GMP, Ox&GMP, Zn Control, NCP-Ox/GMP, NCP-Ox, and NCP-GMP in BxPc-3 pancreatic cancer cells 68

Figure 2.25 Percentage injected dose per gram and percentage injected dose of Pt and GMP in tissues and blood after intravenous administration of NCP-Ox/GMP in CT26 tumor-bearing mice 69

Figure 2.26 Determination of GMP in blood using LC-MS 70

Figure 2.27 *In vivo* tumor growth inhibition curves on subcutaneous BxPc-3 xenografts..... 72

Figure 2.28 Immunogenic response and hypersensitivity of BxPc-3 tumor bearing mice treated with saline and NCP-Ox/GMP..... 73

Figure 2.29 Histology images of resected organs of BxPc-3 tumor bearing mice treated with saline and NCP-Ox/GMP 73

Figure 2.30 *In vivo* tumor growth inhibition curves on subcutaneous AsPc-1 xenografts 74

Figure 2.31 TUNEL assays of BxPc-3 tumor tissues. 76

Figure 3.1 Scheme of Carbo prodrug synthesis 84

Figure 3.2 ESI-MS of Carbo-$(OH)_2$ 84

Figure 3.3 ESI-MS of Carbo-bis(phosphoester) 85

Figure 3.4 ESI-MS of Carbo prodrug 86

Figure 3.5 Schematic representation of NCP-Carbo/GMP.....95

Figure 3.6 Schematic representation showing the core of NCP-Carbo/GMP nanoparticles 96

Figure 3.7 Intensity-average and number-average size distribution of NCP-Carbo/GMP particles. 96

Figure 3.8 TEM micrographs of DOPA-NCP-Carbo/GMP and NCP-Carbo/GMP 97
Figure 3.9 Intensity-average and number-average size distribution of NCP-Carbo/GMP-2 particles. 97
Figure 3.10 TEM micrographs of DOPA-NCP-Carbo/GMP and NCP-Carbo/GMP-2 98
Figure 3.11 Intensity-average distribution of NCP-Carbo particles 98
Figure 3.12 TEM micrographs of DOPA-NCP-Carbo and NCP-Carbo.....99
Figure 3.13 Stability test of NCP-Carbo/GMP after PEGylation in PBS buffer with BSA at 37 ^{o}C 100
Figure 3.14 Pt and GMP release profiles of DOPA-NCP-Carbo/GMP and NCP-Carbo/GMP in 5 mM PBS buffer at 37 ^{o}C. 101
Figure 3.15 *In vitro* cytotoxicity plots and combination index of carbo and GMP combinations on SKOV-3 cells 102
Figure 3.16 *In vitro* cytotoxicity plots and combination index of oxaliplatin and GMP combinations on A2780/CDDP cells 102
Figure 3.17 TEM micrographs of DOPA-RhB-NCP-Carbo/GMP and NCP-RhB-Carbo/GMP 104
Figure 3.18 CLSM images showing cell apoptosis in SKOV-3 cells 105
Figure 3.19 CLSM images showing cell apoptosis in A2780/CDDP cells 106
Figure 3.20 Flow cytometry analysis of PBS, Carbo, GMP, Carbo/GMP, NCP-Carbo, NCP-GMP, and NCP-Carbo/GMP in SKOV-3 ovarian cancer cells. 107
Figure 3.21 Flow cytometry analysis of PBS, Carbo, GMP, Carbo/GMP, NCP-Carbo, NCP-GMP, and NCP-Carbo/GMP in A2780/CDDP ovarian cancer cells..... 108
Figure 3.22 CLSM images of co-localization of RhB from Carbo/GMP particles in SKOV-3 cells 109
Figure 3.23 CLSM images of co-localization of RhB from Carbo/GMP particles in A2780/CDDP cells.....110
Figure 3.24 Cellular uptake of carbo/GMP and NCP-Carbo/GMP in SKOV-3 cells 111
Figure 3.25 Cellular uptake of carbo/GMP and NCP-Carbo/GMP in A2780/CDDP cells..... 111

Figure 3.26 Percentage injected dose per gram and percentage injected dose of Pt and GMP in tissues and blood after intravenous administration of NCP-Carbo/GMP in CT26 tumor-bearing mice 112

Figure 3.27 *In vivo* tumor growth inhibition on subcutaneous SKOV-3 xenografts 113

Figure 3.28 *In vivo* tumor growth inhibition on subcutaneous A2780/CDDP xenografts 114

Figure 3.29 TUNEL assays of SKOV-3 tumor tissues 115

Figure 3.30 TUNEL assays of A2780/CDDP tumor tissues 115

Figure 3.31 Immunogenic response and hypersensitivity induced by saline, Carbo&GMP, and NCP-Carbo/GMP in A2780/CDDP tumor-bearing mice 116

Figure 3.32 Histology images of resected organs of A2780/CDDP tumor bearing mice treated with saline and NCP-Carbo/GMP 116

Figure 4.1 Synthesis of bisphosphonic acid ligands based on PtBp prodrugs 126

Figure 4.2 Intensity-average and number-average size distribution of NCP-Cis/GMP particles 133

Figure 4.3 TEM micrographs of DOPA-NCP-Cis/GMP and NCP-Cis/GMP 135

Figure 4.4 UV-Vis analysis and standard curve of DOPA-NCP-Cis/GMP to determine GMP wt.% loading 135

Figure 4.5 TGA analysis of DOPA-NCP-Cis/GMP to determine GMP wt% loading 136

Figure 4.6 Stability test of NCP-Cis/GMP after PEGylation in PBS buffer with BSA at 37 ^{o}C 136

Figure 4.7 Long-term NCP-Cis/GMP size stability test of NCP-Cis/GMP stored in DEPC-treated water in 4^{o}C 137

Figure 4.8 Pt and GMP release profiles of DOPA-NCP-Cis/GMP and NCP-Cis/GMP in 5 mM PBS buffer at 37 ^{o}C 138

Figure 4.9 *In vitro* cytotoxicity plots and combination index of cisplatin and GMP combinations on H82 cells. 140

Figure 4.10 *In vitro* cytotoxicity plots and combination index of cisplatin and GMP combinations on H69 cells 140

Figure 4.11 *In vitro* cytotoxicity plots and combination index of cisplatin and GMP combinations on H460 cells 140

Figure 4.12 *In vitro* cytotoxicity plots and combination index (of cisplatin and GMP combinations on A549 cells 141

Figure 4.13 Flow cytometry analysis of PBS, cisplatin, GMP, cisplatin/GMP, NCP-Cis, NCP-GMP, and NCP-Cis/GMP in H82 SCLC cells 142

Figure 4.14 Flow cytometry analysis of PBS, cisplatin, GMP, cisplatin/GMP, NCP-Cis, NCP-GMP, and NCP-Cis/GMP in H69 SCLC cells..... 143

Figure 4.15 Flow cytometry analysis of PBS, cisplatin, GMP, cisplatin/GMP, NCP-Cis, NCP-GMP, and NCP-Cis/GMP in H460 NSCLC cells 143

Figure 4.16 Flow cytometry analysis of PBS, cisplatin, GMP, cisplatin/GMP, NCP-Cis, NCP-GMP, and NCP-Cis/GMP in A549 NSCLC cells 144

Figure 4.17 Percentage injected dose per gram and percentage injected dose (% ID) of Pt and GMP in tissues and blood after intravenous administration of NCP-Cis/GMP in CT26 tumor-bearing mice 146

Figure 4.18 Pt and GMP concentration of NCP-Cis/siRNA at a cisplatin dose of 1.0 mg/kg by i.p injection in red/white blood cells layer and plasma layer after centrifugation of whole blood 147

Figure 4.19 Body weight loss of mice treated with NCP-Cis/GMP intraperitoneally to determine maximum tolerated dose 149

Figure 4.20 Body weight loss of S.D./CD rat treated with NCP-Cis/GMP intravenously to determine maximum tolerated dose 149

Figure 4.21 Anticancer efficacy and body weight evolution of NCP-Cis/GMP/siRNAs against A2780/CDDP subcutaneous xenografts 150

Figure 5.1 Intensity-average and number-average size distribution of NCP-Cis/GMP-2 particles 167

Figure 5.2 Intensity-average and number-average size distribution of NCP-Cis/GMP-3 particles 168

Figure 5.3 TGA analysis of DOPA-NCP-Cis/GMP-2 to determine GMP wt% loading..... 169

Figure 5.4 TGA analysis of DOPA-NCP-Cis/GMP-3 to determine GMP wt% loading 169

Figure 5.5 Schematic representation of NCP-Cis/GMP/siRNAs carrying cisplatin and gemcitabine in the solid core and siRNAs in the lipid shell 170

Figure 5.6 MALDI-TOF mass spectrum of DSPE-siRNA conjugate 171

Figure 5.7 Intensity-average and number-average size distribution of NCP-Cis/GMP/siRNAs particles 171

Figure 5.8 TEM micrographs of NCP-Cis/GMP/siRNAs 172

Figure 5.9 Gel retardation of NCP-Cis/GMP/Alexa-siRNA and fluormetry analysis of siRNA concentration on NCP-Cis/GMP/siRNAs..... 172

Figure 5.10 siRNA release from NCP-Cis/siRNAs 173

Figure 5.11 siRNA stability in serum of NCP-Cis/siRNAs by electrophoresis 174

Figure 5.12 Scheme showing the CO_2 generation of PtBp in reducing environment 174

Figure 5.13 Schematic showing the endosomal escape of NCP/siRNAs 175

Figure 5.14 GC spectrum confirming CO_2 generation from PtBp in PBS containing 5 mM cysteine 175

Figure 5.15 Time-dependent endosomal escape of NCP/siRNAs in SKOV-3 cells 176

Figure 5.16 Percent Co-localization of siRNA and endosome quantified by Image J 177

Figure 5.17 mRNA Expression of ERCC-1, Survivin, and Bcl-2 in Cisplatin-Resistant SKOV-3 OCa Cells Transfected with NCP-Cis/GMP/siRNAs 178

Figure 5.18 Bcl-2 relative expression levels in SKOV-3 ovarian cancer cells transfected with PBS, NCP-Cis/GMP, and NCP-Cis/GMP/siRNAs 178

Figure 5.19 *In vitro* cytotoxicity plots and combination index of cisplatin/GMP combinations on SKOV-3 cells 180

Figure 5.20 *In vitro* cytotoxicity plots and combination index of cisplatin/GMP combinations on A2780/CDDP cells..... 180

Figure 5.21 *In vitro* cytotoxicity plots and combination index of cisplatin/GMP combinations on A2780 cells 181

Figure 5.22 CLSM images showing cell apoptosis in A2780/CDDP cells 183

Figure 5.23 CLSM images showing the apoptosis induced by RhB-NCP-Cis/GMP/siRNAs in A2780/CDDP ovarian cancer cells 184

Figure 5.24 Flow cytometry analysis of PBS, cisplatin, GMP, Zn Control, NCP-Cis, NCP-GMP, and NCP-Cis/GMP, and NCP-Cis/GMP/siRNAs in SKOV-3 ovarian cancer cells 185

Figure 5.25 Flow cytometry analysis of PBS, cisplatin, GMP, Zn Control, NCP-Cis, NCP-GMP, and NCP-Cis/GMP, and NCP-Cis/GMP/siRNAs in A2780/CDDP ovarian cancer cells 185

Figure 5.26 Pharmacokinetics of siRNA concentrations in blood after intravenous administration of NCP-Cis/siRNAs in CT26 tumor-bearing mice 187

Figure 5.27 Gel retardation of NCP-Cis/siRNAs in blood serum after 3 h post i.p injection ... 188

Figure 5.28 Anticancer efficacy and body weight evolution of NCP-Cis/GMP/siRNAs against SKOV-3 subcutaneous xenografts starting at tumor volume of ~150 mm^3 189

Figure 5.29 Histology images of resected organs of SKOV-3 tumor-bearing mice treated with saline or NCP-Cis/GMP/siRNAs at the efficacy endpoints 189

Figure 5.30 Anticancer efficacy and body weight evolution of NCP-Cis/GMP/siRNAs against A2780/CDDP subcutaneous xenografts starting at tumor volume of ~75 mm^3..... 190

Figure 5.31 Anticancer efficacy and body weight evolution of NCP-Cis/GMP/siRNAs against SKOV-3 subcutaneous xenografts starting at tumor volume of ~400 mm^3 191

Figure 6.1 Schematic showing the core-shell NCP-Ox@pyrolipid nanoparticles that elicit antitumor immunity by a combination of oxaliplatin and PDT 208

Figure 6.2 Schematic representation showing the core of NCP-Ox nanoparticles 208

Figure 6.3 TEM images of NCP-Ox@pyrolipid..... 209

Figure 6.4 Intensity-average and number-average size distribution of NCP-Ox@pyrolipid particles 210

Figure 6.5 UV-Vis absorption spectra of NCP-Ox@pyrolipid in THF.....211

Figure 6.6 Time-dependent $^1O_2$ generation by NCP-Ox@pyrolipid and porphysome in PBS upon LED light irradiation reported by the SOSG fluorescence intensity for intact particles versus particles with disrupted lipid bilayer 211

Figure 6.7 Cellular uptake of NCP-Ox@pyrolipid, NCP-Ox, free oxaliplatin, and porphysome in CT26 cells determined by ICP-MS and fluorimetry 212

Figure 6.8 *In vitro* cell viability of CT26 cells treated with NCP-Ox@pyrolipid and porphysome at different oxaliplatin or pyroplipid doses 213

Figure 6.9 *In vitro* cell viability of HT29 cells treated with NCP-Ox@pyrolipid and porphysome at different oxaliplatin or pyroplipid doses 213

Figure 6.10 Flow cytometry analysis of saline, oxaliplatin, NCP-Ox, NCP-Ox@pyrolipid, and porphysome under light or dark in CT26 colon cancer cells 215

Figure 6.11 Flow cytometry analysis of saline, oxaliplatin, NCP-Ox, NCP-Ox@pyrolipid, and porphysome under light or dark in HT29 colon cancer cells 215

Figure 6.12 Immunofluorescence microscopy of CRT expression on the cell surface of CT26 cells treated with PBS, free oxaliplatin, NCP-Ox, porphysome, and NCP-Ox@pyrolipid in the absence or presence of light irradiation 217

Figure 6.13 CRT exposure on the cell surface of CT26 cells was assessed after incubation with oxaliplatin, NCP-Ox, NCP-Ox@pyrolipid, or porphysome with or without light irradiation by immunofluorescence staining followed by flow cytometry analysis ..218

Figure 6.14 Percentage injected dose per gram and percentage injected dose (% ID) of Pt and pyrolipid in tissues and blood after intravenous administration of NCP-Ox@pyrolipid in CT26 tumor-bearing mice 219

Figure 6.15 Anticancer efficacy of PBS, NCP-Ox (+), NCP-Ox@pyrolipid (-), and NCP-Ox@pyrolipid (+) in BALB/c mice bearing CT26 xenografts..... 221

Figure 6.16 Anticancer efficacy of PBS, NCP-Ox (+), NCP-Ox@pyrolipid (-), and NCP-Ox@pyrolipid (+) in nude mice bearing HT29 xenografts 221

Figure 6.17 H&E staining of tumor sections harvested from CT26 tumor-bearing mice receiving PBS w/ irradiation, NCP-Ox w/ irradiation, NCP-Ox@pyrolipid w/o irradiation, and NCP-Ox@pyrolipid w/ irradiation 221

Figure 6.18 H&E staining of tumor sections harvested from HT29 tumor-bearing mice receiving PBS w/ irradiation, NCP-Ox w/ irradiation, NCP-Ox@pyrolipid w/o irradiation, and NCP-Ox@pyrolipid w/ irradiation 222

Figure 6.19 Representative CLSM images of TUNEL assays of tumor tissues. DNA fragments in apoptotic CT26 cells were stained with fluorescein-conjugated deoxynucleotides, and the nuclei were stained with DAPI 222

Figure 6.20 Percentages of TUNEL-positive cells in CT26 tumor tissues..... 223

Figure 6.21 Representative CLSM images of TUNEL assays of tumor tissues. DNA fragments in apoptotic HT29 cells were stained with fluorescein-conjugated deoxynucleotides, and the nuclei were stained with DAPI 223

Figure 6.22 Percentages of TUNEL-positive cells in HT29 tumor tissues 224

Figure 6.23 *In vivo* immunogenic responses induced by NCP-Ox@pyrolipid in CT26 tumor bearing BALB/c mice 225

Figure 6.24 NCP-Ox@pyrolipid with irradiation-treated CT26 cells were efficiently vaccinated against live tumor cells 226

Figure 6.25 Abscopal effect of NCP-Ox@pyrolipid observed in bilateral tumor model of CT26 by subcutaneously injecting cancer cells into both the right and left flank regions of each animal 227

LIST OF SYMBOLS AND ABBREVIATIONS

°C	Degrees Celsius
α	Alpha
α*v*β3	An integrin that is overexpressed in some cancer tissues
β	Beta
δ	Delta
λ	Wavelength
λ_{ex}	Wavelength of excitation
μ	Micro-
ζ	Zeta
A2780	Human ovarian cancer cell line
A2780/CDDP	Human cisplatin-resistant ovarian cancer cell line
A549	Human non-small cell lung adenocarcinoma cell line
AA	Anisamide
ACN	Acetonitrile
Ag	Silver
ALT	Alanine aminotransferase
Aq.	Aqueous
AsPc-1	Human pancreatic ductal adenocarcinoma cell line
AST	Aspartate aminotransferase
ATCC	American Type Culture Collection
ATM	Ataxia telangiectasia mutated
ATP	Adenosine triphosphate

AUC	Area under curve
Bbi	1,1’-(1,4 butanediyl)bis(imidazole)
Bcl-2	B-cell lymphoma 2
Bcl-xL	B-cell lymphoma-extra large
BDC	1,4-benzenedicarboxylate
BEV	Bevacizumab
BHC	Benzenehexa-carboxylate
Bix	1,4-bis(imidazole-1-ylmethyl)benzene
BP	Bisphosphonates
BSA	Bovine serum albumin
BT-20	Human breast cancer cell line
BUN	Blood urea nitrogen
BxPc-3	Human pancreatic adenocarcinoma cell line
C_0	Initial blood concentration
Carbo	Carboplatin
Ce6	Chlorin e6
CI	Combination index
CL	Systemic clearance
Cl	Chloride
CLSM	Confocal laser scanning microscopy
cm	Centimeter
CMP	Cytidine monophosphate
c(RGDfk)	Small cyclic peptide known to target the αvβ3 integrin

CRT	Calreticulin
CT26	Murine colon adenocarcinoma 26
CTAB	Cetyltrimethylammonium bromide
Cur	Curcumin
Cys	Cysteine
Da	Dalton
Dach	1,2-(*R*,*R*)-diaminocyclohexane
DachPtBP	Oxaliplatin bisphosphonate prodrug
DAPI	4’,6-diamidino-2-phenylindole
DCM	Dichloromethane
dFdU	2’,2’-difluorodeoxyuridine
DIC	Differential interference contrast microscopy
DLS	Dynamic light scattering
DMF	Dimethylformamide
DMSO	Dimethylsulfoxide
DNA	Deoxyribonucleic acid
DOPA	1,2-dioleoyl-sn-glycero-3-phosphate sodium salt
DOPC	1,2-dioleoyl-sn-glycero-3-phosphocholine
DOX	Doxorubicin
DSCP	Disuccinatocisplatin
DSPC	1,2-distearoyl-sn-glycero-3-phosphocholine
DSPE-PEG_{2k}	1,2-distearoyl-sn-glycero-3-phosphoethanolamine-N-[amino(polyethyleneglycol)2000]

EE	Encapsulation efficiency
Eg.	For example
EGCG	Epigallocatechin gallate
EGFR	Epidermal growth factor receptor
ELISA	Enzyme-linked immunosorbent assays
EPR	Enhanced permeability and retention effect
ERCC-1	Excision repair cross-complementation group 1
EtOH	Ethanol
FBS	Fetal bovine serum
FDA	The Food and Drug administration
Fe	Iron
FITC	Fluorescein isothiocyanate
FOLFOX	Combination of leucovorin, fluorouracil, and oxaliplatin
g	Grams
GC	Gas chromatography
Gd	Gadolinium
GDP	Gemcitabine diphosphate
Gem	Gemcitabine
GMP	Gemcitabine monophosphate
GTP	Gemcitabine triphosphate
GSH	Glutathione
H460	Human non-small cell lung cancer cell line
H69	Human small cell lung cancer cell line

H82	Human small cell lung cancer cell line
h	Hours
H&E	Hematoxylin and erosin
HeLa	Human cervical adenocarcinoma cell line
HPLC	High performance liquid chromatography
HT29	Human colon carcinoma cell line
IC_{50}	Inhibitory concentration 50%
ICD	Immunogenic cell death
ICP-MS	Inductively coupled plasma-mass spectrometry
ID	Injected dose
IFN-γ	Interferon gamma
IgE	Immunoglobulin E
IL-6	Interleukin 6
ILS	Increased life span
i.p.	Intraperitoneal
i.t.	Intratumoral
i.v.	Intravenous
J	Joules
Jurkat	Human acute lymphoblastic leukemia cell line
k	Kilo-
k_0	Elimination rate constant
L	Liter
La	Lanthanum

LC-MS	Liquid chromatography-mass spectrometry
LED	Light-emitting diode
m	Milli-
M	Molar
MALDI-TOF	Matrix-assisted laser desorption/ionization-time of flight
MCF-7	Human breast adenocarcinoma cell line
MDR	Multidrug resistant
Mes	Mesitylene
MeOH	Methanol
MHz	Mega Hertz
min	Minute
mm	Millimeter
MMP9	Matrix-metalloproteinase 9
Mn	Manganese
MOF	Metal organic framework
Mol	Moles
MPS	Mononuclear phagocytic system
MRI	Magnetic resonance imaging
MRT	Mean resident time
MST	Median survival time
MTD	Maximum tolerated dose
MTS	3-(4,5-dimethylthiazol-2-yl)-5-(3-carboxymethoxyphenyl)-2-(4-sulfophenyl)-2H-tetrazolium

MTX	Methotrexate
MW	Molecular weight
MWCO	Molecular weight cutoff
m/z	Mass to charge ratio
n	Nano-
Na	Sodium
NF-κB	Nuclear factor kappa-light-chain-enhancer of activated B cells
nm	Nanometer
NMOF	Nanoscale metal organic framework
NCP	Nanoscale coordination polymer
NCP-Carbo	Carboplatin containing NCP
NCP-Carbo/GMP	Carboplatin and gemcitabine monophosphate containing NCP
NCP-Cis	Cisplatin containing NCP
NCP-Cis/GMP	Cisplatin and gemcitabine monophosphate containing NCP
NCP-Cis@pyrolipid	Cisplatin and pyrolipid containing NCP
NCP-GMP	Gemcitabine monophosphate containing NCP
NCP-Ox	Oxaliplatin containing NCP
NCP-Ox/GMP	Oxaliplatin and gemcitabine monophosphate containing NCP
NCP-Ox@pyrolipid	Oxaliplatin and pyrolipid containing NCP

NER	Nucleotide excision repair
NDK	Nucleoside diphosphate kinase
NMR	Nuclear magnetic resonance
NSCLC	Non-small cell lung cancer
$^1O_2$	Singlet oxygen
OCa	Ovarian cancer
OCT	Optimal cutting temperature
p53	Tumor protein 53
p	Pico-
Pam	Pamidronate
PBS	Phosphate buffered saline
PCR	Polymerase chain reaction
PDAC	Pancreatic ductal adenocarcinoma
PDI	Polydispersity index
PDT	Photodynamic Therapy
PEG	Polyethylene glycol
PFS	Progression-free survival
P-gp	P-glycoprotein
PI	Propidium iodide
PLGA	Poly(lactic-co-glycolic acid)
PK	Pharmacokinetic
Pt	Platinum
PtBp	Cisplatin bisphosphonate prodrug

PTX	Paclitaxel
RhB	Rhoadamine-B
RISC	RNA-induced silencing complex
RNA	Ribonucleic acid
ROS	Reaction oxygen species
r.t.	Room temperature
SCLC	Small cell lung cancer
S.D.	Standard Deviation
siRNA	Small-interfering ribonucleic acid
SEM	Scanning electron microscopy
SKOV-3	Human ovarian cancer cell lines
SOSG	Singlet oxygen sensor green
$t_{1/2}$	Half-life
Tb	Terbium
TEA	Triethylamine
TEM	Transmission electron microscopy
TEOS	Tetraethylorthosilicate
TGA	Thermogravimetric Analysis
THF	Tetrahydrofuran
TIR	Tumor inhibitory rate
TMSBr	Trimethylsilyl bromide
TNF-α	Tumor necrosis factor alpha
Triton X-100	t-octylphenoxypolyethyoxyethanol

TUNEL	Terminal deoxynucleotidyl transferase dUTP nick end labeling
UMP	Uridine monophosphate
UV-Vis	Ultraviolet-visible
V	Volts
v/v	Volume over volume
V_{ss}	Volume of distribution at steady state
W	Watts
W	Water to surfactant ratio
Wt.%	Weight Percent
XPA	XP complementation group A
Zavg	Intensity-weighted cumulative nanoparticle diameter
Zn	Zinc
Zr	Zirconium
Zol	Zoledronate

ABSTRACT

Christopher Poon: Nanoscale Coordination Polymers for Combination Therapy of Cancer

(Under the Direction of Wenbin Lin)

Despite remarkable progress made in conventional therapies, cancer remains one of the deadliest disease in the world. Combination therapy with multiple chemotherapeutics is a successful strategy for treating many cancers. Nanoparticle-based therapeutics have gained popularity due to their many favorable properties, including their high payloads, tunable sizes, tailorable surface properties, controllable drug release kinetics, and improved pharmacokinetics. Recently, nanoscale coordination polymers (NCPs), self-assembled nanoparticles constructed from metal ions and organic bridging ligands, have been used as versatile platforms for cancer drug delivery.

This work highlights the recent development of NCPs for simultaneous delivery of multiple chemotherapeutics for the treatment of various types of cancer. Chapter I introduces the challenges of treating cancers and summarizes current nanoplatforms in clinics and literatures. Chapter II presents a novel NCP containing oxaliplatin and gemcitabine for the treatment of pancreatic cancer. This work constitutes the first time that NCPs could incorporate multiple chemotherapeutics. In Chapter III, the development of NCP nanoparticles that efficiently deliver high payloads of carboplatin and gemcitabine. A strong synergistic effect was observed between carboplatin and gemcitabine against platinum-resistant ovarian cancer, SKOV-3 and A2780/CDDP, *in vitro*, while these particles exhibited long blood circulation and potently inhibit tumor growth *in vivo* when compared to free carboplatin and gemcitabine. Chapter IV introduces

NCP nanoparticles carrying both cisplatin and gemcitabine for effective treatment of both small cell and non-small cell lung cancers. Synergy between cisplatin and gemcitabine was observed *in vitro* and superior potency and efficacy was found *in vivo*. In Chapter V, NCP containing cisplatin and gemcitabine was further enhanced with the addition of siRNAs on the surface of the particle to effectively target multidrug resistant genes. It was found that these NCP particles possesses efficient endosomal escape through a novel carbon dioxide release mechanism to completely eradicate subcutaneous cisplatin-resistant ovarian cancer tumors *in vivo*. Finally, Chapter VI concludes by reporting the synthesis, characterization and evaluation of NCP-based core-shell nanoparticles carrying oxaliplatin and photosensitizer pyrolipid in combination for chemotherapy and photodynamic therapy in colorectal cancers. These particles enable enhanced antitumor immunity for achieving superior anticancer efficacy in colorectal cancers and their potential applications in the treatment of metastatic colorectal cancer.

ACKNOWLEDGEMENTS

Much of these research would not have been possible without the help and support of many people. Firstly, I would like to express my thanks to my advisor Professor Wenbin Lin for providing me with the opportunity to work in his lab along with the exciting and innovative projects he has bestowed upon me over the past five years. I will always remember his advice on doing research with the intent of solving real world problems. If the research does not, then it is not worth doing. Particularly, he has instilled in me with more critical eyes when reading scientific publications as well as my own research. More importantly, his dedication and passion in science has encouraged me to be a more diligent and better researcher. Without his continuous support, patience, motivation, and immense knowledge, I would not be the scientist I am today. Whether it was discussion about science, experience, or life lesson, his advices will always be engraved in my mind, and I will forever be indebted to him.

I would also like to extend my thanks to my thesis committee: Professor Chuan He and Professor Yossi Weizmann, for taking their time in reviewing my dissertation. It is a pleasure to be able to present my research before such prominent scientists.

There are many scientists that I want to acknowledge for helping me along the journey: Professor Xiaosong Li for undergraduate research experience and guidance; Dr. Chang Jin for his mentorship and helpful discussion in mass spectrometry; Dr. Qiti Guo for valuable conversation on scanning electron microscopy and life experience; and Dr. Joe Austin for his help on the transmission electron microscopy.

I thank my fellow labmates, past and present, for their aids in different portions of my PhD study career. Much of the gratitude to my early years are from Dr. Demin Liu, who taught me the basis of nanoparticle synthesis and characterizations. It was an honor to have taken part of the

development of nanoscale coordination polymers in his research. Additionally, I would like to acknowledge and thank Dr. Chunbai He for developing my *in vitro* and *in vivo* skill sets and for her precious mentorship, undying patience and countless advices in conducting my own research. I would like to also thank Dr. Xiaopin Duan and Christina Chan for our work in the carboplatin project. I would like to extend my thank to Dr. Carter Abney, Zekai Lin, and Marek Piechowicz for the works they have done with me in maintaining and operating the ICP-MS. I would also like to thank the undergraduate students that I have had the pleasure to mentor and work with over the years, Amy Li and Alexander Chen. I would also like to thank Dr. Joseph Della Rocca, Dr. Rachel Huxford-Phillips, Dr. Joseph Falkowski, Dr. Marcela Wanderley, Dr. Stephanie Kramer, Dr. Nathan Thacker, Seth Barrett, Kuangda Lu, Dan Micheroni, and Irene Hsiao for their insightful and helpful discussions. Furthermore, I would like to thank any other past or present Lin group members for their support, encouragement, and friendship.

Finally, I would like to thank my family for always being there for me through the hard but yet rewarding time in graduate school. I would not have made it to this point of my life without the constant support of my parents, Cheuk and Angela Poon. They have provided me with the foundation of who I am today and have given me unconditional love during all aspects of my life. Last but not least, I could not have done this without my wife, Xinyue Yang, for being by my side through this long journey, and I look forward to starting a new chapter of our life with you together.

CHAPTER I: Introduction and Background

1.1 Cancer is a World Epidemic

In 2016, 1,685,210 new cases of cancer are expected, and cancer will account for approximately one in four deaths worldwide.[1] Experts expect this number to increase 45% by 2030, to 2.3 million new cases annually. Cancer will overtake heart disease to become the leading cause of death in the United States in 2030. In the last 20 years, many improvements have been made to conventional therapies, such as radiotherapy, chemotherapy, and surgery. As a result, 20% of cancer deaths were estimated to have been averted as compared to 1980.[2]

Cisplatin is a platinum-based anticancer drug that is used in the treatment of many forms of cancer, including lung, ovarian, testicular, and bladder cancer.[3,4] The successful use of cisplatin has led to the synthesis and biological evaluation of other platinum (Pt) complexes, such as oxaliplatin and carboplatin, which, along with cisplatin, make up the three platinum complexes that are approved for clinical use by the Food and Drug Administration (FDA) (Figure 1.2).[3,5,6]

The anticancer activity of Pt drugs depends on their ability to bind with DNA in the nucleus. Once inside the cell, cisplatin undergoes aquation, resulting in the loss of two chloro-ligands because the chloride concentration inside the cell (3-20 mM) is lower than that outside of the cell (100 mM). The resulting active diaquo form of cisplatin reacts with the guanosine bases of DNA to induce major distortion to the helix structure.[7] DNA damage caused by platinum lesions inhibits DNA repair and replication, triggering multiple signal-transduction pathways that ultimately result in apoptosis.[8]

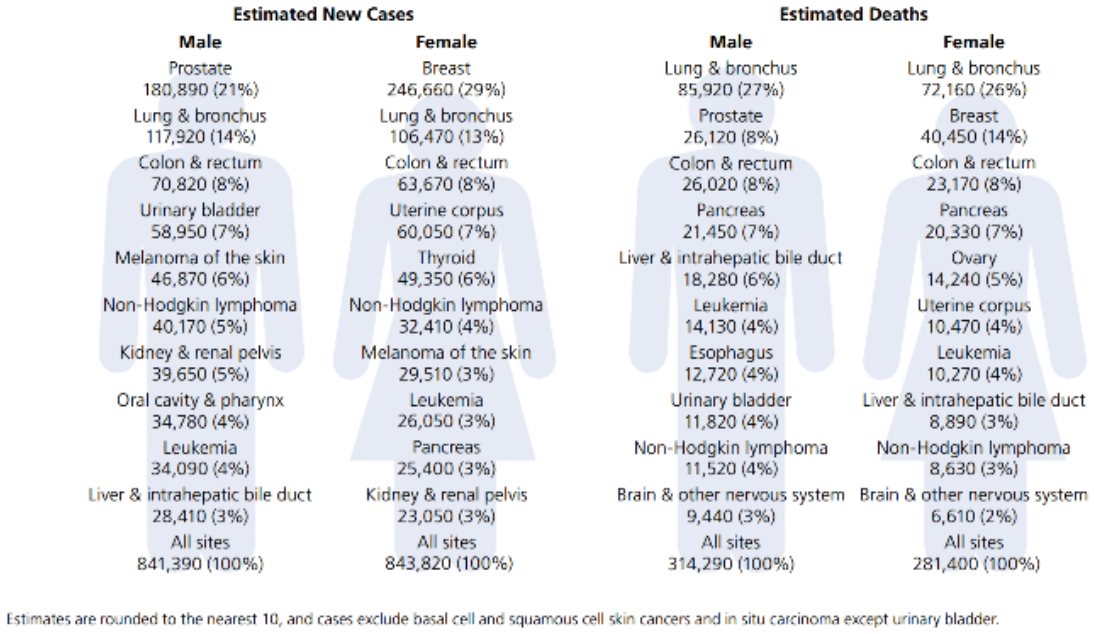

Figure 1.1 Estimated numbers of new cancer cases and deaths in 2016, as reported by the American Cancer Society.[1]

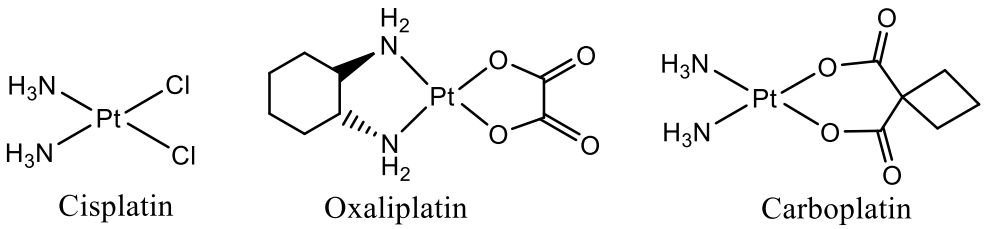

Cisplatin Oxaliplatin Carboplatin

Figure 1.2 Structures of the three FDA-approved Pt-based chemotherapeutics: cisplatin, oxaliplatin, and carboplatin.

Conventional chemotherapy has many drawbacks. Almost 50 years since the discovery of cisplatin, there has not been significant change in overall patient survival in many types of cancer. Of the 72 anticancer drugs approved by the FDA in the last decade, the median overall survival benefit of these drugs was only 2.1 months compared to an estimated cost of $2.7 million per life invested in developing new anticancer agents.[9] Because the annual cost of new cancer medications can exceed $100,000, healthcare bills have been a major reason for personal bankruptcy.[10] Furthermore, most new drugs are merely new formulations or analogs of previously approved

therapeutic agents;[11] thus, they often face a similar inability to differentiate between cancerous and healthy cells, leading to high toxicity and narrow therapeutic windows. Only a small proportion of the drug dose actually penetrates the interior of solid tumors due to poor pharmacokinetics. As a result, higher doses of anticancer drugs are needed to elicit therapeutic effects. Higher doses also lead to higher risk of side effects, such as nausea, hair loss, and loss of appetite.[12] Finally, cancer cells can develop multi-drug resistance, making repeat treatments ineffective.

Two main challenges that hinder successful cancer treatment are intratumor heterogeneity and multidrug resistance. Tumor cells vary in intrinsic or acquired drug resistant mechanisms, depending on their location in the body.[13-19] Because each cancer expresses different resistance genes, cancer cells display great heterogeneity with respect to drug resistance. Even a single tumor can exhibit distinct morphological and phenotypic heterogeneity in signaling pathways that promote drug resistance.[20,21] As a result, cancers often develop genome instability or acquire drug resistance over time. Increased genetic diversity elevates the risk that tumors will adapt to cytotoxic therapy.[22] Thus, some patients who initially respond well to a cancer drug eventually succumb to new tumors that no longer respond to the same drug.

Pt resistance can be crudely divided into two groups: those that limit formation of Pt-DNA adducts and those that prevent cell death occurring after Pt-DNA adduct (Figure 1.3). In the former case, multidrug resistance can result in enhanced drug efflux, decreased drug accumulation, and alteration of cell membrane lipids.[21] Drugs enter cells via diffusion across the plasma membrane, binding to a receptor and transporter, or via endocytosis. Receptor-mediated transport can be undermined by modification of cell surface receptors. One of these, P-glycoprotein (P-gp) regulates the flux of multiple chemotherapeutics, including taxanes, topoisomerase inhibitors, and antimetabolites, across the plasma membrane. However, P-gp overexpression can be induced

during chemotherapy, resulting in the failure of many different drugs.[23] Copper transporters are also responsible for transporting Pt drugs into and out of cells.[24,25] In cisplatin-resistant ovarian cancer patients, overexpression of these copper transporters results in an increased resistance to both cisplatin and copper.[26,27] Overexpression of copper transporters lowers the cisplatin cellular uptake and increases efflux of cisplatin. These changes altered drug metabolism and activated parallel signal transduction pathways to block apoptosis.

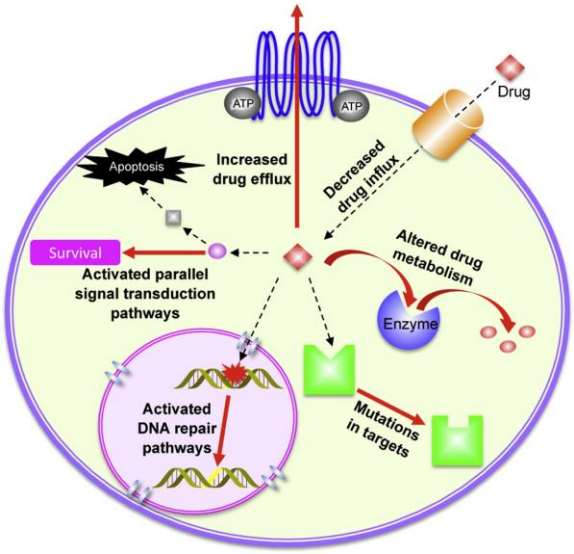

Figure 1.3 Different drug resistance mechanisms in cancer cells.[28]

Activation of these signaling pathways alter the cell cycle and checkpoints responsible for drug resistance, resulting in increased repair to damaged DNA caused by cytotoxic drugs on cancer cells (Figure 1.4). Nucleotide excision repair (NER) is the primary DNA repair mechanism responsible for the removal of Pt-DNA adducts in tumor cells. Overexpression of XP complementation group A (XPA) and excision repair cross-complementation group 1 (ERCC1) increases its excision repair function, leading to poor responses to chemotherapy in many cancer patients.[29-31] NER also accounts for cellular signaling pathways, including the activation of ataxia telangiectasia mutated (ATM) pathway, the reduction of functional p53 tumor suppressor, and the

transcription of Bcl-xL proteins that are responsible for the activation of DNA damage checkpoints.[32] Therefore, attempts to silence these genes are being explored to overcome Pt resistance.[33,34] Monotherapy is not enough to overcome the dynamic nature and adaptive ability of tumor cells.[35] Instead, combination therapies counter resistance mechanisms by targeting multiple targets through different methods of action and entry, allowing synergistic effects to lower the required effective dose, thus reducing side effects and increasing therapeutic efficacy.

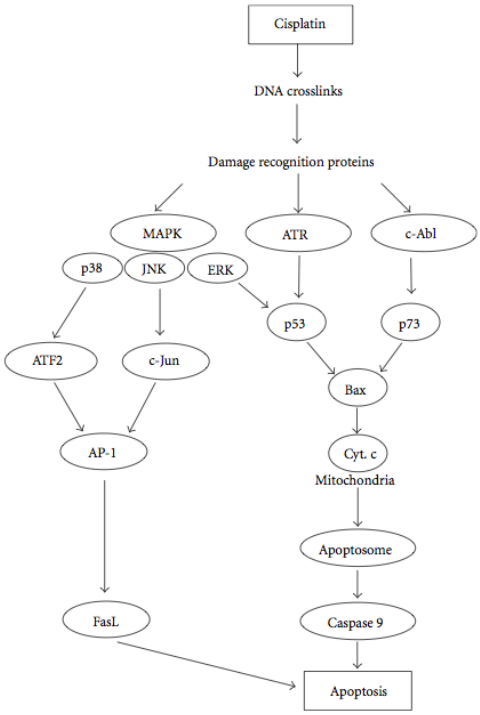

Figure 1.4 Signaling pathways that mediate cisplatin resistance.[36]

1.2 Combination Chemotherapy

Chemotherapy is often used in conjunction with surgery and radiotherapy. Surgery or radiotherapy is used to treat locally cancers, while chemotherapy can kill cancer cells that have spread nearby organs. Sometimes, chemotherapy is used to shrink tumors before surgery in order to facilitate surgical resection. As previously discussed, tumor heterogeneity and drug resistance have made monotherapy less effectual in treating cancer patients, but combination therapy with

multiple chemotherapeutics is a successful strategy for treating many cancers.[37-40] In contrast to conventional single-agent treatment, multi-agent therapy can synergistically eradicate cancer or inhibit tumor growth by increasing therapeutic target selectivity and overcoming drug resistance through diverse mechanisms of actions.[41-43] When drugs with different effects are combined, each of the drugs can increase their therapeutic effects without added side effects. For a combination of multiple therapeutics to be considered to have synergistic effects, the drugs have a higher therapeutic index at a lower dose than the standard dose of each single agent. In 1984, Professor Ting-Chao Chou and Professor Paul Talalay introduced the "combination index" to quantify the collective effects of synergism, additive effects, and antagonism among multiple drugs.[44-46] The combination index (CI) is calculated using the following equation:

$$CI = \frac{D_1}{D_{m1}} + \frac{D_2}{D_{m2}}$$

where D_1 and D_2 are concentrations of drug 1 and drug 2, used in combination at a specific drug effect level (e.g. 50% inhibition concentration), while D_{m1} and D_{m2} are the concentrations of the drugs dosed individually to achieve that same drug effect level. CI values were plotted against drug effect level (IC_x values), with CI values lower than, equal to, and greater than 1 indicating synergism, additivity, and antagonism, respectively. Analyzing synergistic effects is necessary when determining suitable drug combinations to avoid additive effects that could cause systemic toxicity. Finding drug combinations that provide synergistic effects can be difficult and requires understanding of many complex cancer-driven pathways and interactions. Different drug ratios must also be optimized for synergism.[47] Using the combination index can reduce the size of experimental sets of animals and patients used for drug combinations in clinical studies, while paving the road for more current and future drug combinations in cancer applications.

Several FDA-approved drug combinations have been approved for the treatment of cancer,

especially combinations of Pt drugs with gemcitabine. Gemcitabine is a cytidine analog that is FDA-approved for non-small cell lung cancer (NSCLC), pancreatic cancer, breast cancer, and ovarian cancer. Gemcitabine enters the cells through nucleotide transporters[48] and is then phosphorylated to gemcitabine monophosphate (GMP) by deoxycytidine kinase.[49,50] GMP is further phosphorylated by uridine/cytidine monophosphate (UMP/CMP) kinase and nucleoside diphosphate kinase (NDK) to generate pharmacologically active gemcitabine diphosphate (GDP) and gemcitabine triphosphate (GTP).[51] Gemcitabine used in combination with cisplatin is FDA-approved for the treatment of several cancers, including cervical cancer and malignant mesothelioma. Gemcitabine and cisplatin is furthermore the first line of treatment for bladder cancer, pancreatic cancer, biliary tract, and NSCLC. The FDA has also approved combinations of gemcitabine and oxaliplatin for use against pancreatic cancer and gemcitabine and carboplatin for Pt-resistant ovarian cancer and lung cancer.

Recently several multidrug regimens have been tested for the treatment of various cancers, with mixed degrees of success in phase III clinical trials.[28] Pujade-Lauraine and coworkers reported the use of liposomal doxorubicin (DOX), paclitaxel (PTX), or topotecan with monoclonal antibody bevacizumab, which targets vascular endothelial growth factor, in platinum-resistant ovarian cancer patients significantly improved the progression-free survival (PFS) and objective response rate by 2.0- and 2.3-fold, respectively (Figure 1.5).[52] Another recent report by Elter and colleagues described the combination of fludarabine and alemtuzumab, which binds to CD52, improved the PFS by 7.2 months compared with fludarabine alone in patients with chronic lymphocytic leukemia.[53] However, not all recent trials have shown clinical benefits. FOLFOX, the combination of leucovorin, fluorouracil, and oxaliplatin, used with cetuximab has been explored for patients with advanced colon cancer.[54] However, the study showed no improvement in disease-

free survival with the addition of cetuximab over FOLFOX alone. Likewise, when Hauschild and coworkers combined carboplatin and PTX with sorafenib, a tyrosine protein kinase inhibitor, it did not show any improvement over the chemotherapy treatment alone for patients with advanced melanoma.[55] Combination therapy has its own drawbacks as the drugs typically have different pharmacokinetic properties, which often makes it difficult to obtain the optimal dose and increases the chances of adverse side effects.[47,56] As a result, there is a great need to develop a combination drug delivery system that specifically and selectively delivers multiple chemotherapeutics to tumor sites.

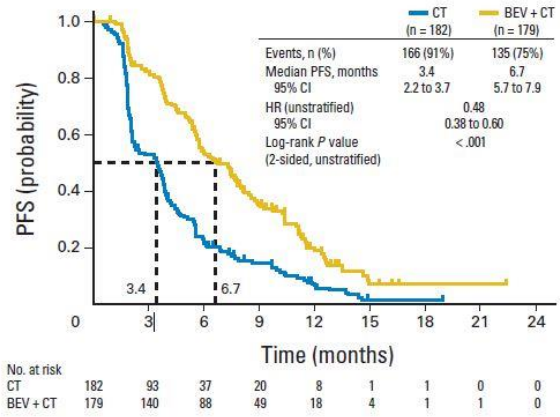

Figure 1.5 Progression-free survival of patients with platinum-resistant ovarian cancer treated with chemotherapy (CT) or chemotherapy with bevacizumab (BEV + CT).[52]

1.3 Nanoparticles for Combination Therapy

Nanotechnology has been explored for new uses in diverse applications, including medicine, electronics, food, fuel cells, and batteries. Nanoparticle-based therapeutics offer an alternative to conventional therapy that can overcome many of the hurdles that have confounded medical treatment using small molecule drugs. This has led researchers to design nanoparticles with unique physiochemical properties, such as their size and surface chemistry, while including multiple diagnostic or therapeutic agents.[57-61] Of the nanotechnology in clinical trials, only

dendrimers[62], micelles,[63-65] hydrogels,[66] nanoparticulates,[67] and liposomes[68-70] are used to carry small molecule drugs and therapeutic macromolecules, such as peptides, aptamers, proteins, and nucleic acids (Figure 1.6).

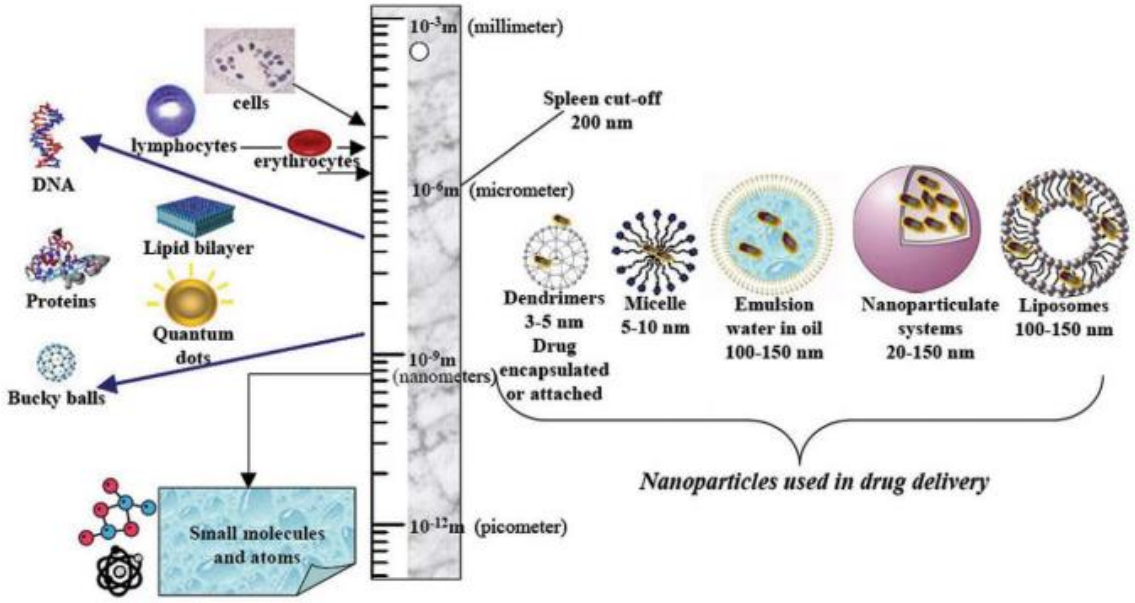

Figure 1.6 Nanoparticles used in drug delivery consist of dendrimers, micelles, emulsions, nanoparticulates, and liposomes for the delivery of small molecule drugs and therapeutic macromolecules, such as proteins, peptides, aptamers, and nucleic acids.[71]

1.3.1 Advantages of Anticancer Nanoparticles

As mentioned above, there are two major weaknesses that prevent conventional small molecule chemotherapeutics from optimal effectiveness against cancer, their short blood circulation time and their inability to select for diseased tissue. Nanoparticles have several advantages over traditional small molecule agents, including high payloads, tunable sizes, tailorable surface properties, controllable drug release kinetics, and improved pharmacokinetics.[72-78] Because of their size, which ranges from 10-200 nm in diameter, nanoparticles can penetrate through leaky neovasculatures of tumor tissues and are retained due to their characteristically ineffective lymphatic drainage, an effect known as the enhanced permeability and retention (EPR)

effect (Figure 1.7).[79] Particles larger than 40 kDa, the threshold for renal clearance, leak out of tumor vessels and accumulate in tumor tissues.[80] Once particles enter the tumor, ineffective lymphatic drainage causes particles to be retained in the tumor. Particles between 50-150 nm in diameter with a neutral, slightly positive, or slightly negative charge are of particular interest because they can penetrate into tumor tissue after systemic administration in animal models.[81,82] Knowing these parameters, I aimed to design nanoparticles of 10-200 nm in size with either a neutral, slight positive or slight negative surface charge to effectively target and treat tumors using the EPR effect.

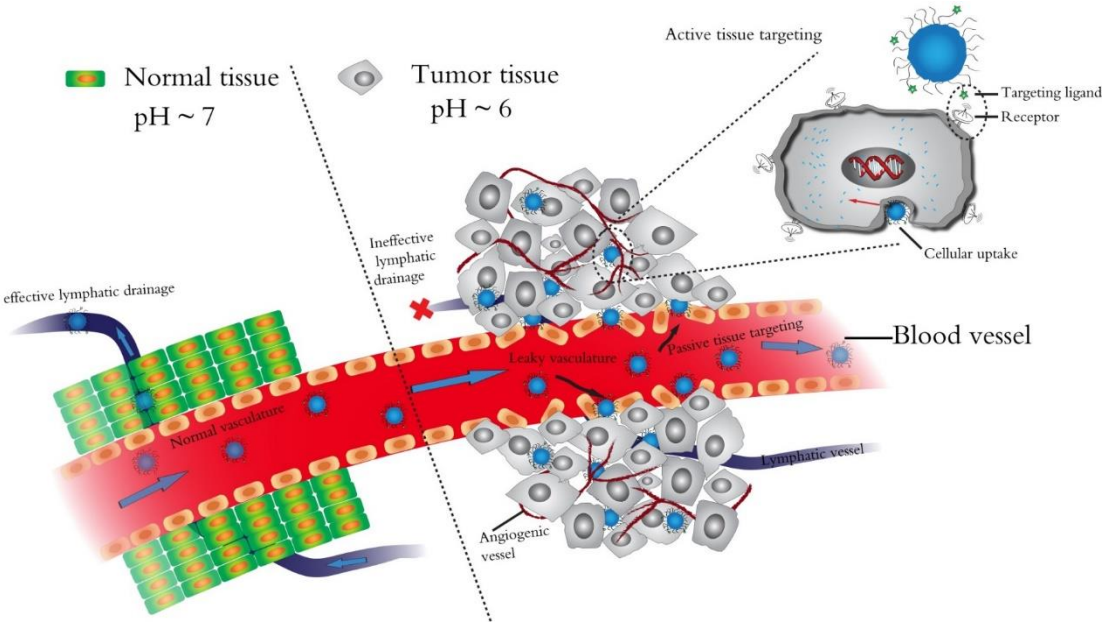

Figure 1.7 Schematic showing enhanced permeability and retention (EPR) effect stemming from the leaky neovasculature and inefficient lymphatic drainage characteristic of tumors. Courtesy of Dr. Demin Liu.

Diffusion, flow force, and protein adsorption are other factors that affect how nanoparticles reach tumor cells.[83] Interactions between nanoparticles and their local environments are dependent on both size and surface properties. For example, when nanoparticle surface charges are highly positive or negative, macrophages take them up, resulting in greater clearance by the mononuclear

phagocytic system (MPS). In order to stabilize particles against rapid decomposition, they can be encapsulated within a lipid layer containing water-soluble polymers such as polyethylene glycol (PEG). This coating shields the nanoparticle from the immune system, prevents degradation, and increases circulation to improve drug accumulation and controlled drug release within the tumor.[84] Furthermore, nanoparticles can be specifically targeted to cancer cells by surface conjugation of a tumor-specific ligand to enhance the accumulation of nanoparticles in tumors, a process that can be amplified by incorporating multiple targeting ligands for multivalent binding to cell-surface receptors.[85,86] Another advantage of nanoparticles is their high surface-to-volume ratio, allowing for high drug loadings on particle surfaces. Nanoparticles can also carry high drug payloads in their cores, while PEG on the surface protects the drug from degradation without affecting the pharmacokinetic properties and biodistribution of the particle. Nanoparticle drug delivery has been shown to promote therapeutic effectiveness and reduce side effects by improving pharmacokinetics.[77,87-89]

1.3.2 FDA-Approved Anticancer Nanoparticles and the Drawbacks of Ongoing Clinical Trials of Single-Agent Nanoplatforms

Despite the advantages of nanoparticle drug delivery, only two nanoparticle platforms containing chemotherapeutics – liposomes and abraxanes--have been FDA-approved for cancer treatment in humans so far.[71] Doxil, a DOX-containing liposome, was the first FDA-approved nanodrug for the treatment of ovarian and breast cancer.[90-92] The use of a stealth liposome enhances its blood circulation time by a hundred-times over free DOX while minimizing cardiotoxicity, a major serious side effect.[71] Abraxane, an albumin-bound nanoparticle of PTX currently used to treat metastatic breast cancer, advanced pancreatic cancer, and in combination with carboplatin for NSCLC, was the second nanoscale drug system to have been approved by the FDA.[63, 70] The use

of Abraxane eliminates the toxicities associated with solubilizer, Cremophor EL, in the PTX formulation of Taxol, while retaining the therapeutic benefits of PTX. The removal of Cremophor EL increases the maximum tolerated dose (MTD) of Abraxane by 70-80% compared to that of Taxol. Abraxane also increases the bioavailability of PTX with biphasic elimination half-life of 27 hours, compared to PTX's half-life of 5.8 hours, resulting in higher intratumoral concentration associated with Abraxane compared with the equivalent dose of Taxol.[69,70]

Despite the success of Doxil and Abraxane, other nanoplatforms have not replicated the same success or demonstrated significant clinical benefits over that of the free drugs. For example, SPI-77 and Lipoplatin, both liposomal formulations of cisplatin, showed superior pharmacokinetic properties but did not perform well in clinical trials, showing no enhanced therapeutic efficacy over free cisplatin because they were not released in tumor tissue.[93-97] ProLindac, an oxaliplatin-containing copolymer conjugate, also failed to demonstrate superior efficacy over oxaliplatin in ovarian cancer patients because the strong covalent attachment of the oxaliplatin prodrug to the polymer prevented its release at the tumor site.[98] Other nanoplatforms have suffered from insufficient pharmacokinetic properties due to their accumulation in the liver, spleen, and bone marrow, which limits their bioavailability to the tumor.[99] Liver entrapment also often results in liver toxicity and chronic inflammatory reactions.[100] Another possibility, cationic nanoparticles, such as gold and polystyrene, have been shown to cause hemolysis and blood clotting.[101]

Although Doxil and Abraxane have shown some value in the clinic, the majority of nanoparticles have not shown significant benefits over small molecule drugs. This can partially be attributed to the fact that most particles undergoing clinical trials only carry a single therapeutic agent. It thus seemed advantageous to develop nanocarriers that would be able to deliver multiple chemotherapeutics with controlled release characteristics and optimal pharmacokinetic profiles.

Multidrug-containing nanoparticles could potentially offer a solution to overcoming drug resistance that has plagued many different single drug-containing particles in clinical trials.

1.3.3 Recent Nanoplatforms for Combination Chemotherapy

The biggest potential of nanoparticles is their ability to deliver multiple therapeutics with controlled kinetic release while evading chemoresistance mechanisms and minimizing adverse side effects. Recent literature indicates that many have explored using nanomaterials containing multiple therapeutics for cancer treatment.

The therapeutic effects of individual drugs can be enhanced when they are administered in combination by controlling their release orders, rates, doses, and durations. For example, epigallocatechin gallate (EGCG), a multiple signaling inhibitor, has been combined with PTX within a targeted core-shell PLGA-Casein nanoparticle for PTX-resistant breast cancer therapy.[102] To overcome PTX resistance, Menon and colleagues developed this nanoparticle to release EGCG first, followed by PTX. EGCG downregulates NF-κB, a major pathway associated with PTX resistance, and resensitized the breast cancer cells to PTX. In another example, Zhao and coworkers designed a multicompartment hydrogel with DOX and PTX encapsulated separately in amphiphilic copolymer nanoparticles, resulting in a synergistic effect against breast cancer.[103] Upon an increase in temperature, the hybrid aqueous solution turned into a semisolid hydrogel that simultaneously released DOX and PTX independently to the desired tumor sites. This combination hydrogel inhibited tumor growth by 82% in xenograft mouse models with reduced toxicity. Hammond and colleagues reported a liposome carrying DOX and EGFR inhibitor erlotinib for time sequenced drug release in BT-20 breast cancer cells and A549 NSCLC cells (Figure 1.8),[104] in which erlotinib is sequestered in the exterior lipid bilayer membrane of the particle, and DOX is encapsulated in the aqueous interior, thereby staggering the release of the erlotinib from the shell

of the nanoparticle before freeing DOX from the core. This nanoparticle demonstrated superior cell uptake, resulting in significant tumor reduction in breast and NSCLC mouse xenograft models.

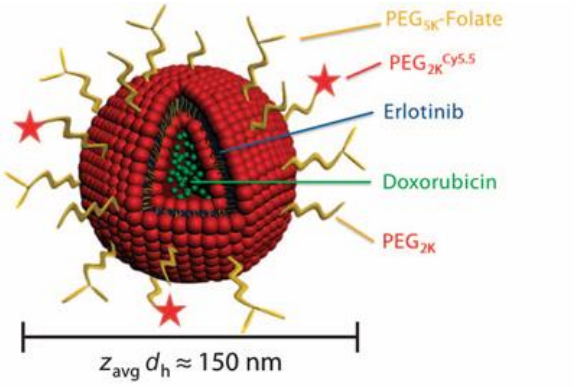

Figure 1.8 Schematic of folate-targeted layer-by-layer liposome containing DOX in the aqueous core and erlotinib on the outer lipid shell for controlled sequential drug release.[104]

The overexpression of protein in tumor microenvironments has also been explored as a means of regulating drug release. Meiners and coworkers developed an avidin-capped mesophorous silica nanoparticle functionalized with linkers that are specifically cleaved by the overexpression of matrix-metalloproteinase 9 (MMP9) to co-deliver cisplatin and bortezomib in lung cancer.[105] The avidin acts as a bulky gatekeeper, blocking the mesopores of the silica nanoparticles, and can only be cleaved open by MMP9 that is overexpressed in advanced stages of lung cancer. This nanoparticle releases drugs when specifically triggered by the MMP9 in lung tumors, showing only minimal release in healthy lung tissue. In another example, liposome containing oxaliplatin is conjugated to cetuximab on the surface through thiol-ether linkage for metastatic colon cancer expressing epidermal growth factor receptor (EGFR).[106] In EGFR-overexpressing cell lines, the targeted liposome showed an intercellular uptake three times higher than oxaliplatin liposome, leading to a 66% inhibition rate compared to the control group.

Prodrug nanoparticles have also been used extensively for drug delivery due to their exceptionally high drug loading and reduced side effects. Liu and colleagues designed prodrug

nanoparticles with a combination of DOX and curcumin (PEG-Dox-Cur) for the treatment of liver cancer (Figure 1.9).[107] To form this prodrug nanoparticle, DOX was conjugated onto the terminal aldehyde group of PEG by Schiff's base reaction, and curcumin was trapped within the nanoparticle through hydrophobic interactions. The acidic environment of the tumor breaks the Schiff's base groups within the nanoparticles, releasing both anticancer drugs inside the tumor. The therapy demonstrated prolonged circulation time, reduced toxicity, and enhanced antitumor efficacy. A self-assembled prodrug nanoparticle was synthesized through amphiphilic irinotecan and chlorambucil conjugation.[108] The hydrolysable ester linkage of the amphiphilic conjugate was cleaved upon cellular internalization to release the drugs, resulting in 71% tumor inhibition in MCF-7 breast cancer tumor.

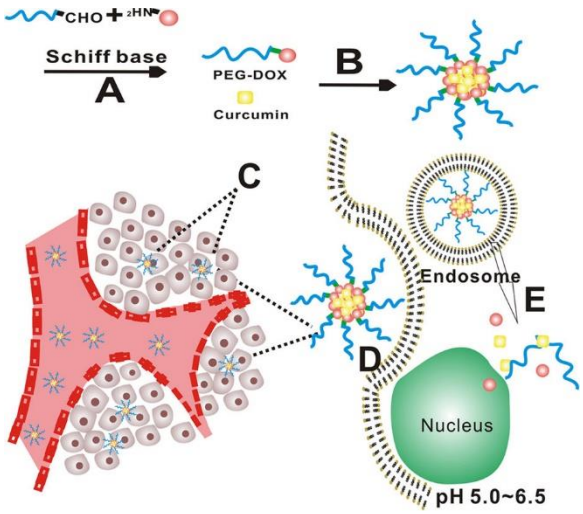

Figure 1.9 Schematic showing the synthesis and mechanistic action of PEG-Dox-Cur nanoparticle.[107]

1.4 Nanoscale Coordination Polymers

1.4.1 Advantages of Hybrid Nanoparticles

Nanoparticles can be categorized as purely organic (eg. liposomes, micelles, hydrogel, and dendrimers) or inorganic (eg. quantum dots, gold nanoparticles, carbon nanotubes, mesoporous

silica nanoparticles, and metal oxide) based on the components that construct the structure. All of the above examples in the last section have demonstrated high agent loadings and innovative release mechanisms to enhance bioavailability and anticancer efficacy. However, all of these nanoparticles were composed of either pure organic or inorganic materials, each with their own advantages and drawbacks. Most organic materials are biocompatible, biodegradable, and nontoxic but have problems with stability, reproducibility, and drug entrapment.[109] In contrast, most inorganic materials have a smaller particle size, improved stability, controlled tunability, enhanced permeability, high drug loadings, and a triggered release profile but face problems with high cellular toxicity, low biocompatibility, and nonbiodegradability.[110,111] Hybrid nanoparticles, consisting of both inorganic and organic materials, can combine the beneficial features of both inorganic and organic components, while allowing for systematic tuning of these properties.

Nanoscale coordination polymers (NCPs) are a unique class of hybrid nanoparticles consisting of polydentate bridging ligands connected by metal ions or clusters that form a larger repeating network (Figure 1.10).[76,112,113] The facile tunability of NCP materials allows for applications in biomedical imaging[114,115] and drug delivery.[76,116-121] These materials have many characteristics beneficial to drug delivery such as chemical diversity, high loading capacity, and intrinsic biodegradability. By incorporating anticancer therapeutic agents into the nanoparticle, one benefit is to control release of the drug over time. NCPs possess many advantages over other existing nanoparticle platforms, including chemically diversity for accommodating different compositions, sizes, shapes, and surface functionalization; high and efficient drug loading; and intrinsically biodegradability due to labile bond between metal ions and polydentate bridging ligand.

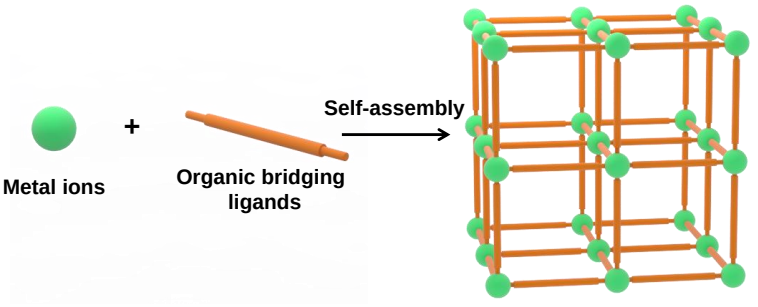

Figure 1.10 Formation of nanoscale coordination polymers from metal-connecting points and organic bridging ligands.[113]

1.4.2 Synthesis of NCPs

Controlling particle size is paramount to influencing the chemical and physical properties of the nanoparticles. As discussed above, nanoparticles between the sizes of 10-200 nm can select for tumors because of the EPR effect. Therefore, it is important to prepare 10-200 nm nanoparticles that are homogenous, monodispersed, and stable. NCPs are prepared by self-assembly using four general methods: reverse microemulsion, surfactant-assisted solvothermal synthesis, surfactant-free solvothermal synthesis, and rapid precipitation. The first two methods depend on surfactants to control particle morphology and stability (Figure 1.11), while the last two methods are surfactant-free (Figure 1.12). Rapid precipitation generally results in the formation of amorphous particles, while the other three methods can yield both amorphous and crystalline materials. The amorphous particles formed from these reactions are NCPs, whereas the crystalline materials are nanoscale metal-organic frameworks (NMOFs). For simplicity, I will only focus on the synthesis of NCPs.

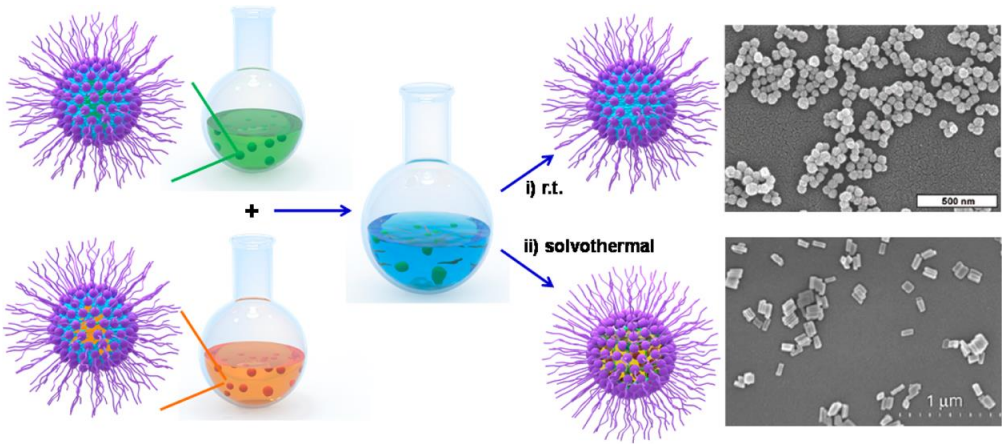

Figure 1.11 Surfactant-templated synthesis of NCPs by reverse microemulsion at room temperature or by surfactant-assisted solvothermal reactions at elevated temperature.[113]

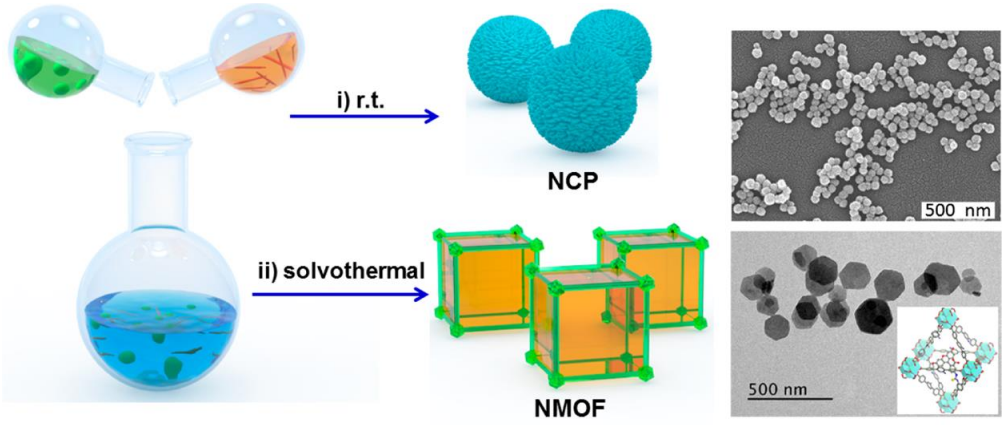

Figure 1.12 Surfactant-free synthesis of NCPs and NMOFs by nanoprecipitation reaction at room temperature or by solvothermal reactions at elevated temperature.[113]

Reverse, or water-in-oil, microemulsion is a room temperature reaction in which the reactants are suspended in surfactant-stabilized aqueous droplets in a nonpolar organic phase. These droplets facilitate the nucleation and growth kinetics of NCP materials. This method allows for a control of particle size by varying the water to surfactant ratio (*W*). For example, $Gd_2(BDC)_3(H_2O)_4$ nanoparticles were synthesized using reverse microemulsion of $GdCl_3$, di(methylammonium) 1,4-benzenedicarboxylate (BDC) organic linkers, and cationic cetyltrimethylammonium bromide surfactant (CTAB) in an isooctane/1-hexanol/water mixture.[122]

These materials provided multimodal bioimaging properties for magnetic resonance imaging (MRI). By decreasing the *W* value from 10 to 5, the nanorod dimension could be changed from 2 μm in length and 100 nm in diameter to 125 nm in length and 40 nm in diameter. The reduction in *W* value reflects the lower particle aspect ratios due to an increase in nucleation sites within the microemulsion, leading to a decrease in particle size. However, CTAB and isooctane are toxic, which limits their use for biomedical applications. More recently, we synthesized zinc-bisphosphonate NCPs containing cisplatin and oxaliplatin prodrugs in the less toxic surfactant mixture of Triton X-100/1-hexanol/cyclohexane/water reverse microemulsion.[119] The detailed synthesis and applications of these NCPs will be discussed in later sections.

Surfactant molecules can also be templated to yield surfactant-assisted solvothermal reaction. Temperature plays an important role in microemulsion reaction, as the kinetics for nucleation and growth change as a function of temperature. Therefore, different NCPs can be formulated solely by changing temperature. $Gd_2(BHC)(H_2O)_6$ nanomaterials were synthesized by heating a reverse microemulsion of hexa(methylammonium) benzenehexa-carboxylate (BHC) and $GdCl_3$ in surfactant mixture of CTAB/1-hexanol/heptane/water at 120 ^oC.[123] The resulting block-like particles have dimensions of 25 x 50 x 100 nm. When changing the pH of same reaction system at 60 ^oC, $[Gd_2(BHC)(H_2O)_8](H_2O)_2$ nanorods of ~100-300 nm was produced. Decreasing the pH gradually protonates the coordinating moieties of the organic ligands and hinders metal binding and subsequent nucleation of the nanomaterials. By changing pH and temperature conditions, new nanoparticles with different compositions and morphologies can be afforded for different applications.

The surfactant-free solvothermal reaction is achieved by heating a solution of metal and ligand molecules by conventional or microwave methods. The dielectric properties of solvents

increases with temperature, leading to weakened interactions of solvent molecules and increased dissociation. For example, $Fe_3(\mu_3\text{-}O)Cl(H_2O)(BDC)_3$ NMOF was synthesized with $FeCl_3$ and BDC ligand through microwave heating.[124] The resulting nanomaterial displayed an octahedral morphology with a diameter of 200 nm and adopted a crystalline MIL-101 structure. The solvothermal reaction was also used to synthesize an Mn-Zol NCP consisted of $MnCl_2$ and zoledronic acid in the presence of 1,2-dioleoyl-sn-glycero-3-phosphate sodium salt (DOPA) in the solvent mixture of dimethylformamide (DMF)/H_2O at 140 ^oC with microwave heating.[115] Zoledronic acid has used for the treatment of bone diseases, and Mn^{2+} centers are a great MRI contrast agents. Mn-Zol NCP is spherical with a diameter size of ~55 nm.

Lastly, NCPs can be formed by room temperature precipitation in which a solution of nanoparticles are insoluble with a given solvent, while the individual precursors remain soluble, resulting in precipitation of the nanoparticles. The use of solvent plays an important role in NCP synthesis, as, typically, the organic bridging ligand is soluble, forming nanoparticles of differing structures. A Tb-DSCP NCP was synthesized with this method by incorporating an aqueous solution of $TbCl_3$ with disuccinatocisplatin (DSCP), a Pt^{4+} cisplatin prodrug, at a pH of 5.5.[76] Methanol was used as the precursor solution to precipitate spherical nanoparticles 60 nm in diameter with high cisplatin loading by dynamic light scattering (DLS). A Zr-based NCP containing a DSCP prodrug was also formulated using acetone-induced precipitation of $ZrCl_4$ and DSCP in the presence of DMF.[118]

1.4.3 NCPs as Drug Delivery Platforms

NCPs have emerged as a promising platform for drug delivery due to their self-assembly under mild synthetic conditions, ability to carry high drug payloads, intrinsic biodegradability, and structural and chemical diversity. NCPs can incorporate different nontoxic prodrugs inside their

frameworks and selectively target tumor sites through the EPR effect due to their optimal particle size and stability. Upon release, these prodrugs can transform into highly potent anticancer drugs, thereby increasing their therapeutic effects and lowering side effects that limit most small molecule chemotherapeutics. In this section, I will describe the developments and applications of some NCPs in drug delivery.

1.4.3.1 Nitrogen-Containing Bisphosphonate When cancer metastasizes, cancerous cells from the primary tumor enter the bloodstream or lymph system, and commonly enter the bone marrow, leading to osteolysis and the formation of new tumors.[125] Pamidronate (Pam) and zoledronate (Zol) are two nitrogen-containing bisphosphonate chemotherapeutic agents used to strengthen bones weakened by cancer. We developed two types of NCPs that carry Pam or Zol incorporated into Ca^{2+} or Mn^{2+} metal centers for cancer treatment and imaging applications (Figure 1.13).[115,117] These particles demonstrated high drug loadings (45-75 wt.%) and colloidal stability *in vitro*. The targeting ligand anisamide (AA) was further conjugated with PEG through amide coupling. AA was chosen as the targeting ligand because it possesses a high affinity for sigma receptors, which are overly expressed by many human cancer cells. Enhanced *in vitro* cellular uptakes and cytotoxicity were observed with the targeting moiety in several cancer cell lines. In addition, the Mn-based NCP carrying Zol provided multifunctional theranostic ability for simultaneous chemotherapy and MRI capabilities.

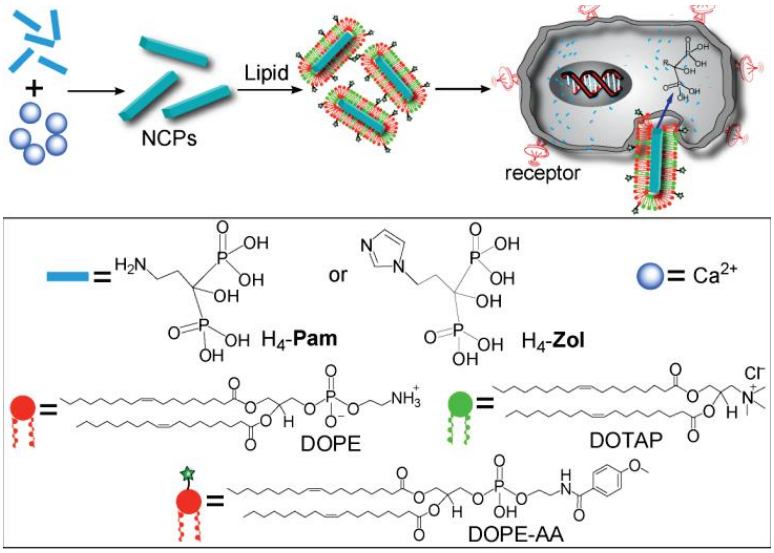

Figure 1.13 Synthesis and cell uptake mechanism of nitrogen-containing bisphosphate NCPs.[117]

1.4.3.2 Methotrexate NCPs were developed using methotrexate (MTX), an antifolate agent that inhibits dehydrofolate reductase and prevents DNA synthesis (Figure 1.14).[116] Like many small molecule chemotherapeutics, MTX suffers from rapid renal clearance, poor pharmacokinetics, and high systemic toxicity. We synthesized Zn-, Zr- and Gd-based NCPs containing MTX using the surfactant-assisted solvothermal reaction to form particles of 40-100 nm with high MTX loadings (~80 wt.%). These particles showed enhanced *in vitro* efficacy and uptakes in Jurkat cells. Similarly, Che and coworkers designed Fe- and Zn-based NCPs carrying MTX of ~150 nm in diameter using nanoprecipitation method.[126] Their synthesis afforded MTX loading of almost 90 wt.% with pH-responsive release in acidic environment. Furthermore, these NCPs showed improved *in vitro* cytotoxicity against HeLa cells as compared to free MTX.

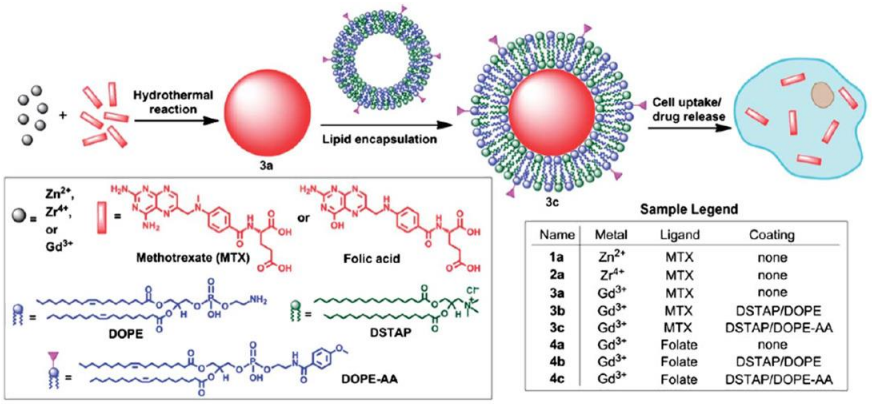

Figure 1.14 Schematic showing the surfactant-assisted solvothermal reaction of MTX-containing NCPs.[116]

1.4.3.3 Doxorubicin Following the commercial success of Doxil, different groups attempted to replicate its success using NCPs as delivery vehicles for DOX. Maspoch and colleagues encapsulated DOX, Zn^{2+} ion, and 1,4-bis(imidazole-1-ylmethyl)benzene (bix) ligand in a NCP (DOX/Zn(bix)) through a nanoprecipitation reaction.[127] Scanning (SEM) and transmission (TEM) electron microscopy showed that DOX/Zn(bix) varies between 100 to 1500 nm, while it exhibited a comparable IC_{50} *in vitro* cytotoxicity to free DOX in HL60 leukemia cells. In another example, Huang and coworkers synthesized a pH-responsive NCP containing DOX, Fe^{2+} ion, and 1,1'-(1,4 butanediyl)bis(imidazole) (bbi) organic ligands using the nanoprecipitation method.[128] The particles were coated with silica to enhance stability, and the folate acid conjugated on the surface enhanced *in vitro* intercellular uptake and cytotoxicity in HeLa cells.

1.4.3.4 Pt-Based Drugs Many nanoparticle carriers carry cisplatin but few NCPs have been developed to do so.[129-131] The first reported NCP to carry cisplatin was amorphous Tb-DSCP synthesized using nanoprecipitation (Figure 1.15).[76] Tb-DSCP was encapsulated with silica to enhance stability, and the surface was further functionalized with c(RGDfk), a cyclic peptide that targets $\alpha_v\beta_3$ integrin, which is overexpressed in many angiogenic cancers. Tb-DSCP demonstrated

slow controlled release of the cisplatin prodrug through the silica shell, leading to improved cytotoxicity against HT-29 human colon adenocarcinoma cells compared to free cisplatin. Unfortunately, the silica-coated NCP released the prodrug prematurely from the particles before they reached targeted sites. Therefore, a new NCP coating strategy was developed using a lipid layer composed of 1,2-dioleoyl-*sn*-*glycero*-3-phosphocholine (DOPC), cholesterol, and 1,2-distearoyl-*sn*-*glycero*-3-phosphoethanolamine-*N*-(polyethylene glycol) (DSPE-PEG_{2k}). This coating shields the nanoparticle from the immune system, prevents degradation, and increases circulation to improve drug accumulation and controlled drug release within the tumor.[84] NCP containing DSCP, $LaCl_3$ and DOPA was synthesized using surfactant-templated method.[118] The particle was further coated using the new lipid layer strategy to afford particle sizes of ~90 nm with DSCP loading of 8.2 wt.%. *In vitro* cytotoxicity against NSCLC cell-lines was comparable to that of free cisplatin. An AA-targeted formulation was also synthesized to induce enhanced cellular uptake and cytotoxicity.

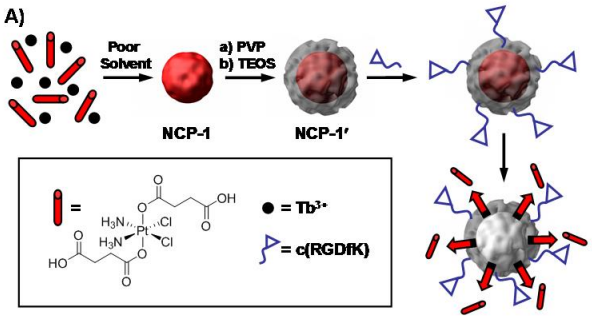

Figure 1.15 Schematic showing the synthesis of Tb-DSCP NCP coated with a silica cell and conjugation with a cyclic peptide (PVP = polyvinylprollidone, TEOS = tetraethylorthosilicate).[76]

Though the NCPs mentioned above showed enhanced *in vitro* efficacy, their lack of stability and unfavorable pharmacokinetics limit their *in vivo* applications. Recently, we formulated a new generation of NCP composed of zinc metal ions and cisplatin (PtBp) or oxaliplatin bisphosphonate prodrug dachPtBP using reverse microemulsion with high drug

loadings (48 wt.% cisplatin prodrug for NCP-Cis or 45 wt.% oxaliplatin prodrug for NCP-Ox) (Figure 1.16).[119] The particle was encapsulated with a DOPC/cholesterol/DSPE-PEG_{2k} lipid layer. The average sizes of these particles are between 40-45 nm with near-neutral zeta potentials as determined by DLS. Both NCP-Cis and NCP-Ox caused a dramatic reduction of viable CT26, H460, and AsPC-1 cells. The optimal size and the addition of PEG on the surface prolonged the blood circulation half-lives of 16 h and 12 h for NCP-Cis and NCP-Ox, respectively. That is a dramatic increase in comparison to free cisplatin and oxaliplatin, which only have blood circulation half-lives of 15 min and 2.3 min.[132,133] These NCPs also exhibited superior *in vivo* efficacy compared to free drugs in multiple tumor xenograft models, including colon, lung, and pancreatic cancer.

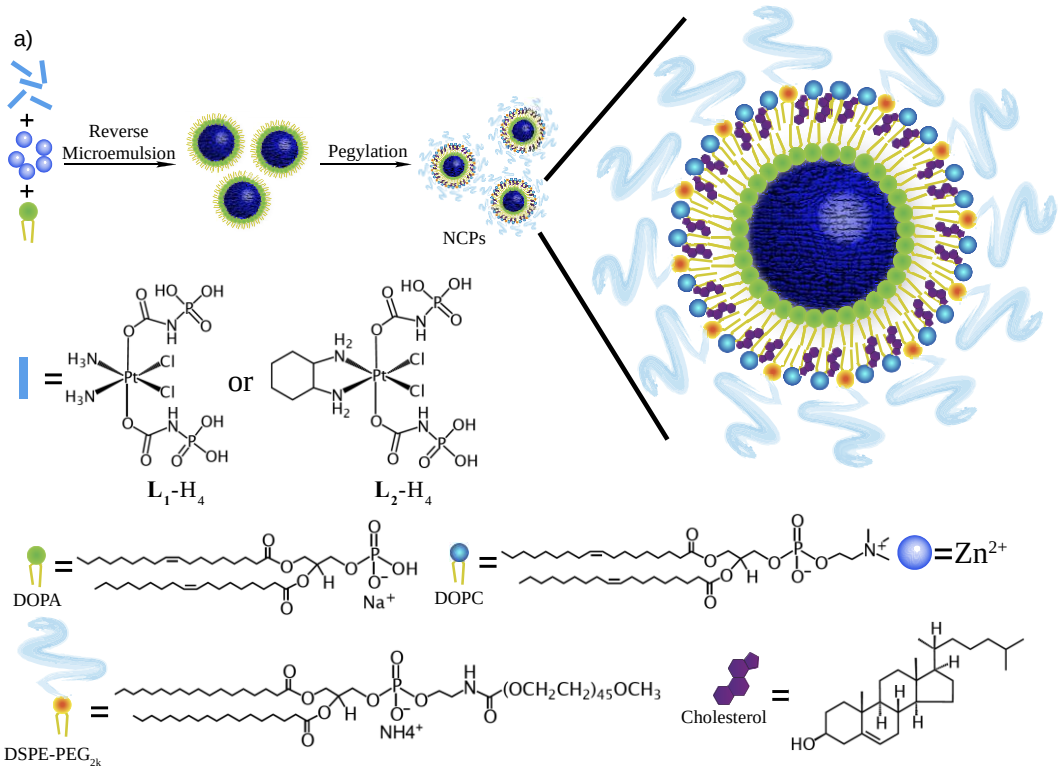

Figure 1.16 Schematic and general procedure for the self-assembly of NCP-Cis and NCP-Ox.

1.5 Summary and Scope of Work

In the last several years, there has been significant progress in the use of nanoparticles for drug delivery. In particular, hybrid nanomaterials consisting of both organic and inorganic building blocks can be specifically tuned and tailored to form new materials for many different applications. Multifunctional nanoparticles have attracted much attention in recent years because of their ability to simultaneously deliver multiple therapeutic modalities into a single platform for synergistic therapeutic efficacy. Taken together with the recent failures of nanoparticle monotherapies in clinical trials and the potential advantages of hybrid nanoparticles as a powerful delivery system, we believed it is critical to develop a combination drug delivery system that would specifically and selectively deliver multiple chemotherapeutics to tumor sites. NCPs are a viable material that can incorporate different drug combinations for the treatment of a variety of difficult-to-treat cancers.

This thesis outlines our recent contributions to the development of NCPs, which improve their ability to deliver multiple chemotherapeutics for synergistic combination therapy. In Chapter II, we develop novel nanoparticle platform based on NCP for simultaneous delivery of oxaliplatin and gemcitabine monophosphate (GMP) for the treatment of pancreatic ductal adenocarcinoma. A strong synergy between oxaliplatin and GMP was observed in both *in vitro* and *in vivo* efficacy against AsPc-1 and BxPc-3 pancreatic cancer cells. Chapter III discusses the therapeutic use of new self-assembled core-shell NCPs that deliver high loadings of carboplatin and GMP for Pt-resistant ovarian cancer. The co-administration of carboplatin and gemcitabine in the NCP was accompanied by prolonged blood circulation and improved tumor uptake of the drugs, resulting in regression and growth inhibition of these drug-resistant tumors. In Chapter IV, a cisplatin- and GMP-containing NCP was synthesized, characterized, and investigated for two different types of

lung cancer. Chapter V focuses on an NCP consisting of high payloads of the chemotherapeutics cisplatin and gemcitabine in the core and pooled siRNAs that target multidrug resistant (MDR) genes in the shell to treat cisplatin-resistant ovarian cancer. Finally, Chapter VI introduces an NCP that carries oxaliplatin and a photosensitizer for effective combination chemotherapy and photodynamic therapy application in colorectal cancers. The materials mediated regression of both a light-irradiated primary tumor and a non-irradiated metastatic tumor by eliciting a strong immunogenic response.

1.6 References

(1) Siegel, R.; Naishadham, D.; Jemal, A. *CA Cancer J. Clin* **2012**, *62*, 10.

(2) Society, A. C. **2013**.

(3) Kelland, L. *Nature Reviews Cancer* **2007**, *7*, 573.

(4) Wheate, N.; Walker, S.; Craig, G.; Oun, R. *Dalton Trans* **2010**, *39*, 8113.

(5) Jung, Y.; Lippard, S. J. *Chemical Reviews (Washington, DC, United States)* **2007**, *107*, 1387.

(6) Wang, D.; Lippard, S. J. *Nature Reviews Drug Discovery* **2005**, *4*, 307.

(7) Jamieson, E. R.; Lippard, S. J. *Chemical Reviews (Washington, D. C.)* **1999**, *99*, 2467.

(8) Takahara, P. M.; Rosenzweig, A. C.; Frederick, C. A.; Lippard, S. J. *Nature (London)* **1995**, *377*, 649.

(9) Kantarjian, H.; Zwelling, L. *Cancer* **2013**, *119*, 3903.

(10) Anon *Blood* **2013**, *121*, 4439.

(11) Della Rocca, J.; Liu, D.; Lin, W. *Nanomedicine (London, U. K.)* **2012**, *7*, 303.

(12) Reijiba, S.; Reddy, H.; Bigand, C.; Parmentier, C.; Couvreur, P.; Hajri, A. *J. Control Release* **2012**, *157*, 132.

(13) Coleman, R. L.; Monk, B. J.; Sood, A. K.; Herzog, T. J. *Nat Rev Clin Oncol* **2013**, *10*, 211.

(14) Vaughan, S.; Coward, J. I.; Bast, R. C.; Berchuck, A.; Berek, J. S.; Brenton, J. D.; Coukos, G.; Crum, C. C.; Drapkin, R.; Etemadmoghadam, D.; Friedlander, M.; Gabra, H.; Kaye,

S. B.; Lord, C. J.; Lengyel, E.; Levine, D. A.; McNeish, I. A.; Menon, U.; Mills, G. B.; Nephew, K. P.; Oza, A. M.; Sood, A. K.; Stronach, E. A.; Walczak, H.; Bowtell, D. D.; Balkwill, F. R. *Nat Rev Cancer* **2011**, *11*, 719.

(15) Roberts, D.; Schick, J.; Conway, S.; Biade, S.; Laub, P. B.; Stevenson, J. P.; Hamilton, T. C.; O'Dwyer, P. J.; Johnson, S. W. *Brit J Cancer* **2005**, *92*, 1149.

(16) Kelland, L. *Nat Rev Cancer* **2007**, *7*, 573.

(17) Agarwal, R.; Kaye, S. B. *Nat Rev Cancer* **2003**, *3*, 502.

(18) van der Zee, A. G.; Hollema, H. H.; de Bruijn, H. W.; Willemse, P. H.; Boonstra, H.; Mulder, N. H.; Aalders, J. G.; de Vries, E. G. *Gynecol Oncol* **1995**, *58*, 165.

(19) Markman, J. L.; Rekechenetskiy, A.; Holler, E.; Ljubimova, J. Y. *Adv Drug Deliver Rev* **2013**, *65*, 1866.

(20) Igney, F. H.; Krammer, P. H. *Nat Rev Cancer* **2002**, *2*, 277.

(21) Gottesman, M. M. *Annu. Rev. Med.* **2002**, *53*, 615.

(22) de Bruin, E. C.; McGranahan, N.; Mitter, R.; Salm, M.; Wedge, D. C.; Yates, L.; Jamal-Hanjani, M.; Shafi, S.; Murugaesu, N.; Rowan, A. J.; Groenroos, E.; Muhammad, M. A.; Horswell, S.; Gerlinger, M.; Varela, I.; Jones, D.; Marshall, J.; Voet, T.; Van Loo, P.; Rassl, D. M.; Rintoul, R. C.; Janes, S. M.; Lee, S.-M.; Forster, M.; Ahmad, T.; Lawrence, D.; Falzon, M.; Capitanio, A.; Harkins, T. T.; Lee, C. C.; Tom, W.; Teefe, E.; Chen, S.-C.; Begum, S.; Rabinowitz, A.; Phillimore, B.; Spencer-Dene, B.; Stamp, G.; Szallasi, Z.; Matthews, N.; Stewart, A.; Campbell, P.; Swanton, C. *Science (Washington, DC, U. S.)* **2014**, *346*, 251.

(23) Thomas, H.; Coley, H. M. *Cancer Control* **2003**, *10*, 159.

(24) Holzer, A. K.; Howell, S. B. *Cancer Research* **2006**, *66*, 10944.

(25) Lin, X.; Okuda, T.; Holzer, A.; Howell, S. B. *Mol. Pharmacol.* **2002**, *62*, 1154.

(26) Samimi, G.; Safaei, R.; Katano, K.; Holzer, A. K.; Rochdi, M.; Tomioka, M.; Goodman, M.; Howell, S. B. *Clin. Cancer Res.* **2004**, *10*, 4661.

(27) Kalayda, G. V.; Wagner, C. H.; Buss, I.; Reedijk, J.; Jaehde, U. *BMC Cancer* **2008**, *8*, 175.

(28) Kemp, J. A.; Shim, M. S.; Heo, C. Y.; Kwon, Y. J. *Adv. Drug Delivery Rev.* **2016**, *98*, 3.

(29) Rosell, R.; Taron, M.; Barnadas, A.; Scagliotti, G.; Sarries, C.; Roig, B. *Cancer Control* **2003**, *10*, 297.

(30) Ferry, K. V.; Hamilton, T. C.; Johnson, S. W. *Biochem. Pharmacol.* **2000**, *60*, 1305.

(31) Lord, R. V. N.; Brabender, J.; Gandara, D.; Alberola, V.; Camps, C.; Domine, M.; Cardenal, F.; Sanchez, J. M.; Gumerlock, P. H.; Taron, M.; Sanchez, J. J.; Danenberg, K. D.; Danenberg, P. V.; Rosell, R. *Clin. Cancer Res.* **2002**, *8*, 2286.

(32) Basu, A.; Krishnamurthy, S. *J. Nucleic Acids* **2010**, No pp. given.

(33) Chang, I.-Y.; Kim, M.-H.; Kim, H. B.; Lee, D. Y.; Kim, S.-H.; Kim, H.-Y.; You, H. J. *Biochem. Biophys. Res. Commun.* **2005**, *327*, 225.

(34) Gossage, L.; Madhusudan, S. *Cancer Treat. Rev.* **2007**, *33*, 565.

(35) Lawrence, M. S.; Stojanov, P.; Polak, P.; Kryukov, G. V.; Cibulskis, K.; Sivachenko, A.; Carter, S. L.; Stewart, C.; Mermel, C. H.; Roberts, S. A.; Kiezun, A.; Hammerman, P. S.; McKenna, A.; Drier, Y.; Zou, L.; Ramos, A. H.; Pugh, T. J.; Stransky, N.; Helman, E.; Kim, J.; Sougnez, C.; Ambrogio, L.; Nickerson, E.; Shefler, E.; Cortes, M. L.; Auclair, D.; Saksena, G.; Voet, D.; Noble, M.; DiCara, D.; Lin, P.; Lichtenstein, L.; Heiman, D. I.; Fennell, T.; Imielinski, M.; Hernandez, B.; Hodis, E.; Baca, S.; Dulak, A. M.; Lohr, J.; Landau, D.-A.; Wu, C. J.; Melendez-Zajgla, J.; Hidalgo-Miranda, A.; Koren, A.; McCarroll, S. A.; Mora, J.; Lee, R. S.; Crompton, B.; Onofrio, R.; Parkin, M.; Winckler, W.; Ardlie, K.; Gabriel, S. B.; Roberts, C. W. M.; Biegel, J. A.; Stegmaier, K.; Bass, A. J.; Garraway, L. A.; Meyerson, M.; Golub, T. R.; Gordenin, D. A.; Sunyaev, S.; Lander, E. S.; Getz, G. *Nature (London, United Kingdom)* **2013**, *499*, 214.

(36) Shen, D.-W.; Pouliot, L. M.; Hall, M. D.; Gottesman, M. M. *Pharmacol. Rev.* **2012**, *64*, 706.

(37) Lehar, J.; Krueger, A. S.; Avery, W.; Heilbut, A. M.; Johansen, L. M.; Price, E. R.; Rickles, R. J.; Short, G. F., III; Staunton, J. E.; Jin, X.; Lee, M. S.; Zimmermann, G. R.; Borisy, A. A. *Nat. Biotechnol.* **2009**, *27*, 659.

(38) Saltz, L. B.; Clarke, S.; Diaz-Rubio, E.; Scheithauer, W.; Figer, A.; Wong, R.; Koski, S.; Lichinitser, M.; Yang, T.-S.; Rivera, F.; Couture, F.; Sirzen, F.; Cassidy, J. *J. Clin. Oncol.* **2008**, *26*, 2013.

(39) Herbst, R. S.; Giaccone, G.; Schiller, J. H.; Natale, R. B.; Miller, V.; Manegold, C.; Scagliotti, G.; Rosell, R.; Oliff, I.; Reeves, J. A.; Wolf, M. K.; Krebs, A. D.; Averbuch, S. D.; Ochs, J. S.; Grous, J.; Fandi, A.; Johnson, D. H. *J. Clin. Oncol.* **2004**, *22*, 785.

(40) Giaccone, G.; Herbst, R. S.; Manegold, C.; Scagliotti, G.; Rosell, R.; Miller, V.; Natale, R. B.; Schiller, J. H.; von Pawel, J.; Pluzanska, A.; Gatzemeier, U.; Grous, J.; Ochs, J. S.; Averbuch, S. D.; Wolf, M. K.; Rennie, P.; Fandi, A.; Johnson, D. H. *J. Clin. Oncol.* **2004**, *22*, 777.

(41) DeVita, V. T., Jr.; Young, R. C.; Canellos, G. P. *Cancer* **1975**, *35*, 98.

(42) Shah, M. A.; Schwartz, G. K. *Drug Resistance Updates* **2000**, *3*, 335.

(43) Ferrari, M. *Nature Reviews Cancer* **2005**, *5*, 161.

(44) Chou, T.-C. *Cancer Research* **2010**, *70*, 440.

(45) Chou, T. C.; Talalay, P. *Trends Pharmacol. Sci.* **1983**, *4*, 450.

(46) Chou, T. C.; Talalay, P. *Adv. Enzyme Regul.* **1984**, *22*, 27.

(47) Mayer, L. D.; Harasym, T. O.; Tardi, P. G.; Harasym, N. L.; Shew, C. R.; Johnstone, S. A.; Ramsay, E. C.; Bally, M. B.; Janoff, A. S. *Mol. Cancer Ther.* **2006**, *5*, 1854.

(48) Mackey, J. R.; Mani, R. S.; Selner, M.; Mowles, D.; Young, J. D.; Belt, J. A.; Crawford, C. R.; Cass, C. E. *Cancer Res* **1998**, *58*, 4349.

(49) Oguri, T.; Achiwa, H.; Sato, S.; Bessho, Y.; Takano, Y.; Miyazaki, M.; Muramatsu, H.; Maeda, H.; Niimi, T.; Ueda, R. *Mol. Cancer Ther.* **2006**, *5*, 1800.

(50) Plunkett, W.; Huang, P.; Gandhi, V. *Anticancer Drugs* **1995**, *6 Suppl 6*, 7.

(51) Mackey, J. R.; Yao, S. Y.; Smith, K. M.; Karpinski, E.; Baldwin, S. A.; Cass, C. E.; Young, J. D. *J Natl Cancer Inst* **1999**, *91*, 1876.

(52) Pujade-Lauraine, E.; Hilpert, F.; Weber, B.; Reuss, A.; Poveda, A.; Kristensen, G.; Sorio, R.; Vergote, I.; Witteveen, P.; Bamias, A.; Pereira, D.; Wimberger, P.; Oaknin, A.; Mirza, M. R.; Follana, P.; Bollag, D.; Ray-Coquard, I. *J. Clin. Oncol.* **2014**, *32*, 1302.

(53) Elter, T.; Gercheva-Kyuchukova, L.; Pylylpenko, H.; Robak, T.; Jaksic, B.; Rekhtman, G.; Kyrcz-Krzemien, S.; Vatutin, M.; Wu, J.; Sirard, C.; Hallek, M.; Engert, A. *Lancet Oncol.* **2011**, *12*, 1204.

(54) Alberts, S. R.; Sargent, D. J.; Nair, S.; Mahoney, M. R.; Mooney, M.; Thibodeau, S. N.; Smyrk, T. C.; Sinicrope, F. A.; Chan, E.; Gill, S.; Kahlenberg, M. S.; Shields, A. F.; Quesenberry, J. T.; Webb, T. A.; Farr, G. H., Jr.; Pockaj, B. A.; Grothey, A.; Goldberg, R. M. *JAMA, J. Am. Med. Assoc.* **2012**, *307*, 1383.

(55) Hauschild, A.; Agarwala, S. S.; Trefzer, U.; Hogg, D.; Robert, C.; Hersey, P.; Eggermont, A.; Grabbe, S.; Gonzalez, R.; Gille, J.; Peschel, C.; Schadendorf, D.; Garbe, C.; O'Day, S.; Daud, A.; White, J. M.; Xia, C.; Patel, K.; Kirkwood, J. M.; Keilholz, U. *J. Clin. Oncol.* **2009**, *27*, 2823.

(56) Ismael, G. F. V.; Rosa, D. D.; Mano, M. S.; Awada, A. *Cancer Treat. Rev.* **2008**, *34*, 81.

(57) Nel, A. E.; Madler, L.; Velegol, D.; Xia, T.; Hoek, E. M. V.; Somasundaran, P.; Klaessig, F.; Castranova, V.; Thompson, M. *Nature Materials* **2009**, *8*, 543.

(58) Albanese, A.; Tang, P. S.; Chan, W. C. W. *Annu. Rev. Biomed. Eng.* **2012**, *14*, 1.

(59) Chen, F.; Ehlerding, E. B.; Cai, W. *J. Nucl. Med.* **2014**, *55*, 1919.

(60) Chen, Q.; Wang, X.; Wang, C.; Feng, L.; Li, Y.; Liu, Z. *ACS Nano* **2015**, *9*, 5223.

(61) Chou, L. Y. T.; Zagorovsky, K.; Chan, W. C. W. *Nature Nanotechnology* **2014**, *9*, 148.

(62) Bosman, A. W.; Janssen, H. M.; Meijer, E. W. *Chemical Reviews (Washington, D. C.)* **1999**, *99*, 1665.

(63) Cabral, H.; Matsumoto, Y.; Mizuno, K.; Chen, Q.; Murakami, M.; Kimura, M.; Terada, Y.; Kano, M. R.; Miyazono, K.; Uesaka, M.; Nishiyama, N.; Kataoka, K. *Nat Nanotechnol* **2011**, *6*, 815.

(64) Kataoka, K.; Harada, A.; Nagasaki, Y. *Adv. Drug Delivery Rev.* **2001**, *47*, 113.

(65) Uziely, B.; Jeffers, S.; Isacson, R.; Kutsch, K.; Wei-Tsao, D.; Yehoshua, Z.; Libson, E.; Muggia, F. M.; Gabizon, A. *Journal of clinical oncology : official journal of the American Society of Clinical Oncology* **1995**, *13*, 1777.

(66) Hamidi, M.; Azadi, A.; Rafiei, P. *Adv. Drug Delivery Rev.* **2008**, *60*, 1638.

(67) Minelli, C.; Lowe, S. B.; Stevens, M. M. *Small* **2010**, *6*, 2336.

(68) Torchilin, V. P. *Nature Reviews Drug Discovery* **2005**, *4*, 145.

(69) Sparreboom, A.; Scripture, C. D.; Trieu, V.; Williams, P. J.; De, T.; Yang, A.; Beals, B.; Figg, W. D.; Hawkins, M.; Desai, N. *Clin. Cancer Res.* **2005**, *11*, 4136.

(70) Gradishar, W. J.; Tjulandin, S.; Davidson, N.; Shaw, H.; Desai, N.; Bhar, P.; Hawkins, M.; O'Shaughnessy, J. *J. Clin. Oncol.* **2005**, *23*, 7794.

(71) Davis, M. E.; Chen, Z.; Shin, D. M. *Nature Reviews Drug Discovery* **2008**, *7*, 771.

(72) Yavuz, M. S.; Cheng, Y.; Chen, J.; Cobley, C. M.; Zhang, Q.; Rycenga, M.; Xie, J.; Kim, C.; Song, K. H.; Schwartz, A. G.; Wang, L. V.; Xia, Y. *Nature Materials* **2009**, *8*, 935.

(73) Lee, J. E.; Lee, N.; Kim, H.; Kim, J.; Choi, S. H.; Kim, J. H.; Kim, T.; Song, I. C.; Park, S. P.; Moon, W. K.; Hyeon, T. *Journal of the American Chemical Society* **2010**, *132*, 552.

(74) Sajja, H. K.; East, M. P.; Mao, H.; Wang, Y. A.; Nie, S.; Yang, L. *Current Drug Discovery Technologies* **2009**, *6*, 43.

(75) Cheon, J.; Lee, J.-H. *Accounts of Chemical Research* **2008**, *41*, 1630.

(76) Rieter, W. J.; Pott, K. M.; Taylor, K. M. L.; Lin, W. *Journal of the American Chemical Society* **2008**, *130*, 11584.

(77) Peer, D.; Karp, J. M.; Hong, S.; Farokhzad, O. C.; Margalit, R.; Langer, R. *Nature Nanotechnology* **2007**, *2*, 751.

(78) Li, S.-D.; Huang, L. *Molecular Pharmaceutics* **2008**, *5*, 496.

(79) Fang, J.; Nakamura, H.; Maeda, H. *Adv. Drug Deliv. Rev.* **2011**, *63*, 136.

(80) Matsumaura, Y.; Maeda, H. *Cancer Res* **1986**, 6387.

(81) Nomura, T.; Koreeda, N.; Yamashita, F.; Takakura, Y.; Hashida, M. *Pharmaceutical Research* **1998**, *15*, 128.

(82) Hu-Lieskovan, S.; Heidel, J. D.; Bartlett, D. W.; Davis, M. E.; Triche, T. J. *Cancer Research* **2005**, *65*, 8984.

(83) Lazarovits, J.; Chen, Y. Y.; Sykes, E. A.; Chan, W. C. W. *Chem Commun (Camb)* **2015**, *51*, 2756.

(84) Knop, K.; Hoogenboom, R.; Dagmer, F.; Schubert, U. *Angew. CHem. Int. Ed.* **2010**, 6288.

(85) Della Rocca, J.; Huxford, R. C.; Comstock-Duggan, E.; Lin, W. *Angewandte Chemie International Edition* **2011**, *50*, 10330.

(86) Hong, S.; Leroueil, P. R.; Majoros, I. J.; Orr, B. G.; Baker, J. R.; Banaszak Holl, M. M. *Chem. Biol. (Cambridge, MA, U. S.)* **2007**, *14*, 107.

(87) Danhier, F.; Feron, O.; Preat, V. *J. Controlled Release* **2010**, *148*, 135.

(88) Devalapally, H.; Chakilam, A.; Amiji, M. M. *J. Pharm. Sci.* **2007**, *96*, 2547.

(89) Haley, B.; Frenkel, E. *Urol. Oncol.: Semin. Orig. Invest.* **2008**, *26*, 57.

(90) O'Brien, M. E. R. *Anti-Cancer Drugs* **2008**, *19*, 1.

(91) Green, A. E.; Rose, P. G. *International Journal of Nanomedicine* **2006**, *1*, 229.

(92) Chanan-Khan, A. A.; Lee, K. *Clin. Lymphoma Myeloma* **2007**, *7*, S163.

(93) Bandak, S.; Goren, D.; Horowitz, A.; Tzemach, D.; Gabizon, A. *Anti-cancer drugs* **1999**, *10*, 911.

(94) Zamboni, W.; Gervais, A.; Egorin, M.; Schellens, J. M.; Zuhowski, E.; Pluim, D.; Joseph, E.; Hamburger, D.; Working, P.; Colbern, G.; Tonda, M.; Potter, D.; Eiseman, J. *Cancer Chemother. Pharmacol.* **2004**, *53*, 329.

(95) White, S. C.; Lorigan, P.; Margison, G. P.; Margison, J. M.; Martin, F.; Thatcher, N.; Anderson, H.; Ranson, M. *Br. J. Cancer* **2006**, *95*, 822.

(96) Kim, E. S.; Lu, C.; Khuri, F. R.; Tonda, M.; Glisson, B. S.; Liu, D.; Jung, M.; Hong, W. K.; Herbst, R. S. *Lung Cancer* **2001**, *34*, 427.

(97) Stathopoulos, G. P.; Antoniou, D.; Dimitroulis, J.; Michalopoulou, P.; Bastas, A.; Marosis, K.; Stathopoulos, J.; Provata, A.; Yiamboudakis, P.; Veldekis, D.; Lolis, N.; Georgatou, N.; Toubis, M.; Pappas, C.; Tsoukalas, G. *Ann Oncol* **2010**, *21*, 2227.

(98) Nowotnik, D. P.; Cvitkovic, E. *Adv. Drug Delivery Rev.* **2009**, *61*, 1214.

(99) Grislain, L.; Couvreur, P.; Lenaerts, V.; Roland, M.; Deprez-Decampeneere, D.; Speiser, P. *Int. J. Pharm.* **1983**, *15*, 335.

(100) Fernandez-Urrusuno, R.; Fattal, E.; Porquet, D.; Feger, J.; Couvreur, P. *Toxicol. Appl. Pharmacol.* **1995**, *130*, 272.

(101) De Jong, W. H.; Borm, P. J. A. *International Journal of Nanomedicine* **2008**, *3*, 133.

(102) Narayanan, S.; Mony, U.; Vijaykumar, D. K.; Koyakutty, M.; Paul-Prasanth, B.; Menon, D. *Nanomedicine (N. Y., NY, U. S.)* **2015**, *11*, 1399.

(103) Wang, W.; Song, H.; Zhang, J.; Li, P.; Li, C.; Wang, C.; Kong, D.; Zhao, Q. *J. Controlled Release* **2015**, *203*, 57.

(104) Morton, S. W.; Lee, M. J.; Deng, Z. J.; Dreaden, E. C.; Siouve, E.; Shopsowitz, K. E.; Shah, N. J.; Yaffe, M. B.; Hammond, P. T. *Sci. Signaling* **2014**, *7*, ra44/1.

(105) van Rijt, S. H.; Boeluekbas, D. A.; Argyo, C.; Datz, S.; Lindner, M.; Eickelberg, O.; Koenigshoff, M.; Bein, T.; Meiners, S. *ACS Nano* **2015**, *9*, 2377.

(106) Zalba, S.; Contreras, A. M.; Haeri, A.; ten Hagen, T. L. M.; Navarro, I.; Koning, G.; Garrido, M. J. *J. Controlled Release* **2015**, *210*, 26.

(107) Zhang, Y.; Yang, C.; Wang, W.; Liu, J.; Liu, Q.; Huang, F.; Chu, L.; Gao, H.; Li, C.; Kong, D.; Liu, Q.; Liu, J. *Sci. Rep.* **2016**, *6*, 21225.

(108) Huang, P.; Wang, D.; Su, Y.; Huang, W.; Zhou, Y.; Cui, D.; Zhu, X.; Yan, D. *Journal of the American Chemical Society* **2014**, *136*, 11748.

(109) Gregoriadis, G. *Trends Biotechnol.* **1995**, *13*, 527.

(110) Turner, C. T.; McInnes, S. J. P.; Voelcker, N. H.; Cowin, A. J. *J. Nanomater.* **2015**, 1.

(111) Dizaj, S. M.; Jafari, S.; Khosroushahi, A. Y. *Nanoscale Res. Lett.* **2014**, *9*, 1.

(112) Huxford, R. C.; de Krafft, K. E.; Boyle, W. S.; Liu, D.; Lin, W. *Chem. Sci.* **2012**, *3*, 198.

(113) He, C.; Liu, D.; Lin, W. *Chemical Reviews (Washington, DC, United States)* **2015**, *115*, 11079.

(114) deKrafft, K. E.; Xie, Z.; Cao, G.; Tran, S.; Ma, L.; Zhou, O. Z.; Lin, W. *Angew. Chem., Int. Ed.* **2009**, *48*, 9901.

(115) Liu, D.; He, C.; Poon, C.; Lin, W. *J. Mater. Chem. B* **2014**, *2*, 8249.

(116) Huxford, R. C.; Dekrafft, K. E.; Boyle, W. S.; Liu, D.; Lin, W. *Chem Sci* **2012**, *3*.

(117) Liu, D.; Kramer, S. A.; Huxford-Phillips, R. C.; Wang, S.; Della Rocca, J.; Lin, W. *Chem Commun (Camb)* **2012**, *48*, 2668.

(118) Huxford-Phillips, R. C.; Russell, S. R.; Liu, D.; Lin, W. *RSC Adv.* **2013**, *3*, 14438.

(119) Liu, D.; Poon, C.; Lu, K.; He, C.; Lin, W. *Nat Commun* **2014**, *5*.

(120) Poon, C.; He, C.; Liu, D.; Lu, K.; Lin, W. *J. Controlled Release* **2015**, *201*, 90.

(121) He, C.; Liu, D.; Lin, W. *Biomaterials* **2015**, *36*, 124.

(122) Rieter, W. J.; Taylor, K. M. L.; An, H.; Lin, W.; Lin, W. *Journal of the American Chemical Society* **2006**, *128*, 9024.

(123) Taylor, K. M. L.; Jin, A.; Lin, W. *Angew. Chem., Int. Ed.* **2008**, *47*, 7722.

(124) Taylor-Pashow, K. M. L.; Della Rocca, J.; Xie, Z.; Tran, S.; Lin, W. *Journal of the American Chemical Society* **2009**, *131*, 14261.

(125) Mundy, G. R. *Nature Reviews Cancer* **2002**, *2*, 584.

(126) Xing, L.; Cao, Y.; Che, S. *Chemical Communications (Cambridge, United Kingdom)* **2012**, *48*, 5995.

(127) Imaz, I.; Rubio-Martinez, M.; Garcia-Fernandez, L.; Garcia, F.; Ruiz-Molina, D.; Hernando, J.; Puntes, V.; Maspoch, D. *Chemical Communications (Cambridge, United Kingdom)* **2010**, *46*, 4737.

(128) Gao, P. F.; Zheng, L. L.; Liang, L. J.; Yang, X. X.; Li, Y. F.; Huang, C. Z. *J. Mater. Chem. B* **2013**, *1*, 3202.

(129) Feazell, R. P.; Nakayama-Ratchford, N.; Dai, H.; Lippard, S. J. *Journal of the American Chemical Society* **2007**, *129*, 8438.

(130) Dhar, S.; Gu, F. X.; Langer, R.; Farokhzad, O. C.; Lippard, S. J. *Proceedings of the National Academy of Sciences of the United States of America* **2008**, *105*, 17356.

(131) Dhar, S.; Daniel, W. L.; Giljohann, D. A.; Mirkin, C. A.; Lippard, S. J. *Journal of the American Chemical Society* **2009**, *131*, 14652.

(132) Johnsson, A.; Olsson, C.; Nygren, O.; Nilsson, M.; Sieving, B.; Cavallin-Stahl, E. *Cancer Chemother Pharmacol* **1995**, 23.

(133) Levi, F.; Metzger, G.; Massari, C.; Miano, G. *Clin Pharmacokinet* **2000**, *38*, 1.

CHAPTER II: Self-Assembled Nanoscale Coordination Polymers Carrying Oxaliplatin and Gemcitabine for Synergistic Combination Therapy of Pancreatic Cancer

2.1 Introduction

Pancreatic cancer has one of the poorest prognoses of all cancer types, with a five-year survival rate of less than 6%.[1,2] Pancreatic ductal adenocarcinoma (PDAC) is the most common type of pancreatic cancer and accounts for 95% of all cases of these tumors. Upon diagnosis, 80% of pancreatic cancer cases are deemed inoperable due to the high risk of surgically resecting tumors connected to surrounding blood vessels and digestive ducts.[3,4] Developing effective chemotherapy is thus of great importance in treating this deadly cancer.

Gemcitabine (gem) alone has long been the standard of care for PDAC in the clinic.[5,6] As a nucleotide analog,[7] gem enters the cells through nucleotide transporters[8] and is then phosphorylated to gemcitabine monophosphate (GMP) by deoxycytidine kinase.[9,10] GMP is further phosphorylated by uridine/cytidine monophosphate (UMP/CMP) kinase and nucleoside diphosphate kinase (NDK) to generate pharmacologically active gemcitabine diphosphate (GDP) and gemcitabine triphosphate (GTP).[11] Although gem is the standard of care for PDAC, the gem treatment has many drawbacks. First, free gem lacks tumor specificity and enters cancerous and healthy cells indiscriminately, leading to high general toxicity and narrow therapeutic windows.[12] Second, about 90% of gem is rapidly deactivated, with a short half-life of a mere 32 minutes in blood circulation due to deamination to the inactive 2',2'-difluorodeoxyuridine (dFdU). Third, many pancreatic cancer cells develop resistance to gem, making repeated treatments with gem ineffective.

Combination therapy with multiple chemotherapeutics is a successful strategy for treating

many cancers.[13-16] In particular, many different multidrug combination regiments have emerged for the treatment of pancreatic cancer, such as FOLFIRNOX and the combination of gemcitabine and nab-paclitaxel.[17,18] Compared to conventional, single-agent treatment, multi-agent therapy can promote synergism of different drugs, increase therapeutic target selectivity, and overcome drug resistance through distinct mechanisms of action.[19-21] However, combination therapy also has drawbacks, as the drugs typically have different pharmacokinetic properties, which often makes it difficult to obtain the optimal dose and increases the chances of adverse side effects.[22,23] A combination drug delivery system that would specifically and selectively deliver multiple chemotherapeutics to tumor sites is thus both a challenge and an endeavor that promises great benefits to cancer patients.

Nanoparticle drug delivery has been shown to promote therapeutic effectiveness and reduce side effects by improving pharmacokinetics.[24-27] Thus, many have aimed to develop nanocarriers capable of delivering multiple chemotherapeutics with controlled release characteristics and optimal pharmacokinetic profiles. Oxaliplatin has been used in combination with gem to treat metastatic pancreatic cancer patients with significantly greater response rates and tumor growth inhibition than their monotherapy counterparts.[28-31] However, this combination is not safe in patients with advanced solid tumors due to serious adverse side effects.[32] In view of this clinical need, we sought to develop a novel nanoparticle system for simultaneous delivery of oxaliplatin and gem for synergistic combination therapy of PDAC.

NCPs can incorporate multiple chemotherapeutics, in particular platinum drugs and gem, for their selective delivery to PDAC cells to elicit synergistic therapeutic effects. This chapter describes the development of NCP-Ox/GMP particles carrying both oxaliplatin and GMP. NCP-Ox/GMP was synthesized in reverse microemulsions and extensively characterized by dynamic

light scattering (DLS), transmission electron microscopy (TEM), and *in vitro* release profiles. Synergistic effects of oxaliplatin and gem of NCP-Ox/GMP on pancreatic cancer cells were demonstrated *in vitro* by cytotoxicity assays, flow cytometry analysis, and confocal scanning laser microscopic (CLSM) imaging. Pharmacokinetics and biodistributions of intravenously injected particles of NCP-Ox/GMP were evaluated in a subcutaneous xenograft mouse model of colon cancer CT26, whereas *in vivo* efficacy studies were carried out on subcutaneous xenograft mouse models of human PDACs including BxPc-3 and AsPc-1. The low general toxicity of NCP-Ox/GMP was indicated by histology analysis and lack of immunogenic responses. Our results indicate that the co-delivery of oxaliplatin and GMP in NCP-Ox/GMP leads to synergistic therapeutic effects and much enhanced antitumor efficacy as compared to their single drug counterparts in human pancreatic cancer xenograft mouse models.

2.2 Experimental Details

2.2.1 General Experimental:

All starting materials, unless otherwise noted, were purchased from Sigma Aldrich or Fisher Scientific and used without further purification. Oxaliplatin was purchased from AK Scientific (USA). 1,2-dioleoyl-sn-glycero-3-phosphocholine (DOPC), 1,2-dioleoyl-sn-glycero-3-phosphate sodium salt (DOPA), and 1,2-distearoyl-sn-glycero-3-phosphoethanolamine-N-[amino(polyethylene glycol)2000] (DSPE-PEG_{2k}) were purchased from Avanti Polar Lipids (USA).

Cell culture supplies, including fetal bovine serum (FBS, Hyclone, USA), RPMI-1640 growth medium (Hyclone, USA), penicillin-streptomycin (Gibco, USA), and phosphate buffered saline (Hyclone, USA) were purchased from Fisher Scientific. AsPC-1 (ATCC# CRL-1682) and

BxPc-3 (ATCC# CRL-1687) human pancreatic adenocarcinoma cells and CT26 (ATCC# CRL-2638) murine colon adenocarcinoma were purchased from the Developmental Therapeutics Core of Northwestern University. All cell lines were maintained in RPMI-1640 growth medium supplemented with 10% FBS and 2% penicillin-streptomycin. All cells were maintained at 37 °C with 5 % CO_2 and were cultured according to ATCC recommendations.

Mice (female nu/nu, 6-8 weeks old) were purchased from Harlan Laboratories, Inc. (USA). All animal work was approved by the Institutional Animal Care and Use Committee (IACUC) at the University of Chicago and University of North Carolina-Chapel Hill.

2.2.2 Synthesis of Prodrugs:

2.2.2.1 Synthesis of dachPtBP: Prodrug dachPtBP was synthesized based on previous literature (Figure 2.1).[33,34] To a suspension of *cis*, *trans*-[Pt(dach)$Cl_2$$(OH)_2$] (2.46 g, 5.94 mmol) in 12 mL DMF was added a 1 mL DMF solution containing 4 mol eq. of diethoxyphosphinyl isocyanate (3.75 mL, 2.4 mmol). The resulting mixture was stirred for 12 h at room temperature in the dark. The solution was filtered, and the desired product was precipitated by the addition of diethyl ether, then washed with ether twice to remove residual DMF. ^{1}H NMR in DMSO-d_6: δ 9.36 (br, 2H); 8.72 (d, 2H); 8.15 (br, 2H); 4.38 (m, 8H); 2.72 (t, 2H); 2.26 (d, 2H); 1.56 (d, 2H); 1.35 (m, 2H); 1.07 (m, 2H); Yield: 62%.

The bisphosphonate ester complex (2.85 g, 3.69 mmol) was put under vacuum for 4 h and dissolved in dry DMF. Trimethylsilyl bromide (5.0 mL, 38 mmol) was added at 0 ^{o}C, and the mixture was allowed to react for 18 h at room temperature in the dark, under N_2. After concentration, the desired product was precipitated by the addition of DCM and then washing with DCM at least two times. The solid was dissolved in MeOH and stirred at room temperature for 8h in order to hydrolyze the silyl ester. After solvent concentration, DCM was poured into the reaction

mixture to precipitate the desired product, and the solid was washed with DCM twice. ^{1}H NMR in D_2O: δ2.79 (d, 2H); 2.18 (d, 2H); 1.52 (d, 2H); 1.40 (m, 2H); 1.11 (m, 2H). Yield: 94%.

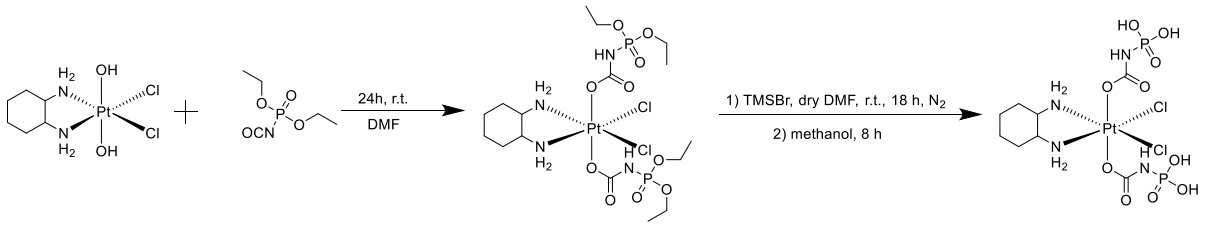

Figure 2.1 Synthesis of bisphosphonic acid ligands based on dachPtBP prodrugs.

2.2.1.1 Synthesis of GMP: Prodrug GMP was prepared from gemcitabine by a protocol slightly modified from the literature (Figure 2.2).[35] Phosphorus oxychloride (13.5mL, 14.5mmol) was stirred with trimethylphosphate (20mL) in 4-5 ^{o}C. Gemcitabine hydrochloride (1.00g, 3.34mmol) was slowly added for 5 minutes. The solution was stirred at 5 ^{o}C for 5 minutes then at room temperature for 4 hours. The mixture was poured into a cold mixture of deionized water (140mL) and diethyl ether (300mL). The aqueous layer was extracted and washed with diethyl ether (2x200mL). The pH of the solution was adjusted to 6.5 with concentrated ammonium hydroxide in an ice bath. The aqueous layer was washed with diethyl ether (200mL). The solution was frozen and lyophilized overnight until it formed a powder. Methanol (100mL) was poured into the solid and was stirred for two hours. The solution was filtered, retaining the aqueous layer. The methanol was evaporated off and washed with diethyl ether (2x100mL), then dried under vacuum for two hours. Methanol (20mL) was poured into the solid and stirred for 10 min. The solution was filtered and rotor vaporized, then washed with diethyl ether (3x30mL) and dried under vacuum. Ethanol (20mL) and acetonitrile (20mL) was poured and rotovaporized off. The solid was washed with ethanol (20mL) and diethyl ether (2x20mL). The methanol/ethanol treatment was repeated three more times. The solid was dried in vacuo at room temperature to give gemcitabine

monophosphate. ^{1}H NMR in CD_3OD. 7.95-7.93 (d, 1H); 6.25-6.22 (m, 1H); 6.01 (m, 1H); 4.39-4.32 (m, 1H); 4.25-4.23 (m, 1H); 4.14-4.10 (m, 1H); 4.00-3.98 (m, 1H); impurity from trimethylphosphate seen at 3.57 (s) and 3.55 (s). Yield: 68%.

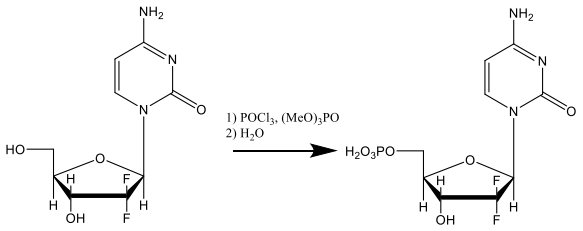

Figure 2.2 Synthesis of gemcitabine monophosphate prodrug.

2.2.3 Preparation of DOPA-NCP Particles:

2.2.3.1 Preparation of NCP-Ox/GMP: A 5 mL mixture of 0.3 M Triton X-100/1.5 M 1-hexanol in cyclohexane consisting of 0.2 mL of an aqueous 25 mg/mL dachPtBP sodium salt solution (7.6 μmol) and 0.030 mL of an aqueous 15 mg/mL GMP sodium salt solution (1.3 μmol) was stirred vigorously at room temperature. Another 5 mL of 0.3 M Triton X-100/1.5 M 1-hexanol in cyclohexane containing 0.2 mL of an aqueous 100 mg/mL $Zn(NO_3)_2$ solution (67 μmol) was stirred in a similar manner. Twenty μL of dioleoyl-sn-glycero-3-phosphate sodium salt (DOPA, 11 μmol in $CHCl_3$) was added to the solution containing dachPtBP and GMP. The two microemulsions were stirred continuously for 15 min until clear solutions were formed. The resulting W=7.4 microemulsions were combined and stirred for an additional 30 minutes. NCP-Ox/GMP particles were obtained by the addition of 20 mL ethanol and washed once with ethanol, once with 50% (v/v) ethanol/cyclohexane, and once with 50% (v/v) ethanol/tetrahydrofuran (THF) before being redispersed in THF. The nanoparticles were purified by filtration through 200 nm

syringe filter. NCP-Ox/GMP was synthesized at a 20x scale, which shows similar prodrug loading, morphology, and size as those obtained at 1x scale.

2.2.3.2 Preparation of NCP-Ox: NCP-Ox, the nanoparticle carrying oxaliplatin, was synthesized according to our previous report.[33] A *W*=7.4 microemulsion was prepared by the addition of 0.2 mL of an aqueous 25 mg/mL dachPtBp sodium salt solution (7.6×10^{-3} mmol) and 0.2 mL of an aqueous 100 mg/mL $Zn(NO_3)_2$ solution (6.7×10^{-2} mmol) to two separate 5 mL aliquots of a 0.3 M Triton X-100/1.5 M 1-hexanol in cyclohexane mixture while vigorously stirring at room temperature. 20 μL DOPA (5.5×10^{-3} mmol in $CHCl_3$) was added to the solution and stirred for 15 min, until clear solution was obtained. The two microemulsions were combined, and the resulting microemulsion was stirred for an additional 30 min. After the addition of 20 mL ethanol, NCP-Ox particles were washed once with ethanol, once with 50% (v/v) EtOH/cyclohexane, and once with 50% (v/v) EtOH/THF before being redispersed in THF.

2.2.3.3 Preparation of NCP-GMP: NCP-GMP particles carrying GMP monotherapy were prepared from our previous report.[33] A *W*=7.4 microemulsion was prepared by the addition of 0.2 mL of an aqueous 25 mg/mL GMP sodium salt solution (1.5×10^{-2} mmol) and 0.2 mL of an aqueous 100 mg/mL $Zn(NO_3)_2$ solution (6.7×10^{-2} mmol) to two separate 5 mL aliquots of a 0.3 M Triton X-100/1.5 M 1-hexanol in cyclohexane mixture while vigorously stirring at room temperature. 40 μL DOPA (1.1×10^{-2} mmol in $CHCl_3$) was added to the solution and stirring was continued for 15 min until clear solution formed. The two microemulsions were combined, and the resulting microemulsion was stirred for an additional 30 min. After the addition of 20 mL ethanol, NCP-GMP particles were washed once with ethanol, once with 50% (v/v) EtOH/cyclohexane, and once with 50% (v/v) EtOH/THF before being redispersed in THF.

2.2.3.4 Preparation of Zn Control: $Na_4P_2O_7 \cdot 10H_2O$ (100 mg, 0.224 mmol) was dissolved in a solution of 3 M NaOH/aq to form a 25mg/mL $Na_4P_2O_7 \cdot 10H_2O$ solution. $Zn(NO_3)_2 \cdot 6H_2O$ (400 mg, 1.344 mmol) was dissolved in H_2O (4 mL) to form an aqueous 100 mg/mL solution. Microemulsions were formed by the addition of 25mg/mL $Na_4P_2O_7 \cdot 10H_2O$ aq. (0.224 mmol)and 100 mg/mL $Zn(NO_3)_2 \cdot 6H_2O$ aq. (2.68 mmol) to two separate Triton-X-100 (0.3 M, 1.5 M hexanol/cyclohexane) surfactant system mixtures. The separate microemulsions were stirred vigorously for 10 to 15 min at room temperature, after which they were combined and stirred vigorously for 30 min at room temperature. After the addition of 20 mL ethanol, particles were washed once with ethanol, once with 50% (v/v) EtOH/cyclohexane, once with 50% (v/v) EtOH/THF, and redispersed in THF.

2.2.3.5 Preparation of Chlorin e6-Doped NCPs: A W=7.4 microemulsion was prepared with the addition of 25 mg/mL dachPtBP sodium salt solution (7.6 μmol), 15 mg/mL GMP sodium salt solution (1.3 μmol), 23 mg/mL chlorin e-6 sodium salt solution (0.8 μmol), and DOPA (22 μmol) to a 5 mL aliquot of Triton-X-100 (0.3 M in 1.5 M hexanol/cyclohexane) solution. Another microemulsion of 5 mL Triton-X-100 (0.3 M, 1.5 M hexanol/cyclohexane) containing $Zn(NO_3)_2 \cdot 6H_2O$ aq. (131 mmol) was also prepared. The two microemulsions were stirred vigorously for 15 min at room temperature, after which they were combined and stirred for 30 min at room temperature. After the addition of 20 mL ethanol, Ce6-NCP-Ox/GMP particles were washed once with ethanol, once with 50% (v/v) ethanol/cyclohexane, twice with 50% (v/v) ethanol/THF, and redispersed in THF. Ce6-NCP-Ox, Ce6-NCP-GMP, and Ce6-Zn controls were prepared in the same fashion.

2.2.4 General Procedures of Lipid Coating and PEGylation:

The lipid-coated and PEGylated particles were obtained by adding a THF solution of 1,2-dioleoyl-sn-glycero-3-phosphocholine (DOPC), cholesterol (1:1 molar ratio), and 1,2-distearoyl-sn-glycero-3-phosphoethanolamine-N-[methoxy(polyethylene glycol)-2000] (DSPE-PEG_{2k}, 20 mol%) to the DOPA-capped NCP nanoparticles. The resulting mixture was added to 500 μL of 30% (v/v) ethanol/H_2O at 50 ^oC. THF was evaporated, and the dispersion was allowed to cool to room temperature before use.

2.2.5 Characterization of NCP Particles:

Particle sizes and zeta potentials were determined using dynamic light scattering (DLS) with a Malvern Instruments Zetasizer Nano-ZS. Morphologies of the nanoparticles were observed by transmission electron microscope (TEM, JEM 100CX-II). Dry nanoparticles were weighed and digested in concentrated nitric acid overnight and then diluted with water for the purpose of determining the oxaliplatin drug loading by inductively coupled plasma-mass spectrometry (ICP-MS, Agilent 7700x ICP-MS). Samples were introduced via a concentric glass nebulizer with a free aspiration rate of 0.4 mL/min, a Peltier-cooled double pass glass spray chamber, and a quartz torch. A peristaltic pump carried samples from an ASX-520 autosampler (Agilent) to the nebulizer. All standards and samples were prepared by digesting a known amount of sample in concentrated nitric acid overnight and then diluting with water to 2% HNO_3 by volume.

GMP loading was determined by UV-Vis spectroscopy and thermogravimetric analyses (TGA). UV-Vis absorption spectra were obtained using a Shimadzu UV-2401PC UV-Vis Spectrophotometer. TGA was performed using a Shimadzu TGA-50 equipped with a platinum pan and heated at 3 ^oC/min in air. Different concentrations of GMP and dachPtBP solution in 6 M HCl were prepared as standards. A baseline spectrum was recorded using 6 M hydrochloric acid. The

absorbance of GMP at 275 nm was recorded. Particles were digested overnight in 6 M hydrochloric acid. The concentration of GMP in the solution was determined by its corresponding absorbance at 275 nm. Using the Pt-drug loading from ICP-MS and comparing it to the standards of oxaliplatin, the absorbance from Pt was subtracted from the total absorbance to determine the GMP-drug loading.

2.2.6 In Vitro *Stability Studies:*

In vitro stability of NCP particles was evaluated by bovine serum albumin (BSA) binding and time-dependent drug release. In the BSA binding analysis, 0.5 mg of NCP-Ox/GMP was dispersed in 1 mL of PBS, and the particle diameter was measured by DLS. BSA (2 mg) was then added to the nanoparticle suspension. DLS measurements were obtained every 10 min for 10 hours to determine the size of nanoparticles in the suspension over time. Differences in the size and count rate of the particles were used to determine extent of protein binding and sedimentation.

2.2.7 In Vitro *Drug Release:*

The release profiles were performed in 400 mL of 5 mM PBS buffer (pH=7.4) kept stirring in a beaker at 37 ^{o}C. DOPA-NCP-Ox/GMP or NCP-Ox/GMP (3 mg) was suspended in 4 mL of the buffer solution in a 10,000 MWCO pleated dialysis bag. The dialysis bag containing the nanoparticle suspension was then added to the beaker, and the system was incubated at 37 ^{o}C. Periodically, 1 mL aliquots of the solution were removed, and 1 mL of fresh buffer solution was added to the beaker. The removed aliquots were collected and analyzed by ICP-MS for Pt content and by UV-Vis for GMP content. For the release experiment under reducing environments, 5 mM cysteine was added to 5 mM PBS to simulate the intracellular reductant concentration.

2.2.8 In Vitro *Cytotoxicity Assays and Synergistic Effects of Drug Combinations:*

In vitro cytotoxicity assays were performed on AsPc-1 and BxPc-3 cancer cell lines. Confluent AsPc-1 and BxPc-3 cells were trypsinized and counted with a hemocytometer. Cells were plated in 96-well plates at a cell density of 2000 cells/well and a total of 100 μL fresh culture media, followed by incubation at 37 °C and 5 % CO_2 for 24 h. The culture medium was replaced by 100 μL of fresh RPMI 1640 containing 10% FBS and different concentrations of oxaliplatin, GMP, free Ox&GMP mixture (at the same NCP-Ox/GMP drug dose), Zn Control, NCP-Ox/GMP, NCP-Ox, and NCP-GMP were added. The cells were incubated at 37 °C and 5 % CO_2 for 48 h, and cell viability was determined by MTS assay (Promega, USA) according to manufacturer's instructions. The concentrations of oxaliplatin or GMP required to inhibit cell growth by 50% (IC_{50} values) were calculated.

The combination index (CI) was calculated using the following equation[36,37]

$$CI = \frac{D_1}{D_{m1}} + \frac{D_2}{D_{m2}}$$

in which D_1 and D_2 are concentrations of drug 1 and drug 2, respectively, in combination at a specific drug effect level (e.g. 50% inhibition concentration), while D_{m1} and D_{m2} are the concentrations of the drugs dosed individually to achieve that same drug effect level. CI values were plotted against drug effect level (IC_x values), with CI values lower than, equal to, and greater than 1 indicating synergism, additivity, and antagonism, respectively.

2.2.9 Intracellular Uptake and Cell Apoptosis In Vitro*:*

Wells containing coverslips in 6-well plates were seeded with AsPc-1 or BxPc-3 cells at a density of 5×10^5 cells per well in RPMI-1640 media (10% FBS, 2% penicillin-streptomycin). The cells were incubated for 24 h at 37ºC and 5% CO_2 prior to drug treatment. Dispersions of

PBS, oxaliplatin, GMP, free Ox&GMP, Ce6-Zn Control, Ce6-NCP-Ox/GMP, Ce6-NCP-Ox, and Ce6-NCP-GMP were incubated with cells for 48 h at 37 ºC and 5% CO_2. The cell suspensions were washed with PBS, fixed with iced 4% paraformaldehyde, and stained with 10 μg/mL of DAPI and Alexa Fluor 488 conjugated Annexin V (Invitrogen, USA), based on manufacturer's instructions. The cells were imaged using a confocal laser scanning microscope (Olympus FV1000, Japan) at excitation wavelengths of 405 nm, 488 nm, and 546 nm to visualize nuclei (blue fluorescence), cell apoptosis (green fluorescence), and nanoparticle internalization from chlorin e6 (red florescence), respectively.

2.2.10 Cell Apoptosis by Flow Cytometry:

AsPc-1 or BxPc-3 cells were seeded at a cell density of 5×10^5 cells per well and 2 mL total volume in a 6-well plate and cultured for 24 h at 37 ºC and 5% CO_2. Media were removed from the wells and aliquots of PBS, oxaliplatin, GMP, Ox&GMP, Zn Control, NCP-Ox/GMP, NCP-Ox, and NCP-GMP in fresh media were added to each well at an oxaliplatin concentration of 3.5 μM for AsPc-1 or 4.8 μM for BxPc-3 and/or a GMP concentration of 1.4 μM for AsPc-1 or 1.9 μM for BxPc-3. After incubating at 37 ºC and 5% CO_2 for 24 h, the floating and adherent cells were collected by a cell scraper and stained with Alexa Fluor 488 Annexin V/dead cell apoptosis kit with Alexa Fluor 488 annexin V and propidium iodide (PI, Invitrogen, USA) according to manufacturer's instructions. Cell apoptosis was analyzed on a flow cytometer (LSRII 3-8, BD, USA).

2.2.11 Pharmacokinetics of NCP-Ox/GMP:

Nude mice bearing C26 tumors were intravenously injected with NCP-Ox/GMP at an oxaliplatin dose of 3 mg/kg. The mice were randomly distributed into different time period groups (n = 3 for each time point). At 5 min, 1 h, 3 h, 8 h, 24 h, and 48 h post injection time point, the

mice were sacrificed, and the liver, lung, spleen, kidney, bladder, tumor, and blood were collected. Organs were digested in concentrated nitric acid overnight and then diluted with water and filtered for ICP-MS measurements of the Pt. Blood circulation half-life was fitted by an one-compartment model with nonlinear elimination using PK solver.[38]

Pharmacokinetics of GMP was analyzed using high-performance liquid chromatography-tandem mass spectrometry (HPLC-MS/MS, Agilent 6460 QQQ MS-MS) following a procedure from the literature.[39] The initial sample was prepared on ice to minimize enzyme-mediated degradation. To 50 μL of blood, 200 μL of ice-cold acetonitrile was added, vortex mixed, and centrifuged. The resulting supernatant was evaporated, and the residue was reconstituted in 100 μL of water. Calibration standard was prepared in mouse blood at GMP concentrations of 10, 25, 50, 100, 250, 500, 1,000, and 2,500 ng/mL. An injection volume of 20 μL was used. The separation was achieved using a PGC Hypercarb column (100 x 2.1 ID, 5 μm, Thermo Fisher Scientific) fitted with a guard column (Hypercarb 10 x 2.1, 5 μm, Thermo Fisher Scientific) and a gradient mobile phase consisting of (A) 10 mM ammonium acetate at pH 10 and (B) acetonitrile. The initial mobile phase consisted of 95% solvent A and 5% solvent B at a flow rate of 0.3 mL/min for 2 min. Solvent A was decreased to 80% in 0.2 min and held at this composition for 5.6 min. The gradient was returned to 95% solvent A over 0.2 min and held at this composition for 7 min to give a total runtime of 15 min. The autosampler and column temperatures were kept at 4 ^{o}C and 30 ^{o}C, respectively. The mass to charge transition was monitored from 342 to 231. A dwell time of 50 ms was used.

2.2.12 Tumor Growth Inhibition:

Tumor growth inhibition studies were conducted on AsPc-1 or BxPc-3 subcutaneous xenograft mouse models. AsPc-1 or BxPc-3 cells (5×10^6 cells in 200 μL of RPMI-1640) were

subcutaneously injected into the right flank regions of the mice. When the tumor volumes reached around 100 mm^3, the mice were randomly distributed into 6 groups (n=6) and intravenously injected with different formulations. For the mice bearing BxPc-3 tumors, the formulations included PBS, free oxaliplatin/gem (5 mg oxaliplatin/kg, 50 mg gem/kg), Zn Control, NCP-Ox/GMP (2 mg oxaliplatin/kg, 0.8 mg GMP/kg), NCP-Ox (2 mg oxaliplatin/kg), and NCP-GMP (0.8 mg GMP/kg). For the mice bearing AsPc-1 tumors, the formulations included PBS, free oxaliplatin/gem (5 mg oxaliplatin/kg, 50 mg gem/kg), and NCP-Ox/GMP (2 mg oxaliplatin/kg, 0.8 mg GMP/kg). The drugs were administered every four days. Tumor sizes were calculated by measuring two perpendicular diameters with a caliper with the formula of $V = 0.5 \times (a \times b^2)$, where V = tumor volume, a = the larger perpendicular diameter and b = the smaller perpendicular diameter. The tumor volumes were measured every other day. The body weight of each mouse was recorded every other day. All the mice were sacrificed when the tumor volume reached the maximum permitted size of 2000 mm^3.

2.2.13 In Vivo *Immunogenic Response, Hypersensitivity, and General Toxicity Evaluation of NCP-Ox/GMP:*

At the endpoint of the in vivo tumor growth inhibition experiment, blood samples were taken from the mice. Serum was separated for immunogenic response analysis. The serum concentrations of TNF-α, IFN-γ, and IL-6 were evaluated by ELISA (R&D Systems, USA). The plasma concentration of IgE was detected by ELISA (R&D Systems, USA) as indications of hypersensitivity triggered by NCP-Ox/GMP. Blood from the control group was also analyzed under the same treatment above for comparisons. Organs (liver, lung, spleen, and kidney) of mice treated with NCP-Ox/GMP were fixed with formalin. Paraffin-embedded 5 μm issue sections were stained with hematoxylin and erosin (H&E) and observed for general toxicity.

2.2.14 In Vivo *Tumor Cell Apoptosis:*

The BxPc-3 tumors were collected at the endpoint of the *in vivo* tumor growth inhibition experiment, embedded in OCT medium, and sectioned at 5 μm thickness. TdT-mediated dUTP nick end labeling (TUNEL) staining was performed using DNA Fragmentation Detection Kit (Life Technology, USA) recommended by the manufacturer and observed under CLSM. The nuclei were stained with DAPI (10 μg/mL). DNA fragments in apoptotic cells were stained with fluorescein-conjugated deoxynucleotides (green). The percentage of apoptotic cells in the samples was determined by dividing the amount of TUNEL-positive cells by the total numbers of cells observed in each microscopic field. Three tumors were randomly selected in each treatment group for analysis.

2.2.15 Statistical analysis:

Results were expressed as means ± standard deviation (S.D.). Student *t*-tests were used to determine statistical significance. A P value < 0.05 was considered statistically significant.

2.3 Results and Discussion

2.3.1 Synthesis of NCP-Ox/GMP:

DOPA-capped NCP-Ox/GMP particles were first synthesized in reverse microemulsions by crosslinking dachPtBP, a Pt^{4+} prodrug, and gemcitabine monophosphate (GMP) with Zn^{2+} ions (Figure 2.3); the Zn^{2+} ions formed coordination bonds with the phophonate groups of dachPtBP and phosphate groups of GMP. Briefly, two separate Triton-X/1-hexanol/cyclohexane microemulsions with W=7.4 were formed containing dachPtBP sodium solution, GMP sodium solution, and DOPA in one microemulsion, while the other containing a solution of $Zn(NO_3)_2$. Once the two microemulsions had formed, they were combined and stirred at room temperature

for an additional 30 minutes. The particles were isolated by centrifugation and washed once with ethanol, once with 50% (v/v) ethanol/cyclohexane, and once with 50% (v/v) ethanol/tetrahydrofuran (THF) before being redispersed in THF.

DOPA-capped NCP-Ox/GMP has a hydrophobic surface, which we coated with a DSPE/DSPE-PEG layer via hydrophobic/hydrophobic interactions to form NCP-Ox/GMP. The resulting particles can then enter the cells through endocytosis and subsequently release oxaliplatin and GMP to disrupt DNA replication. The synthesis of NCPs has been scaled up to hundreds of milligrams and each batch showed consistent prodrug loading, morphology, size, zeta potentials, and pharmacokinetic properties.

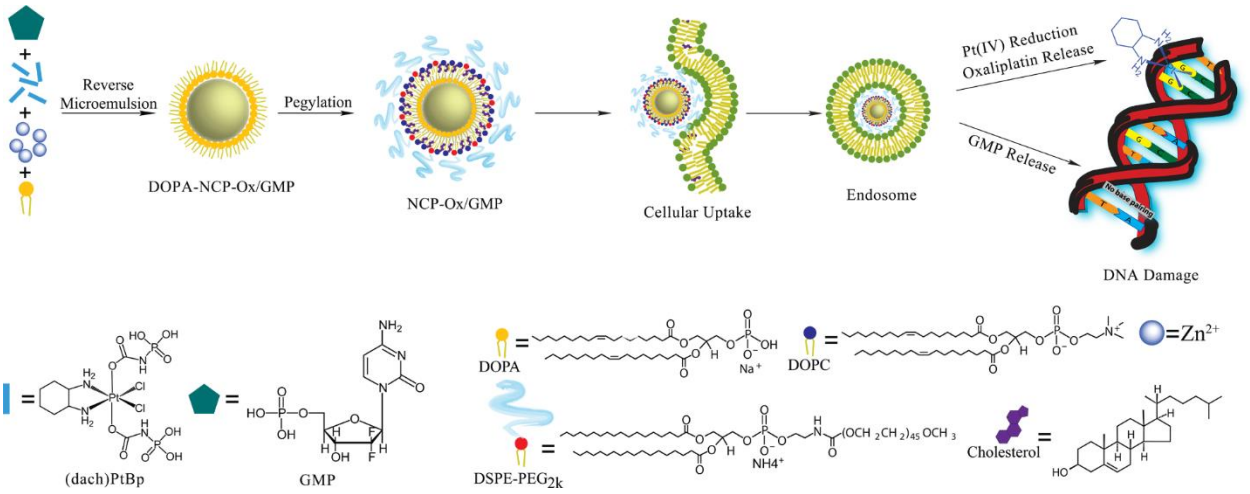

Figure 2.3. Schematic representation of the synthesis, composition, and mechanism of NCP-Ox/GMP showing the endocytosis of NCP-Ox/GMP to release oxaliplatin and GMP and the mechanisms by which oxaliplatin and GMP disrupt DNA replication. Reprinted with permission from Journal of Controlled Release, 2015, *201*, 90-99. Copyright 2016 Elsevier.

2.3.2 Characterization of NCP Particles:

As shown in Figure 2.4, TEM images of DOPA-NCP-Ox/GMP and NCP-Ox/GMP showed well-dispersed, spherical nanoparticles of 26.4 ± 3.4 and 29.9 ± 1.7 nm in diameter, respectively. The average sizes of DOPA-NCP-Ox/GMP and NCP-Ox/GMP are 39.7 ± 0.8 and 49.5 ± 0.6 nm

in diameter, respectively, as determined by DLS (Table 2.1, Figure 2.5). The polydispersity indexes (PDI) for the two particles were 0.032 and 0.062, respectively. NCP-Ox/GMP has a near neutral zeta potential, indicating that PEG chains shield the nanoparticle surface charge, allowing NCP-Ox/GMP to resist opsonization and evade the mononuclear phagocytic system (MPS).

Table 2.1 Sizes, Polydispersities, and Zeta Potentials of NCP and Zn Control Particles.

NCPs	Number-Ave diameter (nm)	PDI	Zeta Potential (mV)
DOPA-NCP-**Ox/GMP**	39.7±0.8	0.032	NA
NCP-**Ox/GMP**	49.5±0.6	0.062	-1.3±0.2
DOPA-NCP-**Ox**	28.7±9.2	0.151	NA
NCP-**Ox**	56.7±6.1	0.130	-1.0±0.6
DOPA-NCP-**GMP**	64.4±0.8	0.058	NA
NCP-**GMP**	97.3±8.2	0.161	-6.6±0.7
DOPA-**Zn Control**	25.4±5.2	0.116	NA
Zn Control	51.6±12.2	0.179	-1.2±0.7

Measured in THF. Data are expressed as means±S.D.

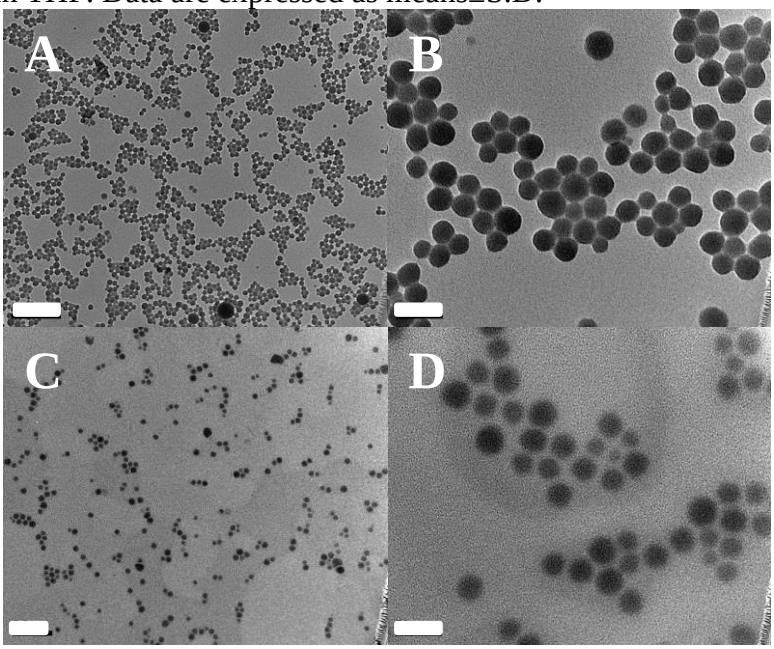

Figure 2.4. TEM micrographs of DOPA-NCP-Ox/GMP (A, B) and NCP-Ox/GMP (C, D). Scale bars represent 200 nm for A and C and 50 nm for B and D. Reprinted with permission from Journal of Controlled Release, 2015, *201*, 90-99. Copyright 2016 Elsevier.

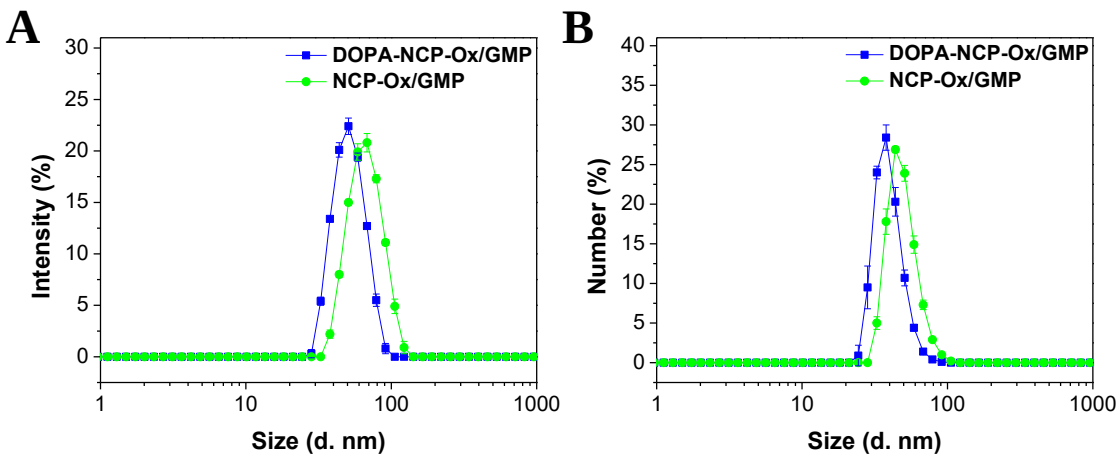

Figure 2.5. Intensity-average (A) and number-average size distribution (B) of NCP-Ox/GMP particles. Bare and PEG particles were measured in THF and PBS buffer, respectively. Reprinted with permission from Journal of Controlled Release, 2015, *201*, 90-99. Copyright 2016 Elsevier.

NCP-Ox, NCP-GMP, and Zn control particles were similarly formulated for comparison purposes. The particle diameters, PDIs, and zeta potentials of these particles are shown in Table 2.1 and Figure 2.6 through 2.11. NCP-Ox containing only dachPtBP and Zn control nanoparticles exhibited similar particle sizes of ~50 nm in diameter and near neutral zeta potential. NCP-GMP containing only GMP was also formulated and exhibited a slightly larger particle size of 97 nm.

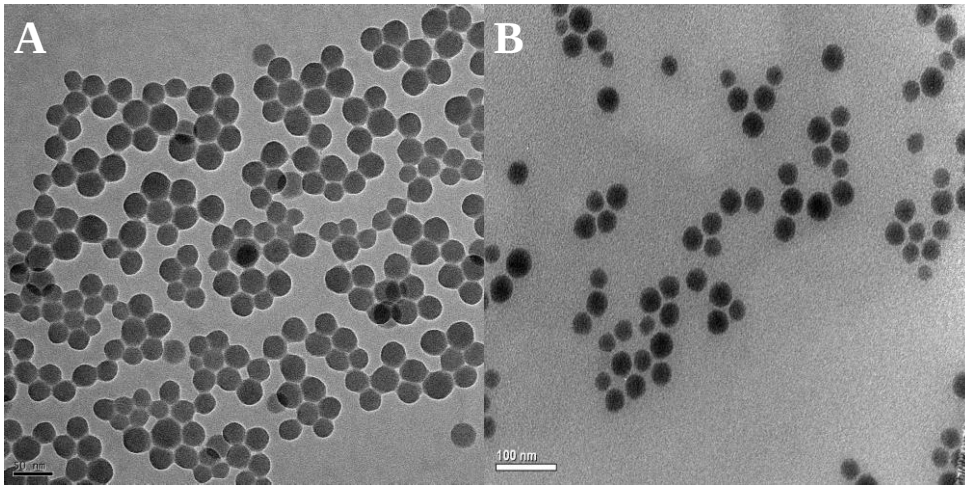

Figure 2.6. TEM micrographs of DOPA-NCP-Ox (A) and NCP-Ox (B). Reprinted with permission from Journal of Controlled Release, 2015, *201*, 90-99. Copyright 2016 Elsevier.

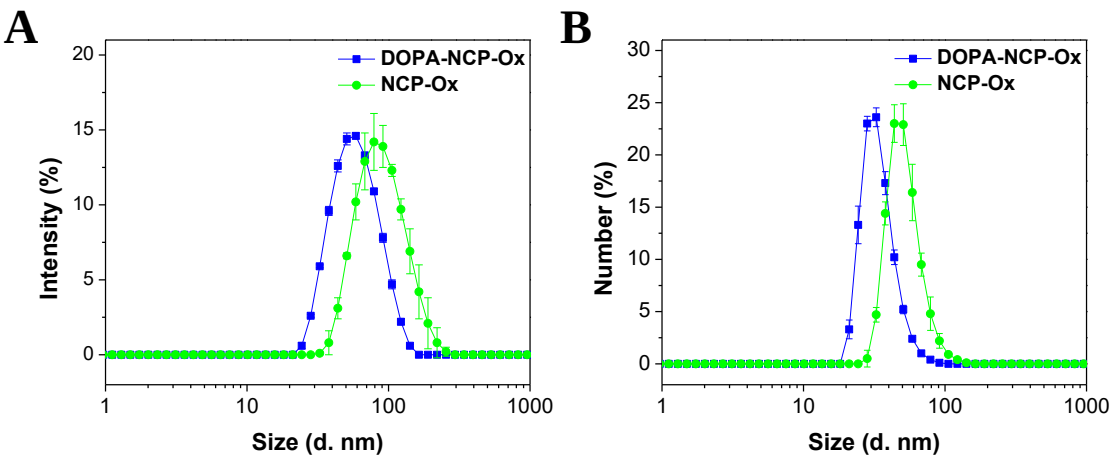

Figure 2.7. Intensity-average (A) and number-average size distribution (B) of NCP-Ox particles. Bare and PEG particles were measured in THF and PBS buffer, respectively. Reprinted with permission from Journal of Controlled Release, 2015, *201*, 90-99. Copyright 2016 Elsevier.

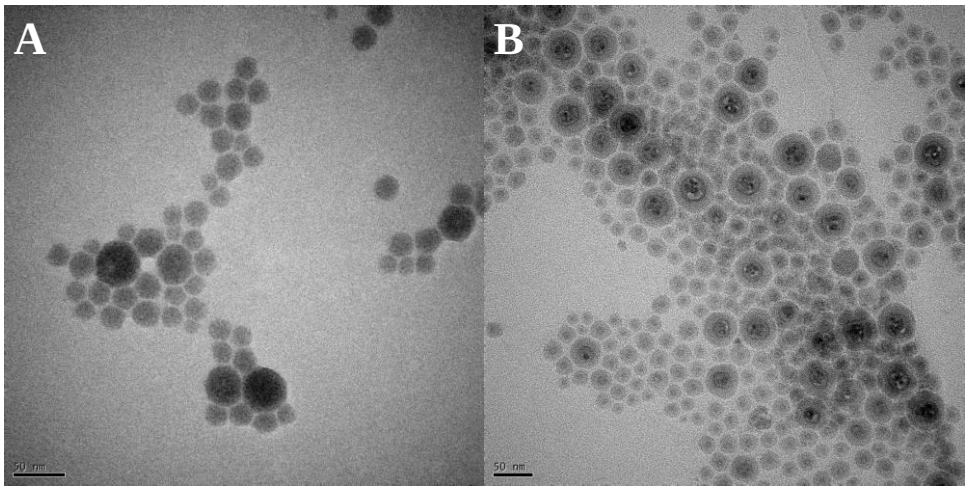

Figure 2.8. TEM micrographs of DOPA-NCP-GMP (A) and NCP-GMP (B). Reprinted with permission from Journal of Controlled Release, 2015, *201*, 90-99. Copyright 2016 Elsevier.

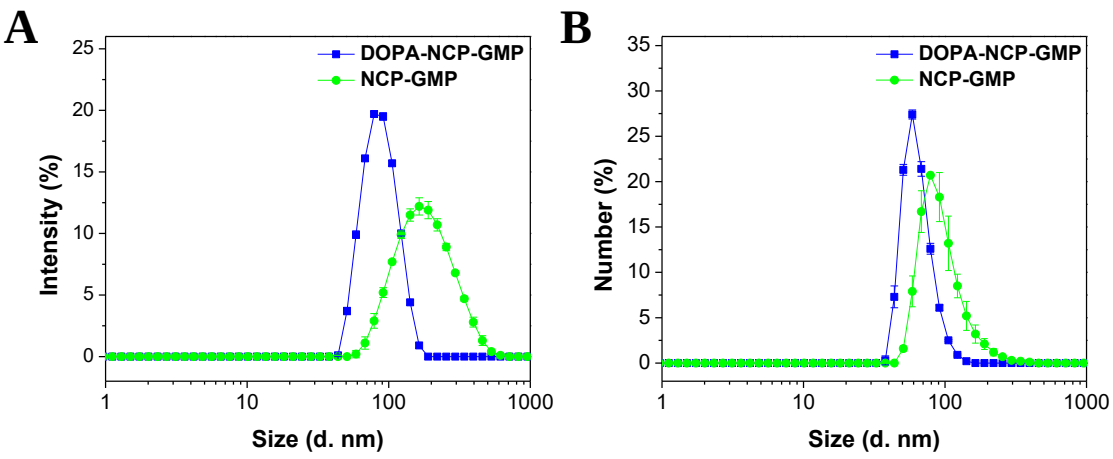

Figure 2.9. Intensity-average (A) and number-average size distribution (B) of NCP-GMP particles. Bare and PEG particles were measured in THF and PBS buffer, respectively. Reprinted with permission from Journal of Controlled Release, 2015, *201*, 90-99. Copyright 2016 Elsevier.

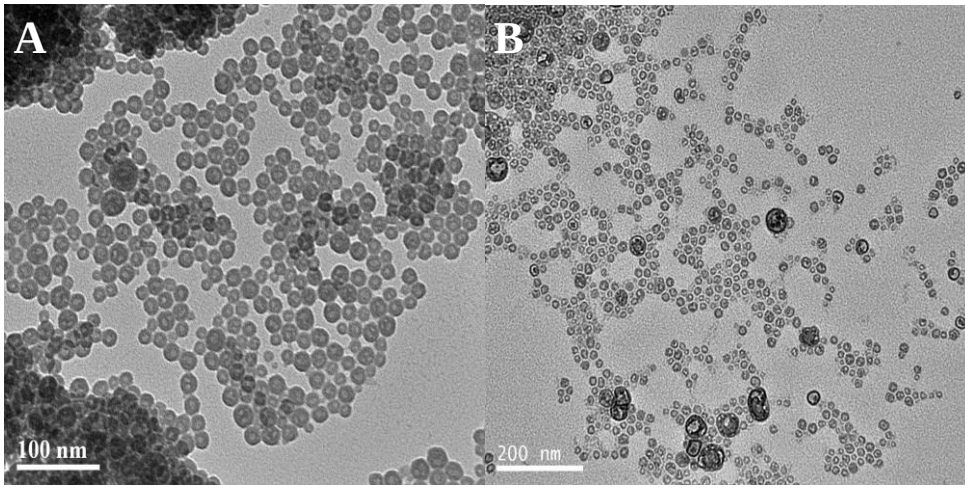

Figure 2.10. TEM micrographs of DOPA-NCP-Zn Control (A) and NCP-Zn Control (B). Reprinted with permission from Journal of Controlled Release, 2015, *201*, 90-99. Copyright 2016 Elsevier.

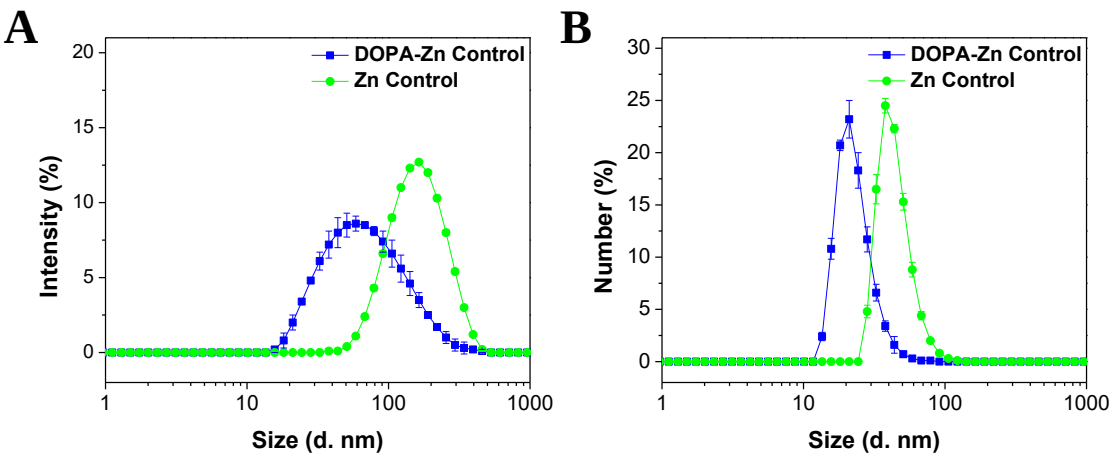

Figure 2.11. Intensity-average (A) and number-average size distribution (B) of NCP-Zn Control particles. Bare and PEG particles were measured in THF and PBS buffer, respectively. Reprinted with permission from Journal of Controlled Release, 2015, *201*, 90-99. Copyright 2016 Elsevier.

ICP-MS measurements of DOPA-NCP-Ox/GMP and DOPA-NCP-Ox gave oxaliplatin loadings of 30 ± 3 wt.% (corresponding to 50 ± 6 wt.% prodrug loading) and 25 ± 2 wt.% (corresponding to 42 ± 5 wt.% prodrug loading), respectively. UV-Vis and TGA analysis of NCP-Ox/GMP and NCP-GMP showed GMP loadings of 12 ± 2 wt.% and 57 ± 2 wt.%, respectively (Figure 2.12 and 2.13). These levels of drug loadings are exceptionally high among known nanotherapeutics. Furthermore, NCP-Ox/GMP was shown to be stable in PBS buffer in the presence of bovine serum albumin (BSA) at 37 ^{o}C (Figure 2.14).

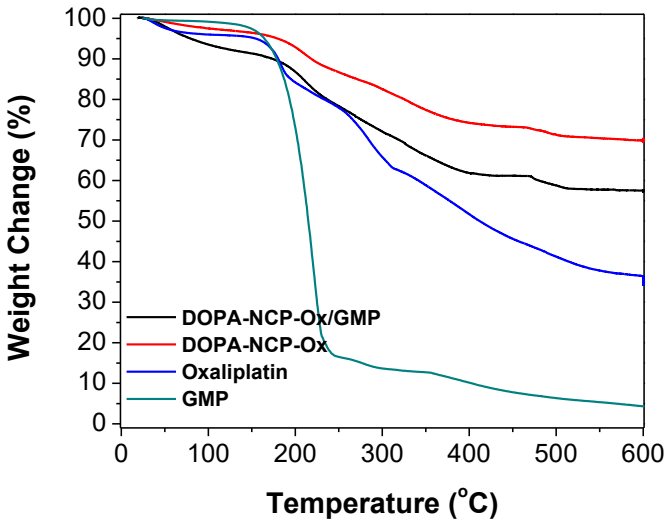

Figure 2.12. TGA analysis of DOPA-NCP-Ox/GMP to determine GMP wt% loading. Reprinted with permission from Journal of Controlled Release, 2015, *201*, 90-99. Copyright 2016 Elsevier.

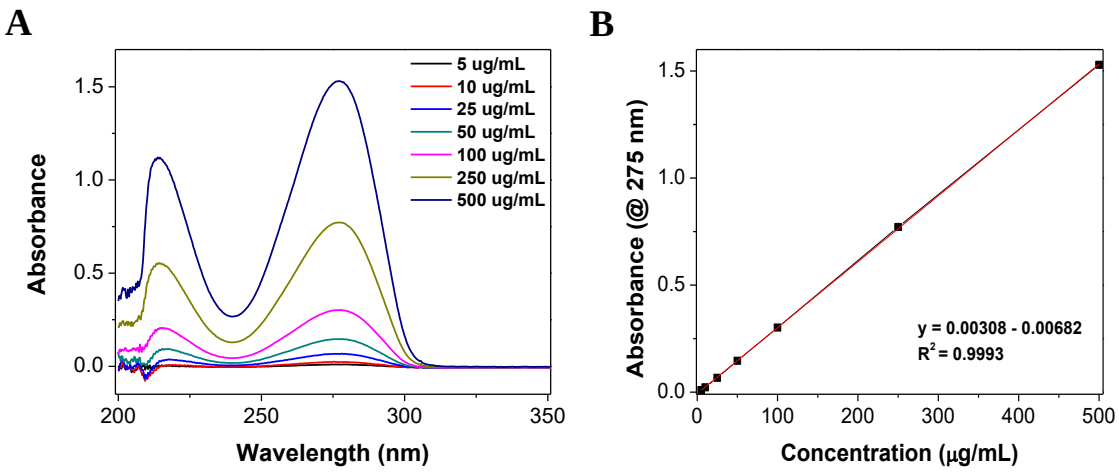

Figure 2.13. UV-Vis analysis and standard curve of DOPA-NCP-Ox/GMP to determine GMP wt% loading. Reprinted with permission from Journal of Controlled Release, 2015, *201*, 90-99. Copyright 2016 Elsevier.

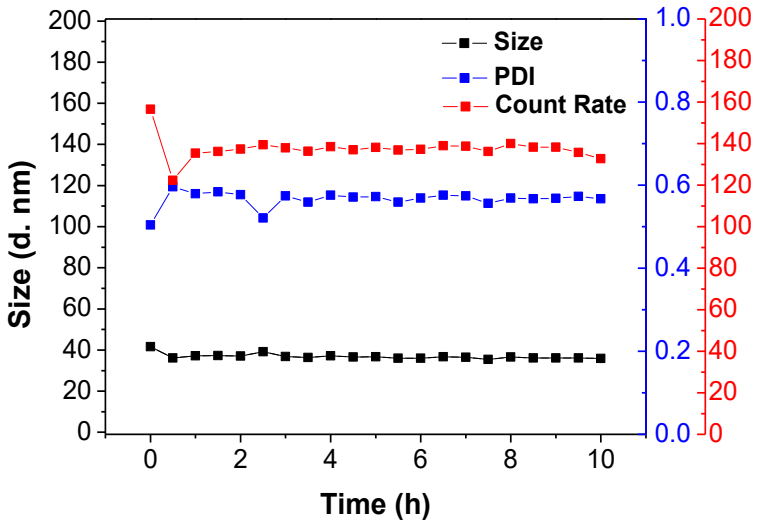

Figure 2.14. Stability test of NCP-Ox/GMP after PEGylation in PBS buffer with BSA at 37 ºC. Reprinted with permission from Journal of Controlled Release, 2015, *201*, 90-99. Copyright 2016 Elsevier.

2.3.3 In Vitro *Drug Release*

In vitro drug release of DOPA-NCP-Ox/GMP and NCP-Ox/GMP was studied in phosphate buffered saline (PBS) at 37 ºC at pH 7.4. Only about 7% of the platinum was released from NCP-Ox/GMP after 72 h, while DOPA-NCP-Ox/GMP showed a rapid burst release, with 70% of the total platinum released before 12 h (Figure 2.14A). Similarly, GMP release experiments revealed that only 21% of the GMP was released from NCP-Ox/GMP after 12 h, as opposed to DOPA-NCP-Ox/GMP, which had a GMP release of 86% after 12 h (Figure 2.14B). No initial burst release was observed for nanoparticles after pegylation, suggesting that the lipid coating strategy adopted herein prevented drug release prior to reaching the tumor sites, while stabilizing the nanoparticles in systemic circulation, prolonging circulation.

To verify the stability of NCP-Ox/GMP in a reducing environment, the drug release was also simulated in the presence of 5 mM cysteine. The results revealed that the addition of 5 mM cysteine triggered a faster drug release of DOPA-NCP-Ox/GMP with 95% of the platinum and

96% of the GMP released after 12 h, suggesting that the NCPs rapidly underwent reductive degradation to release the drugs. However, NCP-Ox/GMP exhibited a similar drug release pattern in 5 mM PBS and 5 mM PBS supplemented with 5 mM cysteine. PEGylation of the particles made it difficult for cysteine to penetrate the lipid layer, improving the stability of the particle in blood circulation. On the other hand, once the NCP-Ox/GMP particles enter cancer cells via endocytosis, some of the lipid coatings may be incorporated into the cell and plasma membranes, making the particle coatings more permeable to cysteine or other endogenous reducing agents, resulting in rapid drug release via reductive degradation of the particles.

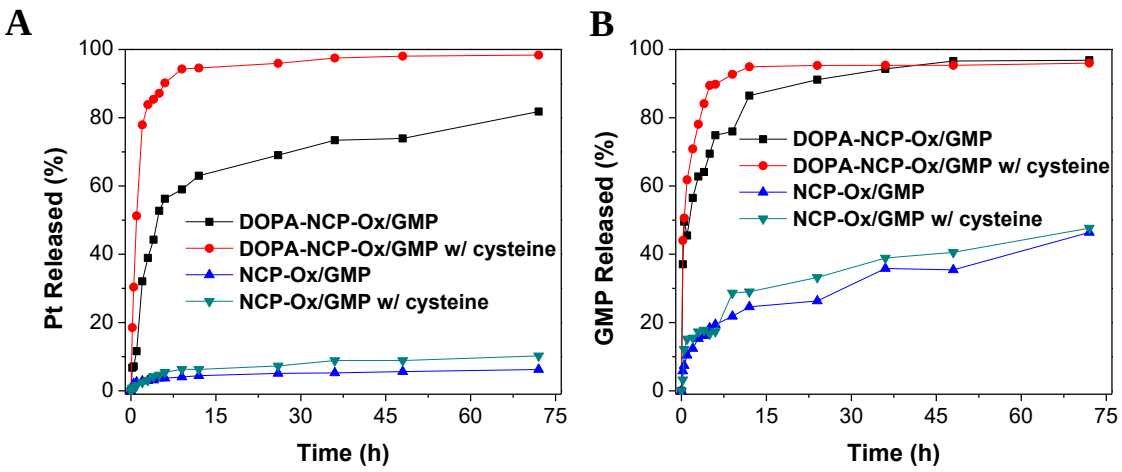

Figure 2.15. Pt (A) and GMP (B) release profiles of DOPA-NCP-Ox/GMP and NCP-Ox/GMP in 5 mM PBS buffer at 37 ^{o}C. Reprinted with permission from Journal of Controlled Release, 2015, *201*, 90-99. Copyright 2016 Elsevier.

2.3.4 In Vitro *Cytotoxicity and Combination Index*

MTS assays of drug-loaded NCPs, Zn Control, and free drugs were carried out against AsPc-1 and BxPc-3 cells. After 48 h of incubation, NCP-Ox/GMP exhibited significantly enhanced anticancer efficacy against AsPc-1 (Figure 2.16A and 2.16B) and BxPc-3 (Figure 2.17A and 2.17B) cells, with IC_{50} values that are about 5-fold, 2-fold, and 4-fold lower than free

oxaliplatin, NCP-Ox, free GMP, and NCP-GMP, respectively. NCP-Ox/GMP and free combination drugs showed comparable cytotoxicity in AsPc-1 (Oxaliplatin IC_{50}=3.5 ± 0.5 μM vs. 3.6 ± 0.6 μM and GMP IC_{50}=1.4 ± 0.1 μM vs.1.4 ± 0.3 μM, respectively) and BxPc-3 (Oxaliplatin IC_{50}=4.8 ± 2.2 μM vs. 3.0 ± 0.2 μM and GMP IC_{50}=1.9 ± 0.9 μM vs. 1.2 ± 0.1 μM, respectively). The results demonstrated that the NCP-Ox/GMP carrying two chemotherapeutics significantly outperformed their platinum and GMP drug counterparts and their NCP monotherapy counterparts in terms of cytotoxicity, which could be ascribed to the synergistic effects exerted by oxaliplatin and GMP (Figure 2.16C and 2.16D, Figure 2.17C and Figure 2.17D).

When comparing the NCP-Ox/GMP and Ox&GMP mixture with their free drug and NCP counterparts, most of the CI values were below 1, indicating synergy between oxaliplatin and GMP. Due to this synergistic effect, oxaliplatin and GMP inside a single nanocarrier exhibited better efficacy than each free drug alone, as well as the single drug nanoparticle formulations over the same concentrations. The synergistic effect between oxaliplatin and GMP in NCP-Ox/GMP can be explained by their different mechanisms of action, which lead to much greater anticancer efficacy against pancreatic tumor models than monotherapy NCPs. We have shown here and previously[33] that NCP-Ox has a tumor-inhibiting effect on PDAC. Oxaliplatin exerts its effect by forming a DNA adduct that interferes with DNA replication.[40,41] However, only 5-10% of platin complex binds covalently to DNA, while 75-85% of the drug binds to proteins.[42,43] Furthermore, tumor cells develop acquired platinum resistance, primarily from high expression levels of resistance genes.[44] Likewise, gem resistance can disrupt signaling pathways during cell apoptosis.[45] GTP works differently from oxaliplatin because it induces apoptosis by replacing cytidine during DNA replication. Combining oxaliplatin and GMP in a single nanocarrier thus

brings together the benefits of each therapy, while overcoming the toxicities of platinum or gem alone because they can act effectively at reduced doses.

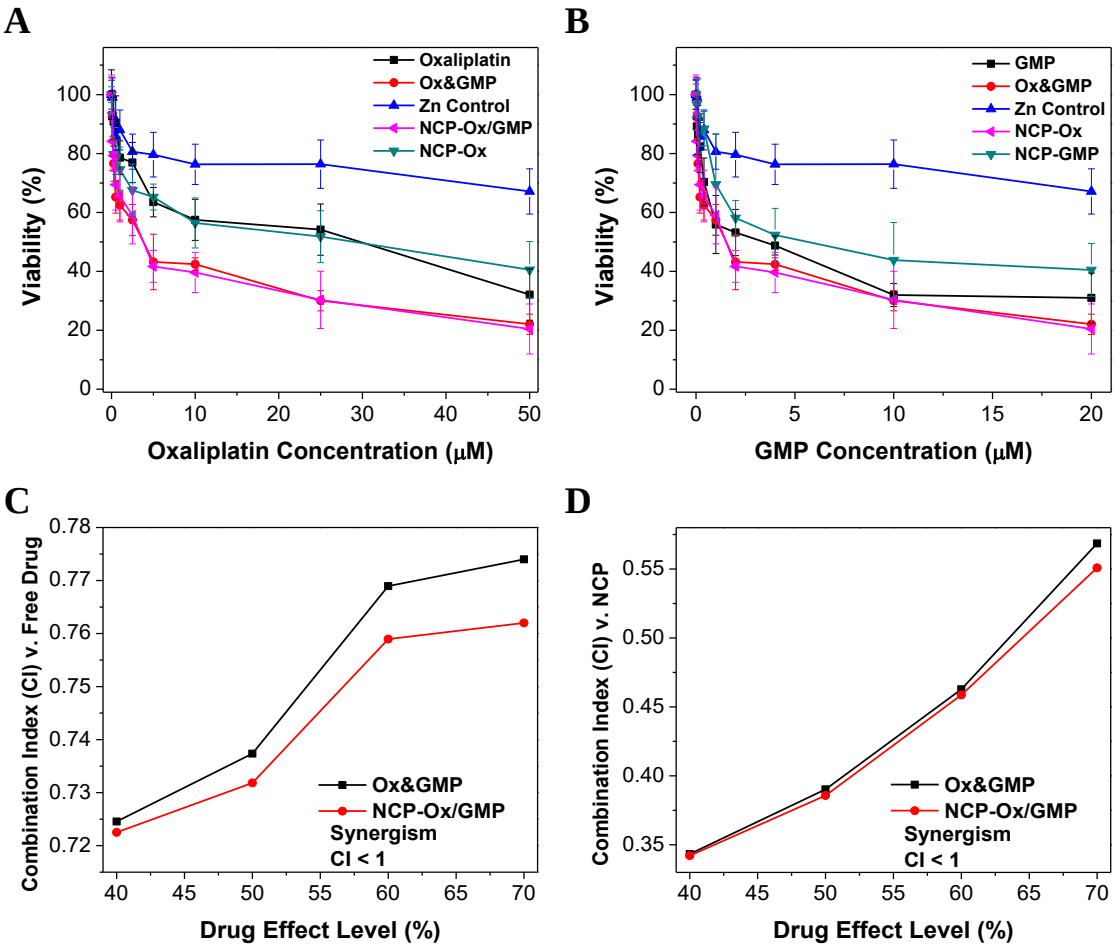

Figure 2.16. *In vitro* cytotoxicity plots and combination index (CI) of oxaliplatin and GMP combinations on AsPc-1 cells. The cell viabilities on AsPc-1 cells were measured after 48 h exposure to Zn Control, NCP-Ox/GMP, NCP-Ox, or free drugs (oxaliplatin, GMP, or Ox&GMP). Data are mean ± S.D. (n=6). Reprinted with permission from Journal of Controlled Release, 2015, *201*, 90-99. Copyright 2016 Elsevier.

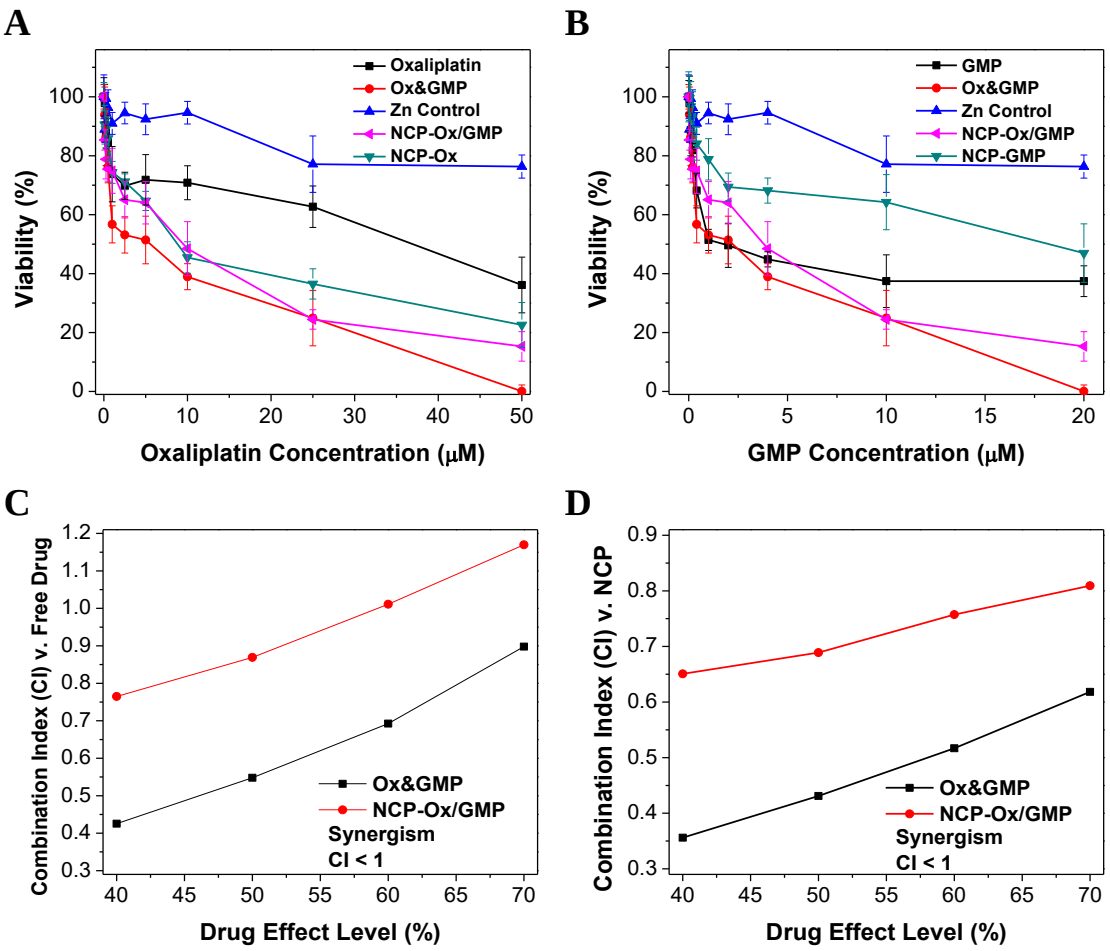

Figure 2.17. *In vitro* cytotoxicity plots and combination index (CI) of oxaliplatin and GMP combinations on BxPc-3 cells. The cell viabilities on BxPc-3 cells were measured after 48 h exposure to Zn Control, NCP-Ox/GMP, NCP-Ox, or free drugs (oxaliplatin, GMP, or Ox&GMP). Data are mean ± S.D. (n=6). Reprinted with permission from Journal of Controlled Release, 2015, *201*, 90-99. Copyright 2016 Elsevier.

Table 2.2 Oxaliplatin IC_{50} Values of Oxaliplatin, GMP, Ox&GMP, NCP-Ox/GMP, NCP-Ox, and NCP-GMP Against AsPc-1 and BxPc-3 Cells (the numbers in parenthesis refer to GMP concentrations).

	Oxaliplatin (μM)	GMP (μM)	Ox&GMP (μM)	Zn Control* (μM)	NCP-Ox/GMP (μM)	NCP-Ox (μM)	NCP-GMP (μM)
AsPc-1	18.1±2.1	(2.6±0.4)	3.6±0.6 (1.4±0.3)	>50 (>20)	3.5±0.5 (1.4±0.1)	22.4±1.4	(6.1±4.1)
BxPc-3	29.0±7.1	(2.7±2.1)	3.0±0.2 (1.2±0.1)	>50 (>20)	4.8±2.2 (1.9±0.9)	7.8±2.5	(25.8±6.3)

*Zn Control does not contain oxaliplatin or GMP as they are used to study the toxicity of NCP excipients. The amount of Zn Control particle was the same as NCP-Ox/GMP under the studied concentrations. Data are expressed as means±S.D.

2.3.5 Intracellular Uptake and Cell Apoptosis In Vitro

Dye-doped particles of NCPs were synthesized by incorporating chlorin-6 into the particles for confocal imaging studies. The bare and lipid-coated Ce6-NCP particles showed similar morphologies as well as particle sizes and distributions (Table 2.3 and Figure 2.18-20). The Ce6 loading was determined to be 0.42 wt.% by fluorimetry. Cellular uptake and intracellular drug release behaviors were observed by CLSM. AsPc-1 (Figure 2.21) or BxPc-3 (Figure 2.22) cells were incubated with free oxaliplatin, GMP, Ox&GMP, Zn Control, NCP-Ox/GMP, NCP-Ox, or NCP-GMP for 48 h. Internalization of the nanoparticles was observed, as shown by strong Ce6 fluorescence found in the cells. Significant FITC-Annexin V signals were found for both AsPc-1 and BxPc-3 cells incubated with Ox&GMP and Ce6-NCP-Ox/GMP, indicating the combination of oxaliplatin and GMP drugs induced substantial cell apoptosis. In comparison, Zn Control showed no cytotoxicity, which was supported by the absence of apoptosis marker in CLSM imaging.

Table 2.3. Sizes, Polydispersities, and Zeta Potentials of Ce6-NCP Particles.

NCPs	Number-Ave diameter (nm)	PDI	Zeta Potential (mV)
DOPA-Ce6-NCP-**Ox/GMP**	58.2±1.8[#]	0.089	NA
Ce6-NCP-**Ox/GMP**	66.9±4.6[$]	0.107	-5.2±1.0
DOPA-Ce6-NCP-**Ox**	40.0±2.3[#]	0.073	NA
Ce6-NCP-**Ox**	50.2±0.8[$]	0.086	-1.0±0.6
DOPA-Ce6-NCP-**GMP**	31.4±1.2[#]	0.174	NA
Ce6-NCP-**GMP**	152.1±7.2[$]	0.159	-3.4±0.3

[#]Measured in THF. [$]Measured in PBS buffer. Data are expressed as means±S.D.

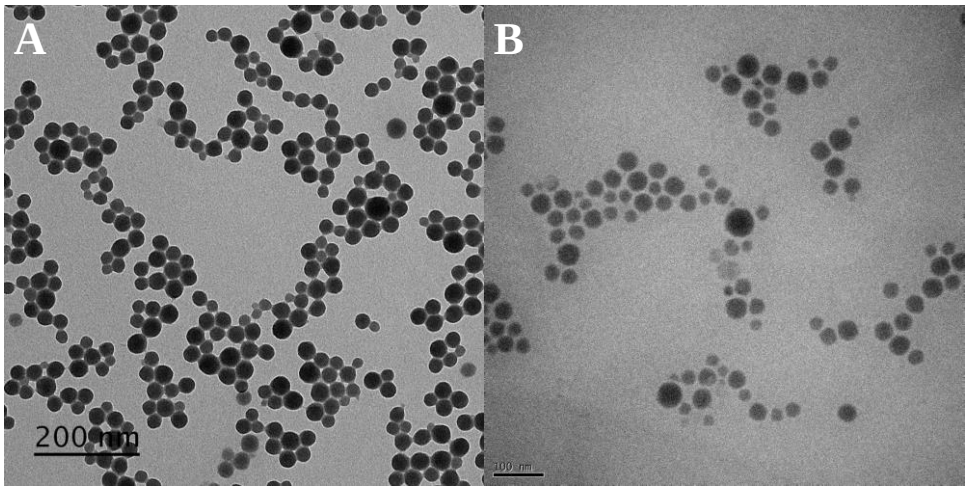

Figure 2.18. TEM micrographs of DOPA-Ce6-NCP-Ox/GMP (A) and NCP-Ce6-Ox/GMP (B). Reprinted with permission from Journal of Controlled Release, 2015, *201*, 90-99. Copyright 2016 Elsevier.

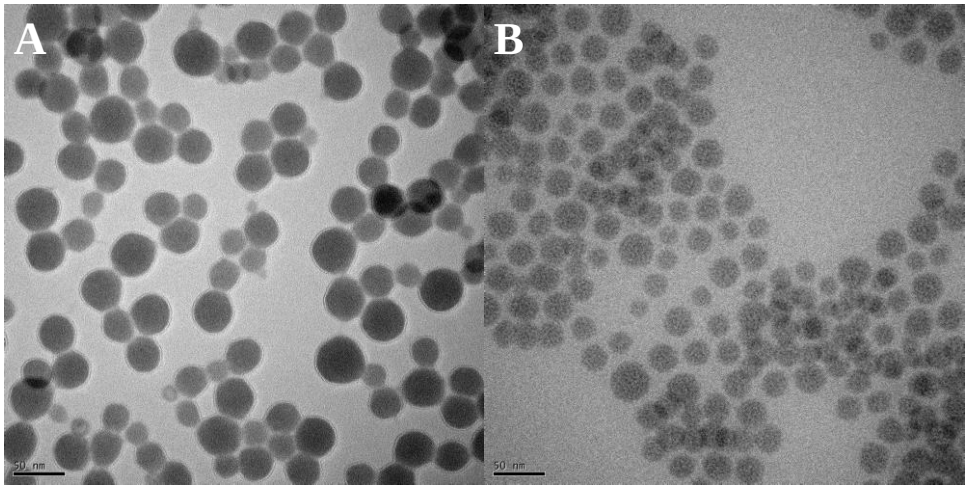

Figure 2.19. TEM micrographs of DOPA-Ce6-NCP-Ox (A) and Ce6-NCP-Ox (B).

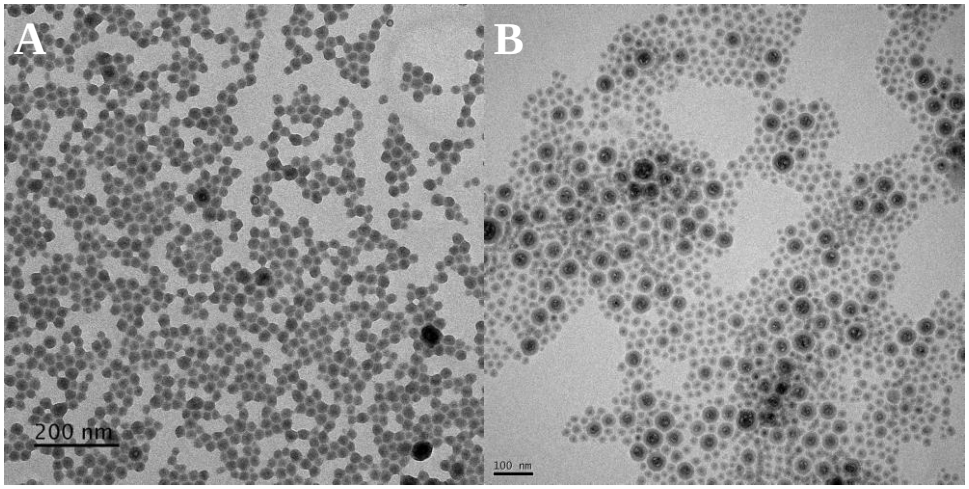

Figure 2.20. TEM micrographs of DOPA-Ce6-NCP-GMP (A) and Ce6-NCP-GMP (B). Reprinted with permission from Journal of Controlled Release, 2015, *201*, 90-99. Copyright 2016 Elsevier.

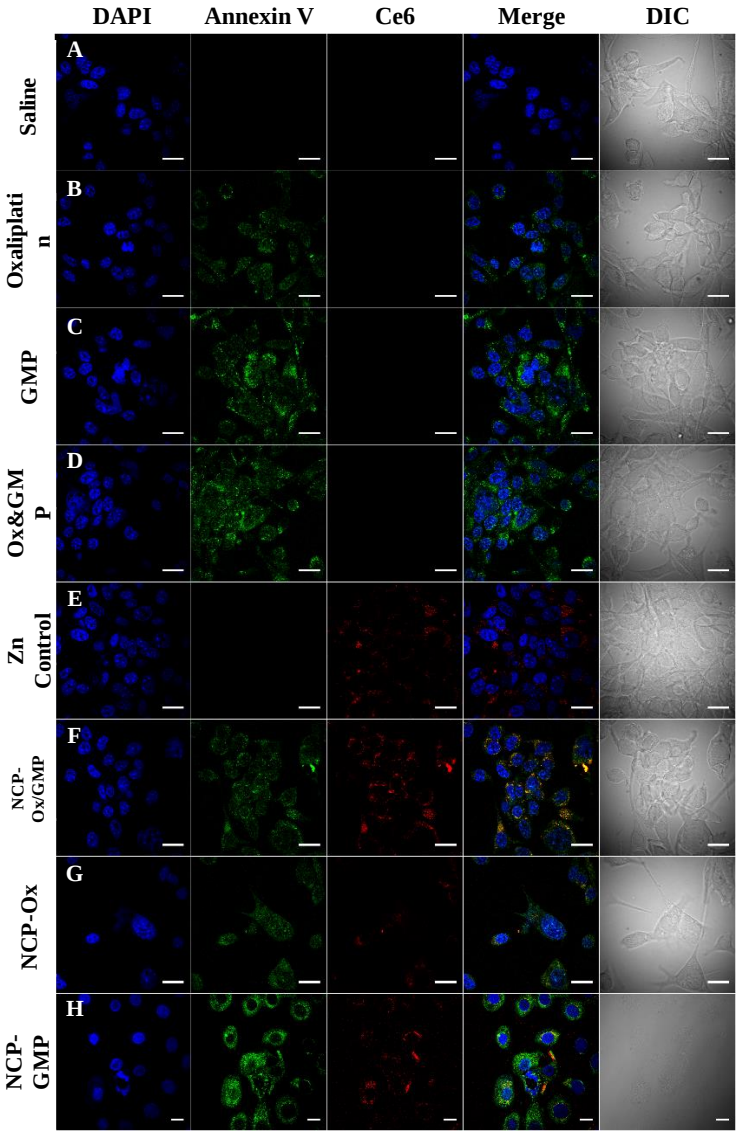

Figure 2.21. CLSM images showing the apoptosis induced by saline (A), oxaliplatin (B), GMP (C), Ox&GMP (D), Ce6-Zn Control (E), Ce6-NCP-Ox/GMP (F), Ce6-NCP-Ox (G), and Ce6-NCP-GMP (H) in AsPc-1 pancreatic cancer cells. First column represents DAPI-stained nucleus. Second column represents annexin-5 stained cells. Third column presents Ce6 labeled particles (only presence in NCP particles). Fourth column is the merged images. Fifth column is the DIC. Bar = 20 μm. Reprinted with permission from Journal of Controlled Release, 2015, *201*, 90-99. Copyright 2016 Elsevier.

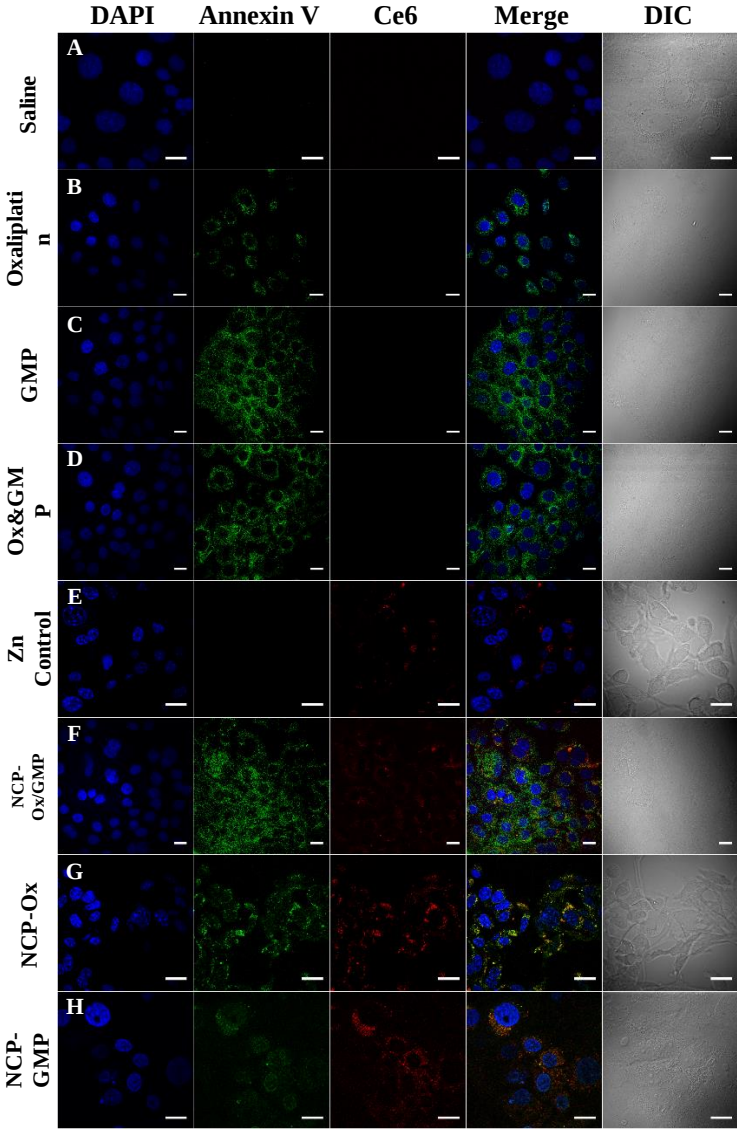

Figure 2.22. CLSM images showing the apoptosis induced by saline (A), oxaliplatin (B), GMP (C), Ox&GMP (D), Ce6-Zn Control (E), Ce6-NCP-Ox/GMP (F), Ce6-NCP-Ox (G), and Ce6-NCP-GMP (H) in BxPc-3 pancreatic cancer cells. First column represents DAPI-stained nucleus. Second column represents annexin-5 stained cells. Third column presents Ce6 labeled particles (only presence in NCP particles). Fourth column is the merged images. Fifth column is the DIC. Bar = 20 μm. Reprinted with permission from Journal of Controlled Release, 2015, *201*, 90-99. Copyright 2016 Elsevier.

Flow cytometry analysis showed increased percentages of early and late apoptosis for Ox&GMP and NCP-Ox/GMP for AsPc-1 (Figure 2.23) and BxPc-3 cells (Figure 2.24). Ox&GMP

induced 63.7% and 50.6% apoptosis for AsPc-1 and BxPc-3 cells, respectively, whereas NCP-Ox/GMP induced 74.6% and 78.6% apoptosis for BxPc-3 cells, respectively. In comparison, oxaliplatin, GMP, and their corresponding monotherapy NCPs showed inferior cytotoxicity, as shown by confocal microscopy imaging and flow cytometry analysis (Figure 2.22 and Figure 2.23). Apoptotic cell percentages for oxaliplatin, GMP, NCP-Ox, and NCP-GMP were determined to be 52.9%, 55.9%, 60.8%, and 54.2%, respectively, for AsPc-1 cells. Oxaliplatin, GMP, NCP-Ox, and NCP-GMP induced 1.5%, 32.3%, 30.2%, and 35.1% apoptosis for BxPc-3 cells, respectively. These results showed an efficient intracellular uptake of NCPs and triggered release of both oxaliplatin and/or GMP from the nanoparticles to lead to high anticancer efficacy.

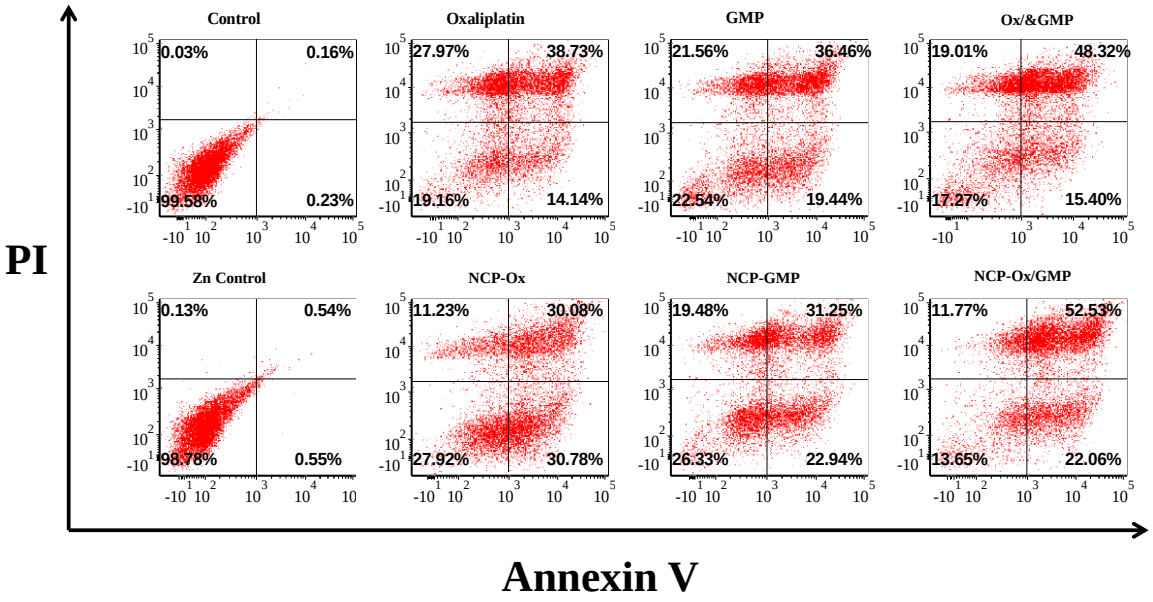

Figure 2.23. Flow cytometry analysis of saline, oxaliplatin, GMP, Ox&GMP, Zn Control, NCP-Ox/GMP, NCP-Ox, and NCP-GMP in AsPc-1 pancreatic cancer cells. Reprinted with permission from Journal of Controlled Release, 2015, *201*, 90-99. Copyright 2016 Elsevier.

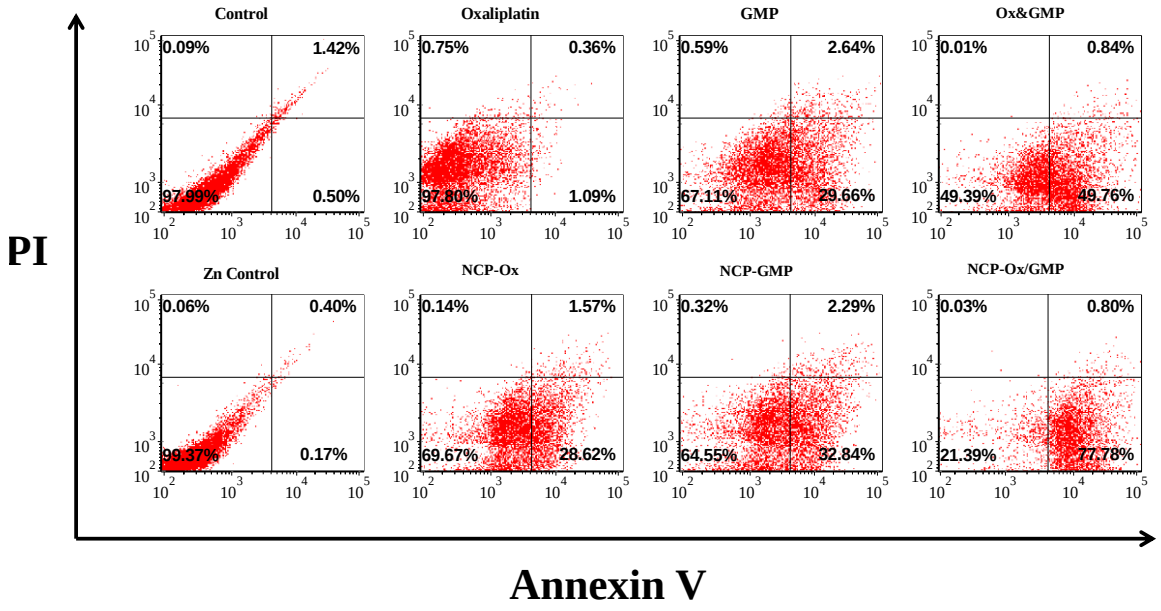

Figure 2.24. Flow cytometry analysis of saline, oxaliplatin, GMP, Ox&GMP, Zn Control, NCP-Ox/GMP, NCP-Ox, and NCP-GMP in BxPc-3 pancreatic cancer cells. Reprinted with permission from Journal of Controlled Release, 2015, *201*, 90-99. Copyright 2016 Elsevier.

2.3.6 Pharmacokinetic Studies

We examined the biodistribution of NCP-Ox/GMP on CT26-tumor-bearing mice in order to assess its ability to evade the MPS and to accumulate in tumor tissues (Figure 2.25). NCP-Ox/GMP showed prolonged blood circulation, with Pt and GMP blood circulation half-lives of 10.1±3.3 h and 8.0±2.3 h, respectively, after intravenous injection (Table 2.4). This blood circulation half-life is more than 1000-fold longer than the reported value of the oxaliplatin prodrug, which is rapidly cleared from blood circulation with an α-half-life of 0.01±0.004 h.[46] NCP-Ox/GMP showed a comparable blood circulation half-life to that of NCP-Ox ($t_{1/2}$=12.0±3.9 h).[33] The tumor uptake of NCP-Ox/GMP reached 8.8 ± 2.0% ID/g (percentage injected dose per gram) after 24 h (Fig. 4A), which is six times higher than that measured in oxaliplatin in the literature.[47] Very low Pt concentrations were observed in other organs, such as the liver, spleen, and kidney (Figure 2.25A). All of these results indicate that NCP-Ox/GMP has the ability to evade

the MPS system, leading to prolonged circulation time and enhanced tumor uptake over small molecule therapeutics, presumably due to the enhanced permeability and retention (EPR) effect.[48,49] Since NCP-Ox/GMP particles are smaller than 50 nm, they can readily accumulate in tumors because of their misaligned and defective vasculatures, as well as by taking advantage of their poor lymphatic drainage. We believe dense PEG layer on NCP-Ox/GMP allows the particles to evade the MPS system, which is supported by the low Pt concentrations observed in organs with high MPS activity such as the liver, spleen, and kidney.

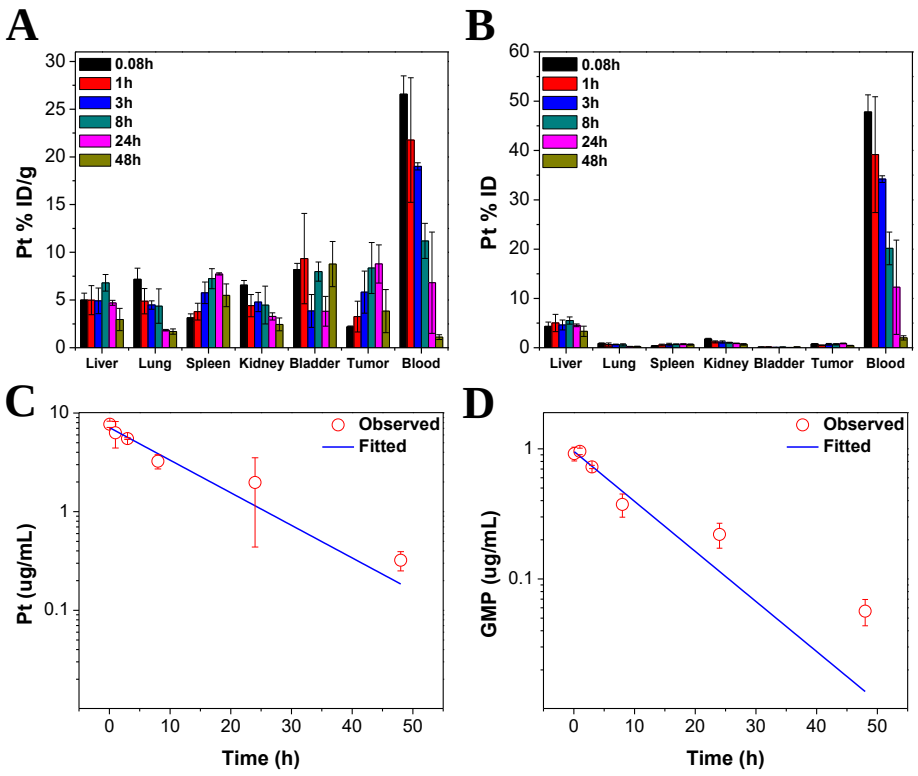

Figure 2.25. (A) Percentage injected dose per gram (% ID/g) and (B) percentage injected dose (% ID) of Pt in tissues and blood after intravenous administration of NCP-Ox/GMP in CT26 tumor-bearing mice at time points 5 min, 1 h, 3 h, 8 h, 24 h, and 48 h. Data are mean ± S.D. (n=3). (C) Average observed and predicted time-dependent Pt distributions in blood after administration of NCP-Ox/GMP (n=3). (D) Average observed and predicted time-dependent GMP distributions in blood after administration of NCP-Ox/GMP (n=3). One-compartment model was used for fitting the Pt and GMP distributions in blood. Reprinted with permission from Journal of Controlled Release, 2015, *201*, 90-99. Copyright 2016 Elsevier.

Table 2.4. Pharmacokinetic Parameters of Pt Distribution for NCP-Ox/GMP in CT26 Bearing Nude Mice*.

C_0 (μg/mL)	k_0 (1/h)	V_{ss} (mg/kg/(μg/mL))	CL ((mg/kg)/(μg/mL)/h)	AUC (μg/mL×h)	MRT (h)	$t_{1/2}$ (h)
7.1±1.0	0.075±0.028	0.428±0.061	0.031±0.008	96.1±23.9	14.5±4.8	10.1±3.3

*C_o, blood concentration at time=0; k_o, elimination rate constant; V_{ss}, volume of distribution at steady state; CL, systemic clearance; AUC, total area under curve; MRT, mean resident time; $t_{1/2}$, the time required to reduce the plasma concentration to one half its initial value

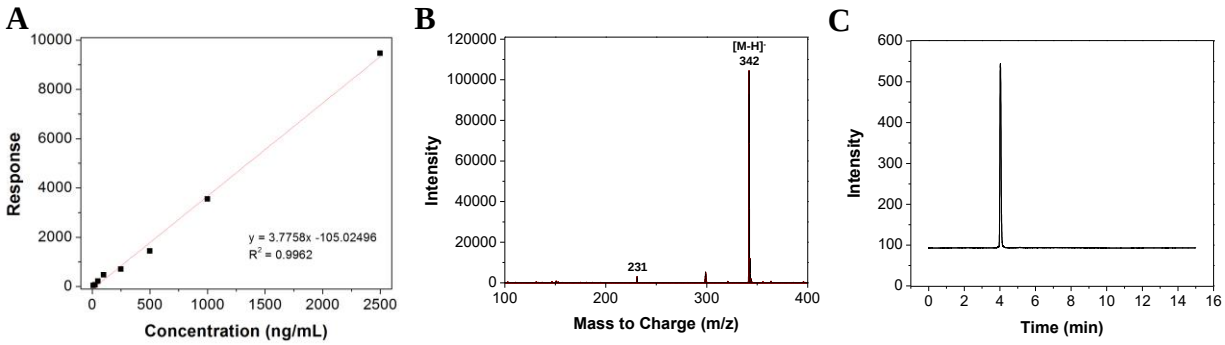

Figure 2.26. (A) Standard curve for the determination of GMP in blood using LC-MS. (B) Product ion and deprotonated parent ion MS/MS spectrum of GMP at m/z 341.9. (C) Chromatograms of GMP at 5 min in blood (retention time = 4.1 min)(m/z transition from 342 to 231). Reprinted with permission from Journal of Controlled Release, 2015, *201*, 90-99. Copyright 2016 Elsevier.

2.3.7 Tumor Growth Inhibition Studies

To determine whether NCP-Ox/GMP possesses synergistic efficacy for pancreatic cancers *in vivo*, tumor growth inhibition was evaluated in BxPc-3 and AsPc-1 subcutaneous xenograft murine models. For mice bearing BxPc-3 tumors, free oxaliplatin/gem (5 mg oxaliplatin/kg, 50 mg gem/kg dose) and NCP-GMP (0.8 mg/kg dose) did not show statistically significant antitumor efficacy. Though tumor growth was more inhibited by NCP-Ox (2 mg/kg dose) as compared to the control (p=0.0085), NCP-Ox/GMP, at a dose of of 2 mg/kg for oxaliplatin and 0.8 mg/kg GMP, showed the most potent anticancer efficacy in BxPc-3 models (Figure 2.27A). Tumor growth was dramatically inhibited in the NCP-Ox/GMP group in comparison to the monotherapy NCP groups (p=0.0319 vs. NCP-Ox and p=0.0030 vs. NCP-GMP): growth in NCP-Ox/GMP was effectively

suppressed, with the average tumor size increasing 1.7-fold, in comparison to the increase of 3.6~14.3-folds in other groups. Tumor weight of NCP-Ox/GMP was also significantly reduced compared with those of other treatment groups; the average tumor weight in the NCP-Ox/GMP group is more than 11-fold smaller than that of the PBS control group (p=0.0002) (Figure 2.27C). Moreover, the average tumor weight of the NCP-Ox/GMP group was 2.7 times smaller than that of the NCP-Ox group (p=0.0342) and 16.6 times smaller than that of the NCP-GMP group (p=0.0031).

The mice were sacrificed 12 days post injection because the tumors in the PBS control and NCP-GMP groups had exceeded the 2000 mm^3 limit. No significant change in body weight was observed for the NCP-treated groups, indicating the safety and tolerance of the NCP vehicles (Figure 2.27B). General toxicity was further investigated by immunogenic responses (Figure 2.28) and histological assessments (Figure 2.29). No statistically significant difference was observed between the control and NCP-Ox/GMP groups in terms of proinflammatory cytokine production and Pt hypersensitivity. From the H&E-stained sectioned tissues of liver, lung, spleen, and kidney, no difference in general toxicity was observed between the control and NCP-Ox/GMP groups.

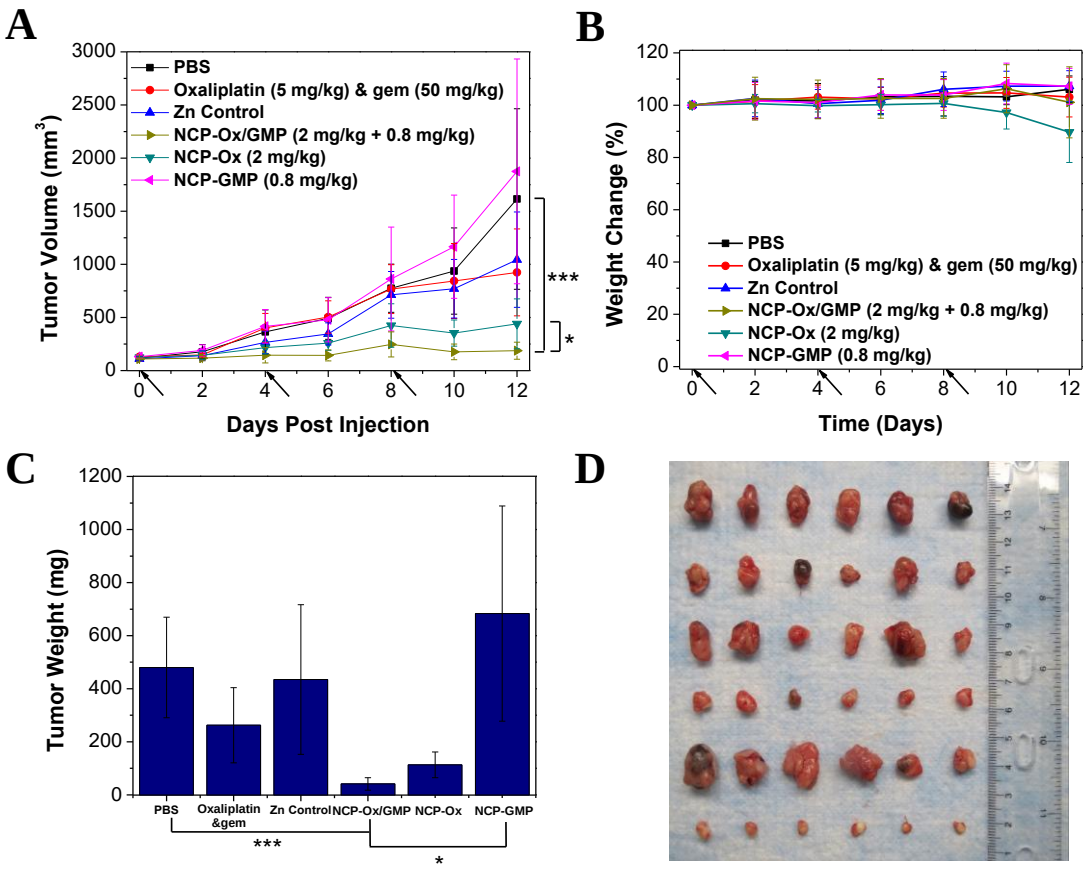

Figure 2.27. (A) *In vivo* tumor growth inhibition curves for PBS(■), oxaliplatin & gem (♦), Zn Control (▲), NCP-Ox/GMP(►), NCP-Ox (▼), and NCP-GMP (◄) on subcutaneous BxPc-3 xenografts. Oxaliplatin (dose, 5 mg/kg) and gem (dose, 50 mg/kg), NCP-Ox/GMP (doses, 2 mg/kg + 0.8 mg/kg), NCP-Ox (dose, 2 mg/kg), and NCP-GMP (dose, 0.8 mg/kg) were administered on day 0, 4, and 8. Data are expressed as means±S.D. (n=6), *p<0.05, **p<0.01, ***p<0.001. (B) Body weights of mice bearing BxPc-3 tumors over the post injection period. (C) End-point tumor weights. Data are expressed as means±S.D. (n=6), *p<0.05, **p<0.01, ***p<0.001. (D) Photos of the resected BxPc-3 tumors from top to bottom: PBS, oxaliplatin & gem, Zn Control, NCP-Ox, NCP-GMP, and NCP-Ox/GMP. Reprinted with permission from Journal of Controlled Release, 2015, *201*, 90-99. Copyright 2016 Elsevier.

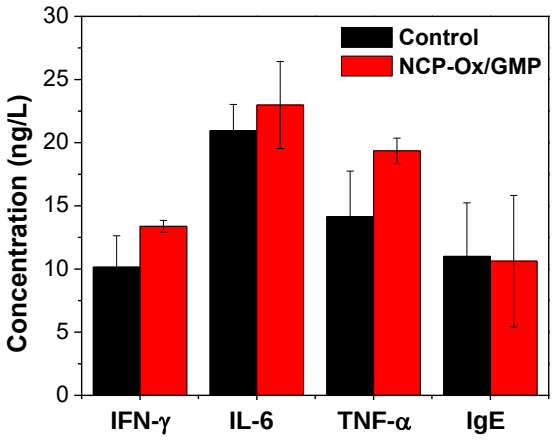

Figure 2.28. Immunogenic response and hypersensitivity of BxPc-3 tumor bearing mice treated with saline and NCP-Ox/GMP. Reprinted with permission from Journal of Controlled Release, 2015, *201*, 90-99. Copyright 2016 Elsevier.

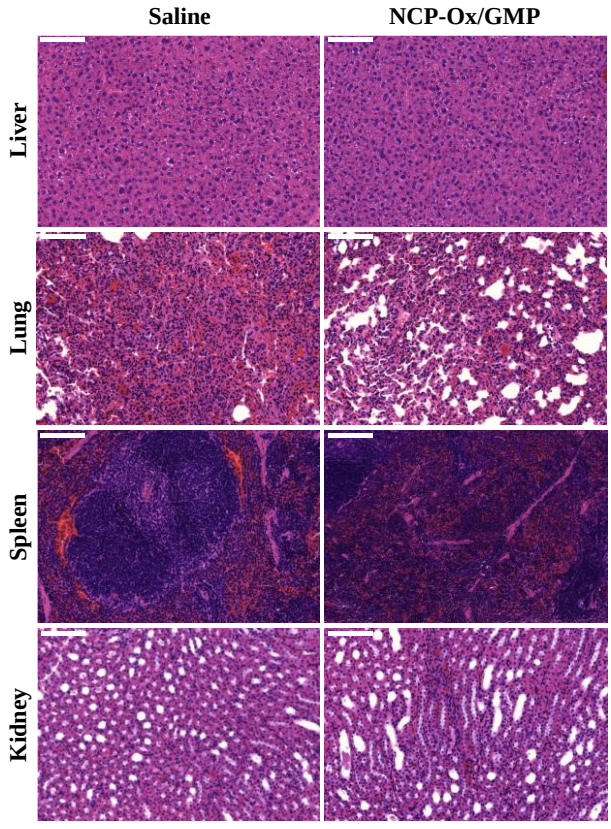

Figure 2.29. Histology images of resected organs (with H&E staining) of BxPc-3 tumor bearing mice treated with saline and NCP-Ox/GMP. Bar = 100 μm. Reprinted with permission from Journal of Controlled Release, 2015, *201*, 90-99. Copyright 2016 Elsevier.

Mice bearing AsPc-1 tumors were also intravenously injected with free oxaliplatin & gem (5 mg/kg oxaliplatin and 50 mg/kg gem) and NCP-Ox/GMP (2 mg/kg for oxaliplatin and 0.8 mg/kg for GMP) every four days for a total of five injected doses to compare their anticancer efficacy. NCP-Ox/GMP showed superior tumor growth inhibition at lower drug doses compared with the combination of free drugs (Figure 2.30A). For the NCP-Ox/GMP treatment, the tumor size 56 days post injection showed only a 3-fold increase, whereas the PBS control and free drug combination groups show nearly a 6-fold increase in tumor size (p=0.00076). Mice treated with NCP-Ox/GMP showed a slight decrease in weight during the treatment but quickly regained weight after the last injection. No adverse effects from the NCP-Ox/GMP were observed as indicated by the relatively stable body weights maintained during the experiment (Figure 2.30B).

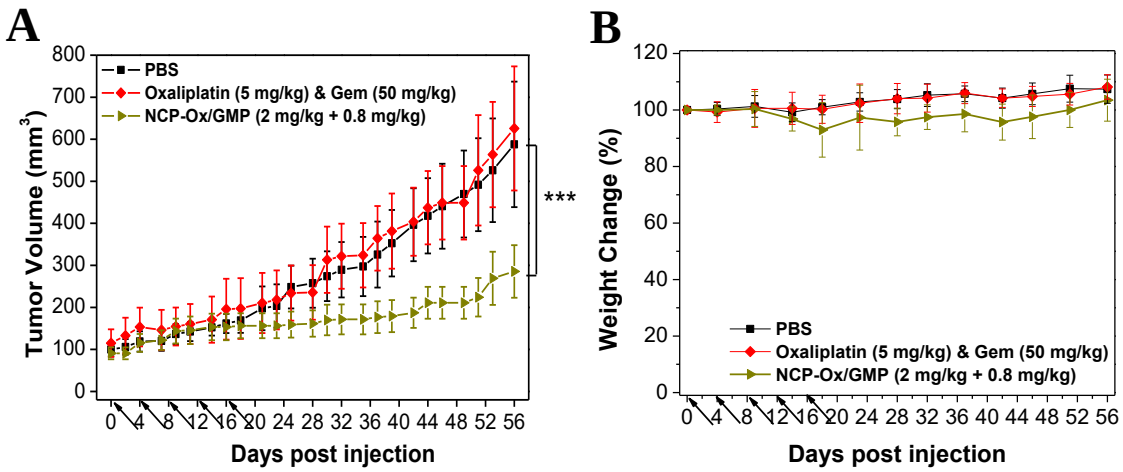

Figure 2.30. (A) *In vivo* tumor growth inhibition curves for PBS(■), oxaliplatin & gem (♦), and NCP-Ox/GMP(►) on subcutaneous AsPc-1 xenografts. Oxaliplatin (dose, 5 mg/kg) and gem (dose, 50 mg/kg) and NCP-Ox/GMP (doses, 2 mg/kg + 0.8 mg/kg) were administered on day 0, 4, 8, 12, 16, and 20. Data are expressed as means±S.D. (n=6), *p<0.05, **p<0.01, ***p<0.001. Body weights of mice bearing AsPc-1 tumors over the post injection period. Reprinted with permission from Journal of Controlled Release, 2015, *201*, 90-99. Copyright 2016 Elsevier.

The oxaliplatin and GMP combination in the NCP-Ox/GMP particle has thus not only shown synergistic effects *in vitro* but also exhibited outstanding antitumor efficacy on pancreatic

cancer cell subcutaneous xenografts *in vivo*. Even at much lower doses, NCP-Ox/GMP achieved much higher potency than free drugs, which is rare among all other existing nanotherapeutics. The high antitumor efficacy of NCP-Ox/GMP as compared to monotherapy NCPs confirmed the synergistic effects of oxaliplatin and gem in NCP-Ox/GMP *in vivo*.

2.3.8 In Vivo *Tumor Cell Apoptosis*

BxPc-3 tumors from the tumor inhibition efficacy study were sectioned for TUNEL assays to investigate cell apoptosis caused by different treatments (Figure 2.31A). NCP-Ox/GMP induced 77.8±7.5% apoptotic tumor cells, which was superior to 46.5±5.7% and 6.5±4.8% apoptotic tumor cells induced by NCP-Ox and NCP-GMP, respectively. No apoptosis was triggered by the control, Zn Control, and free oxaliplatin & gem (Figure 2.31B). The TUNEL assay results are consistent with the tumor growth inhibition results as shown in Figure 2.27. The superior anticancer potency of NCP-Ox/GMP is a result of the enhanced drug delivery to tumors and the synergistic effect of oxaliplatin and GMP. The lack of apoptosis shown in the free oxaliplatin & gem treatment group indicated that the free drugs are rapidly cleared away from the body, leading to subtherapeutic accumulation of the drugs in the tumors.

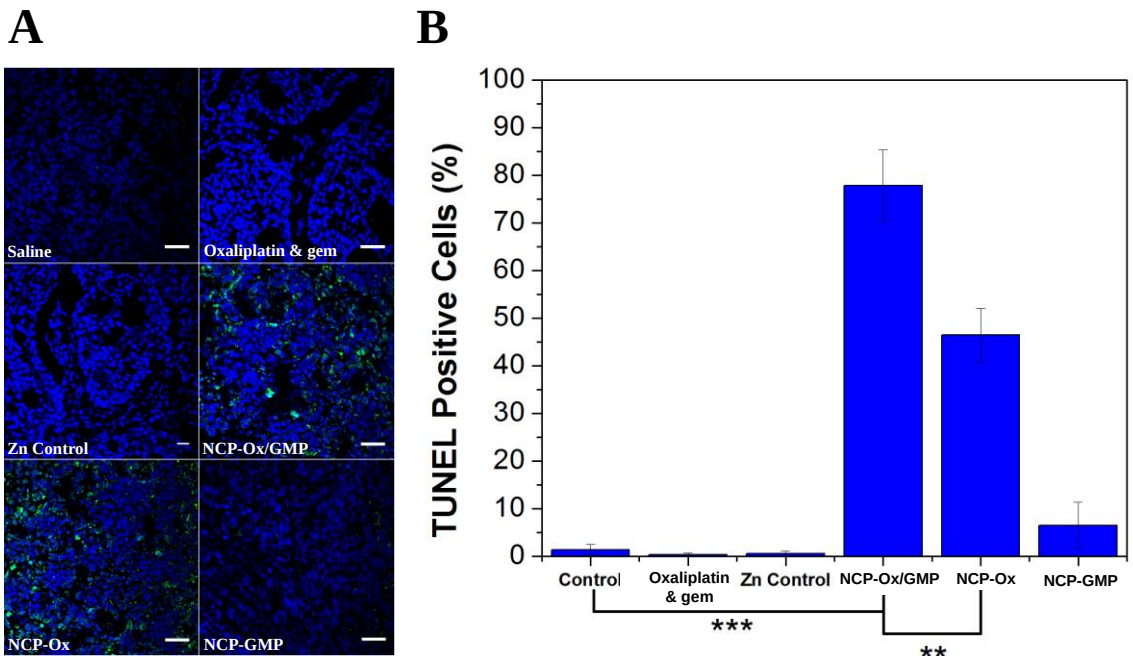

Figure 2.31. (A) Representative CLSM images of TUNEL assays of BxPc-3 tumor tissues. DNA fragment in apoptotic cells was stained with fluorescein-conjugated deoxynucleotides (green) and the nuclei were stained with DAPI (blue). Scale = 40 μm. (B) The percentages of TUNEL-positive cells in tumor tissues. Reprinted with permission from Journal of Controlled Release, 2015, *201*, 90-99. Copyright 2016 Elsevier.

2.4 Conclusion

We developed an NCP-based formulation for the co-delivery of oxaliplatin and GMP as a combination therapy for the treatment of pancreatic cancers. We showed the synergistic effect of oxaliplatin and GMP against pancreatic cancer cell lines in *in vitro* studies. The combination NCP particle, NCP-Ox/GMP, showed a long blood circulation half-life with high drug accumulation in tumors. NCP-Ox/GMP effectively inhibits tumor growth *in vivo* with far greater success than monotherapy NCPs and free combination drugs. As the combination of oxaliplatin and gem is FDA approved for the treatment of pancreatic cancer, this work highlights the potential of combination NCPs to be highly effective delivery vehicles for PDAC treatment in the clinic. The

versatility of NCPs in incorporating other combinations of drugs opens a wide range possibilities for the treatment of many challenging cancers.

2.5 References

(1) Bunt, S.; Mohr, A.; Bailey, J.; Grandgenett, P.; Hollingsworth, M. *Cancer Immunology Immunotherapy* **2013**, *62*, 225.

(2) Society, A. C. *Atlanta: American Cancer Society* **2013**.

(3) El Kamar, F. G.; Grossbard, M. L.; Kozuch, P. S. *Oncologist* **2003**, *8*, 18.

(4) Geer, R. J.; Brennan, M. F. *Am J Surg* **1993**, *165*, 68.

(5) King, R. S. *Cancer Pract* **1996**, *4*, 353.

(6) Burris, H. A., 3rd; Moore, M. J.; Andersen, J.; Green, M. R.; Rothenberg, M. L.; Modiano, M. R.; Cripps, M. C.; Portenoy, R. K.; Storniolo, A. M.; Tarassoff, P.; Nelson, R.; Dorr, F. A.; Stephens, C. D.; Von, H. D. D. *J Clin Oncol* **1997**, *15*, 2403.

(7) Hertel, L. W.; Boder, G. B.; Kroin, J. S.; Rinzel, S. M.; Poore, G. A.; Todd, G. C.; Grindey, G. B. *Cancer Res* **1990**, *50*, 4417.

(8) Mackey, J. R.; Mani, R. S.; Selner, M.; Mowles, D.; Young, J. D.; Belt, J. A.; Crawford, C. R.; Cass, C. E. *Cancer Res* **1998**, *58*, 4349.

(9) Oguri, T.; Achiwa, H.; Sato, S.; Bessho, Y.; Takano, Y.; Miyazaki, M.; Muramatsu, H.; Maeda, H.; Niimi, T.; Ueda, R. *Mol. Cancer Ther.* **2006**, *5*, 1800.

(10) Plunkett, W.; Huang, P.; Gandhi, V. *Anticancer Drugs* **1995**, *6 Suppl 6*, 7.

(11) Mackey, J. R.; Yao, S. Y.; Smith, K. M.; Karpinski, E.; Baldwin, S. A.; Cass, C. E.; Young, J. D. *J Natl Cancer Inst* **1999**, *91*, 1876.

(12) Zhou, B.-B. S.; Bartek, J. *Nature Reviews Cancer* **2004**, *4*, 216.

(13) Lehar, J.; Krueger, A. S.; Avery, W.; Heilbut, A. M.; Johansen, L. M.; Price, E. R.; Rickles, R. J.; Short, G. F., III; Staunton, J. E.; Jin, X.; Lee, M. S.; Zimmermann, G. R.; Borisy, A. A. *Nat. Biotechnol.* **2009**, *27*, 659.

(14) Saltz, L. B.; Clarke, S.; Diaz-Rubio, E.; Scheithauer, W.; Figer, A.; Wong, R.; Koski, S.; Lichinitser, M.; Yang, T.-S.; Rivera, F.; Couture, F.; Sirzen, F.; Cassidy, J. *J. Clin. Oncol.* **2008**, *26*, 2013.

(15) Herbst, R. S.; Giaccone, G.; Schiller, J. H.; Natale, R. B.; Miller, V.; Manegold, C.; Scagliotti, G.; Rosell, R.; Oliff, I.; Reeves, J. A.; Wolf, M. K.; Krebs, A. D.; Averbuch, S. D.; Ochs, J. S.; Grous, J.; Fandi, A.; Johnson, D. H. *J. Clin. Oncol.* **2004**, *22*, 785.

(16) Giaccone, G.; Herbst, R. S.; Manegold, C.; Scagliotti, G.; Rosell, R.; Miller, V.; Natale, R. B.; Schiller, J. H.; von Pawel, J.; Pluzanska, A.; Gatzemeier, U.; Grous, J.; Ochs, J. S.; Averbuch, S. D.; Wolf, M. K.; Rennie, P.; Fandi, A.; Johnson, D. H. *J. Clin. Oncol.* **2004**, *22*, 777.

(17) Conroy, T.; Desseigne, F.; Ychou, M.; Bouche, O.; Guimbaud, R.; Becouarn, Y.; Adenis, A.; Raoul, J.-L.; Gourgou-Bourgade, S.; de la Fouchardiere, C.; Bennouna, J.; Bachet, J.-B.; Khemissa-Akouz, F.; Pere-Verge, D.; Delbaldo, C.; Assenat, E.; Chauffert, B.; Michel, P.; Montoto-Grillot, C.; Ducreux, M. *N. Engl. J. Med.* **2011**, *364*, 1817.

(18) Von Hoff, D. D.; Ervin, T.; Arena, F. P.; Chiorean, E. G.; Infante, J.; Moore, M.; Seay, T.; Tjulandin, S. A.; Ma, W. W.; Saleh, M. N.; Harris, M.; Reni, M.; Dowden, S.; Laheru, D.; Bahary, N.; Ramanathan, R. K.; Tabernero, J.; Hidalgo, M.; Goldstein, D.; Van Cutsem, E.; Wei, X.; Iglesias, J.; Renschler, M. F. *N. Engl. J. Med.* **2013**, *369*, 1691.

(19) DeVita, V. T., Jr.; Young, R. C.; Canellos, G. P. *Cancer* **1975**, *35*, 98.

(20) Shah, M. A.; Schwartz, G. K. *Drug Resistance Updates* **2000**, *3*, 335.

(21) Lehar, J.; Krueger, A. S.; Avery, W.; Heilbut, A. M.; Johansen, L. M.; Price, E. R.; Rickles, R. J.; Short, G. F., 3rd; Staunton, J. E.; Jin, X.; Lee, M. S.; Zimmermann, G. R.; Borisy, A. A. *Nat Biotechnol* **2009**, *27*, 659.

(22) Mayer, L. D.; Harasym, T. O.; Tardi, P. G.; Harasym, N. L.; Shew, C. R.; Johnstone, S. A.; Ramsay, E. C.; Bally, M. B.; Janoff, A. S. *Mol. Cancer Ther.* **2006**, *5*, 1854.

(23) Ismael, G. F. V.; Rosa, D. D.; Mano, M. S.; Awada, A. *Cancer Treat. Rev.* **2008**, *34*, 81.

(24) Danhier, F.; Feron, O.; Preat, V. *J. Controlled Release* **2010**, *148*, 135.

(25) Peer, D.; Karp, J. M.; Hong, S.; Farokhzad, O. C.; Margalit, R.; Langer, R. *Nature Nanotechnology* **2007**, *2*, 751.

(26) Devalapally, H.; Chakilam, A.; Amiji, M. M. *J. Pharm. Sci.* **2007**, *96*, 2547.

(27) Haley, B.; Frenkel, E. *Urol. Oncol.: Semin. Orig. Invest.* **2008**, *26*, 57.

(28) Louvet, C.; Labianca, R.; Hammel, P.; Lledo, G.; Zampino, M. G.; Andre, T.; Zaniboni, A.; Ducreux, M.; Aitini, E.; Taieb, J.; Faroux, R.; Lepere, C.; de Gramont, A. *Journal of clinical oncology : official journal of the American Society of Clinical Oncology* **2005**, *23*, 3509.

(29) Poplin, E.; Feng, Y.; Berlin, J.; Rothenberg, M. L.; Hochster, H.; Mitchell, E.; Alberts, S.; O'Dwyer, P.; Haller, D.; Catalano, P.; Cella, D.; Benson, A. B., III *J. Clin. Oncol.* **2009**, *27*, 3778.

(30) Demols, A.; Peeters, M.; Polus, M.; Marechal, R.; Gay, F.; Monsaert, E.; Hendlisz, A.; Van Laethem, J. L. *Br. J. Cancer* **2006**, *94*, 481.

(31) Louvet, C.; Andre, T.; Lledo, G.; Hammel, P.; Bleiberg, H.; Bouleuc, C.; Gamelin, E.; Flesch, M.; Cvitkovic, E.; De Gramont, A. *J. Clin. Oncol.* **2002**, *20*, 1512.

(32) Wong, E.; Giandomenico, C. M. *Chem. Rev. (Washington, D. C.)* **1999**, *99*, 2451.

(33) Liu, D.; Poon, C.; Lu, K.; He, C.; Lin, W. *Nat Commun* **2014**, *5*.

(34) Rieter, W. J.; Pott, K. M.; Taylor, K. M. L.; Lin, W. *Journal of the American Chemical Society* **2008**, *130*, 11584.

(35) Risbood, P.; Kane Jr., C. T.; Hossain, T.; Vadapalli, S.; Chadda, S. *Bioorganic & Medicinal Chemistry Letters* **2008**, *18*, 2957.

(36) Chou, T.-C. *Cancer Research* **2010**, *70*, 440.

(37) Xiao, H.; Li, W.; Qi, R.; Yan, L.; Wang, R.; Liu, S.; Zheng, Y.; Xie, Z.; Huang, Y.; Jing, X. *J. Controlled Release* **2012**, *163*, 304.

(38) Zhang, Y.; Huo, M.; Zhou, J.; Xie, S. *Comput Methods Programs Biomed* **2010**, *99*, 306.

(39) Bapiro, T. E.; Richards, F. M.; Goldgraben, M. A.; Olive, K. P.; Madhu, B.; Frese, K. K.; Cook, N.; Jacobetz, M. A.; Smith, D.-M.; Tuveson, D. A.; Griffiths, J. R.; Jodrell, D. I. *Cancer Chemother. Pharmacol.* **2011**, *68*, 1243.

(40) Raymond, E.; Faivre, S.; Woynarowski, J. M.; Chaney, S. G. *Semin Oncol* **1998**, *25*, 4.

(41) Woynarowski, J. M.; Faivre, S.; Herzig, M. C.; Arnett, B.; Chapman, W. G.; Trevino, A. V.; Raymond, E.; Chaney, S. G.; Vaisman, A.; Varchenko, M.; Juniewicz, P. E. *Mol Pharmacol* **2000**, *58*, 920.

(42) Raymond, E.; Faivre, S.; Chaney, S.; Woynarowski, J.; Cvitkovic, E. *Mol. Cancer Ther.* **2002**, *1*, 227.

(43) Alian, O. M.; Azmi, A. S.; Mohammad, R. M. *Clin Transl Med* **2012**, *1*, 26.

(44) Cooke, S. L.; Brenton, J. D. *Lancet Oncol.* **2011**, *12*, 1169.

(45) Fryer, R. A.; Barlett, B.; Galustian, C.; Dalgleish, A. G. *Anticancer Res* **2011**, *31*, 3747.

(46) Levi, F.; Metzger, G.; Massari, C.; Miano, G. *Clin Pharmacokinet* **2000**, *38*, 1.

(47) Rafi, M.; Cabral, H.; Kano, M. R.; Mi, P.; Iwata, C.; Yashiro, M.; Hirakawa, K.; Miyazono, K.; Nishiyama, N.; Kataoka, K. *J. Controlled Release* **2012**, *159*, 189.

(48) Matsumura, Y.; Maeda, H. *Cancer Res* **1986**, *46*, 6387.

(49) Maeda, H.; Sawa, T.; Konno, T. *J Control Release* **2001**, *74*, 47.

CHAPTER III: Nanoscale Coordination Polymers with High Payloads of Carboplatin and Gemcitabine for Synergistic Combination Treatment of Platinum-Resistant Ovarian Cancer

3.1 Introduction

Ovarian cancer (OCa) is the deadliest of all gynecological cancers, accounting for 5% of all cancer deaths among women.[1] Despite the progress made using a platinum-taxane combination as first-line treatment for OCa, the development of platinum (Pt) resistance often leads to relapse, and patients eventually succumb to tumors.[2-4] OCa cells can resist multiple chemotherapeutics, hindering successful treatment, with 85% of OCa patients relapsing following successful initial treatment.[5,6] A Pt-resistant disease is seen when cancer recurs within six months of initial Pt treatment.[7,8] Retreating the disease with Pt/taxane or other Pt-based therapies following first relapse has shown to be ineffectual.[9] Mechanisms of drug resistance include decreased metabolic transformation of drugs to active chemotherapeutics,[10] reduced uptake and efflux of the drugs,[11,12] increased tolerance to drugs,[13] or increased DNA repair within tumors.[14-16] Combination therapy can counter these mechanisms of resistance without increasing dosages to the point of toxicity by taking advantage of synergism between individual drugs to more efficiently treat disease.

The combination of carboplatin (carbo) and gemcitabine (gem) was approved by the FDA in 2006 for the treatment of advanced ovarian cancer recurring at least 6 months after completion of Pt-based (e.g., carbo or cisplatin) therapy. Gem, a nucleotide analog, induces apoptosis by replacing cytidine during DNA replication.[17] Together with carbo, this combination therapy has been shown to work effectively against drug-resistant tumors without the added toxicity of other Pt cytotoxins (e.g., cisplatin).[18-21] However, gem is often limited by its poor pharmacokinetics and rapid metabolic deactivation.[22-24] Furthermore, the combination with Pt often enhances gem's

hematological toxicity.[25,26] Therefore, there is an urgent need to develop a delivery system for combination drugs that can overcome the limitations imposed by free platinum drugs and gem.

We have developed nanoscale coordination polymers (NCPs) as a novel delivery vehicle for various cancer therapies,[27-30] including a combination therapy delivery system carrying oxaliplatin and gem for the synergistic treatment of pancreatic cancer.[31] These nanoparticles combine the organic and inorganic properties of nanoparticles, as well as their intrinsic biodegradability, to prolong blood circulation half-lives and effectively treat tumors with minimal side effects.[32,33] This chapter reports that NCPs can co-deliver carbo and gem for synergistic therapy of Pt-resistant OCa. More importantly, a superior synergistic effect was found *in vitro* against two Pt-resistant OCa cell lines, SKOV-3 and A2780/CDDP. NCP-Carbo/GMP shows enhanced cellular uptake, prolonged blood circulation, and elevated tumor uptake, resulting in improved antitumor efficacy in Pt-resistant OCa tumor xenograft models.

3.2 Experimental Details

3.2.1 General Experimental:

All starting materials were purchased from Sigma-Aldrich (Louis, MO) and Fisher Scientific (Pittsburgh, PA) unless otherwise noted and used without further purification. 1,2-dioleoyl-sn-glycero-3-phosphate (DOPA), 1,2-distearoyl-sn-glycero-3-phosphocholine (DSPC), cholesterol, and 1,2-distearoyl-sn-glycero-3-phosphoethanolamine-N-[amino(polyethylene glycol)2000] (DSPE-PEG2k) were purchased from Avanti Polar Lipids (Alabaster, AL). Gemcitabine monophosphate (GMP) was synthesized from gem following the literature.[34]

^{1}H NMR spectra were recorded on a Bruker NMR 400 DRX Spectrometer at 400 MHz. The mass spectra of Carbo prodrug, Carbo-bis(phosphonic acid), and its intermediates were

determined using electrospray ionization mass spectrometry (ESI-MS, Agilent 6130) after dissolving the prodrug in water, deprotonating it with excess 3 M NaOH, and then filtering it through a 0.2 μm syringe filter. ESI-MS was taken in positive mode, with a fragmentation voltage of 100 V from 620-720 MW/z.

Human ovarian cancer cells SKOV-3 and murine colon cancer cells CT26 were purchased from the American Type Culture Collection (Rockville, MD) and grown in McCoy's 5A and RPMI 1640, respectively, supplemented with 10% fetal bovine serum (FBS, Gibco, Grand Island, NY). Cisplatin-resistant human ovarian cancer cells A2780/CDDP were obtained from Developmental Therapeutics Core, Northwestern University, and cultured in RPMI 1640 containing 10% FBS. All cells were cultured in a humidified atmosphere containing 5% CO_2 at 37 ^{o}C.

BALB/c female mice (6 weeks, 18-22 g) and athymic female nude mice (6 weeks, 18-22 g) were provided by Harlan Laboratories, Inc (USA). The study protocol was reviewed and approved by the Institutional Animal Care and Use Committee (IACUC) at the University of Chicago.

3.2.2 Synthesis of Carbo Prodrug:

Carbo synthesis was based on previous literatures (Figure 3.1).[35-37] Carbo was synthesized by adding equivalent amounts of Ag salt of cyclobutanedicarboxylic acid (Ag-carbo, 1.51 g) to $Pt(NH_3)_2I_2$ (2.05 g) in minimal H_2O and stirred at room temperature and in darkness for 48 h. The solution was filtered, and the filtrate was evaporated, resulting in a white solid. The product cis-diammine(1, 1-cyclobutanedicarboxylato)-platinum(II) (Carbo) was recrystallized in 1:1 H_2O : EtOH. Yield: 80%. ^{1}H NMR in D_2O: δ 2.8 (t, 4H); δ 1.8 (quintet, 2H).

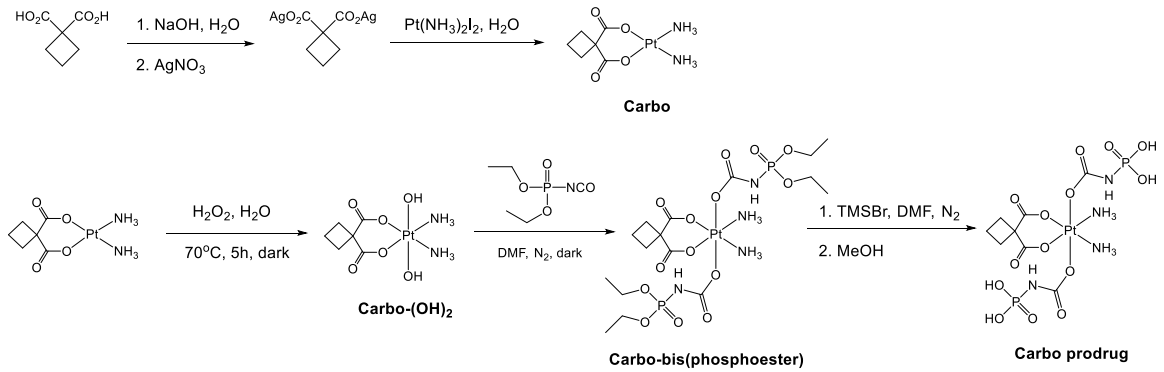

Figure 3.1. Scheme of Carbo prodrug synthesis.

Carbo (1.04 g) was reacted with 30% H_2O_2 (8 mL) in H_2O (16 mL) at 70 °C for 5 h in darkness. Addition of EtOH precipitated a white solid, Carbo-$(OH)_2$, which was washed twice with EtOH. Yield: 80%. ^{1}H NMR in D_2O: δ 2.67 (t, 4H); δ 2.0 (quintet, 2H). The M/Z of $[M+H]^+$ was determined to be 406.1 (expected M/Z= 406.1) (Figure 3.2).

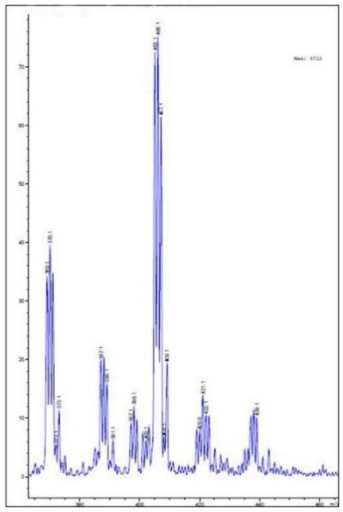

Figure 3.2. ESI-MS of Carbo-$(OH)_2$ showing the peak for $[M+H]^+$ at M/Z=406.1 (expected 406.1).

Carbo-$(OH)_2$ (0.8 g) was dissolved in minimal DMF, to which was added 4 equivalents of diethoxyphosphinyl isocyanate (1.2 mL). The mixture was allowed to react overnight in darkness.

The solution was filtered, and the resulting lightly yellow Carbo-bis(phosphoester) product was precipitated by addition of Et_2O. The product was then washed twice with Et_2O. Yield: 78%. ^1H NMR in D_2O: δ 4.1 (quintet, 4H); δ 3.55 (q, 8H); δ 1.3 (t, 2H); δ 1.16 (t, 12H). The M/Z of $[M+H]^+$ was determined to be 764.2 (expected M/Z= 764.1) (Figure 3.3).

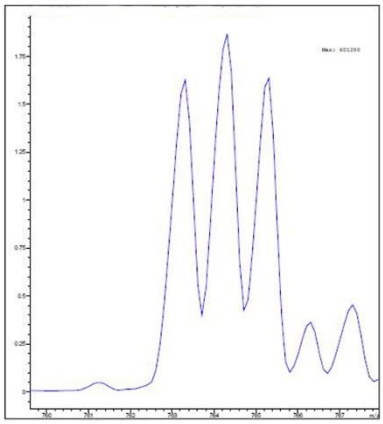

Figure 3.3. ESI-MS of Carbo-bis(phosphoester) showing the peak for $[M+H]^+$ at M/Z=764.2 (expected 764.1).

Trimethylsilyl bromide (TMSBr, 800 μL) was added slowly to the Carbo-bis(phosphoester) (0.8 g) dissolved in minimal DMF at 4 °C, and the solution was stirred for 18 h at room temperature in darkness under N_2 protection. A lightly yellow solid was collected after addition of DCM and then washed twice with additional DCM. The solid was dissolved in MeOH and stirred overnight to hydrolyze the acid. The final product, cis,trans-[Pt(1,1-cyclobutanedicarboxylato)$(NH_3)_2$$(OCONHP(O)(OH)_2)_2$], [Carbo-bis(phosphonic acid) prodrug], was collected by precipitation by DCM and then washed twice with additional DCM. Yield: 73%. ^1H NMR in D_2O: δ 4.1 (quintet, 4H); δ 1.3 (t, 2H). The M/Z of $[M+H]^+$ was determined to be 648.2 (expected M/Z= 648.0) (Figure 3.4).

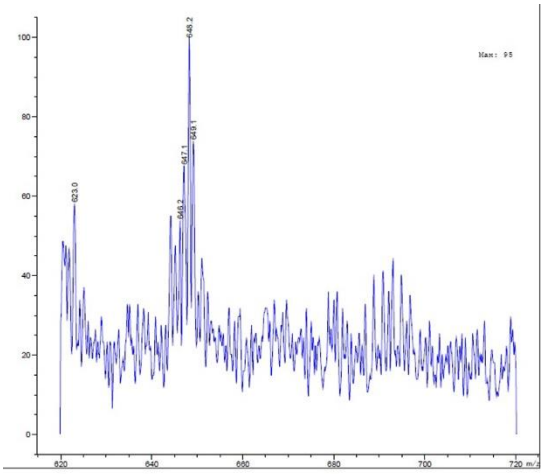

Figure 3.4. ESI-MS of Carbo prodrug showing the peak for $[M+H]^+$ at M/Z=648.2 (expected 648.0).

3.2.2.1 Synthesis of GMP: Prodrug GMP was prepared from gem by a slightly modified literature protocol.[35] Phosphorus oxychloride (13.5mL, 14.5mmol) was stirred with trimethylphosphate (20mL) in 4-5^{o}C. Gemcitabine hydrochloride (1.00g, 3.34mmol) was slowly added for 5 minutes. The solution was stirred at 5^{o}C for 5 minutes then at room temperature for 4 hours. The mixture was poured into cold mixture of deionized water (140mL) and diethyl ether (300mL). The aqueous layer was extracted and washed with diethyl ether (2x200mL). The pH of the solution was adjusted to 6.5 with concentrated ammonium hydroxide in an ice bath. The aqueous layer was washed with diethyl ether (200mL). The solution was freeze overnight. They were lyophilized overnight until powder form. Methanol (100mL) was poured in the solid and was allowed to be stirred for two hours. The solution was filtered, keeping the aqueous layer. The methanol was evaporated off and washed with diethyl ether (2x100mL). It was allowed to dried under vacuum for two hours. Methanol (20mL) was poured into solid and stirred for 10 min. The solution was filtered and rotor vaporized. They were washed with diethyl ether (3x30mL) and dried under vacuum. Ethanol (20mL) and acetonitrile (20mL) was poured and rotovaporized off.

The solid was washed with ethanol (20mL) and diethyl ether (2x20mL). The methanol/ethanol treatment was repeated for three more times. The solid was dried in vacuo at room temperature to give gemcitabine monophosphate. ^{1}H NMR in CD_3OD. 7.95-7.93 (d, 1H); 6.25-6.22 (m, 1H); 6.01 (m, 1H); 4.39-4.32 (m, 1H); 4.25-4.23 (m, 1H); 4.14-4.10 (m, 1H); 4.00-3.98 (m, 1H); impurity from trimethylphosphate seen at 3.57 (s) and 3.55 (s). Yield: 68%.

3.2.3 Particle Synthesis and Characterization:

3.2.3.1 Preparation of NCP-Carbo/GMP: DOPA-NCP-Carbo/GMP was synthesized in reverse microemulsions. To synthesize DOPA-NCP-Carbo/GMP, carbo prodrug (331.3 μL, 11.5 μmol), GMP sodium salt solution (68.7 μL, 5.0 μmol), and DOPA (44 μmol) were added to a 10 mL aliquot of Triton-X-100 (0.3 M in 1.5 M hexanol/cyclohexane) solution to form a W=7.4 microemulsion. Another microemulsion of 10 mL Triton-X-100 (0.3 M, 1.5 M hexanol/cyclohexane) containing $Zn(NO_3)_2 \cdot 6H_2O$ (262 μmol) was also prepared. The two microemulsions were stirred vigorously at room temperature for 15 min. The microemulsion containing the Zn complex was added to the other microemulsion dropwise. The combined emulsion was stirred for an additional 30 min at room temperature. After the addition of 20 mL ethanol, the particles were washed once with ethanol and twice with 50% (v/v) ethanol/tetrahydrofuran (THF) before being redispersed in THF.

Different ratios of carbo and GMP can be loaded into the particle. Another set of NCP-Carbo/GMP with different drug ratios were thus also synthesized. DOPA-NCP-Carbo/GMP-2 was synthesized using carbo prodrug (200 μL, 6.9 μmol), GMP sodium salt solution (200 μL, 14.6 μmol) under the same microemulsion conditions mentioned above.

3.2.3.2 *Preparation of NCP-Carbo:* DOPA-NCP-Carbo was synthesized in reverse microemulsions. 25 mg/mL cis,trans-[Pt(1,1-cyclobutanedicarboxylato)$(NH_3)_2$

$(OCONHP(O)(OH)_2)_2$] (8.6 μmol), and DOPA (11 μmol) were added to a 5 mL aliquot of Triton-X-100 (0.3 M in 1.5 M hexanol/cyclohexane) solution to form a *W*=7.4 microemulsion. Another microemulsion of 5 mL Triton-X-100 (0.3 M, 1.5 M hexanol/cyclohexane) containing $Zn(NO_3)_2 \cdot 6H_2O$ aq. (131 mmol) was also prepared. The two microemulsions were separately stirred vigorously for 15 min at room temperature and then combined and stirred for an additional 30 min at room temperature. NCP-Carbo particles were washed once with ethanol, once with 50% (v/v) ethanol/cyclohexane, twice with 50% (v/v) ethanol/THF, and then redispersed in THF.

3.2.3.3 Preparation of Rhodamine B-Doped NCP-Carbo/GMP: A *W*=7.4 microemulsion was prepared with the addition of 25 mg/mL cis,cis,trans-[$Pt(NH_3)_2Cl_2(OCONHP(O)(OH)_2)_2$] sodium salt solution (7.6 μmol), 15 mg/mL GMP sodium salt solution (1.3 μmol), 23 mg/mL rhodamine B sodium salt solution (0.8 μmol), and DOPA (22 μmol) to a 5 mL aliquot of Triton-X-100 (0.3 M in 1.5 M hexanol/cyclohexane) solution. Another microemulsion of 5 mL Triton-X-100 (0.3 M, 1.5 M hexanol/cyclohexane) containing $Zn(NO_3)_2 \cdot 6H_2O$ aq. (131 mmol) was also prepared. The two microemulsions were stirred vigorously for 15 min at room temperature, after which they were combined. The resulting microemulsion was stirred for 30 min at room temperature. After the addition of 20 mL ethanol, RhB-NCP-Carbo/GMP particles were washed once with ethanol, once with 50% (v/v) ethanol/cyclohexane, twice with 50% (v/v) ethanol/THF, and then redispersed in THF.

3.2.3.4 *Characterization of NCP Particles:* The carbo-loaded nanoparticles were dried, weighed, digested in concentrated nitric acid overnight, and diluted with water to determine the carbo loading by inductively coupled plasma-mass spectrometry (ICP-MS, Agilent 7700x ICP-MS). GMP loading was determined by UV-Vis spectroscopy and thermogravimetric analyses (TGA). Particles were digested overnight in 6 M hydrochloric acid, and the concentration of GMP

in the solution was determined by the absorbance at 275 nm using a Shimadzu UV-2401PC UV-Vis Spectrophotometer.

3.2.3.5 *General Procedures of Lipid Coating and PEGylation:* DOPA-capped NCP-Carbo/GMP nanoparticles were further coated with DSPC, cholesterol, and DSPE-PEG2k to increase their stability and allow them to circulate longer in the blood. A THF solution of DSPC, cholesterol, DSPE-PEG2k (molar ratio 1:1:0.75), and DOPA-capped NCP nanoparticles was added dropwise to 500 μL of 30% (v/v) ethanol/H_2O at 60 °C under strong stirring. THF was evaporated, and the dispersion was allowed to cool to room temperature before use. NCP-Carbo nanoparticle carrying only carbo, and NCP-GMP particles carrying gem monotherapy were prepared similarly as NCP-Carbo/GMP.

3.2.4 In Vitro *Stability Studies:*

Particle stability was evaluated *in vitro* in phosphate buffered saline (PBS) buffer with bovine serum albumin (BSA)-binding and time-dependent drug release. BSA binding analysis was done by dispersing 0.45 mg of NCP-Carbo/GMP in 1 mL PBS containing BSA (30 nM) at 37 ^oC. DLS measurements were detected every hour for 24 hours to determine the size of nanoparticles in suspension over time.

3.2.5 In Vitro *Drug Release:*

In vitro release profiles of Carbo and GMP from NCP-Carbo/GMP were performed in 250 mL 1× PBS buffer with or without 5 mM cysteine at 37 ^oC and pH 7.4. DOPA-NCP-Carbo/GMP or NCP-Carbo/GMP (0.75 mg) were suspended in 4 mL of 1x PBS buffer solution with or without 5 mM cysteine in a 10,000 MWCO pleated dialysis bag. The dialysis bag containing the nanoparticle suspension was added into a beaker containing 250 mL of 1x PBS buffer, incubated at 37 ^oC at pH 7.4, while stirring. Periodically, 1 mL aliquots of solution were taken from the

solution, and a fresh 1 mL of buffer solution with or without cysteine was added to the beaker. The removed aliquot was digested in nitric acid or HCl and analyzed by ICP-MS for Pt or UV-Vis for GMP, respectively.

3.2.6 In Vitro *Cytotoxicity and Synergistic Effect:*

In vitro cytotoxicity assays were carried out on SKOV-3 and A2780/CDDP ovarian cancer cells. In 96-well plates, SKOV-3 or A2780/CDDP ovarian cancer cells were seeded at a density of 1000 cells/well and 750 cells/well, respectively, in a total of 100 μL RPMI-1640 or McCoy containing 10% FBS. The cells were incubated at 37 ^{o}C for 24 h prior to drug treatment. The culture medium was replaced by fresh medium. Different concentrations of carbo, GMP, free carbo plus GMP (Carbo&GMP) mixture (at the same NCP-Carbo and NCP-GMP drug dose), NCP-Carbo, NCP-GMP, and NCP-Carbo/GMP were added and incubated at 37 ^{o}C and 5% CO_2 for 72 h, and cell viability was measured by MTS assay (Promega, USA) based on the manufacturer's manual. IC_{50} values were calculated from curves constructed by plotting cell viability (%) versus drug concentration (μM).

3.2.7 Cell Apoptosis by Confocal Microscopy:

SKOV-3 and A2780/CDDP cells were seeded in 6-well plates (5×10^4 cells/well), and the cells were treated with free drugs or particles at a concentration of 1.9 μM carbo or 0.7 μM GMP for 24 h. Treated cells were harvested, washed twice with ice-cold PBS, stained with Alexa Fluor 488 conjugated Annexin V and prodium iodide (PI) for 15 min at room temperature in the dark, and then analyzed by flow cytometry.

For CLSM imaging, cells were seeded on 10 mm^2 glass coverslips placed in 6-well plates at a density of 5×10^4 cells per well and incubated with free drugs or particles at a concentration of 1.9 μM carbo or 0.7 μM GMP for 24 h. After fixing with 4% paraformaldehyde, cells were

stained with 10 μg/mL of DAPI and Alexa Fluor 488 conjugated Annexin V and observed using CLSM at excitation wavelengths of 405 and 488 nm to visualize nuclei (blue fluorescence) and cell apoptosis (green fluorescence), respectively.

3.2.8 Cell Apoptosis by Flow Cytometry:

SKOV-3 or A2780/CDDP were seeded at 500,000 cells/well in a 6-well plate containing 2 mL total volume of cell culture medium for 24 h at 37 ^{o}C and 5% CO_2. The culture medium was replaced with fresh medium containing different drug treatments at carbo concentration of 1.9 μM for SKOV-3 and 1.3 μM for A2780/CDDP and/or a GMP concentration of 0.7 μM for SKOV-3 and 0.5 μM for A2780/CDDP. Following a 24 h incubation, the floating and adherent cells were collected and stained with Annexin V/dead cell apoptosis kit with Alexa Fluor 488 annexin V and propidium iodide (PI, Invitrogen, USA) based on manufacturer's instructions. The apoptosis was analyzed on a flow cytometer (LSRII 3-8, BD, USA).

3.2.9 In Vitro *Cellular Uptakes and Intercellular Distribution:*

SKOV-3 or A2780/CDDP cells were seeded at a cell density of $5x10^5$ cells per well and 2 mL total volume media containing 10% FBS. Following 24 h of incubation at 37 ^{o}C and 5% CO_2, the culture medium was replaced by 2 mL of fresh media containing aliquots of free carbo and GMP or NCP-Carbo/GMP at 0.96 μM carbo (or 0.35 μM GMP) for SKOV-3 and 0.65 μM carbo (or 0.24 μM GMP) for A2780/CDDP. The cells were cultured for different time points (1 h, 2 h, 4 h, and 24 h) at 37 ^{o}C and 5% CO_2. Media were removed and the cells were washed with 1× PBS three times. The adherent cells were collected by trypsinization and washed with 1× PBS three times. The cells were counted prior to the last wash. They were then digested with concentrated nitric acid or 6 M HCl and analyzed using ICP-MS for Pt content or UV-Vis for GMP content.

To directly observe the internalization and intracellular distribution of particles under CLSM, Rhodamine B (RhB), a fluorescence marker, was doped into the particle by adding it into the prodrug microemulsion during particle preparation. Cells were seeded on 10 mm^2 glass coverslips placed in 6-well plates and incubated with RhB-doped NCP-Carbo/GMP for 1 h, 2 h, 4 h, and 24 h. Cells were washed with PBS three times, fixed with 4% paraformaldehyde, stained with DAPI and LysoTracker Green, and observed under CLSM (FV1000, Olympus, Japan).

3.2.10 In Vivo *Pharmacokinetic and Biodistribution Studies:*

To evaluate the pharmacokinetics and biodistribution of NCP-Carbo/GMP, balb/c mice bearing CT26 tumors were intraperitoneally injected with NCP-Carbo/GMP at 5 mg/kg carbo dose (or 1.5 mg/kg GMP dose). Mice were sacrificed at 5 min, 1h, 3 h, 5h, 8 h, 24 h, and 48 h post-injection. Their liver, lung, spleen, kidney, heart, bladder, tumor, and blood were harvested and digested in concentrated nitric acid for 24 h, and the Pt concentrations were analyzed by ICP-MS.

Pt concentration were analyzed using ICP-MS. GMP concentrations in plasma were further analyzed using high-performance liquid chromatography-tandem mass spectrometry (HPLC-MS/MS, Agilent 6460 QQQ MS-MS). The extraction method followed a procedure reported in the literature.[34] To a 50 μL plasma, 200 μL ice-cold acetonitrile was added, vortexed, mixed, and centrifuged. The resulting supernatant was evaporated and reconstituted in 100 μL of water. An injection volume of 20 μL of sample was used. The autosampler and column temperatures were kept at 4 and 30 ^oC, respectively. The samples were separated via a PGC Hypercarb column (100 x 2.1 ID, 5 μm, Thermo Fisher Scientific) fitted with a guard column (Hypercarb 10 x 2.1, 5 μm, Thermo Fisher Scientific). A gradient mobile phase of (A) 10 mM ammonium acetate at pH 10 and (B) acetonitrile were used with the initial mobile phase of 95% solvent A and 5% solvent B at a flow rate of 0.3 mL/min. After 2 min, solvent A was gradually decreased to 80% over 0.2 min

and held at this condition for 5.6 min. The gradient was returned to 95% solvent A over 0.2 min, and this condition was held for an additional 7 min, for a total run time of 15 min. The mass to charge transition was monitored from 342 to 231.

3.2.11 Antitumor Activity In Vivo*:*

Assessing antitumor activity was conducted in two subcutaneous xenograft mouse models. SKOV-3 cells (5×10^6 cells in 100 μL medium/matrix gel (v/v 1:1)) or A2780/CDDP cells (5×10^6 cells in 100 μL medium) were subcutaneously injected in the right flank of mice. When the tumor volume reached around 100 mm^3, mice were randomly divided into 3 groups (n = 5), and i.p. injected with PBS, Carbo&GMP, and NCP-Carbo/GMP at a dose of 10 mg carbo/kg and 2.4 mg Gem/kg every three days. Tumor sizes were measured every day by a caliper and calculated as follows: (length × $width^2$)/2. Body weight was also recorded every day as an indicator of systemic toxicity. All mice were sacrificed when the tumor volume of PBS group reached 2000 mm^3.

3.2.12 In Vivo *Immunogenic Response, Hypersensitivity, and General Toxicity Evaluation of NCP:*

At the endpoint of the *in vivo* efficacy study, blood was collected, and the serum was separated for immunogenic response analysis. TNF-α, IFN-γ, and IL-6 production was determined by ELISA (R&D Systems, USA). Blood from the control group was also analyzed using the same treatment for comparison. Organs (heart, liver, spleen, lung and kidney) were also harvested, sectioned at 5-μm thickness, stained with H&E, and observed for histological examination of toxicity with light microscopy (Panoramic Scan Whole Slide Scanner, PerkinElmer, USA).

3.2.13 In Vivo *Tumor Cell Apoptosis:*

SKOV-3 and A2780/CDDP tumors were excised and embedded in optimal cutting temperature (OCT) medium, sectioned at 5-μm thickness. TdT-mediated dUTP nick end labeling (TUNEL) assay was performed using DNA Fragmentation Detection Kit (Invitrogen, USA) and observed under CLSM to quantify *in vivo* apoptosis. Nuclei were stained with DAPI (10 μg/mL), and DNA fragments in apoptotic cells were stained with fluorescein-conjugated deoxynucleotides (green). The number of TUNEL-positive cells was divided by the total number of cells to calculate the percentage of apoptotic cells in the sample.

3.2.14 Statistical Analysis:

Results were expressed as means ± standard deviation (S.D.). Two-ways ANOVA was used to determine statistical significance. A P value < 0.05 was considered statistically significant.

3.3 Results

3.3.1 Synthesis and Characterization of NCP-Carbo/GMP:

The carbo prodrug, carbo-bis(phosphonic acid), was synthesized and characterized by NMR and mass spectrometry (Figure 3.2 through 3.4). DOPA-capped NCP-Carbo/GMP nanoparticles containing the carbo prodrug and gemcitabine monophosphate (GMP) were initially synthesized by reverse microemulsion (Figure 3.5 and Figure 3.6). The surface of particles was coated with DOPA as a monolayer via Zn-phosphate interactions between particles and DOPA molecules and hydrophobic-hydrophobic interactions among DOPA molecules, making the particles dispersible in organic solvents. The surface was then additionally coated with DSPC, cholesterol, and DSPE-PEG2k at 1:1:0.75 mol ratio, respectively. The Z-average, number-average, PDI, and zeta-potential for NCP-Carbo/GMP were 85.3±0.7 nm, 64.9±1.7 nm,

0.069±0.013, and -6.02±0.55 mV, respectively, by dynamic light scattering (DLS) measurement (Figure 3.7 and Table 3.1). The near-neutral surface charge indicated that the PEG chains were successfully coated on the particle surface. Transmission electronic microscopy (TEM) showed uniform spherical nanoparticles with a diameter of ~20 nm (Figure 3.8), implying that the lipid coating did not disrupt the NCP core. DOPA-NCP-Carbo/GMP gave carbo loadings of 28.0±2.6 wt.% (54.4±5.1 wt.% prodrug loading) by ICP-MS. Gemcitabine monophosphate (GMP) loadings were found to be 8.6±1.5 wt.% by UV-Vis. Different Pt and GMP loadings of NCP-Carbo/GMP were also formulated (NCP-Carbo/GMP-2), showing the versatility of the NCP system. NCP-Carbo/GMP-2 showed Carbo loading of 17.5 wt.% (34.0 wt.% prodrug loading) and GMP loading of 22.7 wt.%. The different formulations of NCP-Carbo/GMP showed similar particle size and surface charge (Figure 3.9 and Figure 3.10, Table 3.1). NCP-Carbo and NCP-GMP particles containing only Carbo prodrug and GMP, respectively, were similarly formulated for comparison purposes and exhibited similar particle sizes and near neutral zeta potential as NCP-Carbo/GMP (Figure 3.11 and Figure 3.12). No change was seen in the NCP-Carbo/GMP particle size upon exposure to 30 nM bovine serum albumin in phosphate buffer saline at 37 ^{o}C after 24 h (Figure 3.13). The *in vitro* study showed that NCP-Carbo/GMP exhibited excellent stability.

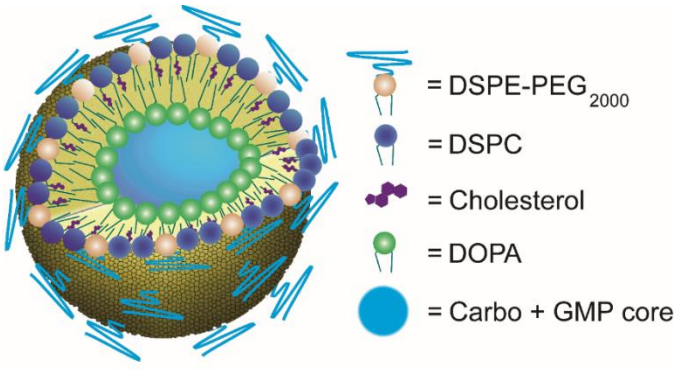

Figure 3.5. Schematic representation of NCP-Carbo/GMP.

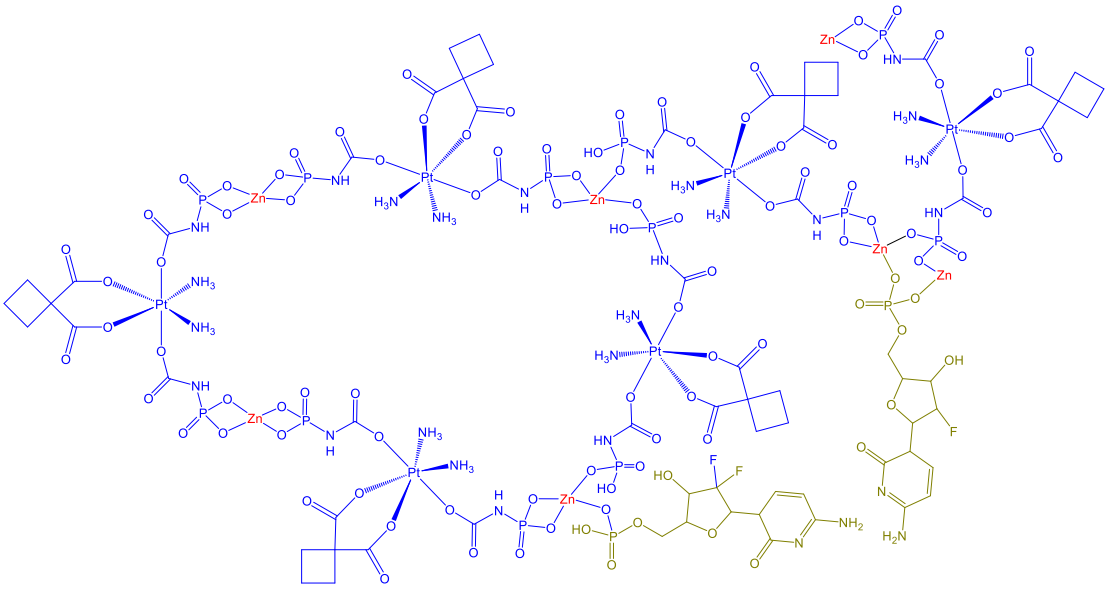

Figure 3.6. Schematic representation showing the core of NCP-Carbo/GMP nanoparticles.

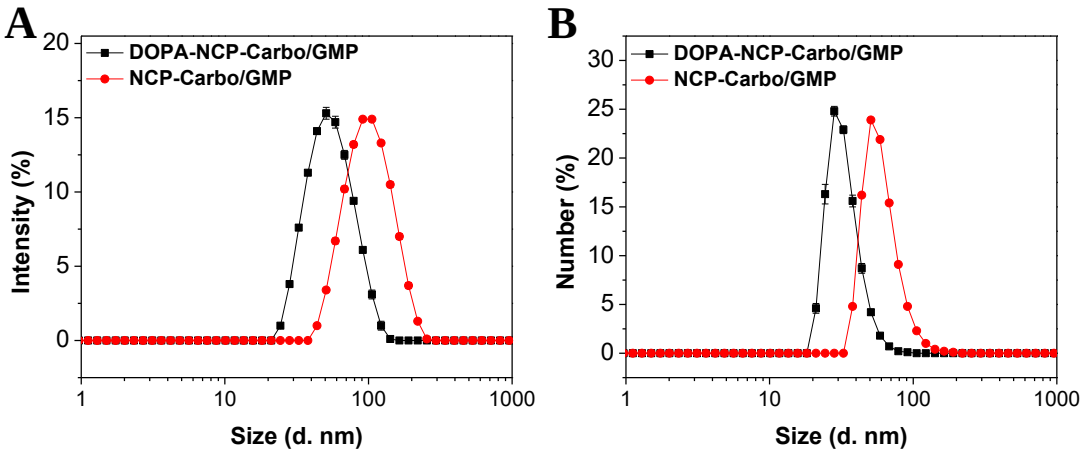

Figure 3.7. (A) Intensity-average and (B) number-average size distribution of NCP-Carbo/GMP particles. Bare and lipid-coated particles were measured in THF and PBS, respectively.

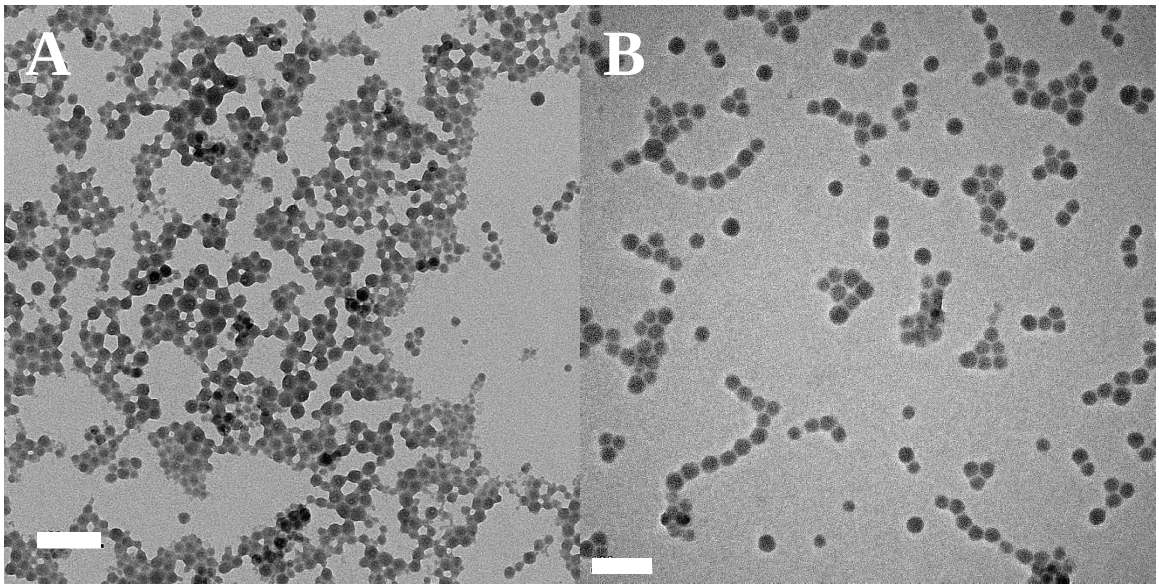

Figure 3.8. TEM micrographs of (A) DOPA-NCP-Carbo/GMP and (B) NCP-Carbo/GMP. Scale = 100 nm.

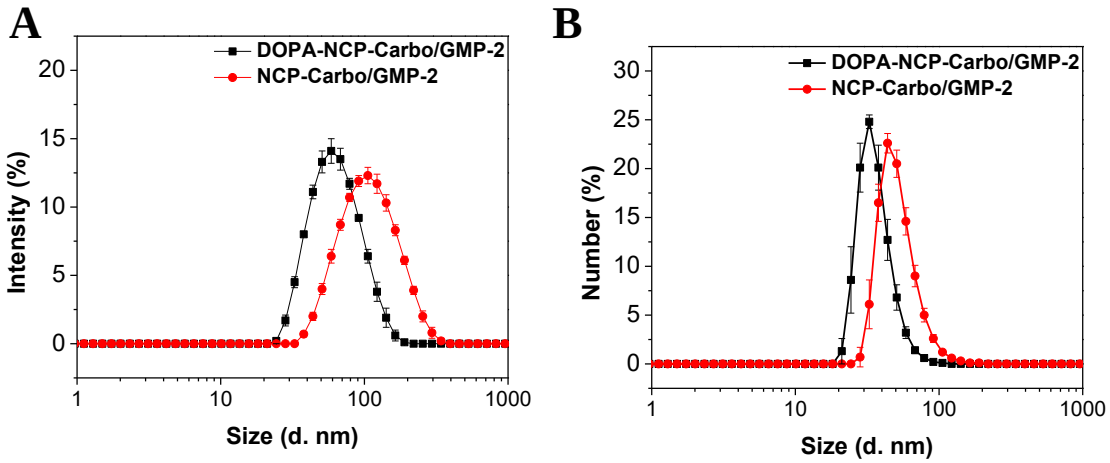

Figure 3.9. (A) Intensity-average and (B) number-average size distribution of NCP-Carbo/GMP-2 particles. Bare and lipid-coated particles were measured in THF and PBS, respectively.

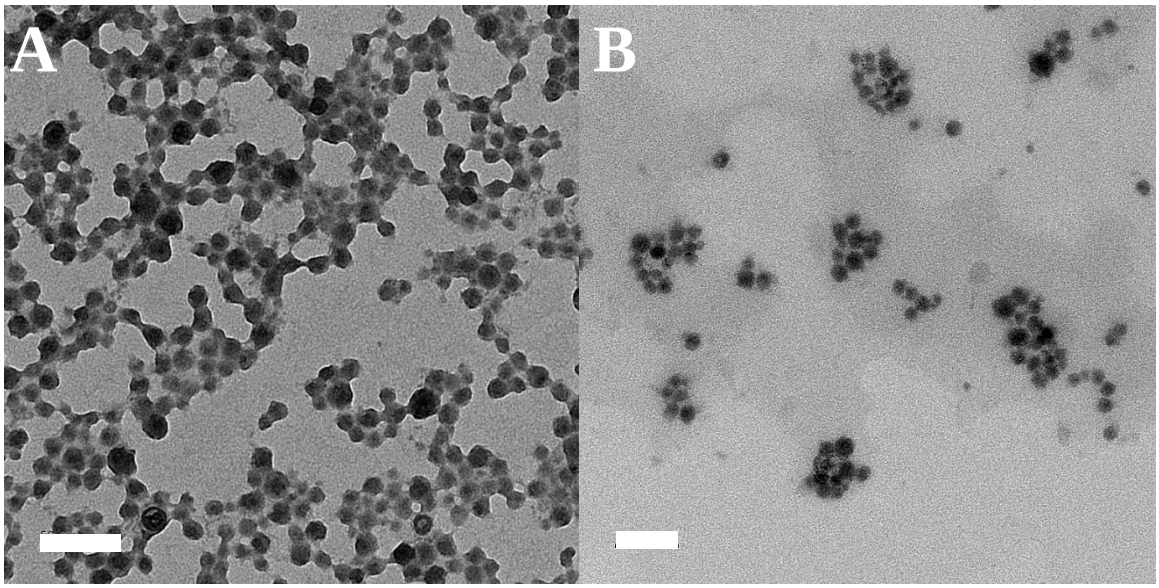

Figure 3.10. TEM micrographs of (A) DOPA-NCP-Carbo/GMP-2 and (B) NCP-Carbo/GMP-2. Scale = 100 nm.

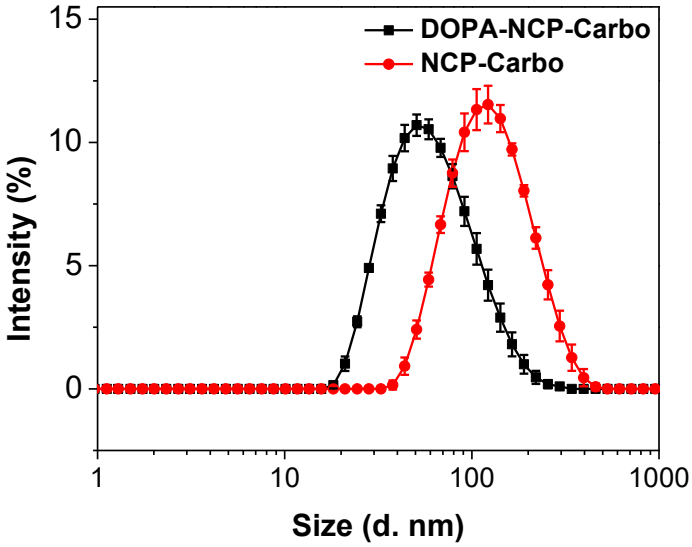

Figure 3.11. Intensity-average size distribution of NCP-Carbo particles. Bare and lipid-coated particles were measured in THF and PBS, respectively.

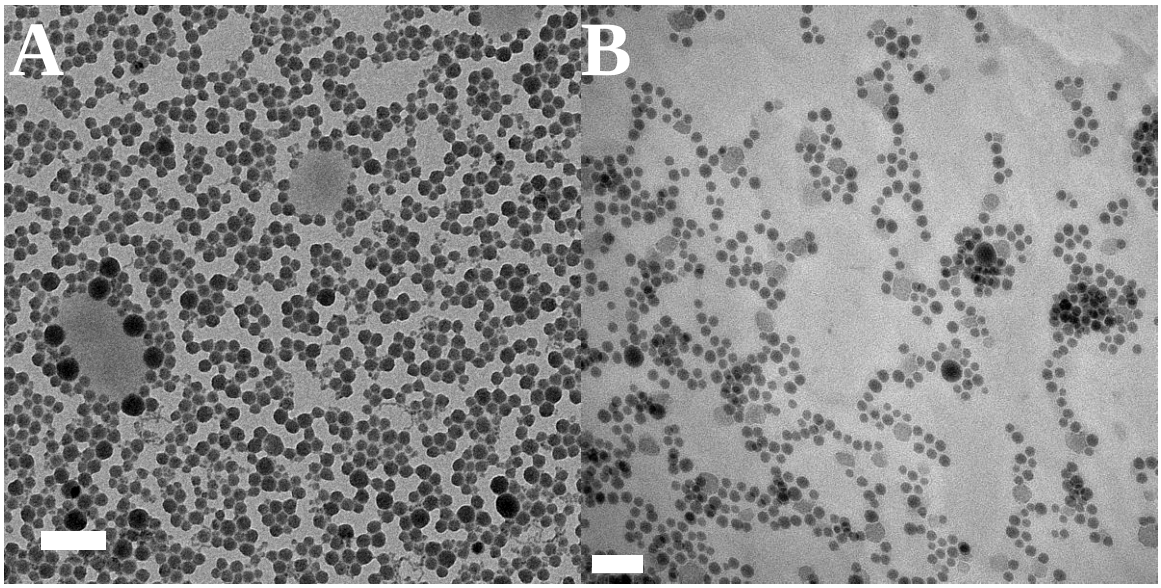

Figure 3.12. TEM micrographs of (A) DOPA-NCP-Carbo and (B) NCP-Carbo. Scale = 100 nm.

Table 3.1. Sizes, Polydispersities, and Zeta Potentials of NCP Particles.

NCPs	Z-Ave diameter (nm)	Number-Ave diameter (nm)	PDI	Zeta Potential (mV)
DOPA-NCP-**Carbo/GMP**	56.9±0.2[#]	37.1±0.4[#]	0.112±0.003	NA
NCP-**Carbo/GMP**	85.3±0.7[$]	64.9±1.7[$]	0.069±0.013[$]	-6.02±0.55[$]
DOPA-NCP-**Carbo/GMP-2**	58.4±0.2[#]	36.4±1.5[#]	0.136±0.002	NA
NCP-**Carbo/GMP-2**	92.8±0.2[$]	52.6±1.8[$]	0.193±0.007[$]	-4.89±0.31[$]
DOPA-NCP-**Carbo**	54.1±0.2[#]	27.3±1.3[#]	0.203±0.006	NA
NCP-**Carbo**	89.7±1.1[$]	40.4±3.8[$]	0.191±0.012	-0.02±0.01[$]
DOPA-NCP-**GMP**	54.1±0.2[#]	27.3±1.3[#]	0.203±0.006	NA
NCP-**GMP**	108.6±1.9[$]	63.1±2.9[$]	0.172±0.018	-5.87±0.40[$]

[#]Measured in THF. [$]Measured in PBS. Data are expressed as means±S.D.

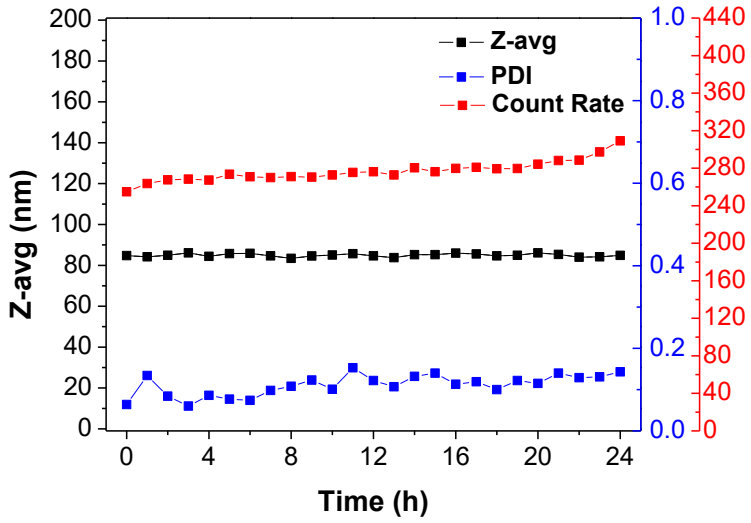

Figure 3.13. Stability test of NCP-Carbo/GMP after PEGylation in PBS buffer with BSA at 37 ^{o}C. Z-avg diameters were evaluated over a 24 h-period.

3.3.2 In Vitro *Drug Release*

The release profiles of carbo and GMP from DOPA-NCP-Carbo/GMP and NCP-Carbo/GMP were investigated in PBS with or without 5 mM cysteine at 37 ^{o}C at pH 7.4 (Figure 3.14). In the absence of cysteine, DOPA-NCP-Carbo/GMP revealed rapid burst release, with 57% and 33% cumulative release of Pt and GMP before 2 h, respectively. In contrast, only 19% Pt and 21% GMP release were observed for NCP-Carbo/GMP after 96 h. Drug release was also studied in the presence of 5 mM cysteine to simulate intracellular environment. The addition of 5 mM cysteine led to a faster drug release of DOPA-NCP-Carbo/GMP with 82% of Pt and 57% of GMP release after 2 h, indicating that the NCPs underwent reductive degradation to release the drugs. However, NCP-Carbo/GMP exhibited similarly slow drug release patterns in PBS and PBS supplemented with 5 mM cysteine. The lipid coating on the particle surface prevented the penetration of cysteine into the NCP core, thereby improving the stability of the particle. In contrast, once the particles undergo endocytosis and enter the cell, the lipid coatings may be

incorporated into the cell and plasma membrane. The disruption of the lipid coatings on NCPs allows cysteine to penetrate the particle core, triggering rapid release of the drugs via reductive degradation of NCPs.

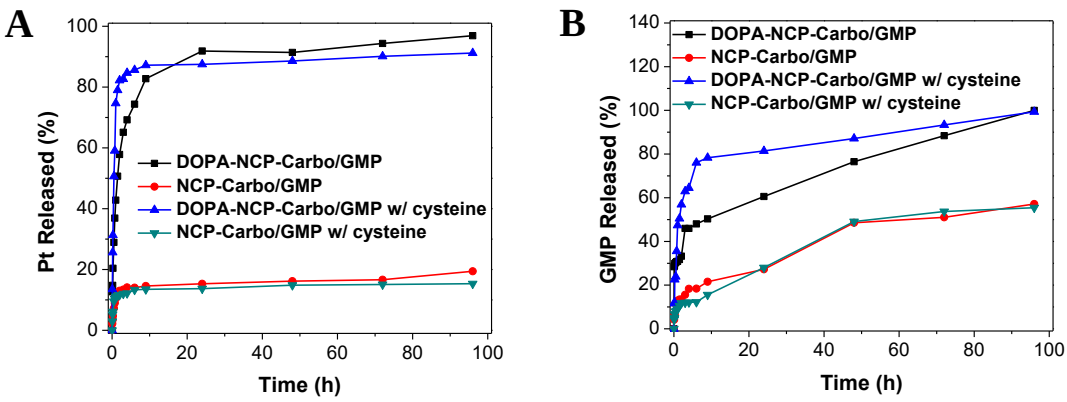

Figure 3.14. Pt (A) and GMP (B) release profiles of DOPA-NCP-Carbo/GMP and NCP-Carbo/GMP in 1x PBS buffer with or without 5 mM cysteine at 37 ^{o}C.

3.3.3 In Vitro *Cytotoxicity and Synergistic Effect*

To evaluate the potency of NCP-Carbo/GMP, *in vitro* cytotoxicity was performed on SKOV-3 (Figure 3.15) or A2780/CDDP (Figure 3.16) ovarian cancer cells treated with nanoparticles or free drugs at different carbo or gem concentrations for 72 h. The cell viability was measured by MTS assay. As seen in Figure 3.15 and Table 3.2, the IC_{50} of carbo and GMP against SKOV-3 were 24.21 ± 0.96 μM and 1.89 ± 0.26 μM, respectively. When free carbo and GMP were combined (Carbo&GMP), the carbo and GMP IC_{50} values were dramatically decreased by 12-fold and 2.5-fold, respectively (carbo IC_{50}= 2.01 ± 0.62 μM or GMP IC_{50}=0.74 ± 0.23 μM). NCP-Carbo/GMP showed comparable cytotoxicity as their corresponding free drug counterparts, with carbo IC_{50}=1.91 ± 0.55 μM and GMP IC_{50}=0.70 ± 0.20 μM. In contrast, monotherapeutic NCPs IC_{50} values of carbo and GMP were 22.82 ± 2.49 μM and 1.98 ± 0.34 μM, respectively. Similar results were shown with A2780/CDDP cells with NCP-Carbo/GMP, with IC_{50} values that

are about 7.6-fold, 14.4-fold, 2.3-fold, and 2.4-fold lower than free carbo, NCP-Carbo, free GMP, and NCP-GMP, respectively.

The CI provides a quantitative measure of synergism (CI < 1), additivity (CI = 1), or antagonism (CI > 1) for the drug combinations. The CI was around 0.5 for NCP-Carbo/GMP against the monotherapeutic NCP and free drugs over a large range of drug effect level for both SKOV-3 (Figure 3.15C) and A2780/CDDP (Figure 3.16C). Synergy was thus seen between carbo and GMP in both Pt-resistant ovarian cancer cells. These results suggest that co-delivery of carbo and gem could overcome drug resistance, leading to much enhanced anticancer efficacy against ovarian tumor models.

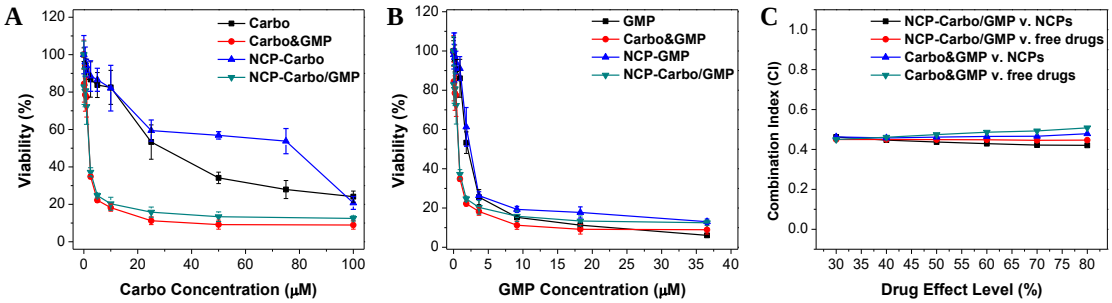

Figure 3.15. *In vitro* cytotoxicity plots and combination indices (CI) of carbo and GMP combinations on SKOV-3 cells. The cell viabilities on SKOV-3 cells were measured after a 72 h exposure to NCP-Carbo, NCP-GMP, NCP-Carbo/GMP, or free drugs (carbo, or GMP). Data are mean ± S.D. (n=6).

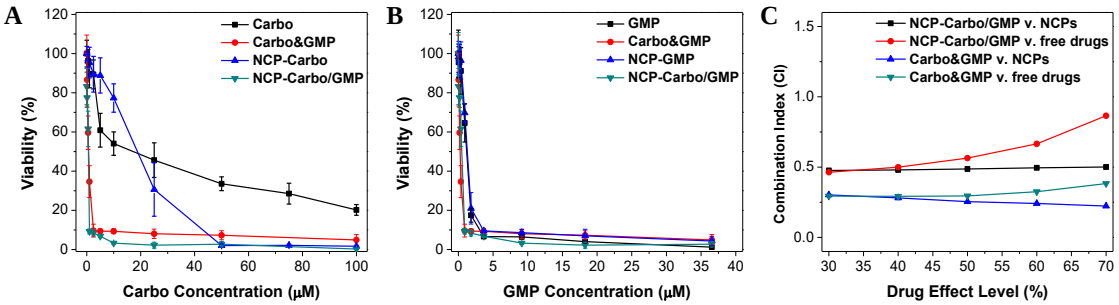

Figure 3.16. *In vitro* cytotoxicity plots and combination indices (CI) of carbo/GMP combinations on A2780/CDDP cells. The cell viabilities on A2780/CDDP cells were measured after a 72 h exposure to NCP-Carbo, NCP-GMP, NCP-Carbo/GMP, or free drugs (carbo, or GMP). Data are mean ± S.D. (n=6).

Table 3.2. Carbo IC_{50} Values of Carbo, GMP, NCP-Carbo, NCP-GMP, NCP-Carbo/GMP against SKOV-3, and A2780/CDDP Cells (the numbers in parentheses refer to GMP concentrations).

	Carbo(μM)	GMP (μM)	Carbo&GMP (μM)	NCP-Carbo (μM)	NCP-GMP (μM)	NCP-Carbo/GMP (μM)
SKOV-3	24.2±1.0	(1.9±0.3)	2.0±0.6 (0.7±0.2)	22.8±2.5	(2.0±0.3)	1.9±0.6 (0.7±0.2)
A2780/CDDP	9.9±2.2	(1.1±0.2)	0.7±0.2 (0.3±0.1)	18.7±1.0	(1.2±0.2)	1.3±0. 2 (0.5±0.1)

Data are expressed as means±S.D.

3.3.4 In Vitro *Cell Apoptosis*

To investigate the synergistic effect of carbo and GMP on cell apoptosis, Annexin V staining and flow cytometry analysis were performed to investigate cell apoptosis induced by free drugs or nanoparticle formulations. Rhodamine-B-doped NCP-Carbo/GMP (RhB-NCP-Carbo/GMP) nanoparticles were synthesized for confocal microscopy. As seen in the DLS (Table 3.3) and TEM images (Figure 3.17), no difference was observed in the size distribution and morphology between dye-doped particles and NCP-Carbo/GMP. After incubation for 24 h, SKOV-3 and A2780/CDDP cells were stained with Alexa Fluor 488 conjugated Annexin V and observed using CLMS. NCP-Carbo/GMP induced the highest level of cell apoptosis, as evidenced by the presence of the most and brightest green fluorescence. Carbo&GMP, NCP-GMP and GMP also induced a high level of cell apoptosis, while carbo and NCP-Carbo resulted in much less cell apoptosis (Figure 3.18 and Figure 3.19).

Table 3.3. 3 Sizes, Polydispersities, and Zeta potentials of RhB-NCP-Carbo/GMP.

NCPs	Z-Ave diameter (nm)	Number-Ave diameter (nm)	PDI	Zeta Potential (mV)
DOPA-RhB-NCP-Carbo/GMP	59.9±0.3[#]	27.17±1.8[#]	0.204±0.004	NA
RhB-NCP-Carbo/GMP	108.6±1.9[$]	63.1±2.9[$]	0.172±0.018	-12.9±3.2

[#]Measured in THF. [$]Measured in PBS buffer. Data are expressed as means±S.D.

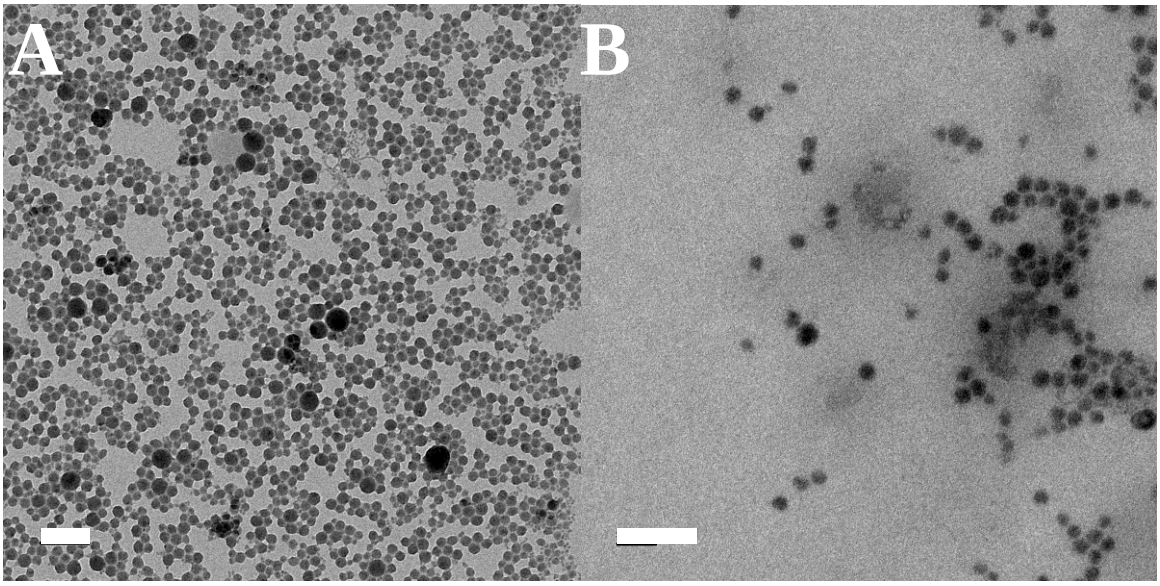

Figure 3.17. TEM micrographs of (A) DOPA-RhB-NCP-Carbo/GMP and (B) RhB-NCP-Carbo/GMP. Scale = 100 nm.

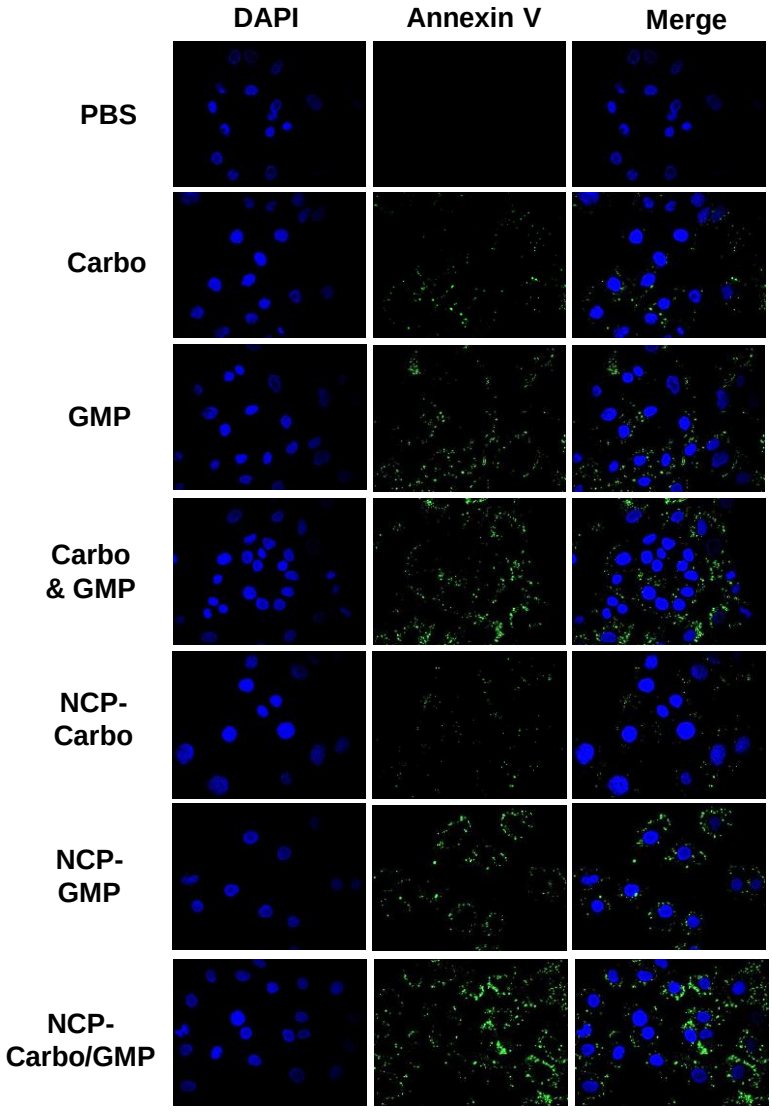

Figure 3.18. CLSM images showing cell apoptosis in SKOV-3 cells after incubation with free drugs or particles for 24 h. Cells were stained with Alexa Fluor 488 conjugated Annexin V and the nuclei were stained with DAPI. Scale bars: 20 μm.

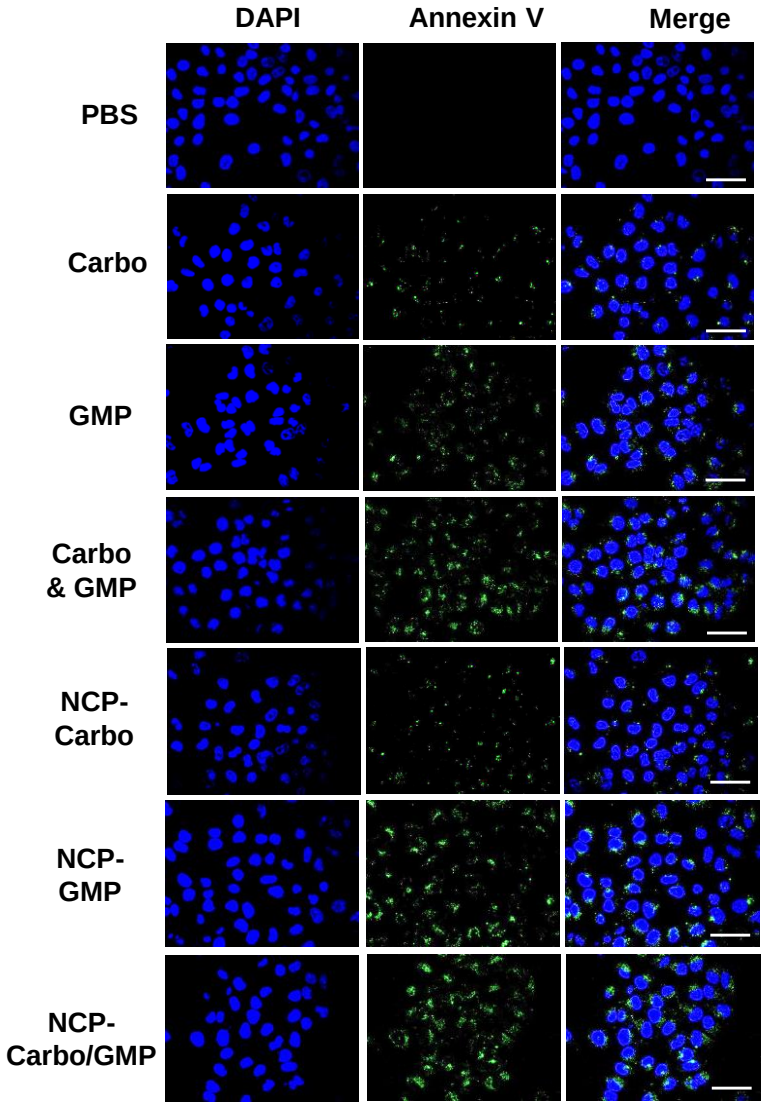

Figure 3.19. CLSM images showing cell apoptosis in A2780/CDDP cells after incubation with free drugs or particles for 24 h. Cells were stained with Alexa Fluor 488 conjugated Annexin V and the nuclei were stained with DAPI. Scale bars: 20 μm.

We further quantified cell apoptosis by flow cytometry (Figure 3.20 and Figure 3.21). Similar to the cytotoxicity assay and CLSM analysis, NCP-Carbo/GMP showed the highest ability to induce cell apoptosis, resulting in 62.05% and 65.94% apoptosis for SKOV-3 and A2780/CDDP cells, respectively. Carbo&GMP also showed significantly increased cell apoptosis in both ovarian

cancer cell lines with 52.67% and 35.43% of cells undergoing apoptosis in SKOV-3 and A2780/CDDP, respectively. Free GMP and NCP-GMP showed comparable apoptotic cells, ranging from 47-49% in SKOV-3 and 26-35% in A2780/CDDP. Little or no apoptotic cells were seen in PBS, carbo, and NCP-carbo for both ovarian cancer cell lines.

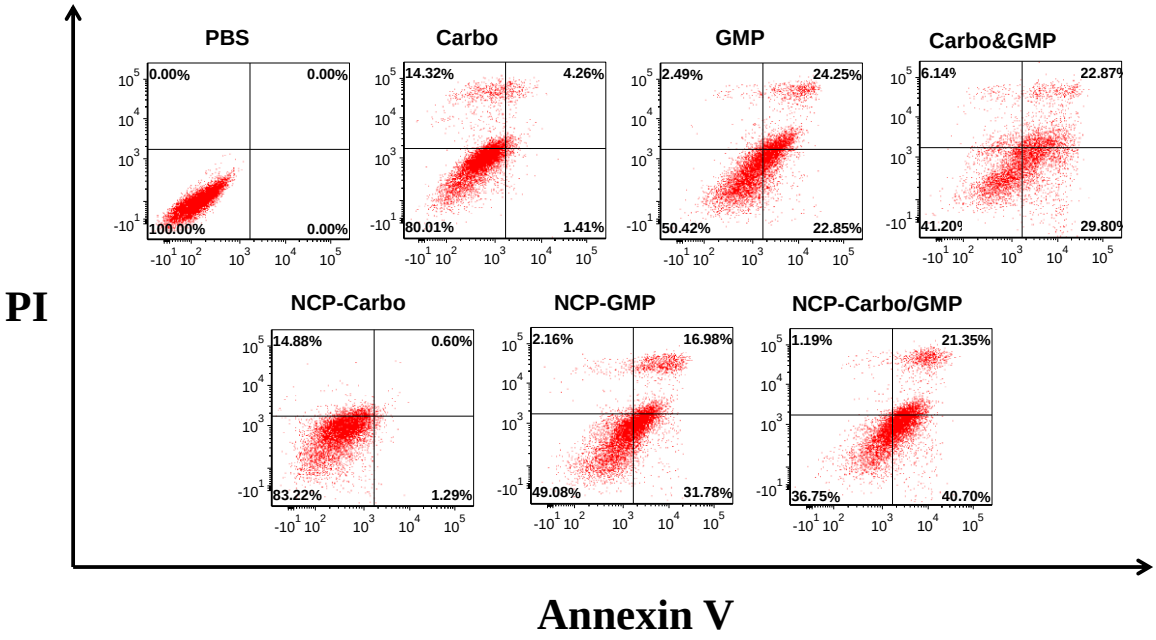

Figure 3.20. Flow cytometry analysis of PBS, Carbo, GMP, Carbo/GMP, NCP-Carbo, NCP-GMP, and NCP-Carbo/GMP in SKOV-3 ovarian cancer cells.

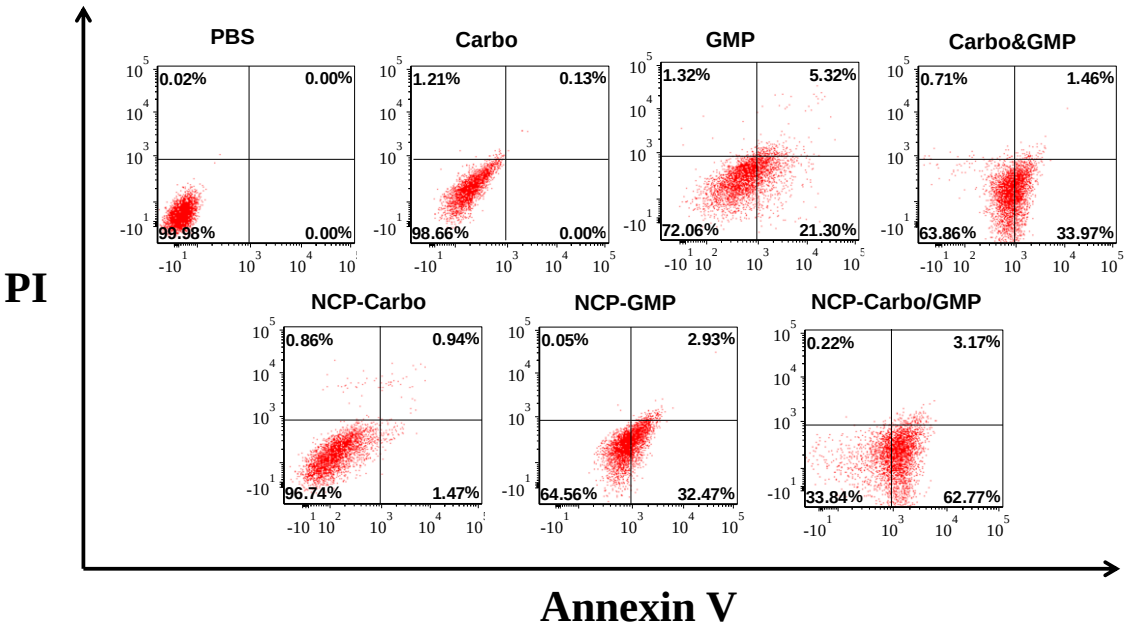

Figure 3.21. Flow cytometry analysis of PBS, Carbo, GMP, Carbo/GMP, NCP-Carbo, NCP-GMP, and NCP-Carbo/GMP in A2780/CDDP ovarian cancer cells.

3.3.5 In Vitro *Cellular Uptakes*

To directly observe the NCP-Carbo/GMP uptake, Rhodamine B-dyed nanoparticles were incubated with either SKOV-3 (Figure 3.22) or A2780/CDDP (Figure 3.23) human ovarian cancer cells and then observed under CLSM. After a 1 h incubation, the nanoparticles were readily taken up by the cells, as evidenced by the co-localization of green fluorescence (Lysotracker Green-stained endosome) and red fluorescence (Rhodamine B-dyed nanoparticle) seen around the exterior of the nucleus. The red fluorescence signal was greatly enhanced after 4 h and 24 h, indicating an increased uptake of this nanoparticle over time.

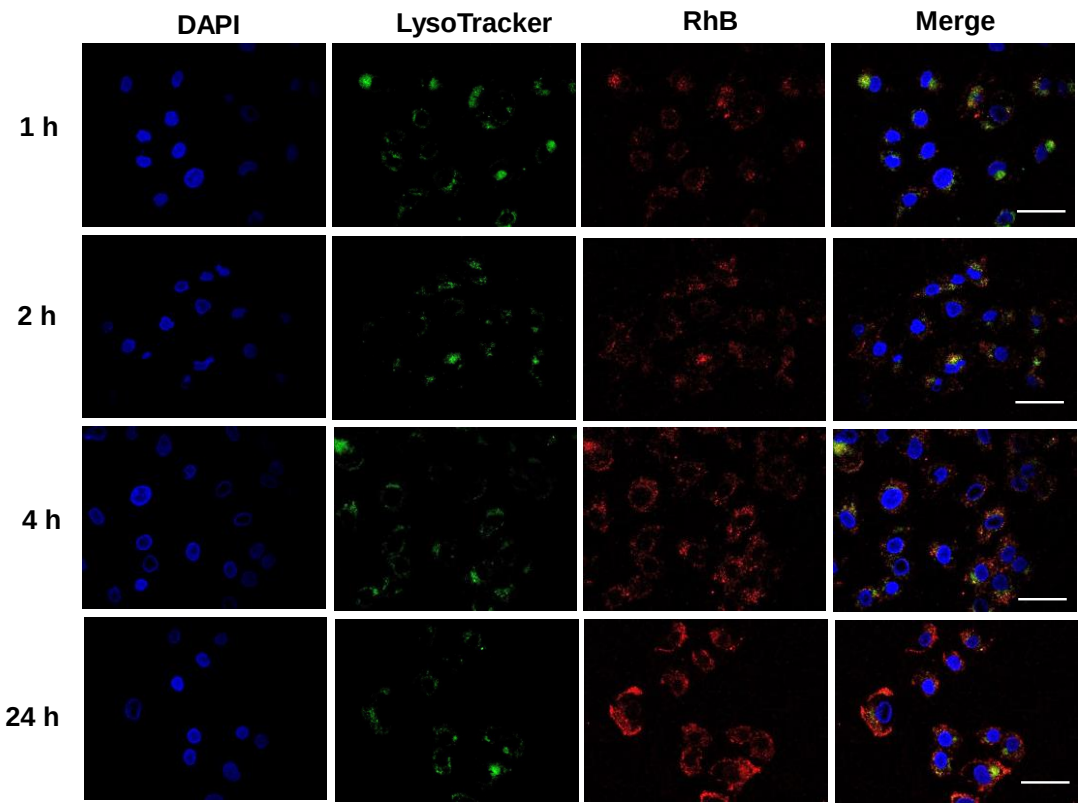

Figure 3.22. CLSM images of co-localization of RhB (red) from Carbo/GMP particles with a late endosome and lysosome marker, LysoTracker (green), in SKOV-3 cells after incubation for varying lengths of time. Scale bars: 20 μm.

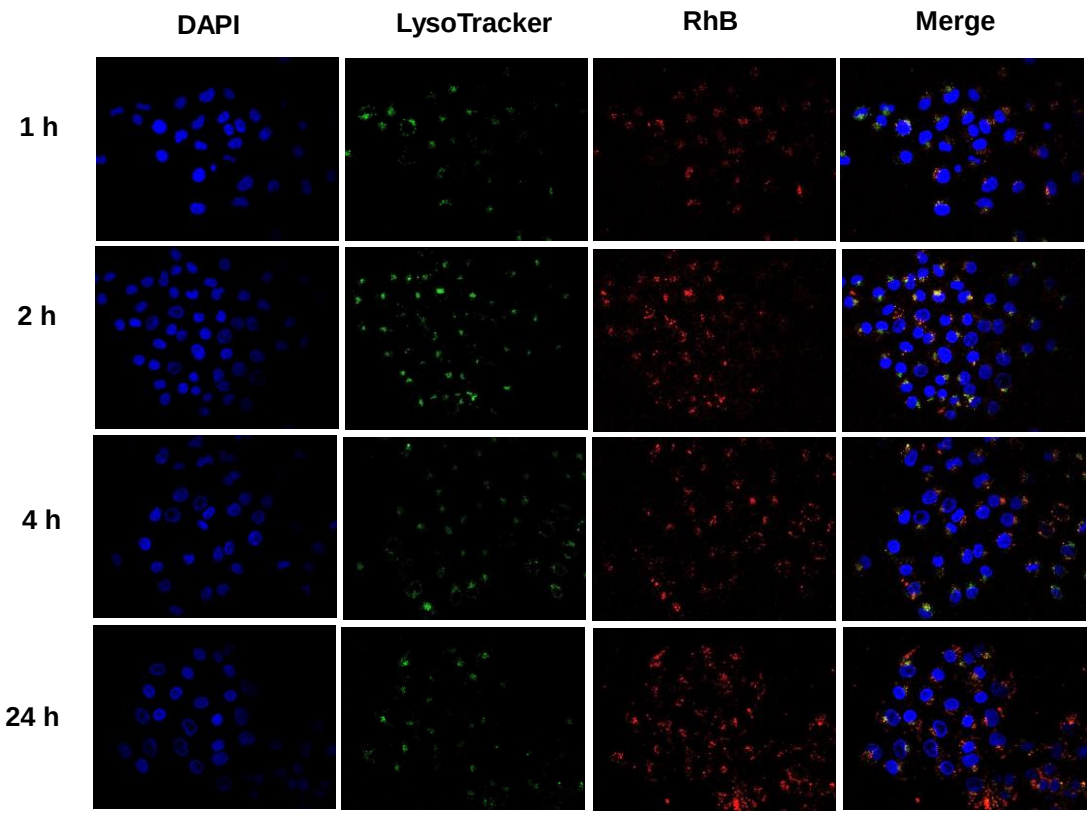

Figure 3.23. CLSM images of co-localization of RhB (red) from Carbo/GMP particles with a late endosome and lysosome marker, LysoTracker (green), in A2780/CDDP cells after incubation for varying lengths of time. Scale bars: 20 μm.

This result was further supported by time-dependent cellular uptake of NCP-Carbo/GMP in SKOV-3 (Fig. 3C, D) and A2780/CDDP (Fig. 3E, F) as determined by ICP-MS. Free carbo showed highest cellular uptake at 1 h, but it decreased by ~50% at 24 h, indicating that the uptake of free carbo is rapid. In contrast, the cellular uptake of NCP-Carbo/GMP increased gradually over time and was significantly higher compared to the free combination drugs. At 24 h, the Pt uptake was 4 times and 5 times higher than the free combination treatments in SKOV-3 and A2780/CDDP, respectively. The cellular uptake of free GMP remained constant throughout the 24-h experiment in A2780/CDDP cells, but decreased by ~50% at 24 h in SKOV-3 cells. The

uptake of NCP-Carbo/GMP, in term of GMP, also showed a slight gradual increase over time, but no significant difference was observed.

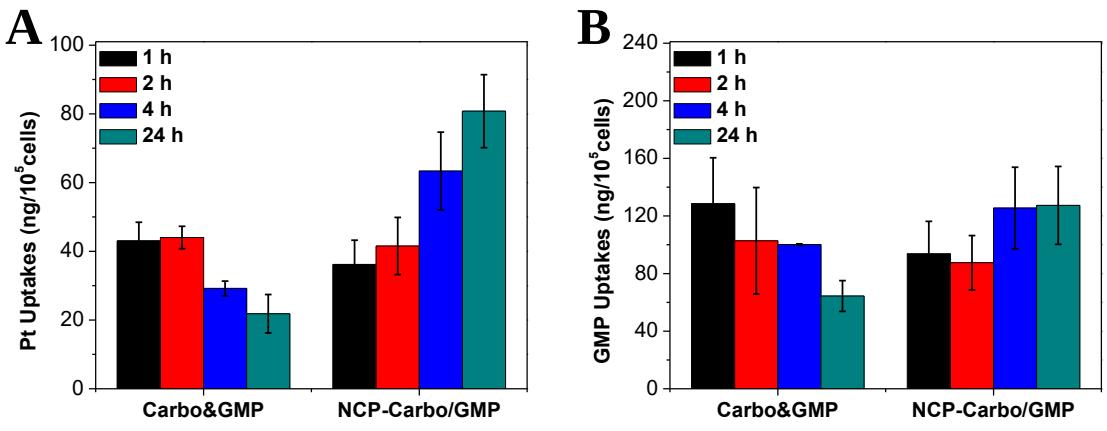

Figure 3.24. Cellular uptake of carbo/GMP and NCP-Carbo/GMP in SKOV-3 cells determined by ICP-MS (Pt uptake) and UV-Vis (GMP uptake). Data expressed as means±S.D. (n=3).

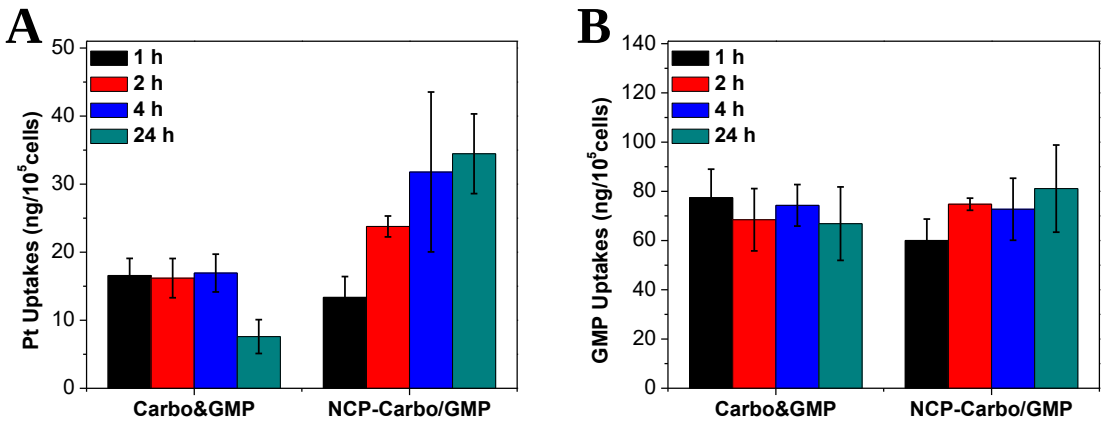

Figure 3.25. Cellular uptake of carbo/GMP and NCP-Carbo/GMP in A2780/CDDP cells determined by ICP-MS (Pt uptake) and UV-Vis (GMP uptake). Data expressed as means±S.D. (n=3).

3.3.6 Pharmacokinetics and Biodistribution

The pharmacokinetics and biodistribution of NCP-Carbo/GMP was investigated in CT26 tumor-bearing mice in order to assess its ability to evade the MPS and accumulate in tumor tissues

(Figure 3.26A). The Pt distribution was quantified by ICP-MS, and the GMP amount in the blood was quantified by HPLC-MS/MS. By i.p. injection, the blood circulation half-lives were fitted with a one-compartment model using PK solver. NCP-Carbo/GMP resulted in Pt and GMP blood circulation half-lives of 11.8 ± 4.8 h (Figure 3.26C) and 9.4 ± 1.4 h (Figure 3.26D), respectively. In addition to the prolonged blood circulation time, tissue Pt distribution profiles of NCP-Carbo/GMP showed its ability to avoid uptake by the MPS, as evidenced by the low percentage of injected dose per gram tissue (% ID/g) in the organs with high MPS activity such as the liver (3.8 ± 2.8 % ID/g), spleen (3.7 ± 3.6 % ID/g), and kidney (4.8 ± 2.2 % ID/g). The slow blood clearance and low MPS uptake led to high tumor accumulation of the drug. The Pt distribution in tumor tissue increased over time, reaching a maximum at 24 h (10.2 ± 4.4 %ID/g), which indicated the high accumulation and long retention of NCP-Carbo/GMP in tumor tissue.

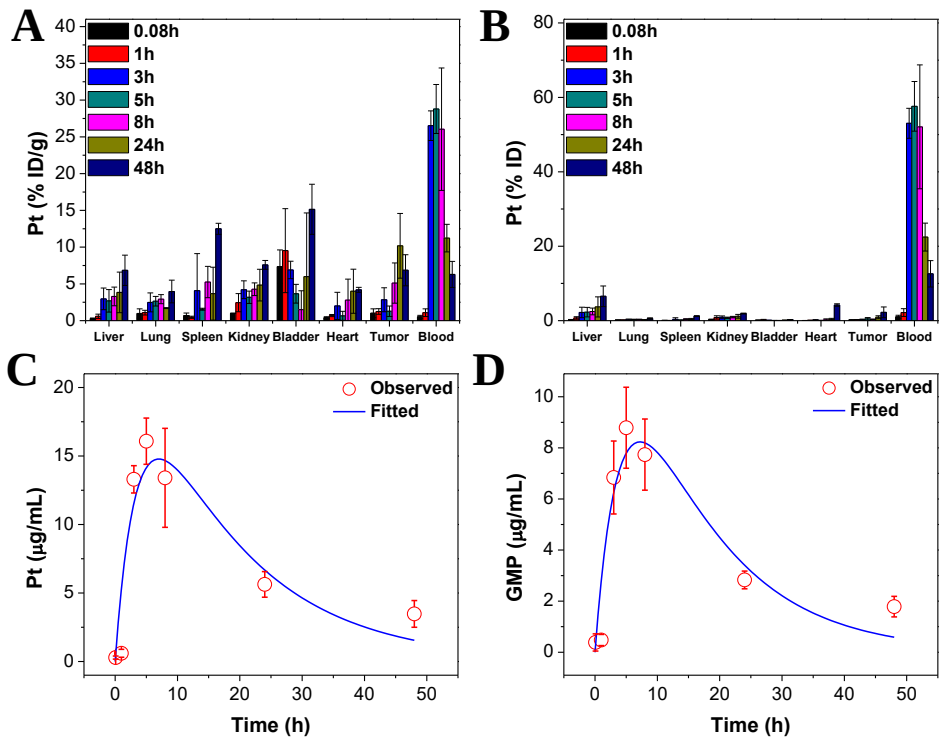

Figure 3.26. (A) Percentage injected dose per gram (% ID/g) and (B) percentage injected dose (% ID) of Pt in tissues and blood after intravenous administration of NCP-Carbo/GMP in CT26 tumor-

Figure 3.26, continued bearing mice at time points 5 min, 1 h, 3 h, 5 h, 8 h, 24 h, and 48 h. Data are mean ± S.D. (n=3). (C) Average observed and predicted time-dependent Pt distributions in blood after administration of NCP-Carbo/GMP (n=3). (D) Average observed and predicted time-dependent GMP distributions in blood after administration of NCP-Carbo/GMP (n=3). One-compartment model was used for fitting the Pt and GMP distributions in blood.

3.3.7 Antitumor Activity In Vivo

The antitumor activity of NCP-Carbo/GMP was evaluated in SKOV-3 and A2780/CDDP subcutaneous xenograft murine models. Mice bearing SKOV-3 or A2780/CDDP tumors were treated once every three days, for a total of three i.p. injections at a dose of 10 mg carbo/kg and 2.4 mg GMP/kg. All of the mice were sacrificed at day 19 for SKOV-3 and day 8 for A2780/CDDP, when the control tumors reached above 2000 mm^3. As shown in Figure 3.27A, NCP-Carbo/GMP showed significant tumor regression in SKOV-3 tumors, with a reduction of 71% compared to the initial tumor volume. For the more aggressive A2780/CDDP tumors, NCP-Carbo/GMP also demonstrated dramatic tumor inhibition, with a tumor inhibitory rate (TIR) of 80% (Figure 3.28A). The tumor weight of NCP-Carbo/GMP-treated group was 90-fold and 12-fold smaller than that of the control in SKOV-3 (Figure 3.27B) and A2780/CDDP (Figure 3.28B) tumors, respectively. On the contrary, mice treated with Carbo&GMP showed a similar tumor growth pattern as PBS, suggesting that free combination drugs caused no antitumor efficacy, possibly because free carbo and GMP do not significantly accumulate in tumor tissue.

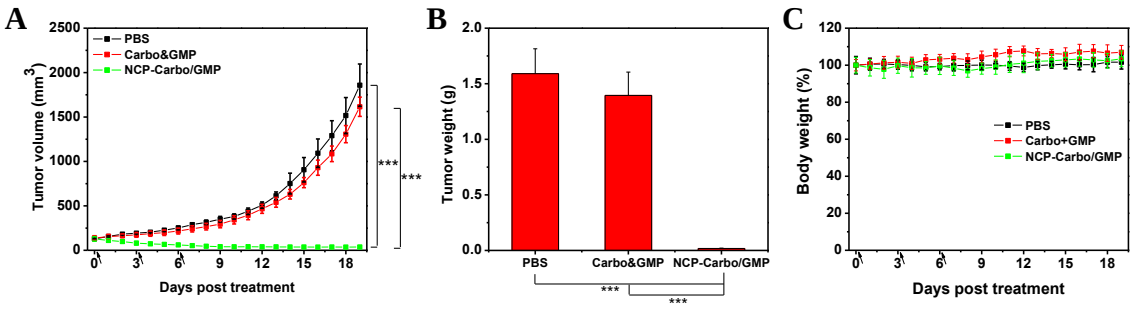

Figure 3.27. Subcutaneous SKOV-3 xenografts: (A) *In vivo* tumor growth inhibition. Carbo (dose, 10 mg/kg) and gem (4.6 mg/kg) and NCP-Carbo/GMP (doses, 10 mg/kg and 4.6 mg/kg) were

Figure 3.27, continued administered on day 0, 3, and 6. (B) End-point tumor weights. (C) Body weight evolution of SKOV-3 tumor-bearing athymic mice treated with NCP-Carbo/GMP (10 mg carboplatin/kg and 2.4 GMP mg/kg). Data are expressed as means±S.D. (n=5), ***p<0.001.

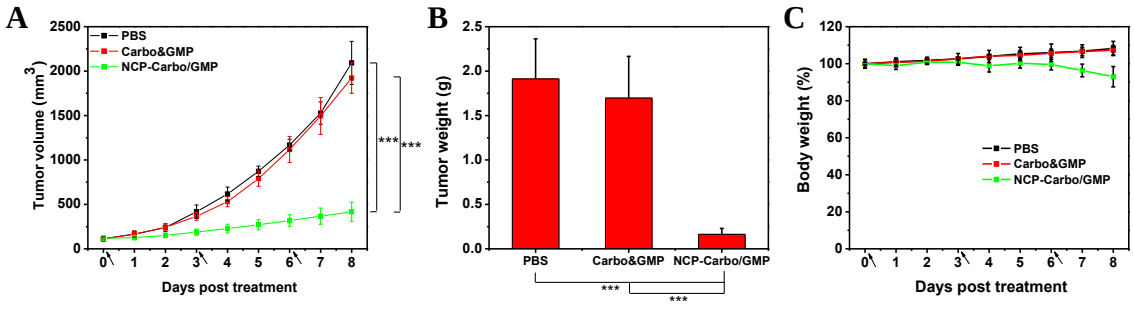

Figure 3.28. Subcutaneous A2780/CDDP xenografts: (A) *In vivo* tumor growth inhibition. Carbo (dose, 10 mg/kg) and gem (4.6 mg/kg) and NCP-Carbo/GMP (doses, 10 mg/kg and 4.6 mg/kg) were administered on days 0, 3, and 6. (B) End-point tumor weights. (C) Body weight evolution of A2780/CDDP tumor-bearing athymic mice treated with NCP-Carbo/GMP (10 mg carboplatin/kg and 2.4 GMP mg/kg). Data are expressed as means±S.D. (n=5), ***p<0.001.

TUNEL assay was performed on the resected tumors to further substantiate and quantify the *in vivo* apoptosis. Figure 3.29B and Figure 3.30B showed that the fluorescence intensity of DNA fragmentation and the relative percentage of apoptotic cells in the NCP-Carbo/GMP-treated group were significantly higher than those in the other groups. NCP-Carbo/GMP induced 92.7±2.4% and 89.3±2.8% tumor cell apoptosis for SKOV-3 and A2780/CDDP, respectively, whereas Carbo&GMP caused 4.0±0.4% and 3.6±0.5% apoptosis for SKOV-3 and A2780/CDDP, respectively. NCP-Carbo/GMP thus exhibited superior anticancer efficacy compared to the free drugs. The histological analysis of tumor tissues also showed that NCP-Carbo/GMP induced tumor tissue apoptosis and necrosis at the highest level, while Carbo&GMP only induced slight tumor tissue apoptosis and necrosis when compared to the PBS-treated group (Figure 3.29A and Figure 3.30A).

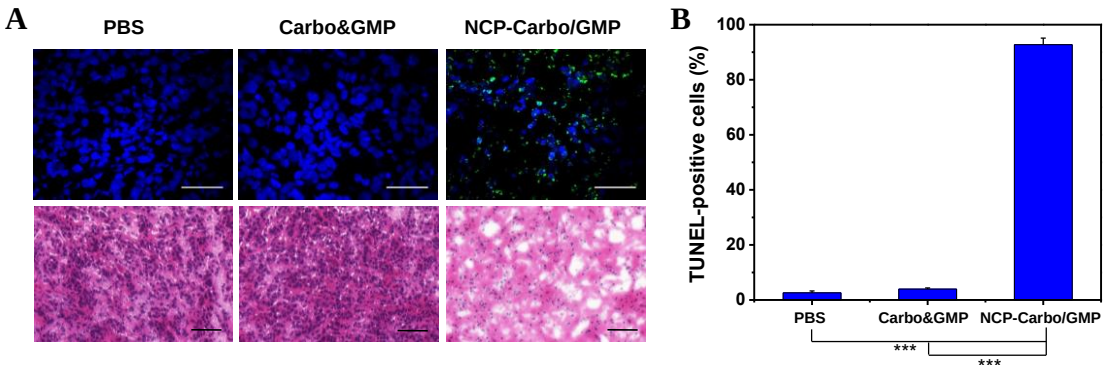

Figure 3.29. (A) Representative CLSM images of TUNEL assays and H&E staining of SKOV-3 tumor tissues. DNA fragment in apoptotic cells was stained with fluorescein-conjugated deoxynucleotides (green) and the nuclei were stained with DAPI (blue). Top bar = 50 μm. Bottom bar = 100 μm. (B) Percentages of TUNEL-positive cells in SKOV-3 tumor tissues.

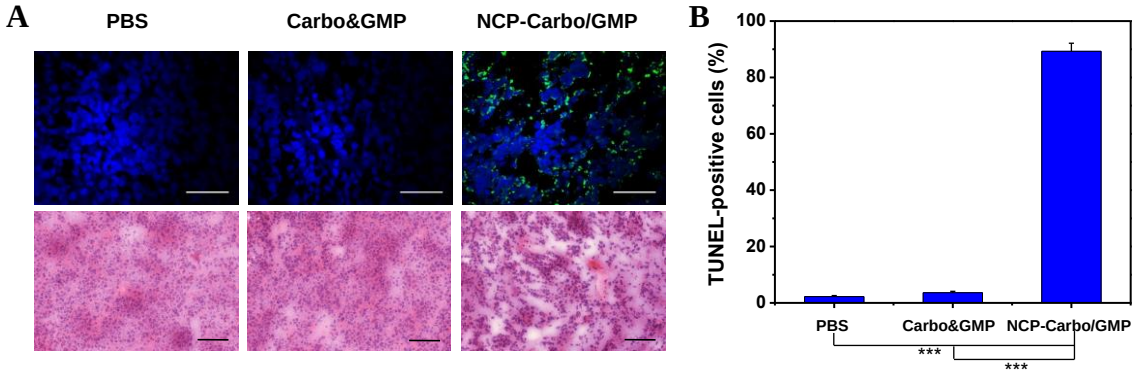

Figure 3.30. (A) Representative CLSM images of TUNEL assays and H&E staining of A2780/CDDP tumor tissues. DNA fragment in apoptotic cells was stained with fluorescein-conjugated deoxynucleotides (green) and the nuclei were stained with DAPI (blue). Top bar = 50 μm. Bottom bar = 100 μm. (B) Percentages of TUNEL-positive cells in A2780/CDDP tumor tissues. Data are expressed as means±S.D. (n=3), ***p<0.001.

No obvious reduction in body weight, immunogenic responses, or histological toxicities were observed after repeated treatment with NCP-Carbo/GMP, suggesting it is safe when applied *in vivo*. No significant weight loss was observed in the NCP-Carbo/GMP treated group, suggesting that it incurs no severe systemic toxicity (Figure 3.27C and Figure 3.28C). The general toxicity was further investigated by immunogenic responses (Figure 3.31) and histological assessments

(Figure 3.32). No statistically significant differences were observed between the control and NCP-Carbo/GMP group in terms of the proinflammatory cytokine production. As seen in the H&E-stained sectioned tissues of the heart, liver, lung, spleen, and kidney, no acute pathological changes were detected in the NCP-Carbo/GMP-treated groups.

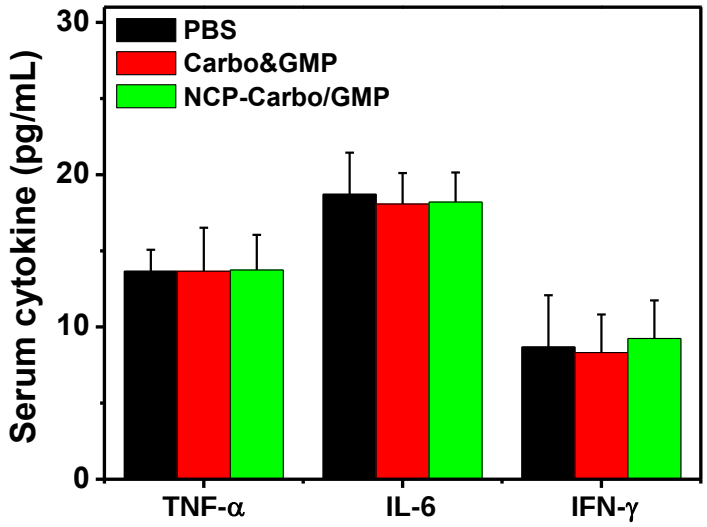

Figure 3.31. Immunogenic response and hypersensitivity induced by saline, Carbo&GMP, and NCP-Carbo/GMP in A2780/CDDP tumor-bearing mice.

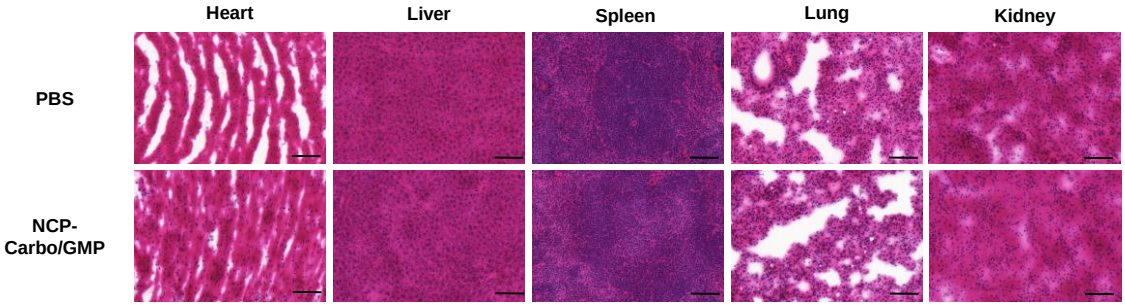

Figure 3.32. Histology images of resected organs (with H&E staining) of A2780/CDDP tumor-bearing mice treated with saline or NCP-Carbo/GMP. Bar = 100 μm.

3.4 Discussion

Treatment of OCa is often limited by the development of Pt resistance after first-line chemotherapy, leading to relapse and ultimately the demise of the patients. Although the combination of cisplatin and gem is FDA-approved for first-line treatment in patients with advanced ovarian cancer, the high toxicity associated with cisplatin often limits the dosage that patients can tolerate, preventing patients from taking advantage of optimal therapeutic effects.[38-40] Furthermore, the combination of cisplatin and gem increases the hematological toxicities of gem. To treat patients with advanced OCa following the failure of initial chemotherapy, either from Pt resistance or high systematic toxicity, a second-line treatment involving the combination of carbo and gem is often used to overcome multidrug-resistant OCa. Currently, carbo is the preferred Pt-based treatment for ovarian cancer because it has fewer side effects than cisplatin. Compared to patients treated with cisplatin, those treated with carbo are far less likely to develop lasting kidney and gastrointestinal damage.[41] Moreover, side effects such as nausea and vomiting are milder under a carbo regimen. In clinical trials, the combination therapy of carbo and gem has been shown to be an effective treatment for patients with Pt-resistant OCa. The combination of carbo and gem has been shown to have a higher response rate and median survival rate than carbo or gem alone in advanced OCa patients.[18,42] Furthermore, the combination of carbo and gem has a comparable median survival rate to cisplatin and gem in non-small cell lung cancer and OCa patients, without the added toxicity of cisplatin.[43-45]

Nanoparticle drug delivery systems that are able to deliver multiple therapeutics agents have shown to enhance antitumor efficacy, overcome multidrug resistance, and reduce addictive toxicity.[46-54] We developed a NCP-platform that combines the chemotherapeutic effect of carbo and gem in a single nanocarrier. We demonstrated that the co-delivery of carbo and gem provides

enhanced synergy and overcomes Pt resistance in OCa. We found that NCP-Carbo/GMP was able to effectively regress Pt-resistant SKOV-3 tumors and dramatically inhibit aggressive A2780/CDDP tumors *in vivo*. The enhanced synergy results from the differing mechanism of actions for carbo and gem, which can delay the development of drug resistance in tumors, thereby reducing the possibility of cancer cell mutations. On the other hand, both carbo and gem target DNA and can function synergistically for better therapeutic efficacy with higher target selectivity. Carbo works by forming an adduct with DNA, thus interfering with DNA replication and inducing cell apoptosis,[55] while gem induces apoptosis by replacing cytidine during DNA replication.[17,56] Due to this synergistic effect, the combination of carbo and gem in a single nanocarrier results in higher therapeutic efficacy with lower toxicity by reducing the administration dosages of each drug.

A major benefit of using nanoparticles of about 10-200 nm in size for drug delivery is their intrinsic ability to target tumors by the enhanced permeability and retention (EPR) effect.[57,58] The particle size of NCP-Carbo/GMP was large enough to avoid renal filtration and small enough to penetrate through the leaky vasculatures in the tumor region, while reducing mononuclear phagocytic system (MPS)-mediated clearance. In addition, the near-neutral surface charge of NCP-Carbo/GMP allows particles to resist opsonization and evade the MPS. The enhanced stability of NCP-Carbo/GMP prevents premature drug leakage before reaching the diseased site, which reduces side effects and increases therapeutic benefits. Once the particles enter the cells, the lipid coating incorporates into the cell and plasma membranes, making the particle coatings more permeable to cysteine or other endogenous reducing agents that cause rapid drug release via reductive degradation of the particles. Our time-dependent drug release showed that NCP-Carbo/GMP exhibited similar drug release profiles both with and without cysteine. On the

contrary, cellular uptake rapidly decreased for free drugs over time, which is attributed to the efflux effect of cells. As a result, NCP-Carbo/GMP has an *in vitro* cell uptake five times higher than that of free drugs. Prolonged blood circulation and enhanced tumor uptake also led to ~90-fold and ~12-fold lower tumor weights, compared to those treated by the control and free combination drugs.

3.5 Conclusion

We developed an NCP platform that combines carbo and gem for successful treatment of Pt-resistant OCa. We show here that carbo and gem produce a synergistic effect in SKOV-3 and A2780/CDDP, and this synergy is retained when this combination is encapsulated inside an NCP. NCP-Carbo/GMP showed a long blood circulation half-life and high drug accumulation in the tumor, resulting in superior tumor regression *in vivo* when compared to free combination drugs. The high antitumor effect, together with the lack of systemic toxicity, suggests that NCPs could be an ideal platform for the smart co-delivery of chemotherapeutic drugs to tumors for more effective cancer treatment.

3.6 References

(1) Arend, R. C.; Londono-Joshi, A. I.; Straughn, J. M., Jr.; Buchsbaum, D. J. *Gynecologic Oncology* **2013**, *131*, 772.

(2) McGuire, W. P.; Markman, M. *Br. J. Cancer* **2003**, *89*, S3.

(3) Markman, M.; Bookman, M. A. *Oncologist* **2000**, *5*, 26.

(4) Neijt, J. P.; ten, B. H. W. W.; van, d. B. M. E.; van, O. A. T.; Willemse, P. H.; Vermorken, J. B.; van, L. A. C.; Heintz, A. P.; Aartsen, E.; van, L. M. *Eur J Cancer* **1991**, *27*, 1367.

(5) Foley, O. W.; Rauh-Hain, J. A.; del, C. M. G. *Oncology (Williston Park)* **2013**, *27*, 288.

(6) Agarwal, R.; Kaye, S. B. *Nature Reviews Cancer* **2003**, *3*, 502.

(7) Pujade-Lauraine, E.; Hilpert, F.; Weber, B.; Reuss, A.; Poveda, A.; Kristensen, G.; Sorio, R.; Vergote, I.; Witteveen, P.; Bamias, A.; Pereira, D.; Wimberger, P.; Oaknin, A.; Mirza, M. R.; Follana, P.; Bollag, D.; Ray-Coquard, I. *J. Clin. Oncol.* **2014**, *32*, 1302.

(8) Bookman, M. A. *Oncologist* **1999**, *4*, 87.

(9) Blackledge, G.; Lawton, F.; Redman, C.; Kelly, K. *Br J Cancer* **1989**, *59*, 650.

(10) Gottesman, M. M. *Annu. Rev. Med.* **2002**, *53*, 615.

(12) Borges-Walmsley, M. I.; McKeegan, K. S.; Walmsley, A. R. *Biochem. J.* **2003**, *376*, 313.

(13) Karran, P. *Carcinogenesis* **2001**, *22*, 1931.

(14) Masuda, H.; Ozols, R. F.; Lai, G. M.; Fojo, A.; Rothenberg, M.; Hamilton, T. C. *Cancer Research* **1988**, *48*, 5713.

(15) Chabner, B. A.; Roberts, T. G. *Nature Reviews Cancer* **2005**, *5*, 65.

(16) Helleday, T.; Petermann, E.; Lundin, C.; Hodgson, B.; Sharma, R. A. *Nature Reviews Cancer* **2008**, *8*, 193.

(17) Hertel, L. W.; Boder, G. B.; Kroin, J. S.; Rinzel, S. M.; Poore, G. A.; Todd, G. C.; Grindey, G. B. *Cancer Research* **1990**, *50*, 4417.

(18) Pfisterer, J.; Plante, M.; Vergote, I.; du Bois, A.; Hirte, H.; Lacave, A. J.; Wagner, U.; Staehle, A.; Stuart, G.; Kimmig, R.; Olbricht, S.; Le, T.; Emerich, J.; Kuhn, W.; Bentley, J.; Jackisch, C.; Lueck, H.-J.; Rochon, J.; Zimmermann, A. H.; Eisenhauer, E. *J. Clin. Oncol.* **2006**, *24*, 4699.

(19) du, B. A.; Luck, H. J.; Pfisterer, J.; Schroeder, W.; Blohmer, J. U.; Kimmig, R.; Moebus, V.; Quaas, J. *Ann Oncol* **2001**, *12*, 1115.

(20) Pfisterer, J.; Vergote, I.; Du, B. A.; Eisenhauer, E. *Int J Gynecol Cancer* **2005**, *15 Suppl 1*, 36.

(21) Lorusso, D.; Di, S. A.; Fanfani, F.; Scambia, G. *Ann Oncol* **2006**, *17 Suppl 5*, v188.

(22) Zhou, B.-B. S.; Bartek, J. *Nature Reviews Cancer* **2004**, *4*, 216.

(23) Bergman, A. M.; Pinedo, H. M.; Peters, G. J. *Drug Resistance Updates* **2002**, *5*, 19.

(24) Hung, S. W.; Marrache, S.; Cummins, S.; Bhutia, Y. D.; Mody, H.; Hooks, S. B.; Dhar, S.; Govindarajan, R. *Cancer Lett. (N. Y., NY, U. S.)* **2015**, *359*, 233.

(25) Burris, H. A., 3rd; Moore, M. J.; Andersen, J.; Green, M. R.; Rothenberg, M. L.; Modiano, M. R.; Cripps, M. C.; Portenoy, R. K.; Storniolo, A. M.; Tarassoff, P.; Nelson, R.; Dorr, F. A.; Stephens, C. D.; Von, H. D. D. *Journal of clinical oncology : official journal of the American Society of Clinical Oncology* **1997**, *15*, 2403.

(26) Sandler, A. B.; Nemunaitis, J.; Denham, C.; Von Pawel, J.; Cormier, Y.; Gatzemeier, U.; Mattson, K.; Manegold, C.; Palmer, M. C.; Gregor, A.; Nguyen, B.; Niyikiza, C.; Einhorn, L. H. *J. Clin. Oncol.* **2000**, *18*, 122.

(27) Liu, D.; Poon, C.; Lu, K.; He, C.; Lin, W. *Nat Commun* **2014**, *5*.

(28) He, C.; Liu, D.; Lin, W. *Biomaterials* **2015**, *36*, 124.

(29) Liu, D.; He, C.; Poon, C.; Lin, W. *J. Mater. Chem. B* **2014**, *2*, 8249.

(30) Rieter, W. J.; Pott, K. M.; Taylor, K. M. L.; Lin, W. *Journal of the American Chemical Society* **2008**, *130*, 11584.

(31) Poon, C.; He, C.; Liu, D.; Lu, K.; Lin, W. *J. Controlled Release* **2015**, *201*, 90.

(32) Yavuz, M. S.; Cheng, Y.; Chen, J.; Cobley, C. M.; Zhang, Q.; Rycenga, M.; Xie, J.; Kim, C.; Song, K. H.; Schwartz, A. G.; Wang, L. V.; Xia, Y. *Nature Materials* **2009**, *8*, 935.

(33) Lee, J. E.; Lee, N.; Kim, H.; Kim, J.; Choi, S. H.; Kim, J. H.; Kim, T.; Song, I. C.; Park, S. P.; Moon, W. K.; Hyeon, T. *Journal of the American Chemical Society* **2010**, *132*, 552.

(34) Risbood, P.; Kane Jr., C. T.; Hossain, T.; Vadapalli, S.; Chadda, S. *Bioorganic & Medicinal Chemistry Letters* **2008**, *18*, 2957.

(35) Liu, W.; Chen, X.; Ye, Q.; Hou, S.; Lou, L.; Xie, C. *Platinum Met. Rev.* **2012**, *56*, 248.

(36) Rochon, F. D.; Massarweh, G. *Inorg. Chim. Acta* **2006**, *359*, 4095.

(37) Singh, M. M.; Szafran, Z.; Pike, R. M. *J. Chem. Educ.* **1990**, *67*, A261.

(38) Dunton, C. J. *Oncologist* **2002**, *7*, 11.

(39) Ozols, R. F.; Young, R. C. *Semin Oncol* **1985**, *12*, 21.

(40) Adams, M.; Kerby, I. J.; Rocker, I.; Evans, A.; Johansen, K.; Franks, C. R. *Acta Oncol* **1989**, *28*, 57.

(41) Canetta, R.; Rozencweig, M.; Carter, S. K. *Cancer Treat Rev* **1985**, *12 Suppl A*, 125.

(42) Fung-Kee-Fung, M.; Oliver, T.; Elit, L.; Oza, A.; Hirte, H. W.; Bryson, P. *Curr Oncol* **2007**, *14*, 195.

(43) Lokich, J.; Anderson, N. *Ann Oncol* **1998**, *9*, 13.

(44) Mazzanti, P.; Massacesi, C.; Rocchi, M. B. L.; Mattioli, R.; Lippe, P.; Trivisonne, R.; Buzzi, F.; De, S. G.; Tuveri, G.; Rossi, G.; Di, L. L.; Sturba, F.; Morale, D.; Catanzani, S.; Pilone, A.; Bonsignori, M.; Battelli, T. *Lung Cancer* **2003**, *41*, 81.

(45) Zatloukal, P.; Petruzelka, L.; Zemanova, M.; Kolek, V.; Skrickova, J.; Pesek, M.; Fojtu, H.; Grygarkova, I.; Sixtova, D.; Roubec, J.; Horenkova, E.; Havel, L.; Prusa, P.; Novakova, L.; Skacel, T.; Kuta, M. *Lung Cancer* **2003**, *41*, 321.

(46) Pathak, R. K.; Dhar, S. *Journal of the American Chemical Society* **2015**, *137*, 8324.

(47) Kolishetti, N.; Dhar, S.; Valencia, P. M.; Lin, L. Q.; Karnik, R.; Lippard, S. J.; Langer, R.; Farokhzad, O. C. *Proceedings of the National Academy of Sciences of the United States of America* **2010**, *107*, 17939.

(48) Salzano, G.; Navarro, G.; Trivedi, M. S.; De Rosa, G.; Torchilin, V. P. *Mol. Cancer Ther.* **2015**, *14*, 1075.

(49) Sarisozen, C.; Abouzeid, A. H.; Torchilin, V. P. *Eur. J. Pharm. Biopharm.* **2014**, *88*, 539.

(50) Wu, X.; He, C.; Wu, Y.; Chen, X.; Cheng, J. *Adv. Funct. Mater.* **2015**, *25*, 6744.

(51) Liu, T.; Yacoub, R.; Taliaferro-Smith, L. D.; Sun, S.-Y.; Graham, T. R.; Dolan, R.; Lobo, C.; Tighiouart, M.; Yang, L.; Adams, A.; O'Regan, R. M. *Mol. Cancer Ther.* **2011**, *10*, 1460.

(52) Lammers, T.; Subr, V.; Ulbrich, K.; Peschke, P.; Huber, P. E.; Hennink, W. E.; Storm, G. *Biomaterials* **2009**, *30*, 3466.

(53) Tardi, P. G.; Dos Santos, N.; Harasym, T. O.; Johnstone, S. A.; Zisman, N.; Tsang, A. W.; Bermudes, D. G.; Mayer, L. D. *Mol. Cancer Ther.* **2009**, *8*, 2266.

(54) Patel, N. R.; Rathi, A.; Mongayt, D.; Torchilin, V. P. *Int. J. Pharm.* **2011**, *416*, 296.

(55) Di Pasqua, A. J.; Goodisman, J.; Dabrowiak, J. C. *Inorg. Chim. Acta* **2012**, *389*, 29.

(56) Plunkett, W.; Huang, P.; Xu, Y.-Z.; Heinemann, V.; Grunewald, R.; Gandhi, V. *Semin. Oncol.* **1995**, *22*, 3.

(57) Matsumura, Y.; Maeda, H. *Cancer Research* **1986**, *46*, 6387.

(58) Maeda, H.; Sawa, T.; Konno, T. *J. Controlled Release* **2001**, *74*, 47.

CHAPTER IV: Nanoscale Coordination Polymers Carrying Cisplatin and Gemcitabine for Synergistic Combination Treatment of Lung Cancers

4.1 Introduction

In the previous two chapters, I described nanoscale coordination polymer (NCP)-platform carrying oxaliplatin or carboplatin with gemcitabine for the synergistic combination treatment of pancreatic and ovarian cancers. In this chapter, my focus shifts to the third of three FDA-approved platin drugs, cisplatin in combination with gemcitabine (gem), for the treatment of both small cell and non-small cell lung cancers. Although progress has been made recently in the treatment of lung cancers, it remains the most deadly cancer, accounting for about 27% of all cancer deaths in the United States, according to the American Cancer Society.[1] Lung cancer is categorized into small cell (SCLC) and non-small cell (NSCLC), which account for 13% and 87% of total lung cancers, respectively. Recent developments in chemotherapy in conjugation with radiotherapy have increased the 5-year survival rate for stage I-III NSCLC patients by 4 to 5%, but the five-year survival rates of SCLC and NSCLC remain abysmal, at about 6% and 21%, respectively.[2]

As described in previous chapters, combination therapy can reduce the side effects induced by high doses of single drugs, enhance the effects of individual drugs, and overcome drug resistance mechanisms.[3,4] The combination of cisplatin and gem is the preferred of only two FDA-approved drug combinations for first-line treatment of NSCLC.[5,6] Recent clinical trials have also shown benefits for the combination of cisplatin and gem for the treatment of SCLC.[7,8] Because most drugs have different pharmacokinetic profiles, nanocarriers must be tailored to control release and optimize their pharmacokinetics.[9] Platinum drugs are often used in

combination for patients with non-small cell lung, ovarian, and metastatic breast cancers. However, the combination of free platinum drugs and gem is not safe in patients with advanced solid tumors due to serious adverse side effects, such as bone marrow suppression, anemia, and neuropathy.[10] Although combination therapy has been shown to be effective in promoting synergism of different drugs and preventing drug resistance through different mechanism of actions,[11-13] the ability of lung cancer cells to resist multiple chemotherapeutics hinders successful treatment, with high recurrence among NSCLC (33%-63%)[14,15] and SCLC patients (50%).[16,17]

Our group has developed NCPs as promising platforms for anticancer drug delivery.[18,19] NCPs consist of polydentate bridging ligands connected by metal ions or clusters that form into a larger repeating network.[20-26] These materials have many characteristics beneficial to drug delivery, such as chemical diversity, high loading capacity, and intrinsic biodegradability, and can be tuned to control drug release. These materials also demonstrate long blood circulation time and dramatic reductions in tumor growth *in vivo*. In this chapter, I describe an NCP platform we developed that contains cisplatin and gem for the combination treatment of SCLC and NSCLC. Cisplatin with gem achieved significantly better response rates and survival benefits than either drug individually administered.[27,28] *In vitro* cytotoxicity assays showed that the combination therapy NCP particles displayed anticancer efficacies superior to those of the monotherapies. *In vivo* studies showed that the Pt-based NCP particles displayed long circulation in the bloodstream, leading to higher drug accumulation in the tumors and a reduction in tumor growth. These results demonstrated the feasibility and benefits of using NCPs as delivery vehicles for multiple drugs.

4.2 Experimental Details

4.2.1 General Experimental:

All starting materials were purchased from Sigma-Aldrich and Fisher (USA), unless otherwise noted, and used without further purification. 1,2-dioleoyl-*sn*-glycero-3-phosphate (DOPA), 1,2-distearoyl-*sn*-glycero-3-phosphocholine (DSPC), cholesterol, and 1,2-distearoyl-*sn*-glycero-3-phosphoethanolamine-N-[amino(polyethylene glycol)2000] (DSPE-PEG2k) were purchased from Avanti Polar Lipids (USA).

Human small cell lung cancer cells H82 and H69 were a gift from Professor Ravi Salgia of University of Chicago Medicine and cultured in RPMI 1640 medium (Gibco, Grand Island, NY, USA) supplemented with 10% FBS. Human non-small cell lung cancer cells H460 and A549 were purchased from Developmental Therapeutics Core, Northwestern University and cultured in RPMI 1640 medium (Gibco, Grand Island, NY, USA) supplemented with 10% FBS.

Athymic female nude mice (6 weeks, 24-26 g), BALB/c female mice (6 weeks, 22-24 g), and SD/CD female rat (6 weeks, 220-250 g) were provided by Harlan Laboratories, Inc (USA). The study protocol was reviewed and approved by the Institutional Animal Care and Use Committee (IACUC) at the University of Chicago.

4.2.2 Synthesis of Cisplatin Prodrug:

Cisplatin prodrug PtBp was synthesized based on protocols in the literature (Figure 4.1).[18,29] To a suspension of cis,cis,trans-[$Pt(NH_3)_2Cl_2(OH)_2$](0.5 g, 1.5 mmol) in 2mL DMF was added a 1mL DMF solution containing 4 mol eq. of diethoxyphosphinyl isocyanate (0.92mL, 6.0 mmol). The resulting mixture was stirred for 12 h at room temperature in the dark. The solution was filtered, and the desired product was precipitated by the addition of diethyl ether and washed

with ether twice to remove residual DMF. ^{1}H NMR in DMSO-d^6. δ 6.59 (s, 6H); 3.99 (m, 8H); 1.20 (m, 12H); Yield: 80%.

The bisphosphonate ester complex (250 mg, 0.36 mmol) was put under vacuum for 4 h and dissolved in dry DMF. Trimethylsilyl bromide (475 μL, 3.6 mmol) was added at 0^{o}C, and the mixture was allowed to react for 18 h at room temperature in the dark under N_2. After concentrating, the desired product was precipitated by the addition of DCM and then washed with DCM at least twice. The solid was dissolved in MeOH and stirred at room temperature for 8 h in order to hydrolyze the silyl ester. After concentrating the mixture, DCM was poured into the reaction mixture to precipitate the desired product, and the solid was washed with DCM twice. ^{1}H NMR in D_2O. δ 6.49 (t, 6H); 5.32 (s, 2H); 3.21 (m, 1H); 3.00 (m, 1H); 2.88 (s, 1H); 2.72 (s, 1H); 2.58 (s, 1H). Yield: 60%.

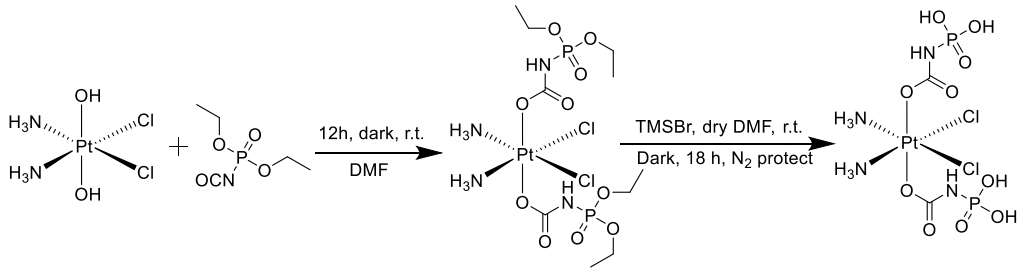

Figure 4.1 Synthesis of bisphosphonic acid ligands based on PtBp prodrugs.

4.2.3 Particle Synthesis and Characterization:

4.2.3.1 Preparation of NCP-Cis/GMP: DOPA-capped NCP-Cis/GMP nanoparticles carrying a cisplatin prodrug and gemcitabine monophosphate (GMP) were synthesized by reverse microemulsion. Twenty-five mg/mL cis,cis,trans-[$Pt(NH_3)_2Cl_2(OCONHP(O)(OH)_2)_2$] (8.6 μmol), 25 mg/mL GMP sodium salt solution (14.6 μmol), and DOPA (22 μmol) were added to a 5 mL aliquot of Triton-X-100 (0.3 M in 1.5 M hexanol/cyclohexane) solution to form a *W*=7.4

microemulsion. Another microemulsion of 5 mL Triton-X-100 (0.3 M, 1.5 M hexanol/cyclohexane) containing $Zn(NO_3)_2 \cdot 6H_2O$ aq. (131 mmol) was also prepared. The two microemulsions were stirred vigorously for 15 min at room temperature, and then combined and stirred for an additional 30 min at room temperature. After the addition of 20 mL ethanol, the NCP-Cis/GMP particles were washed once with ethanol, once with 50% (v/v) ethanol/cyclohexane, twice with 50% (v/v) ethanol/THF, and then redispersed in THF.

4.2.3.2 Preparation of NCP-Cis: A *W*=7.4 microemulsion was prepared by the addition of 0.2 mL of a 25mg/mL PtBp sodium salt aqueous solution and 0.2 mL of a 100mg/mL $Zn(NO_3)_2$ aqueous solution to separate 5 mL aliquots of a 0.3 M Triton X-100/1.5 M 1-hexanol in cyclohexane mixture while vigorously stirring at room temperature. 20 μL DOPA (200 mg/mL in $CHCl_3$) was added to the complex solution and stirred for 15mins, until a clear solution formed. The two microemulsions were combined, and the resulting 10 mL microemulsion with *W*=7.4 was stirred for an additional 30 minutes. After the addition of 20 mL ethanol, NCP-Cis was washed once with ethanol, once with 50% EtOH/cyclohexane, and once with 50% EtOH/THF, then redispersed in THF.

4.2.3.3 Preparation of NCP-GMP: A *W*=7.4 microemulsion was prepared by the addition of 0.2 mL of a 25mg/mL GMP sodium salt aqueous solution and 0.2 mL of a 100mg/mL $Zn(NO_3)_2$ aqueous solution to separate 5 mL aliquots of a 0.3 M Triton X-100/1.5 M 1-hexanol in cyclohexane mixture while vigorously stirring at room temperature. 40 μL DOPA (200 mg/mL in $CHCl_3$) was added to the complex solution and stirred another 15 mins, until a clear solution formed. The two microemulsions were combined, and the resultant 10 mL microemulsion with *W*=7.4 was stirred for an additional 30 minutes. After adding 20 mL ethanol, NCP-GMP was

washed once with ethanol, once with 50% EtOH/cyclohexane, and once with 50% EtOH/THF, then redispersed in THF.

4.2.3.4 General Procedures of Lipid Coating and PEGylation: NCP-Cis/GMP was prepared by adding a THF solution (80 μL) of DOPC, cholesterol, DSPE-PEG_{2k} (cholesterol:DSPC:DSPE-PEG2k=1:1:0.75 in molar ratio) and DOPA-NCP-Cis/GMP to 500 μL of 30% (v/v) ethanol/water at 60 °C. The mixture was stirred at 1,700 rpm for 1 min. THF and ethanol were completely evaporated and the NCP-Cis/GMP/siRNAs solution was allowed to cool to room temperature.

4.2.3.5 Characterization of NCP Particles: ICP-MS (Agilent 7700X, Agilent Technologies, USA) was utilized to analyze the Pt concentration of NCP to calculate cisplatin loadings. GMP loading was determined by UV-Vis spectroscopy and thermogravimetric analyses (TGA). Particles were digested overnight in 6 M hydrochloric acid, and the concentration of GMP in the solution was determined by the absorbance at 275 nm using a Shimadzu UV-2401PC UV-Vis Spectrophotometer. Transmission electron microscopy (TEM, Tecnai Spirit, FEI, USA) was used to observe the morphology of NCP-Cis/GMP/siRNAs.

4.2.4 In Vitro *Stability Studies:*

Particle stability was evaluated *in vitro* in phosphate buffered saline (PBS) buffer with bovine serum albumin (BSA)-binding and time-dependent drug release. BSA binding analysis was performed by dispersing 0.45 mg of NCP-Carbo/GMP in 1 mL PBS containing BSA (30 nM) at 37 ^{o}C. DLS measurements were detected every hour for 24 hours to determine the size of nanoparticles in suspension over time.

The long-term stability of NCP-Cis/GMP was evaluated by storing the nanoparticle in DEPC-treated water at 4 ºC. DLS measurements were detected periodically for six months to determine the size of nanoparticles in suspension over time.

4.2.5 In Vitro *Drug Release:*

In vitro release profiles of cisplatin and GMP from NCP-Cis/GMP were performed in 400 mL in PBS buffer with or without 5 mM cysteine at 37 °C in pH 7.4. DOPA-NCP-Cis/GMP or NCP-Cis/GMP (2 mg) were suspended in 4 mL of 1x PBS buffer solution with or without 5 mM cysteine in a 10,000 MWCO pleated dialysis bag. The dialysis bag containing the nanoparticle suspension was added into the beaker containing 400 mL of 1x PBS buffer, incubated at 37 °C at pH 7.4, while stirring. 1 mL aliquots of solution were taken from the solution at preset time intervals, and a fresh 1 mL of buffer solution with or without cysteine was added to the beaker. The removed aliquot was digested in nitric acid or HCl and analyzed by ICP-MS for Pt or UV-Vis for GMP.

4.2.6 In Vitro *Cytotoxicity of NCP-Cis/GMP:*

Confluent H82, H69, H460 and A549 cells were trypsinized and counted with a hemocytometer. Cells were plated in 96-well plates at a cell density of 4000 cells/well for H82 and H69, and 750 cells/well for H460 and A549 in 100 μL media. Plates were incubated at 37 °C and 5 % CO2 overnight. Media was removed from wells, and then the wells were redispersed with fresh media. Afterwards, different concentrations of cisplatin, GMP, free cisplatin/GMP mixture [at the same NCP-Cis and GMP-NCP (NCP carrying GMP) drug dose], Zn Control (NCP carrying no drugs), NCP-Cis, NCP-Cis/GMP in PBS were added to wells. The plates were incubated at 37 °C and 5 % CO2 for 72 h, and viability was determined *via* MTS assay (Promega, USA) according to manufacturer's instructions. IC_{50} values were measured.

4.2.7 Cell Apoptosis by Flow Cytometry:

H82, H69, H460, or A549 cells were seeded at 5×10^5 cells/well in 6-well plates containing 2 mL total volume of cell culture medium for 24 hours at 37 °C and 5% CO_2. The culture medium was replaced with fresh medium containing different drug treatments at a cisplatin concentration of 0.4 μM for H82 cells, 0.8 μM for H69 cells, 1.7 μM for H460 cells, and 0.04 μM for A549 cells and/or a GMP concentration of 0.8 μM for H82 cells, 1.8 μM for H69 cells, 3.3 μM for H460 cells, and 0.09 μM for A549 cells. Following a 24-hour incubation, the floating and adherent cells were collected and stained with Annexin V/dead cell apoptosis kit with Alexa Fluor 488 annexin V and propidium iodide (PI, Invitrogen, USA) according to manufacturer's instructions. The apoptosis was analyzed on a flow cytometer (LSRII 3-8, BD, USA).

4.2.8 In Vivo *Pharmacokinetic and Biodistribution of NCP-Cis/GMP:*

BALB/c mice bearing CT26 tumors were intravenously injected with NCP-Cis/GMP at 1 mg/kg cisplatin dose (or 2 mg/kg GMP dose). Mice were sacrificed at 5 minutes, 1 hour, 3 hours, 8 hours, 24 hours, and 48 hours post-injection. Their livers, lungs, spleens, kidneys, hearts, bladders, tumors, and blood were harvested and analyzed for Pt concentration using ICP-MS. GMP concentrations in plasma were further analyzed using LC-MS (Agilent 6460 QQQ MS-MS) according to the following procedure. 200 μL ice-cold acetonitrile was added to 50 μL plasma, which was then vortexed, mixed, and centrifuged. The resulting supernatant was evaporated and reconstituted in 100 μL of water. 20 μL samples were used for injections. The autosampler and column temperatures were kept at 4 and 30 °C, respectively. The samples were separated via a PGC Hypercarb column (100 × 2.1 ID, 5 μm, Thermo Fisher Scientific) fitted with a guard column (Hypercarb 10 × 2.1, 5 μm, Thermo Fisher Scientific). A gradient mobile phase of (A) 10 mM ammonium acetate at pH 10 and (B) acetonitrile were used with an initial mobile phase of 95%

solvent A and 5% solvent B at a flow rate of 0.3 mL/min. After 2 minutes, solvent A was gradually decreased to 80% over 0.2 minutes and held at this condition for 5.6 minutes. The gradient was then returned to 95% solvent A over 0.2 minutes and held at this condition for an additional 7 minutes, for a total run time of 15 minutes. The mass to charge transition was monitored from 342 to 231.

4.2.9 In Vivo *Pharmacokinetics of NCP in Red and White Blood Cell Layer and Plasma Layer:*

BALB/c mice were intraperitoneally injected with Alexa Fluor 647 labeled siRNA NCP containing cisplatin (NCP-Cis/siRNA) at 1 mg/kg cisplatin dose. Blood was drawn from the mouse at 3 h, 5 h, and 8 h post-injection. Whole blood was centrifuged at 3000 rpm for 10 min to separate the red and white blood cell layer and plasma layer. The two layers were digested with nitric acid and analyzed for Pt concentration by ICP-MS.

BALB/c mice bearing CT26 tumors were intravenously injected with NCP-Cis/GMP at 1 mg/kg cisplatin dose (or 2 mg/kg GMP dose). Blood was drawn from each mouse 5 minutes post-injection. Whole blood was centrifuged at 3000 rpm for 10 min to separate the red and white blood cell layer and plasma layer. The two layers were digested with hydrochloric acid and acetonitrile and analyzed for GMP concentration by LC-MS.

4.2.10 In Vivo *Maximum Tolerated Dose:*

BALB/c mice were intraperitoneally injected with NCP-Cis/GMP at different dosing schedules: 1) 1.5 mg cisplatin/kg and 3.3 mg GMP/kg once, 2) 1.0 mg/kg cisplatin/kg and 2.2 mg GMP/kg every 3 days for a total of three injections, and 3) 0.6 mg cisplatin/kg and 1.3 mg GMP/kg every five days for a total of five injections. Body weights were measured every day. Mice with over 20% weight loss were euthanized. The maximum tolerated dose was inferred based on the group in which all mice survived and did not lose over 20% weight.

SD/CD rats were intravenously injected with NCP-Cis/GMP at 2 mg cisplatin/kg and 4.4 mg GMP/kg for a total of four injections. Body weights were measured every day. Rats with over 20% weight loss were euthanized. The maximum tolerated dose was inferred based on the group in which all rats survived and did not lose over 20% of their body weight.

4.2.11 In Vivo *Anticancer Efficacy of NCP-Cis/GMP in Subcutaneous Xenograft Mouse Models:*

H82 tumor cells (5 x 10^6 cells per mouse) were subcutaneously injected in the right flank region of 6-week old female athymic mice. When the tumor volumes reached about 150-200 mm^3, the mice were randomly divided into groups and intraperitoneally injected with PBS or NCP-Cis/GMP (0.6 mg cisplatin/kg or 1.3 mg GMP/kg). Tumor sizes were calculated by measuring two perpendicular diameters with a caliper as follows: ($width^2 \times length)/2$. The tumor volumes were measured daily. Body weights for each mouse were recorded every other day. Humane sacrifice of the mice was performed when tumors reached 2000 mm^3 or at the completion of the experiment.

4.2.12 Statistical Analysis:

Results were expressed as means ± standard deviation (S.D.).

4.3 Results and Discussion

4.3.1 Synthesis and Characterization of NCP-Cis/GMP:

DOPA-capped NCP-Cis/GMP nanoparticles containing cisplatin prodrug, cis,cis,trans-$[Pt(NH_3)_2Cl_2(OCONHP(O)(OH)_2)_2]$ (PtBp), and gem prodrug, gemcitabine monophosphate (GMP), were coated with DSPC, cholesterol, and DSPE-PEG2k at 1:1:0.75 mol ratio. The Z-average, number-average, PDI, and zeta-potential for NCP-Cis/GMP were 83.0±1.0 nm, 51.2±0.1 nm, 0.143±0.011, and -2.84±0.22 mV, as measured by dynamic light scattering (DLS) (Figures

4.2, Table 4.1). Transmission electronic microscopy (TEM) showed that NCP-Cis/GMP particles were well-dispersed, with spherical morphology, implying that the lipid coating did not disrupt the NCP core. The particle size of NCP-Cis/GMP was beneficial for tumor-targeting delivery, which was large enough to avoid renal filtration and small enough to penetrate through the leaky vasculatures in tumors, while reducing mononuclear phagocytic system (MPS)-mediated clearance. In addition, NCP-Cis/GMP had a near neutral zeta potential, indicating that the PEG chains were successfully coated on the particle surface, allowing them to resist opsonization and evade the MPS.

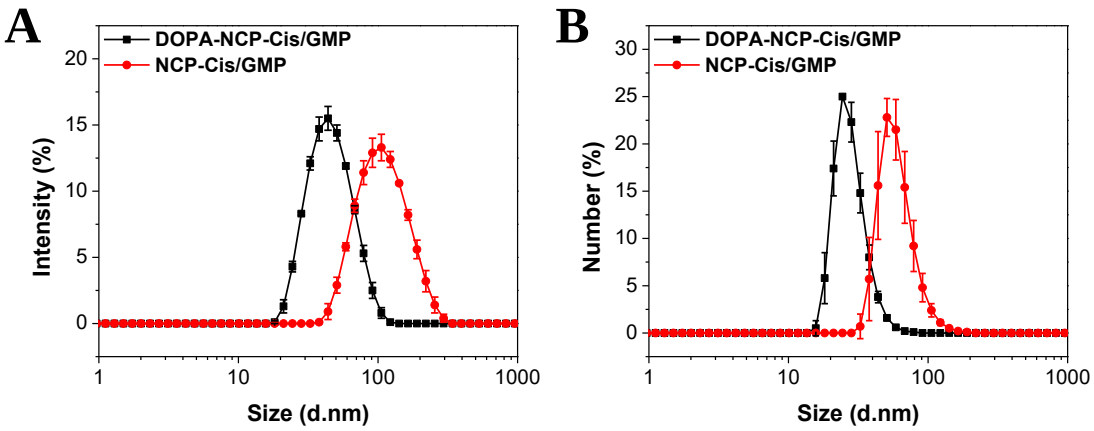

Figure 4.2. (A) Intensity-average and (B) number-average size distribution of NCP-Cis/GMP particles. Bare and lipid-coated particles were measured in THF and PBS, respectively. Reprinted with permission from Journal of the American Chemical Society, 2016, *138*, 6010-19. Copyright 2016 American Chemical Society.

Table 4.1. Sizes, Polydispersities, and Zeta Potentials of NCP Particles.

NCPs	Z-Ave diameter (nm)	Number-Ave diameter (nm)	PDI	Zeta Potential (mV)
DOPA-NCP-**Cis/GMP**	42.4±0.1[#]	28.0±1.0[#]	0.116±0.006	NA
NCP-**Cis/GMP**	83.0±1.0[$]	51.2±0.1[$]	0.143±0.011	-2.84±0.22[$]
DOPA-NCP-**Cis**	59.4±0.2[#]	28.1±3.3[#]	0.190±0.007	NA
NCP-**Cis**	88.8±1.6[$]	50.0±2.9[$]	0.166±0.004	-0.90±0.50[$]
DOPA-NCP-**GMP**	66.6±0.1[#]	40.4±0.7[#]	0.128±0.008	NA
NCP-**GMP**	95.2±1.4[$]	56.4±2.2[$]	0.179±0.009	-5.87±0.40[$]

[#]Measured in THF. [$]Measured in PBS buffer. Data are expressed as means±S.D.

DOPA-NCP-Cis/GMP gave cisplatin loadings of 12.9±1.4 wt.% (24.9±2.7 wt.% prodrug loading), as measured by inductively coupled plasma mass spectrometry (ICP-MS). UV-Vis and thermogravimetric analysis (TGA) measurement of DOPA-NCP-Cis/GMP gave gemcitabine monophosphate (GMP) loadings of 26.7±2.3 wt.% (Figure 4.4 and Figure 4.5). TGA analysis between DOPA-NCP-Cis/GMP with and without DOPA gave DOPA loading of 8.2 wt.% (Figure 4.5).

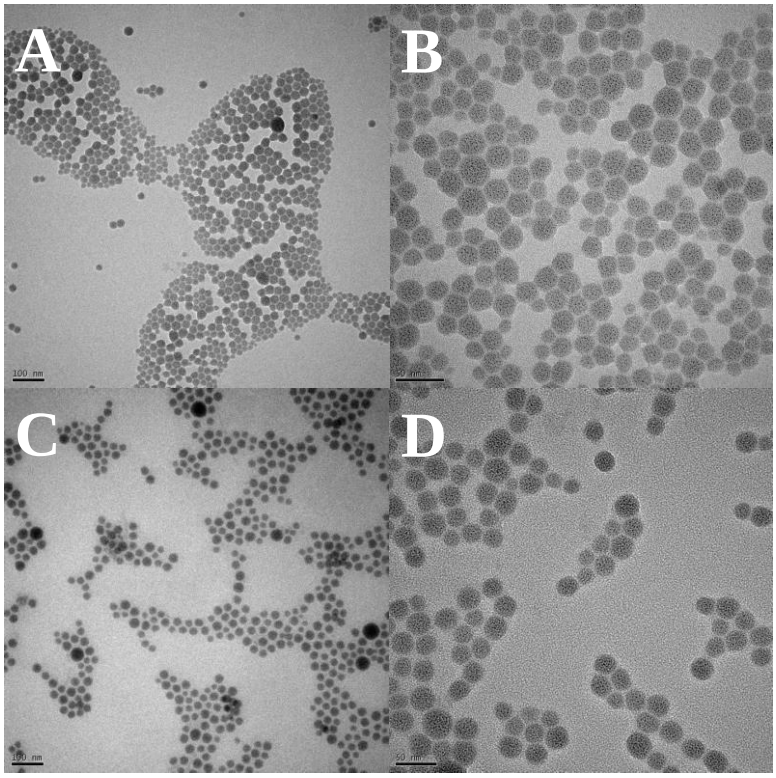

Figure 4.3. TEM micrographs of DOPA-NCP-Cis/GMP (A, B) and NCP-Cis/GMP (C, D). Reprinted with permission from Journal of the American Chemical Society, 2016, *138*, 6010-19. Copyright 2016 American Chemical Society.

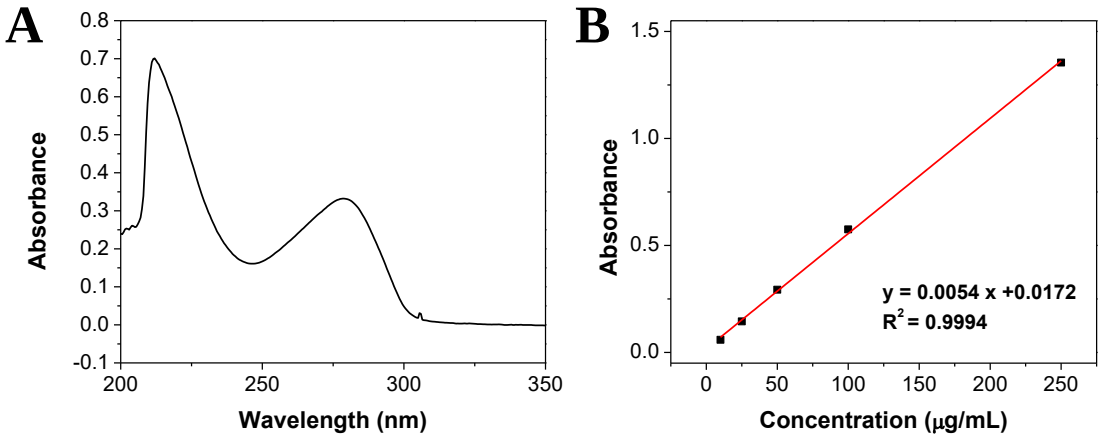

Figure 4.4. UV-Vis analysis and standard curve of DOPA-NCP-Cis/GMP to determine GMP wt.% loading.

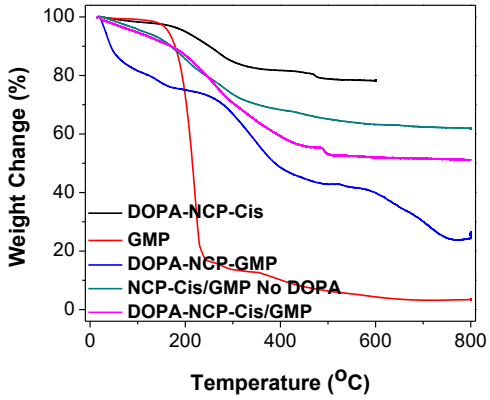

Figure 4.5. TGA analysis of DOPA-NCP-Cis/GMP to determine GMP wt% loading. Reprinted with permission from Journal of the American Chemical Society, 2016, *138*, 6010-19. Copyright 2016 American Chemical Society.

The particle stability was evaluated *in vitro* in phosphate buffered saline (PBS) buffer with bouvine serum albumin (BSA) binding and time dependent drug release (Figure 4.6). BSA binding analysis was done by dispersing 0.5 mg of NCP-Cis/GMP in 1 mL PBS containing BSA (30 nM) at 37°C. DLS measurements were detected every 1 hour for 24 hours to determine the size of nanoparticles in suspension over time. The particle sizes, PDI, and count rate remained constant over a 24-h period.

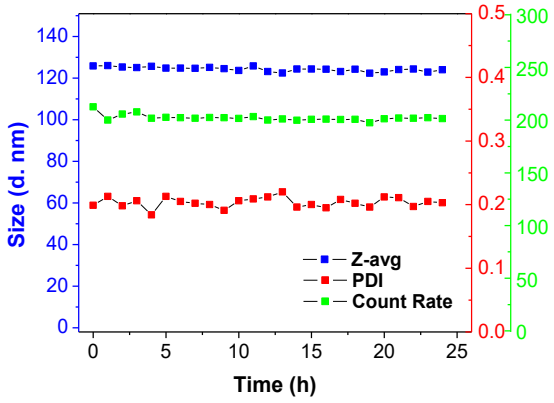

Figure 4.6. Stability test of NCP-Cis/GMP after PEGylation in PBS buffer with BSA at 37 °C over a 24 h-period. Reprinted with permission from Journal of the American Chemical Society, 2016, *138*, 6010-19. Copyright 2016 American Chemical Society.

The long-term stability of NCP-Cis/GMP was evaluated by storing the nanoparticle in DEPC-treated water at 4 ºC (Figure 4.7). The particle size remained consistent over the span of 160 days, demonstrating the incredible stability of the nanoparticle for long-term storage. The ability for the particle to remain in suspension for such a long duration without compromising its stability will ultimately make it easier for clinicians to administer the drug. All of these characters give the particles prolonged circulation time and improved tumor uptake, enhancing their antitumor effect.

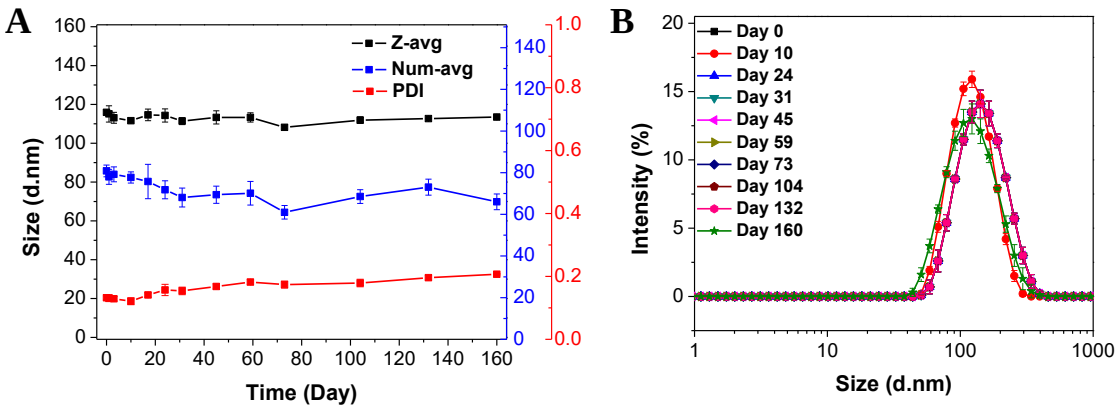

Figure 4.7. (A) Long-term NCP-Cis/GMP size stability test of NCP-Cis/GMP stored in DEPC-treated water in 4ºC. (B) Intensity-average size distribution of NCP-Cis/GMP over a 160-day duration.

4.3.2 In Vitro *Drug Release*

In vitro release profiles of cisplatin and GMP from NCP-Cis/GMP were performed in 400 mL in 1x PBS buffer with or without 5 mM cysteine at 37ºC in pH 7.4 (Figure 4.8). DOPA-NCP-Cis/GMP or NCP-Cis/GMP (2 mg) were suspended in 4 mL of 1x PBS buffer solution with or without 5 mM cysteine in a 10,0000 MWCO pleated dialysis bag. The dialysis bag containing the nanoparticle suspension was added to a beaker containing 400 mL of 1x PBS buffer and incubated at 37ºC in pH 7.4, while stirring. Periodically, 1 mL aliquots of solution were taken from the

solution, and a fresh 1 mL of buffer solution with or without cysteine was added to the beaker. The removed aliquot was digested in nitric acid or HCl and analyzed by ICP-MS for Pt or UV-Vis for GMP, respectively. Pt release showed only 6.3% for NCP-Cis/GMP after 96 h, while DOPA-NCP-Cis/GMP showed rapid burst release, with 47% total Pt release before 12 h. Only 11% GMP release was observed after 12 h as compared to 29% for DOPA-NCP-Cis/GMP. Drug release was also simulated in the presence of 5 mM cysteine with 92% Pt release and 63% GMP release before 12 h, indicating that the NCPs undergo reductive degradation to release the drugs; NCP-Cis/GMP exhibited a similar drug release pattern in both PBS and PBS with cysteine. PEGylation of particles made it difficult for cysteine to penetrate lipid layer, improving the stability of the particle in the bloodstream. Once the particles enter the cells, the lipid coating is incorporated into the cell and plasma membranes, allowing cysteine to penetrate the core particle, triggering release of the drugs.

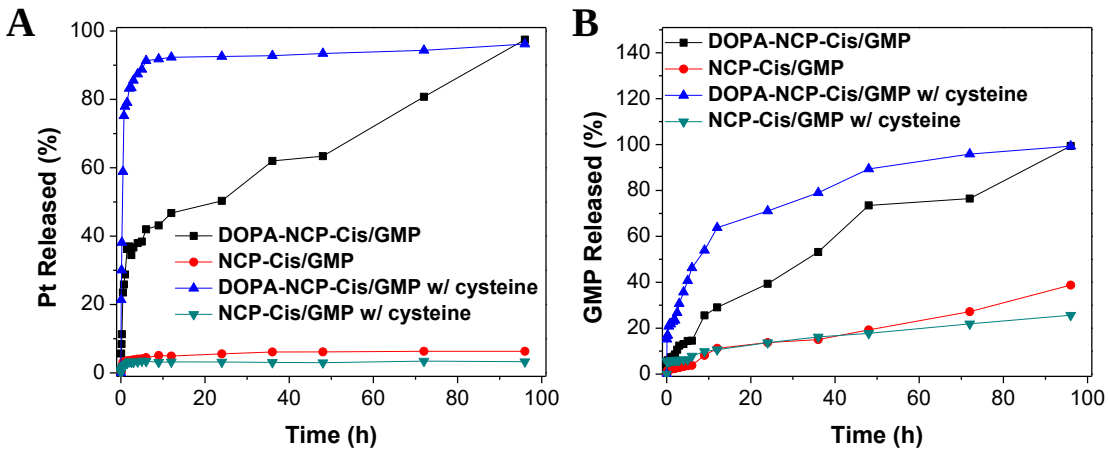

Figure 4.8. Pt (A) and GMP (B) release profiles of DOPA-NCP-Cis/GMP and NCP-Cis/GMP in 1xPBS buffer with or without 5 mM cysteine at 37 ºC. Reprinted with permission from Journal of the American Chemical Society, 2016, *138*, 6010-19. Copyright 2016 American Chemical Society.

4.3.3 In Vitro Cytotoxicity and Synergistic Effects

In vitro cytotoxicity assays of NCP-Cis/GMP were carried out against H82 and H69 SCLC cells, H460 and A549 NSCLC cells (Figure 4.9 through 4.12). As shown in Table 4.2, the cisplatin

IC_{50} of NCP-Cis/GMP decreased by 6.5-, 1.9-, 3.8, and 30-fold compared to NCP-Cis on H82, H69, H460, and A549 cells, respectively. Likewise, the GMP IC_{50} of NCP-Cis/GMP decreased by a 2.4-, 1.6-, 1.2-, and 3.3-fold compared to NCP-GMP on H82, H69, H460, and A549 cells, respectively. Monotherapeutic NCPs did not significantly differ from their free drug counterparts in cytotoxicity. The low IC_{50} values indicate that NCP-Cis/GMP particles were effectively internalized in cells through fusion of the cationic lipid bilayer with cell membranes and sigma receptor-mediated endocytosis. The stability of NCPs allows the particles to circulate longer in the body, resulting in enhanced accumulation in the tumor, followed by a slow, controlled release. This also limits adverse side effects, compared to the free drugs. The result demonstrated that multidrug NCPs are comparable, or in some cases better, than their cisplatin and GMP counterparts, thus reducing the amount of anticancer drugs required for efficient treatment of a deadly disease.

The CI was calculated to define drug interactions, with CI values lower than, equal to, and greater than 1 indicating synergism, additivity, and antagonism, respectively. The CI was around 0.5-0.9 for NCP-Cis/GMP against the monotherapeutic NCP nanoparticles and free drugs over a large range of drug effect level for H82 (Figure 4.9C), H69 (Figure 4.10C), H460 (Figure 4.10C) and A549 cells (Figure 4.12C), indicating synergism between cisplatin and GMP. Due to this synergism, cisplatin and GMP combined within a single nanocarrier exhibited higher cytotoxicity than the free drug alone and individual nanoparticle formulations. The enhanced synergy might be due to their different mechanism of actions: both cisplatin and GMP target the DNA—cisplatin forms an adduct with DNA, interfering with its replication and inducing cell apoptosis, while GMP induces apoptosis by replacing cytidine during DNA replication. Combined in a platform that

ensures effective targeting of tumor tissue, they can function synergistically for better therapeutic efficacy.

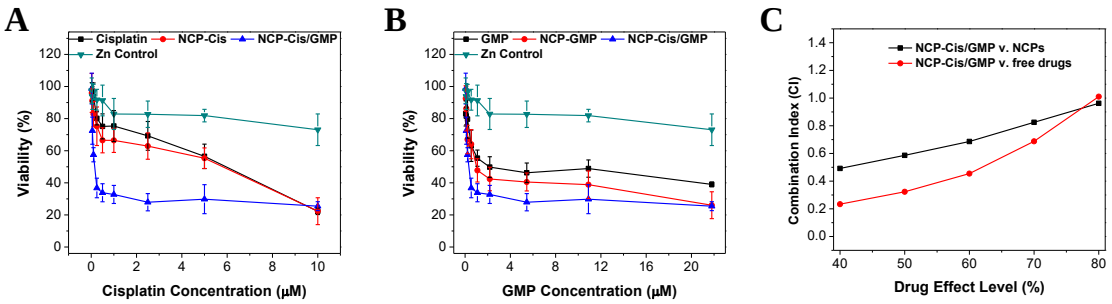

Figure 4.9. *In vitro* cytotoxicity plots (A, B) and combination index (CI) (C) of cisplatin/GMP combinations on H82 cells. The cell viabilities on H82 cells were measured after 72 h exposure to Zn Control, NCP-Cis, NCP-GMP, NCP-Cis/GMP, or free drugs (cisplatin, or GMP). Data are mean ± S.D. (n=6).

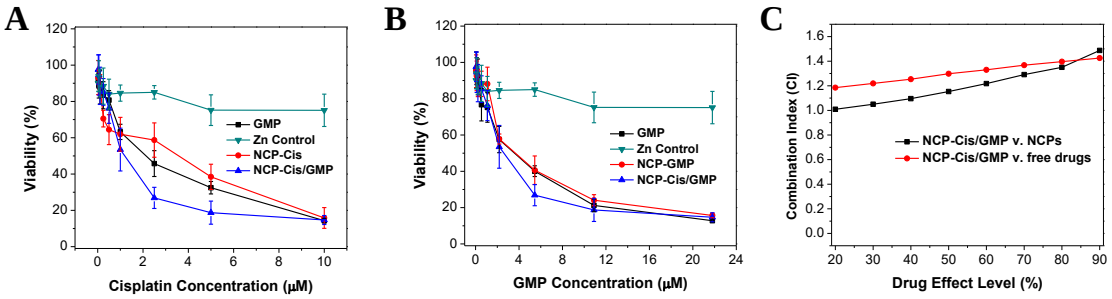

Figure 4.10. *In vitro* cytotoxicity plots (A, B) and combination index (CI) (C) of cisplatin/GMP combinations on H69 cells. The cell viabilities on H69 cells were measured after 72 h exposure to Zn Control, NCP-Cis, NCP-GMP, NCP-Cis/GMP, or free drugs (cisplatin, or GMP). Data are mean ± S.D. (n=6).

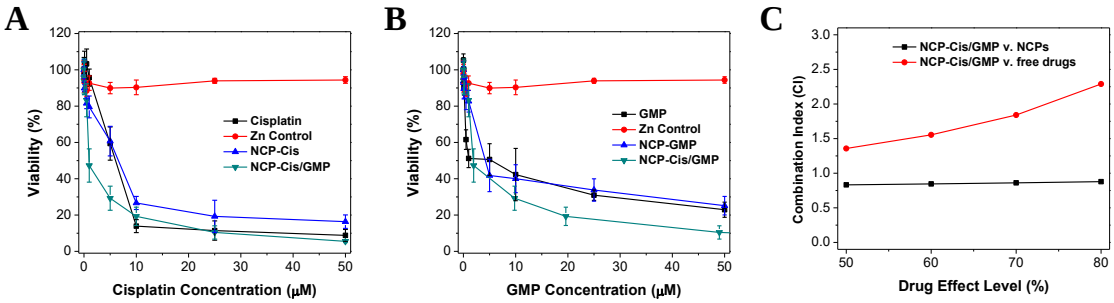

Figure 4.11. *In vitro* cytotoxicity plots (A, B) and combination index (CI) (C) of cisplatin/GMP combinations on H460 cells. The cell viabilities on H460 cells were measured after 72 h exposure

Figure 4.11, continued to Zn Control, NCP-Cis, NCP-GMP, NCP-Cis/GMP, or free drugs (cisplatin, or GMP). Data are mean ± S.D. (n=6).

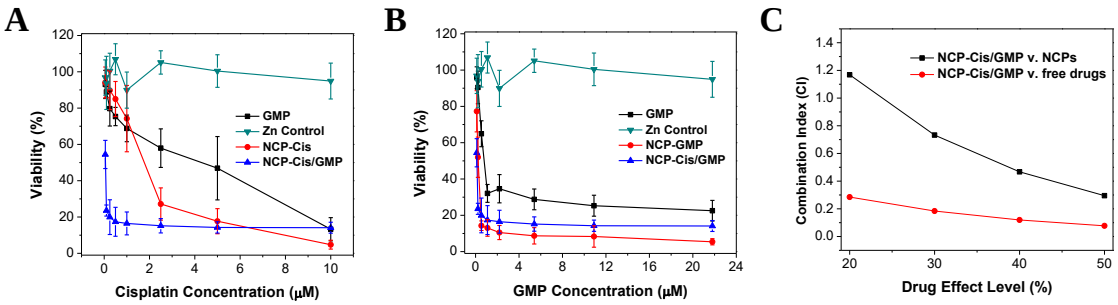

Figure 4.12. *In vitro* cytotoxicity plots (A, B) and combination index (CI) (C) of cisplatin/GMP combinations on A549 cells. The cell viabilities on A549 cells were measured after 72 h exposure to Zn Control, NCP-Cis, NCP-GMP, NCP-Cis/GMP, or free drugs (cisplatin, or GMP). Data are mean ± S.D. (n=6).

Table 4.2. Cisplatin IC_{50} Values of Cisplatin, GMP, NCP-Cis, NCP-GMP, and NCP-Cis/GMP Against H82, H69, H460, and A549 Cells (the numbers in parenthesis refer to GMP concentrations).

	Cisplatin(μM)	GMP (μM)	Zn Control* (μM)	NCP-Cis (μM)	NCP-GMP (μM)	NCP-Cis/GMP (μM)
H82	3.4±0.7	(3.9±1.1)	>10 (>22)	2.6±2.0	(1.9±0.9)	0.4±0.1 (0.8±0.2)
H69	1.5±0.3	(2.5±0.4)	>10 (>22)	1.6±0.5	(2.9±0.3)	0.8±0.3 (0.8±0.2)
H460	4.6±0.6	(3.3±1.3)	>50 (>50)	6.4±0.6	(4.1±1.6)	1.8±0.7 (3.3±1.2)
A549	2.1±0.5	(1.5±0.3)	>10 (>22)	1.2±0.2	(0.3±0.1)	0.04±0.02 (0.09±0.05)

*Zn Control does not contain cisplatin or GMP as they are served as a control to study the toxicity of NCP formulations. The amount of Zn Control particle was the same as NCP-Cis/GMP under the studied concentrations. Data are expressed as means±S.D.

4.3.4 In Vitro *Cell Apoptosis*

To investigate the synergistic effect of cisplatin and GMP on cell apoptosis, flow cytometry analysis was performed to quantify the cell apoptosis induced by free drugs or nanoparticle formulations (Figure 4.13 through 4.16, Table 4.3). A 24-hour incubation with NCP-Cis/GMP

treatment yielded superior cell apoptosis compared to other treatment groups in all SCLC and NSCLC cell lines. The total apoptosis induced by monotherapeutic groups was similar through reduced, with nearly half of the amount of that of NCP-Cis/GMP, while cells treated with PBS and Zn Control remained healthy. This further supported our hypothesis that combination therapy with multiple chemotherapeutics successfully promotes synergy of different drugs, increasing therapeutic target selectivity, and overcoming drug resistance by utilizing different mechanisms of action.

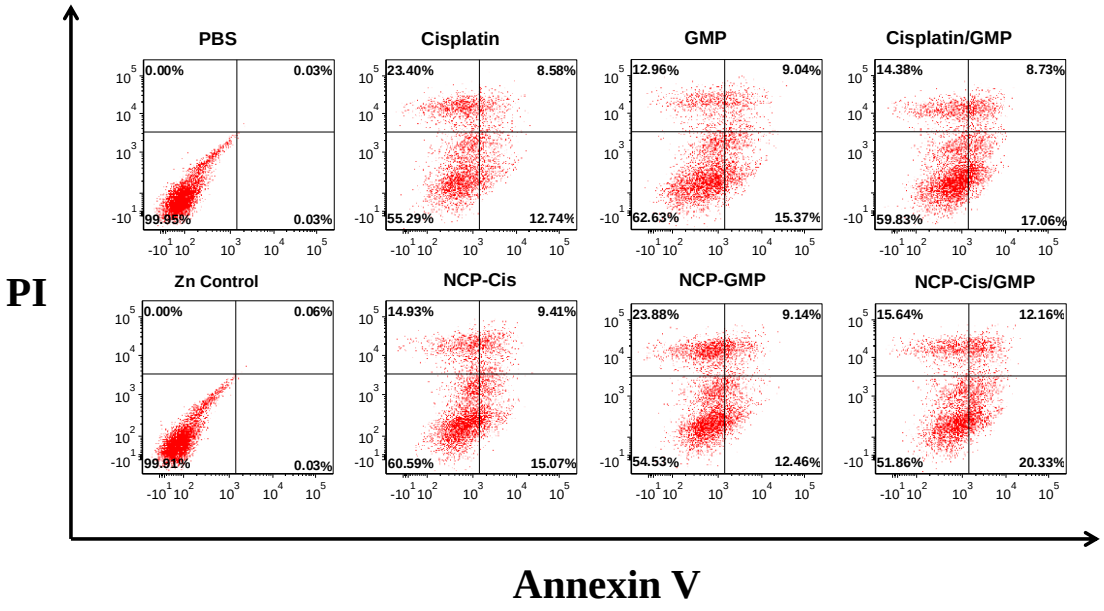

Figure 4.13. Flow cytometry analysis of PBS, cisplatin, GMP, cisplatin/GMP, NCP-Cis, NCP-GMP, and NCP-Cis/GMP in H82 SCLC cells.

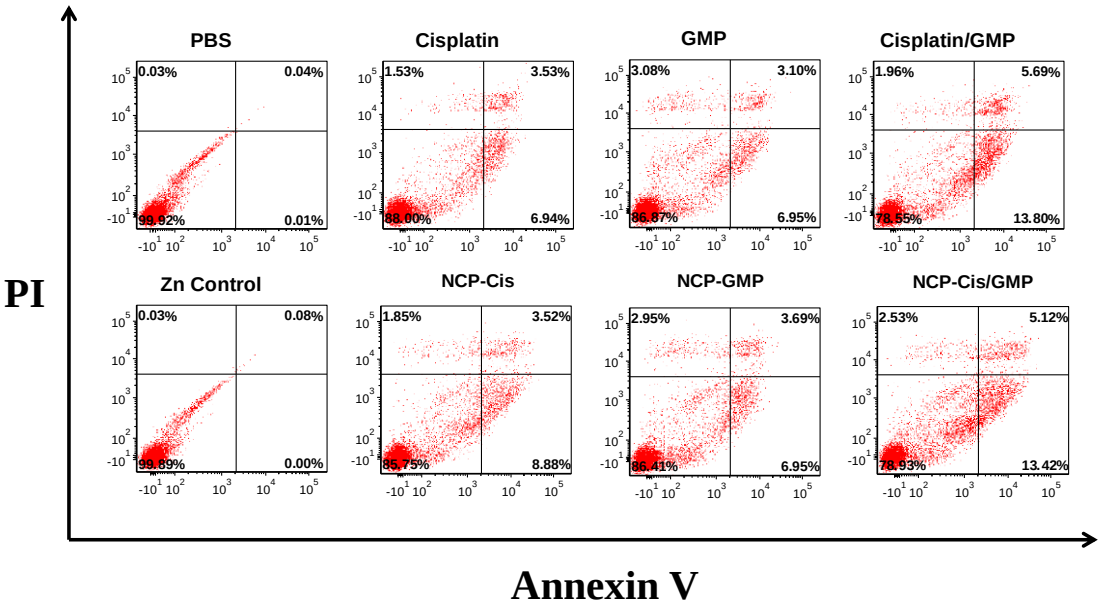

Figure 4.14. Flow cytometry analysis of PBS, cisplatin, GMP, cisplatin/GMP, NCP-Cis, NCP-GMP, and NCP-Cis/GMP in H69 SCLC cells.

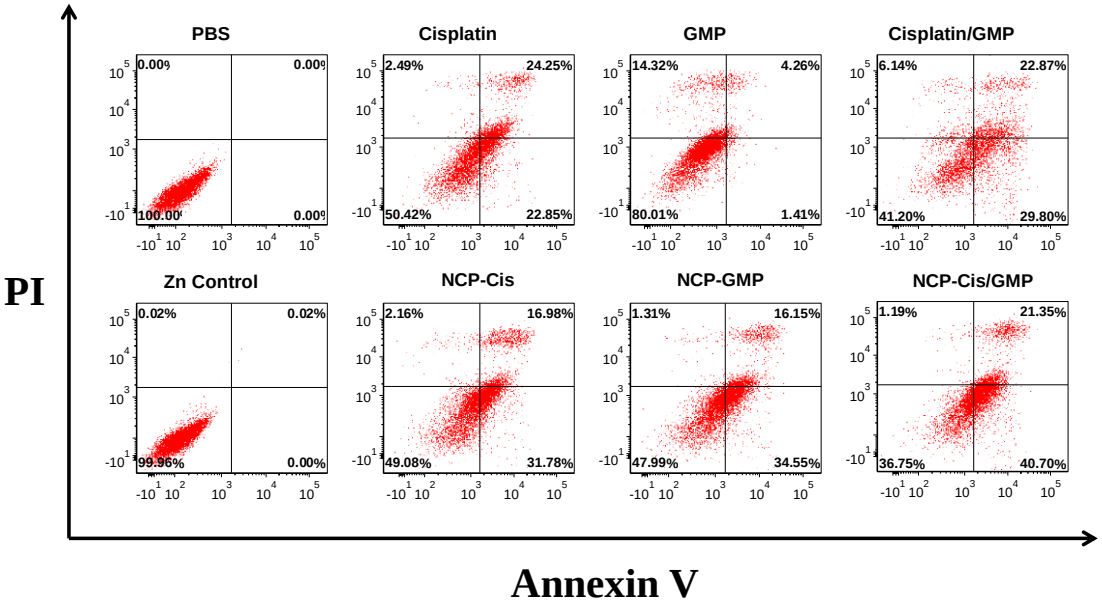

Figure 4.15. Flow cytometry analysis of PBS, cisplatin, GMP, cisplatin/GMP, NCP-Cis, NCP-GMP, and NCP-Cis/GMP in H460 NSCLC cells.

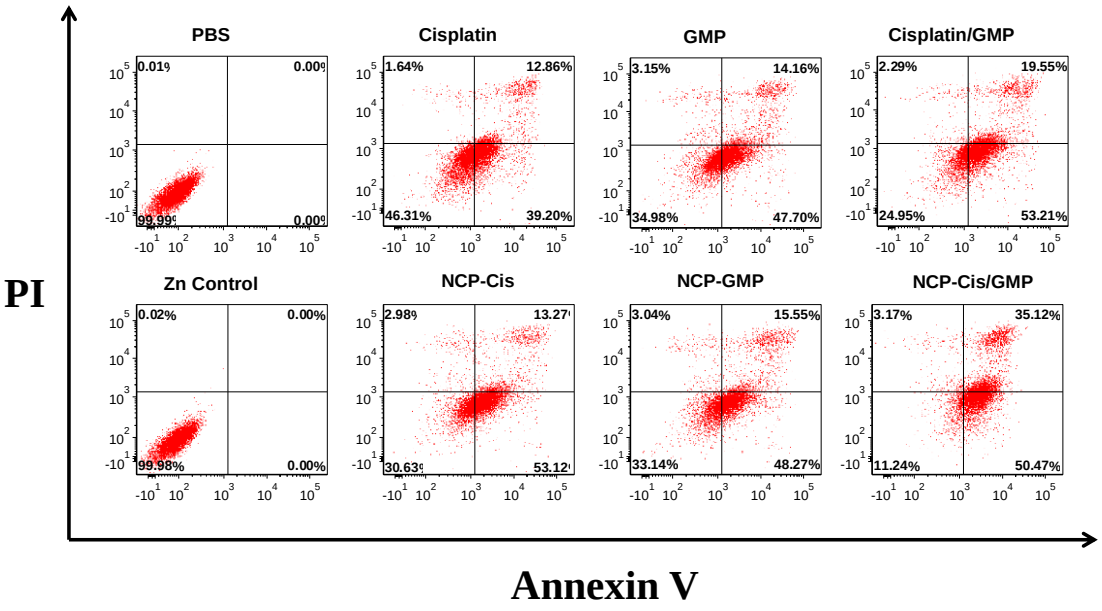

Figure 4.16. Flow cytometry analysis of PBS, cisplatin, GMP, cisplatin/GMP, NCP-Cis, NCP-GMP, and NCP-Cis/GMP in A549 NSCLC cells.

Table 4.3. Percentages of Healthy, Apoptotic, and Necrotic H82, H69, H460 and A549 Cells After a 24-Hour Treatment of PBS, Cisplatin, GMP, Cisplatin/GMP, Zn control, NCP-Cis, NCP-GMP, and NCP-Cis/GMP.

	Healthy (%)	Apoptosis (%)	Necrosis (%)
H82			
PBS	99.9	0.1	0.0
Cisplatin	55.3	21.3	23.4
GMP	62.6	24.4	13.0
Cisplatin/GMP	59.8	25.8	14.4
Zn Control	99.9	0.1	0.0
NCP-Cis	60.7	24.5	14.9
NCP-GMP	54.5	21.6	23.9
NCP-Cis/GMP	51.9	32.5	15.6
H69			
PBS	99.9	0.1	0.0
Cisplatin	88.0	10.5	1.5
GMP	86.9	10.1	3.1
Cisplatin/GMP	78.6	19.5	2.0
Zn Control	99.9	0.1	0.0
NCP-Cis	85.8	12.4	1.9
NCP-GMP	86.4	10.6	3.0
NCP-Cis/GMP	78.9	18.5	2.5
H460			
PBS	100.0	0.0	0.0
Cisplatin	50.4	47.1	2.5
GMP	80.0	5.7	14.3
Cisplatin/GMP	41.2	52.7	6.1
Zn Control	100.0	0.0	0.0
NCP-Cis	49.1	48.8	2.2
NCP-GMP	48.0	50.7	1.3
NCP-Cis/GMP	36.8	62.1	1.2
A549			
PBS	100.0	0.0	0.0
Cisplatin	46.3	52.1	1.6
GMP	35.0	61.9	3.2
Cisplatin/GMP	25.0	72.8	2.3
Zn Control	100.0	0.0	0.0
NCP-Cis	30.6	66.4	3.0
NCP-GMP	33.1	63.8	3.0
NCP-Cis/GMP	11.2	85.6	3.2

4.3.5 Pharmacokinetics and Biodistribution

The pharmacokinetics and biodistribution of NCP-Cis/GMP was investigated in CT26 tumor-bearing mice to assess its ability to evade the MPS and accumulate in tumor tissues (Figure

4.17A). The Pt distribution was quantified by ICP-MS, and the GMP amount in the blood was quantified by HPLC-MS/MS. The concentrations of drugs in the blood were fitted using two-compartment models. As shown in Figure 4.17, NCP-Cis/GMP exhibited half-lives ($t_{1/2\beta}$) of 18.5 ± 5.2 h and 14.7 ± 2.8 h for Pt and GMP, respectively. The Pt distribution of other organs and tumor tissues were also analyzed. The peak tumor uptake was achieved at 10.4 ± 0.8 %ID/g at 24 h post injection. These results indicate NCP-Cis/GMP have prolong circulation time and tumor accumulation of cisplatin. NCP-Cis/GMP particles are able to avoid uptake by MPS as evidenced by lower and kidney % ID/g.

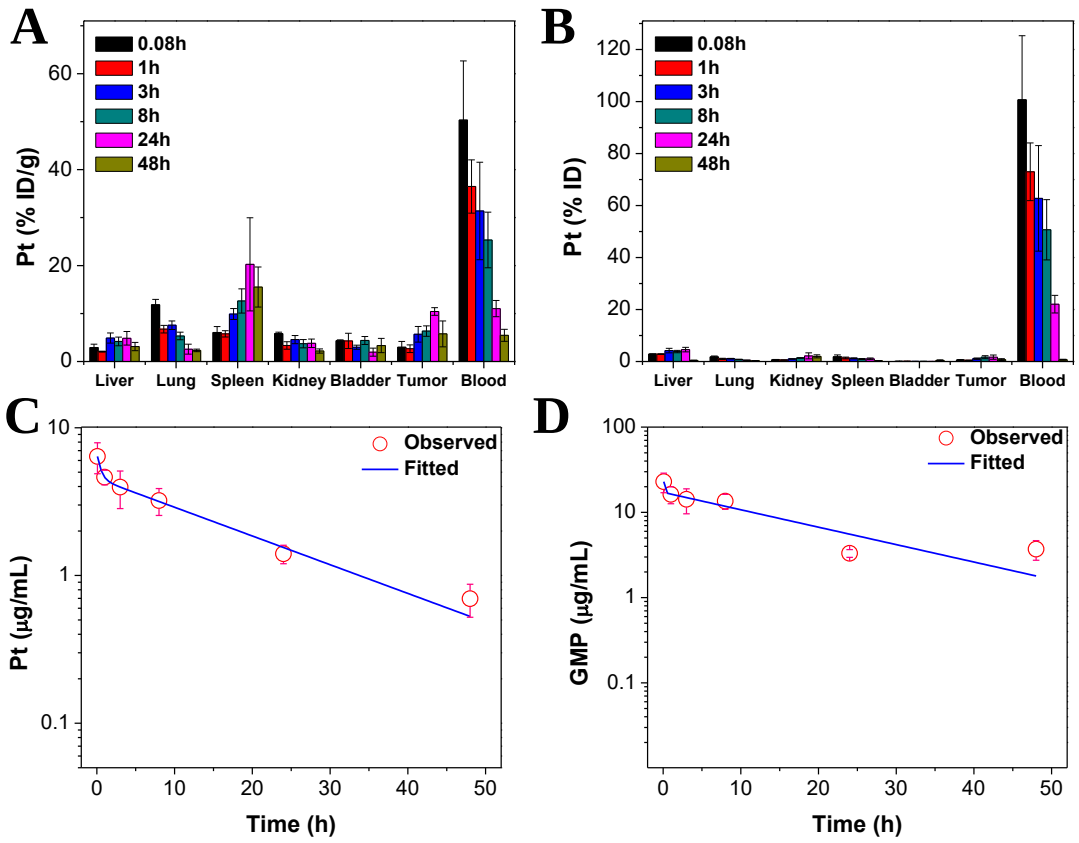

Figure 4.17. (A) Percentage injected dose per gram (% ID/g) and (B) percentage injected dose (% ID) of Pt in tissues and blood after intravenous administration of NCP-Cis/GMP in CT26 tumor-bearing mice at time points 5 min, 1 h, 3 h, 5 h, 8 h, 24 h, and 48 h. Data are mean ± S.D. (n=3). (C) Average observed and predicted time-dependent Pt distributions in blood after administration of NCP-Cis/GMP (n=3). (D) Average observed and predicted time-dependent GMP distributions in blood after administration of NCP-Cis/GMP (n=3). Two-compartment model was used for

Figure 4.17, continued fitting the Pt and GMP distributions in blood. Reprinted with permission from Journal of the American Chemical Society, 2016, *138*, 6010-19. Copyright 2016 American Chemical Society.

We also performed an experiment to quantify the amounts of Pt and GMP in both the red/white blood cell and plasma layers after separating them from whole blood by centrifugation (Figure 4.18). The majority of Pt content was seen in the plasma layer at three different time points post injection; only 5-10% of Pt was seen in the red/white blood cell layer. Similarly, when whole blood was separated into red/white blood cells and plasma, no GMP concentration was detected in the layer containing red/white blood cells, while 770.5 ng of GMP was detected in the plasma layer.

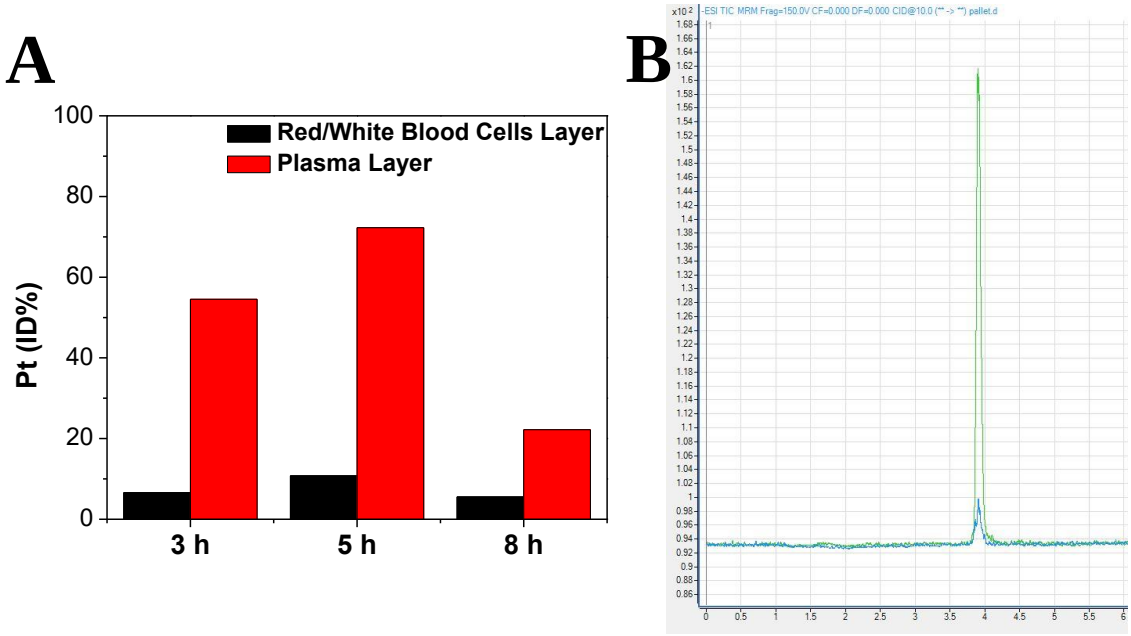

Figure 4.18. (A) Pt injected dose percentage (ID %) of NCP-Cis/siRNA at a cisplatin dose of 1.0 mg/kg by i.p injection in red/white blood cells layer and plasma layer after centrifugation of whole blood. (B) Chromatogram of GMP concentration in plasma layer (green) and red/white blood cells layer (blue) after i.v injection of NCP-Cis/GMP at a cisplatin dose 1.0 mg/kg and GMP dose 2.2 mg/kg (m/z transition from 342 to 231).

4.3.6 Maximum Tolerated Dose for NCP-Cis/GMP

We determined the maximum tolerated dose (MTD) of NCP-Cis/GMP after intraperitoneal injection to BALB/c mice (Figure 4.19). The MTD was inferred based on the group in which all mice survived and did not lose over 20% of their body weight. With a single injection of NCP-Cis/GMP at 1.5 mg cisplatin/kg and 3.3 mg GMP/kg, all three mice were not able to tolerate such high dosage as they lost over 20% of their body weight within the first six days post injection and were euthanized. We also injected NCP-Cis/GMP at 1.0 mg/kg cisplatin/kg and 2.2 mg GMP/kg every 3 days, for a total of three injections. After the third dose, one mouse showed a weight loss of over 20% but eventually regained the weight a week later. However, the toxicity at this dosing schedule was still significant. Therefore, the dosing concentration was lowered and the injections made less frequent. At a cisplatin dose of 0.6 mg/kg and a GMP dose of 1.3 mg/kg every five days, the mice were able to tolerate five total injections, which is equivalent of 3.0 mg cisplatin/kg and 6.5 mg GMP/kg over the span of 25 days. The mice regained weight after the last injection and remained healthy until 30 days after the last injection or the completion of the experiment. MTD was also evaluated in rats injected with NCP-Cis/GMP intravenously at 2.0 mg cisplatin/kg and 4.4 mg GMP/kg doses every five days for a total of four injections (Figure 4.20). The rats could tolerate higher doses than mice and did not show any weight loss until after the forth injection (total dose: 8.0 mg cisplatin/kg and 17.6 mg GMP/kg). A week after the last injection, the rats returned to their original body weights.

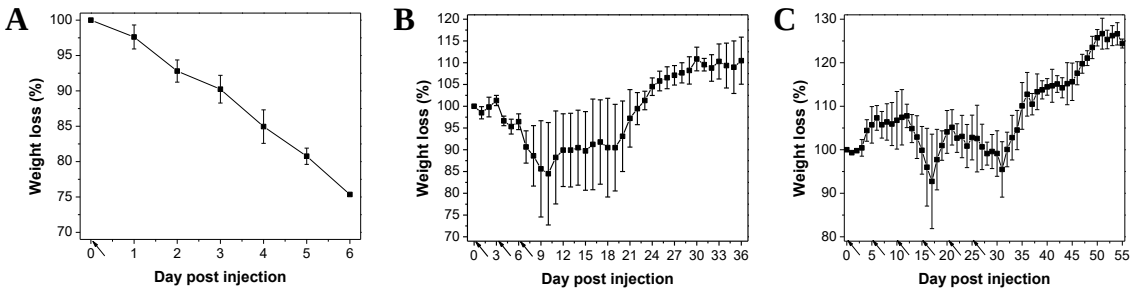

Figure 4.19. Weight loss of mice treated with NCP-Cis/GMP intraperitoneally at (A) 1.5 mg cisplatin/kg and 3.3 mg GMP/kg once, (B) 1.0 mg/kg cisplatin/kg and 2.2 mg GMP/kg every 3 days for a total of three injections, and (C) 0.6 mg cisplatin/kg and 1.3 mg GMP/kg every five days for a total of five injections. Data are mean ± S.D. (n=3).

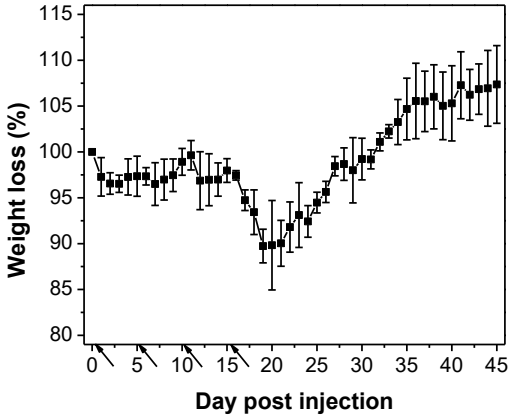

Figure 4.20. Weight loss of SD/CD rat treated with NCP-Cis/GMP intravenously at 2.0 mg cisplatin/kg and 4.4 mg GMP/kg every five days for a total of four injections. Data are mean ± S.D. (n=3).

4.3.7 Antitumor Activity In Vivo

Using the MTD of NCP-Cis/GMP determined previously, we evaluated the *in vivo* antitumor effect of NCP-Cis/GMP at a cisplatin dose of 0.75 mg/kg and a GMP dose of 1.6 mg/kg in H82 SCLC subcutaneous xenografts (Figure 4.21). The treatments started when the tumors reached ~200 mm^3. As shown in Figure 4.21A, NCP-Cis/GMP demonstrated tumor inhibition by 4-fold as compared to the control at day 6 post-first injection or the endpoint of the PBS control study. One of three mice exhibited significant weight loss during the efficacy study, but the loss

did not exceed our 20% toxicity limit. A study with lower doses and smaller starting tumor volumes is currently in progress to optimize efficacy. The high antitumor effect suggested that NCPs could act as an ideal nanoplatform for the smart co-delivery of chemotherapeutic drugs into tumors for more effective cancer treatment.

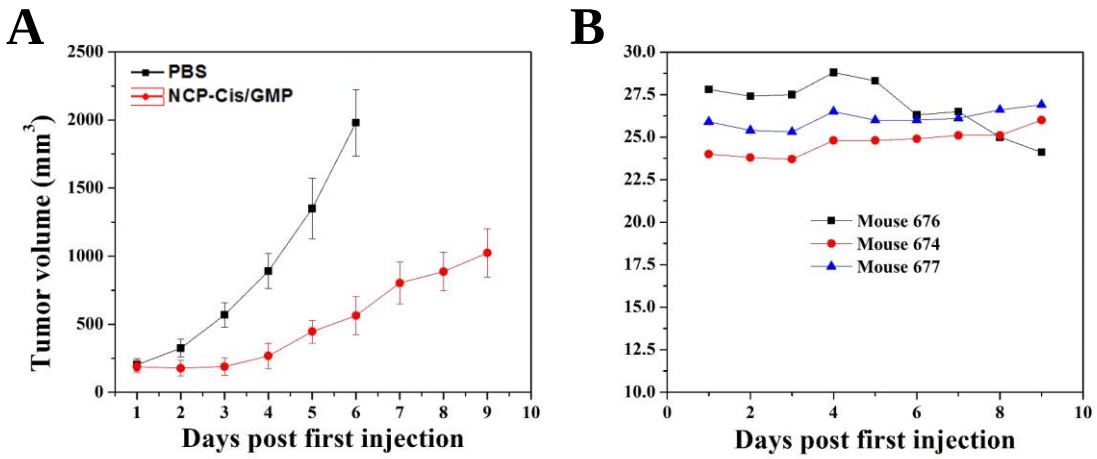

Figure 4.21. (A) Anticancer efficacy of NCP-Cis/GMP against H82 subcutaneous xenografts. Free drug combination or nanoparticles were intraperitoneally injected at 0.75 mg cisplatin/kg and 1.6 mg GMP/kg on Day 0, Day 3, and Day 6 for a total of three injections. (B) Individual mouse body weight evolution of H82 tumor-bearing athymic mice treated with NCP-Cis/GMP. Data are expressed as means±S.D. (n=3).

4.4 Conclusion

I describe here NCP-Cis/GMP containing high chemotherapeutic drug loadings of cisplatin and gem for the treatment of lung cancer. These particles are stable under normal physiological conditions but readily release their therapeutic payloads once the nanoparticles enter tumors. Encapsulating the NCPs with a lipid layer allows them to overcome chemoresistance and reduce the dosages and toxicity of the drugs. The NCP particles exhibited efficacy against lung cancer cell lines in *in vitro* and *in vivo* studies. NCP-Cis/GMP had high tumor uptake and an extraordinary blood circulation half-life. Furthermore, NCP-Cis/GMP was much more effective than its

monotherapeutic NCP counterparts. This work highlights the potential of combination NCPs as highly effective delivery vehicles for cancer therapeutics.

4.5 References

(1) Society, A. C. *Atlanta: American Cancer Society* **2013**.

(2) Johnson, D. H.; Schiller, J. H.; Bunn, P. A., Jr. *J. Clin. Oncol.* **2014**, *32*, 973.

(3) Berhoune, M.; Banu, E.; Scotte, F.; Prognon, P.; Oudard, S.; Bonan, B. *Annals of Pharmacotherapy* **2008**, *42*, 1640.

(4) Muggia, F. *Gynecologic Oncology* **2009**, *112*, 275.

(5) Scagliotti, G. V.; Parikh, P.; von Pawel, J.; Biesma, B.; Vansteenkiste, J.; Manegold, C.; Serwatowski, P.; Gatzemeier, U.; Digumarti, R.; Zukin, M.; Lee, J. S.; Mellemgaard, A.; Park, K.; Patil, S.; Rolski, J.; Goksel, T.; de Marinis, F.; Simms, L.; Sugarman, K. P.; Gandara, D. *J. Clin. Oncol.* **2008**, *26*, 3543.

(6) Sandler, A. B.; Nemunaitis, J.; Denham, C.; Von Pawel, J.; Cormier, Y.; Gatzemeier, U.; Mattson, K.; Manegold, C.; Palmer, M. C.; Gregor, A.; Nguyen, B.; Niyikiza, C.; Einhorn, L. H. *J. Clin. Oncol.* **2000**, *18*, 122.

(7) Steele, J. P. C. *Semin. Oncol.* **2001**, *28*, 15.

(8) Hesketh, P. J.; Chansky, K.; Israel, V.; Grapski, R. T.; Mekhail, T. M.; Spiridonidis, C. H.; Mills, G. M.; Kelly, K.; Crowley, J. J.; Gandara, D. R. *J Thorac Oncol* **2007**, *2*, 440.

(9) Vincent, M. J.; Greco, F.; Nicholson, R. I.; Paul, A.; Griffiths, P. C.; Duncan, R. **2006**, 4061.

(10) Kuenen, B.; Rosen, L.; Smit, E.; Parson, M.; Levi, M.; Ruijter, R.; Huisman, H.; Kedde, M.; Noordhusi, P.; Van Der Vijgh, W. *JCO* **2002**, *20*, 1657.

(11) DeVita, V. T., Jr.; Young, R. C.; Canellos, G. P. *Cancer* **1975**, *35*, 98.

(12) Shah, M. A.; Schwartz, G. K. *Drug Resistance Updates* **2000**, *3*, 335.

(13) Lehar, J.; Krueger, A. S.; Avery, W.; Heilbut, A. M.; Johansen, L. M.; Price, E. R.; Rickles, R. J.; Short, G. F., 3rd; Staunton, J. E.; Jin, X.; Lee, M. S.; Zimmermann, G. R.; Borisy, A. A. *Nat Biotechnol* **2009**, *27*, 659.

(14) Crino, L.; Weder, W.; van, M. J.; Felip, E. *Ann Oncol* **2010**, *21 Suppl 5*, v103.

(15) Shepherd, F. A. *Semin. Oncol.* **1999**, *26*, 3.

(16) Nagy-Mignotte, H.; Guillem, P.; Vignoud, L.; Coudurier, M.; Vesin, A.; Bonneterre, V.; Toffart, A.-C.; Sakhri, L.; Brambilla, C.; Brambilla, E.; Timsit, J.-F.; Moro-Sibilot, D. *Lung Cancer* **2012**, *78*, 112.

(17) Sukumvanich, P.; Einstein, M.; Wagner, B.; Gucalp, R.; Goldberg, G. L. *Gynecol Oncol* **2005**, *96*, 232.

(18) Rieter, W. J.; Pott, K. M.; Taylor, K. M. L.; Lin, W. *Journal of the American Chemical Society* **2008**, *130*, 11584.

(19) Huxford, R. C.; de Krafft, K. E.; Boyle, W. S.; Liu, D.; Lin, W. *Chem. Sci.* **2012**, *3*, 198.

(20) Liu, D.; Poon, C.; Lu, K.; He, C.; Lin, W. *Nat Commun* **2014**, *5*, 4182.

(21) He, C.; Liu, D.; Lin, W. *Biomaterials* **2015**, *36*, 124.

(22) Huxford-Phillips, R. C.; Russell, S. R.; Liu, D.; Lin, W. *RSC Adv* **2013**, *3*, 14438.

(23) Rieter, W. J.; Pott, K. M.; Taylor, K. M.; Lin, W. *J Am Chem Soc* **2008**, *130*, 11584.

(24) Huxford, R. C.; Dekrafft, K. E.; Boyle, W. S.; Liu, D.; Lin, W. *Chem Sci* **2012**, *3*.

(25) Liu, D.; Kramer, S. A.; Huxford-Phillips, R. C.; Wang, S.; Della Rocca, J.; Lin, W. *Chem Commun (Camb)* **2012**, *48*, 2668.

(26) Poon, C.; He, C.; Liu, D.; Lu, K.; Lin, W. *Journal of controlled release : official journal of the Controlled Release Society* **2015**, *201*, 90.

(27) Cardenal, F.; Lopez-Cabreizo, M.; Anton, A. *17* **1999**.

(28) Le Chevalier, T.; Thezenas, S.; Breton, J. In *ASCO Annual Meeting Proceedings* 2006; Vol. 24.

(29) Liu, D.; Poon, C.; Lu, K.; He, C.; Lin, W. *Nat Commun* **2014**, *5*.

(30) Risbood, P.; Kane Jr., C. T.; Hossain, T.; Vadapalli, S.; Chadda, S. *Bioorganic & Medicinal Chemistry Letters* **2008**, *18*, 2957.

CHAPTER V: Nanoscale Coordination Polymers Co-deliver Chemotherapeutics and siRNAs to Eradicate Tumors of Cisplatin-Resistant Ovarian Cancer

5.1 Introduction

Previously, we examined the therapeutic use of new self-assembled core-shell nanoscale coordination polymer (NCP) nanoparticles carrying carboplatin and gemcitabine (NCP-Carbo/GMP) and cisplatin and gemcitabine (NCP-Cis/GMP) for the treatment of various cancers. A strong synergistic effect was observed between platinum (Pt) drugs and gemcitabine (gem) against platinum-resistant ovarian cancer (OCa) cells and both types of lung cancer cells *in vitro*. The co-administration of Pt drugs and gem in the NCPs led to prolonged blood circulation and improved tumor uptake of the drugs, resulting in regression and growth inhibition of these tumors. While it is true that carboplatin offers much less toxicity than cisplatin, this combination failed to completely eradicate tumors due to the reduced therapeutic efficacy of carboplatin compared to cisplatin in OCa. Using the NCP system shown in the last chapter for lung cancer, in this chapter, we develop nanoscale coordination polymers carrying two chemotherapeutics, cisplatin and gem, as well as gene therapeutic agents that will assist in combatting drug resistance pathways in OCa.

OCa is the fifth leading cause of death by cancer for women in the United States, accounting for 5% of all cancer-related deaths in the United States.[1] Currently, the first-line treatment for advanced OCa is upfront surgery, followed by Pt/taxane-based chemotherapy, but the majority of patients have tumors that do not respond to chemotherapy or will eventually recur as multidrug resistant (MDR) OCa.[2-10] After repeated treatments with anticancer chemotherapeutic agents, drug resistance may develop because diseased cells activate signal transduction pathways to avoid death.[11] As a result, 85% of patients with epithelial OCa who achieve full remission

following first-line therapy will develop a recurrent disease. Although combination chemotherapy is often use to counter drug resistance mechanisms in cancer patients, cancer cells can adapt and acquire resistance to one or more drugs, eventually leading to ovarian cancer untreatable by current methods.[12] Because intrinsically resistant and recurring OCa is incurable with current therapeutic methods, novel therapeutic strategies are needed to overcome the disease.[3,6]

Tumor cells can vary in intrinsic or acquired drug resistance mechanisms that differ from patient to patient.[2-5,13-15] Even cancer cells within the same tumor can display a wide array of heterogeneity in signaling pathways that promote drug resistance.[16,17] Drug resistance often involves multiple and dynamically acquired MDR mechanisms as a result of the overexpression of damage recognition proteins (e.g., ERCC-1) and anti-apoptotic proteins (e.g., Bcl-2, survivin). ERCC-1 encodes a subunit of nucleotide excision repair complex required for the incision step of nucleotide excision repair during DNA repair and DNA recombination.[18] Bcl-2 is responsible for the activation of cellular anti-apoptotic defense.[19] Survivin has a functional role in caspase inhibition to lead to negative regulation of apoptosis, and is upregulated in most human tumors, making it a potential target for cancer treatment.[20] Small interfering RNA (siRNA) has the ability to inhibit cellular MDR pathways by silencing the expression of relevant genes and enhancing the accumulation of anticancer drugs at the tumor site.[21-30] Simultaneously delivering pooled siRNAs targeting multiple distinct molecular signaling pathways would provide an effective approach to overcoming drug resistance in OCa.[27,28,31] We hypothesized that co-administration of chemotherapeutics and siRNAs targeting MDR genes can increase the efficacy of existing OCa treatments.

Efficient delivery of siRNAs to the tumor has been a challenge because of the instability of siRNAs in systemic circulation and their inability to cross cell membranes. Therefore, siRNAs

must be either synthetically modified or delivered with effective vehicles to facilitate its intracellular uptake and elicit gene silencing *in vivo*. Although nanoparticulate delivery systems have overcome many drawbacks of small molecule therapeutics,[32-42] issues associated with *in vivo* siRNA delivery, including the contradictory surface charge requirements for efficient endosomal escape (cationic) and long blood circulation (neutral), remain largely unaddressed. Although cationic lipids have been developed with NCPs for the co-delivery of cisplatin and pooled siRNAs to regress tumor growth in a cisplatin-resistant OCa mouse model via intratumoral injection,[43] this system suffers from poor pharmacokinetics and biodistribution upon systemic administration and are unsuitable for clinical translation.

This chapter describes a robust self-assembled, core-shell NCP-based nanomedicine platform for the co-delivery of multiple chemotherapeutic agents and siRNAs (NCP/siRNAs) targeting MDR genes for the effective treatment of resistant OCa. The novel nanomedicine, NCP-Cis/GMP/siRNAs, carries cisplatin and gem in the core and siRNAs in the lipid layer with built-in mechanisms for triggered release and endosomal escape and shows enhanced anticancer efficacy in subcutaneous xenograft mouse models of resistant OCa. Given the dramatically improved therapeutic window of NCP-Cis/GMP/siRNAs, we believe that these particles hold great promise for clinical translation for the treatment of resistant OCa.

5.2 Experimental Details

5.2.1 General Experimental:

All of the starting materials were purchased from Sigma-Aldrich (Louis, MO) and Fisher Scientific (Pittsburgh, PA) unless otherwise noted and used without further purification. 1,2-dioleoyl-sn-glycero-3-phosphate (DOPA), 1,2-distearoyl-sn-glycero-3-phosphoethanolamine

(DSPE), cholesterol , 1,2-distearoyl-sn-glycero-3-phosphocholine (DSPC), and 1,2-distearoyl-sn-glycero-3-phosphoethanolamine-N-[amino(polyethylene glycol)2000] (DSPE-PEG2k) were purchased from Avanti Polar Lipids (Alabaster, AL). The siRNA duplexes were supplied by Integrated DNA Technologies (USA) and dissolved in diethylpyrocarbonate (DEPC)-treated water before use. Survivin siRNA (*sisurvivin*), Bcl-2 siRNA (*siBcl-2*), ERCC-1 siRNA (*siERCC-1*) , and ctrl siRNA contained the anti-sense sequences of 5'-GGACCACCGCAUCUCUACAdTdT-3', 5'-UUCGGCAUUAGGCCUUCCGdTdG-3', 5'-GAGGCUGUGAGAUGGCAUATT-3', and 5'-CGUUAAUCGCGUAUAAUACGCGUAT-3', respectively. A thiol modification was put on the 5' end of the sense strand of each siRNA in order to avoid potential inhibition on the antisense strand. Alexa Fluor 647-labeled survivin siRNA with a thiol modification was used for the quantification and imaging of siRNAs.

Human ovarian cancer cell lines resistant to cisplatin SKOV-3 and A2780/CDDP were obtained from the American Type Culture Collection (Rockville, MD, USA) and Developmental Therapeutics Core, Northwestern University, respectively. The human ovarian cancer cell line sensitive to cisplatin A2780 was from Developmental Therapeutics Core, Northwestern University. SKOV-3 cells were cultured in McCoy's 5a medium containing 10% fetal bovine serum (FBS). A2780 and A2780/CDDP cells were cultured in RPMI-1640 medium (Gibco, Grand Island, NY, USA) containing 10% FBS.

BALB/c and athymic female nude mice (6-8 weeks old, 20-25 g) were provided by Harlan Laboratories, Inc. (USA). The study protocol was reviewed and approved by the Institutional Animal Care and Use Committee (IACUC) at the University of Chicago.

5.2.2 Synthesis of DSPE-siRNA Conjugate:

Succinimidyl 3-(2-pyridyldithio)propionate (SPDP, 21mg, 0.067 mmol) and 1,2-distearoyl-sn-glycero-3-phosphoethanolamine (DSPE, 50mg, 0.067 mmol) were dissolved in chloroform (40mL) and refluxed under N_2 in darkness for 48 hours. After removal of chloroform by rotary evaporation, the crude product was purified by diol-functionalized silica gel column chromatography. Yield: 40%. ^{1}H NMR in $CDCl_3$: δ8.47 (d, 1H); δ7.72 (m, 2H); δ7.14 (d, 1H); δ5.25 (s, 1H); δ4.38 (d, 1H); δ4.17 (s, 2H); δ3.99 (t, 4H); δ3.52 (s, 1H); δ3.03 (t, 2H); δ2.65 (s, 2H); δ2.30 (d, 2H); δ1.70 (bs, 1H); δ1.59 (s, 2H); δ1.28 (s, 60H); δ0.90 (t, 6H). Thiolated siRNAs (IDT, USA) were conjugated to DSPE-SPDP to afford DSPE-siRNA conjugates via the disulfide bond.

5.2.3 Mass spectroscopy analysis of DSPE-siRNA:

The matrix solution was prepared by dissolving 2,5 dihydroxybenzoic acid (10 mg, 0.065 mmol) in a mixture of 1 mL acetonitrile/0.1% trifluoroacetic acid (30:70, v/v). DSPE-siRNA (1 μg, 76.9 pmol) was dissolved in 10 μL of the matrix solution. After vortexing, the sample/matrix solution (1 μL) was spotted onto a Bruker MTP 384 ground steel plate and dried at room temperature. The mass spectrometry analysis was carried out using a Bruker Ultraflextreme matrix-assisted laser desorption/ionization mass spectrometer (MALDI-TOF) MS. The analysis was carried out using a positive reflective ion mode at a mass range of 5000-16000 Da.

5.2.4 Particle Synthesis and Characterization:

5.2.4.1 Preparation of NCP-Cis/GMP: DOPA-capped NCP-Cis/GMP nanoparticles carrying a cisplatin prodrug and gemcitabine monophosphate (GMP) were synthesized by reverse microemulsion. Twenty-five mg/mL cis,cis,trans-$[Pt(NH_3)_2Cl_2(OCONHP(O)(OH)_2)_2]$ (8.6 μmol), 25 mg/mL GMP sodium salt solution (14.6 μmol), and DOPA (22 μmol) were added to a 5 mL

aliquot of Triton-X-100 (0.3 M in 1.5 M hexanol/cyclohexane) solution to form a *W*=7.4 microemulsion. Another microemulsion of 5 mL Triton-X-100 (0.3 M, 1.5 M hexanol/cyclohexane) containing $Zn(NO_3)_2 \cdot 6H_2O$ aq. (131 mmol) was also prepared. The two microemulsions were stirred vigorously for 15 min at room temperature. The two microemulsions were combined and stirred for an additional 30 min at room temperature. After the addition of 20 mL ethanol, NCP-Cis/GMP particles were washed once with ethanol, once with 50% (v/v) ethanol/cyclohexane, twice with 50% (v/v) ethanol/THF, and redispersed in THF.

Different ratios of cisplatin and GMP can be loaded into the particle. Two other sets of NCP-Cis/GMP with different drug ratios were thus also synthesized. DOPA-NCP-Cis/GMP-2 was synthesized using cisplatin prodrug (400 μL, 17.2 μmol) and GMP sodium salt solution (60 μL, 4.4 μmol). DOPA-NCP-Cis/GMP-3 was synthesized using cisplatin prodrug (32 μL, 1.4 μmol) and GMP sodium salt solution (400 μL, 29.2 μmol). Both of these particles were synthesized under the same microemulsion conditions mentioned above.

5.2.4.2 Preparation of NCP-Cis: A *W*=7.4 microemulsion was prepared by the addition of 0.2 mL of a 25 mg/mL cis,cis,trans-$[Pt(NH_3)_2Cl_2(OCONHP(O)(OH)_2)_2]$ aqueous solution (obtained by deprotonation with 3M NaOH) and 0.2 mL of a 100 mg/mL $Zn(NO_3)_2$ aqueous solution to separate 5 mL aliquots of a 0.3 M Triton X-100/1.5 M 1-hexanol in cyclohexane mixture while vigorously stirring at room temperature. 20 μL of DOPA solution (200 mg/mL in $CHCl_3$) was added to the complex solution and the stirring was continued for 15 min until a clear solution formed. The two microemulsions were combined, and the resultant 10 mL microemulsion with *W* =7.4 was stirred for 30 minutes. After the addition of 20 mL ethanol, NCP-Cis was obtained by centrifugation at 12000 rpm. The resulting pellet was washed once with ethanol and twice with

50% EtOH/THF, and redispersed in THF. Particles were purified by filtration through 200 nm syringe filter.

5.2.4.3 Preparation of NCP-GMP: Microemulsions were first formed by the addition of 25mg/mL GMP and 100 mg/mL $Zn(NO_3)_2 \cdot 6H_2O$ to two separate TritonX-100 (100 mL, 0.3 M, 1.5 M cyclohexane/hexanol) surfactant system mixtures. The separate microemulsions were stirred vigorously for 10 to 15 min at room temperate, after which they were combined, and the resultant microemulsion was allowed to stir vigorously for 30 min at room temperature. After the adding of 20 mL ethanol, particles were washed once with ethanol and twice with 50% EtOH/THF, and redispersed in THF.

5.2.4.4 Preparation of Rhodamine B-Doped NCP-Cis/GMP: DOPA-NCP-Cis/GMP was synthesis by reverse microemulsion. Twenty-five mg/mL cis,cis,trans-$[Pt(NH_3)_2Cl_2(OCONHP(O)(OH)_2)_2]$ (8.6 μmol), 25 mg/mL GMP sodium salt solution (14.6 μmol), and DOPA (22 μmol) were added to a 5 mL aliquot of Triton-X-100 (0.3 M in 1.5 M hexanol/cyclohexane) solution to form a W=7.4 microemulsion. Another microemulsion of 5 mL Triton-X-100 (0.3 M, 1.5 M hexanol/cyclohexane) containing $Zn(NO_3)_2 \cdot 6H_2O$ aq. (131 mmol) was also prepared. The two microemulsions were stirred vigorously for 15 min at room temperature. The two microemulsions were combined and stirred for an additional 30 min at room temperature. After the addition of 20 mL ethanol, NCP-Cis/GMP particles were washed once with ethanol, once with 50% (v/v) ethanol/cyclohexane, twice with 50% (v/v) ethanol/THF, and redispersed in THF.

5.2.4.5 General Procedures of Lipid Coating and PEGylation of NCP-Cis/siRNAs: NCP-Cis/siRNAs was prepared by adding 10 μL of aqueous solution of DSPE-siRNA (DSPE-siRNA/DOPA-coated NCP = 1:16 in weight ratio) and a THF solution (80 μL) of cholesterol,

DSPC (cholesterol/DOPC=1:2 in molar ratio), 20 mol% DSPE-PEG2k, and DOPA-coated NCP to 500 μL of 30% (v/v) ethanol/water at 50 °C. The mixture was stirred at 1,700 rpm for 1 min. THF and ethanol were completely evaporated, and the NCP-Cis/siRNAs solution was allowed to cool down to room temperature.

5.2.4.6 General Procedures of Lipid Coating and PEGylation of NCP-Cis/GMP/siRNAs: NCP-Cis/GMP/siRNAs was prepared by adding 10 μL of aqueous solution of DSPE-siRNA conjugates (DSPE-siRNA/DOPA-NCP-Cis/GMP = 1:16 in weight ratio) and a THF solution (80 μL) of cholesterol, DSPC, DSPE-PEG2k (cholesterol:DSPC:DSPE-PEG2k=1:1:0.75 in molar ratio) and DOPA-NCP-Cis/GMP to 500 μL of 30% (v/v) ethanol/water at 60 °C. The mixture was stirred at 1,700 rpm for 1 min. THF and ethanol were completely evaporated and the NCP-Cis/GMP/siRNAs solution was allowed to cool to room temperature.

5.2.4.7 Characterization of NCP Particles: ICP-MS (Agilent 7700X, Agilent Technologies, USA) was utilized to analyze the Pt concentration of NCP to calculate cisplatin loadings. GMP loading was determined by UV-Vis spectroscopy and thermogravimetric analyses (TGA). Particles were digested overnight in 6 M hydrochloric acid, and the concentration of GMP in the solution was determined by the absorbance at 275 nm using a Shimadzu UV-2401PC UV-Vis Spectrophotometer. The particle size and Zeta potential of NCP-Cis/GMP/siRNAs in PBS were determined by Zetasizer (Nano ZS, Malvern, UK). Transmission electron microscopy (TEM, Tecnai Spirit, FEI, USA) was used to observe the morphology of NCP-Cis/GMP/siRNAs. The association of siRNA on NCP was determined by gel retardation assay on 4% (w/v) agarose gel electrophoresis containing 0.25 μg/mL of EB at 56 V for 1 h. Lane 1 was loaded with free Alexa Fluor siRNAs, while lane 2 was loaded with NCP-Cis/GMP/Alexa-siRNAs. siRNA loading amount was quantified by Quant-iT RiboGreen RNA kit (Invitrogen, USA).

5.2.5 siRNA Protection and Release of NCP-Cis/siRNAs:

NCP-Cis/siRNAs, DSPE-siRNA conjugate, or free siRNA containing 10 μg of siRNA was incubated with 20 μL of fetal bovine serum (FBS) for 0.5, 2, 12, and 24 h. After incubation, 0.5% (w/v) Triton X-100 was added to the mixture to disassociate the lipid from the nanoparticle core. The mixture was centrifuged at 13,000 rpm for 15 min, and the supernatant was subjected to electrophoresis to evaluate the siRNA integrity. The electrophoresis was run on a 2% (w/v) agarose gel at 56 V for 1 h. The intensity of each siRNA band on the gel was quantified by Image Lab software.

The siRNA release of NCP-Cis/siRNAs was evaluated in PBS supplemented with 4.5 μM GSH (extracellular environment) or 10 mM GSH (intracellular environment). NCP-Cis/siRNAs containing 1 μg of siRNA were incubated with 1 mL of PBS at 37 °C with shaking. At predetermined time intervals, the suspension was centrifuged at 13,000 rpm for 10 min, and 0.5 mL of the supernatant was quantified for the siRNA content by Quant-iT RiboGreen RNA kit. An equal volume of the release medium was added, and the precipitate was resuspended before further incubation.

5.2.6 Endosomal Escape Mechanism:

The cisplatin prodrug PtBp used to construct NCP-Cis was dissolved in PBS followed by the addition of 5 mM cysteine. Vigorous gas bubbling was observed while no gas generation was noted before adding cysteine. The gas generated from PtBp in the reducing environment was confirmed by gas chromatography (GC).

Alexa Fluor 647-labeled siRNA was used to prepare NCP-Cis/siRNAs. NCP-Cis/siRNAs were incubated with A2780/CDDP cells for 5, 10, 20, and 30 min, respectively. The cells were washed with PBS three times, stained with 100 nM Lysotracker Green for 2 h, fixed with 4%

paraformaldehyde, and stained with 10 μg/mL DAPI for 20 min. The cells were observed by CLSM. The colocalization of green fluorescence (Lysotracker Green-stained endosome/lysosome) and red fluorescence (Alexa Fluor 647-labeled siRNA) was calculated by ImageJ.

5.2.7 In Vitro *Transfection of NCP-Cis/GMP/siRNAs:*

In 24-well plates, SKOV-3 cells were seeded at 2 x 10^5 cells/well and incubated for 24 h. Nanoparticles were added to the cells at a siRNA dose of 15.4 nM, corresponding to a cisplatin dose of 0.39 μg and a GMP dose of 0.81 μg per well. Following a 4-h incubation, the medium was replaced with McCoy with 10% FBS and incubated for an additional 20 h. RNA was isolated from the transfected cells according to the Trizol reagent protocol (Invitrogen, USA), and cDNA was synthesized from 500 ng of total RNA using PrimeScript®RT reagent kit (Takara Biotechnology Co. Ltd) according to the manufacturer's instructions. Synthesized cDNA, forward and reverse primers, and the SYBR Premix Ex Taq™ (Takara Biotech. Co., Ltd.) were run on the CFX96 Real-Time PCR Detection System (Bio-Rad, USA) to evaluate cellular *ERCC-1, Bcl-2, and survivin* mRNA levels. Sequences of the primers used were designed with Primer Bank (Table 5.1). β-actin was used as an internal loading control. In addition, the cells were lysed, and the Bcl-2 amount was quantified by enzyme-linked immunosorbent assays (ELISA, R&D Systems, USA) according to manufacturer's instructions. Bcl-2 gene silencing efficacy of NCP-Cis/GMP/siRNAs was compared to PBS and NCP-Cis/GMP in the same procedural manner.

Table 5.1 Primer Sequences of β-actin, ERCC-1, Bcl-2, and Survivin for Real-Time PCR.

	Primer F	Primer R
β-actin	5'-CCACCCATGGCAAATTCCATGGCA-3'	5'-TCTAGACGGCAGGTCAGGTCCACC-3'
ERCC-1	5'-CTCCGACACTCTACCGTATAA -3'	5'-GAGGCTGTGAGATGGCATATT-3'
Bcl-2	5'-GTGGAGGAGCTCTTCAGGGA-3'	5'-AGGCACCCAGGGTGATGCAA-3'
survivin	5'-GGCATGGGTGCCCCGACGTT-3'	5'-AGAGGCCTCAATCCATGGCA-3'

5.2.8 In Vitro *Cytotoxicity of NCP-Cis/GMP/siRNAs:*

In vitro cytotoxicity assays were carried out on A2780/CDDP and SKOV-3 ovarian cancer cells. In 96-well plates, A2780/CDDP or SKOV-3 cells were seeded at a density of 2000 cells/well in a total of 100 μL RPMI-1640 or McCoy containing 10% FBS. The cells were incubated for 24 hours at 37°C prior to drug treatment. The culture medium was then replaced by fresh medium. Different concentrations of cisplatin, GMP, free cisplatin/GMP mixture [at the same NCP-Cis and NCP-GMP (NCP carrying GMP) drug dose], Zn Control (NCP carrying no drugs), NCP-Cis, NCP-Cis/GMP, NCP-GMP, and NCP-Cis/GMP/siRNAs were added and incubated at 37 °C and 5% CO_2 for 72 hours. Cell viability was measured by MTS assay (Promega, USA) according to the manufacturer's instructions. IC_{50} values were measured.

5.2.9 Cell Apoptosis by Confocal Microscopy:

Six-well plates with coverslips were seeded with A2780/CDDP cells at a density of 5×10^5 cells/well. The cells were incubated at 37 °C and 5% CO_2 for 24 hours prior to drug treatment. Dispersion of free drugs and RhB-doped particles were incubated with A2780/CDDP cells at 37 °C and 5% CO_2 for 24 hours. Then, the cells were washed with PBS, fixed with iced 4% paraformaldehyde, and stained with Alexa Fluor 488 conjugated Annexin V (Invitrogen, USA) according to the manufacturer's instructions. The cells were imaged using a confocal laser scanning microscope (CLSM, Olympus FV1000, Japan) at excitation wavelengths of 405 nm, 488 nm, 546 nm, and 647 nm to visualize nuclei (blue fluorescence), cell apoptosis (green fluorescence), nanoparticle internalization from rhodamine B (red florescence), and siRNAs uptake (violet fluorescence).

5.2.10 Cell Apoptosis by Flow Cytometry:

A2780/CDDP or SKOV-3 cells were seeded at 5×10^5 cells/well in 6-well plates containing 2 mL total volume of cell culture medium for 24 hours at 37 °C and 5% CO_2. The culture medium was replaced with fresh medium containing different drug treatments at a cisplatin concentration of 0.1 μM for A2780/CDDP cells and 1.0 μM for SKOV-3 cells and/or a GMP concentration of 0.2 μM for A2780/CDDP cells and 2.0 μM for SKOV-3 cells. Following incubation of 24 hours, the floating and adherent cells were collected and stained with Annexin V/dead cell apoptosis kit with Alexa Fluor 488 annexin V and propidium iodide (PI, Invitrogen, USA) according to manufacturer's instructions. The apoptosis was analyzed on a flow cytometer (LSRII 3-8, BD, USA).

5.2.11 Gel Retardation Assay of NCP/siRNAs in Blood Serum:

BALB/c mice intraperitoneally injected with NCP-Cis/Alexa-siRNAs at 1 mg/kg cisplatin dose (or 0.25 mg/kg siRNAs dose). Blood was drawn from the mice at 3 hours post-injection. The blood was centrifuged at 12,000 rpm for 4 min to obtain the serum. The association of siRNA with NCP-Cis in blood serum was determined with gel retardation assay on 4% (w/v) agarose gel electrophoresis containing 0.25 μg/mL of EB at 56 V for 1 h. Lane 1 was loaded with free Alexa Fluor siRNAs, while lane 2 was loaded with NCP-Cis/Alexa-siRNAs.

5.2.12 In Vivo *Maximum Tolerated Dose:*

We measured the maximum tolerated dose (MTD) in the BALB/c mouse model by intraperitoneal injecting NCP-Cis/GMP/siRNAs (0.6 cisplatin mg/kg, 1.32 mg/kg GMP/kg, 0.3 siRNAs mg/kg) every five days for total of 6 doses (n=3). Body weight of each mouse was measured every day.

5.2.13 In Vivo *Anticancer Efficacy of NCP-Cis/GMP/siRNAs in a SKOV-3 Subcutaneous Xenograft Mouse Model:*

Tumor-bearing mice were established by subcutaneous inoculations of SKOV-3 cell suspension (5×10^6 cells per mouse) into the right flank region of 6-week-old athymic female nude mice. After tumor volumes reached approximately 150 mm^3, the mice were randomly divided into 4 groups (n = 6 for PBS, free drugs, and NCP-Cis/GMP/siRNAs; n = 3 for NCP-Cis/GMP) and given the following treatments: (1) PBS by i.p., (2) free cisplatin + GMP + siRNAs by i.p., (3) NCP-Cis/GMP by i.p., and (4) NCP-Cis/GMP/siRNAs by i.p. at equivalent cisplatin doses of 0.3 mg/kg, GMP doses of 0.67 mg/kg, and siRNA doses of 0.15 mg/kg on Day 0 and Day 5, for a total of two injections. Tumor volumes and body weights were monitored everyday up until day 84 post first injection and once every week afterward until 156 post first injection or the completion of the experiment. Tumor volumes were calculated as follows: ($width^2$ × length)/2. Mice were sacrificed when tumor volumes reached 2000 mm^3, or 156 days after the first treatment.

5.2.14 In Vivo *General Toxicity Evaluation of NCP in SKOV-3 Subcutaneous Xenograft Mouse Model:*

Livers, lungs, spleens, and kidneys were also excised and embedded in OCT medium. Five μm frozen tissue sections were stained with hematoxylin and erosin (H&E) and observed for toxicity with light microscopy.

5.2.15 In Vivo *Anticancer Efficacy of NCP-Cis/GMP/siRNAs in a A2780/CDDP Subcutaneous Xenograft Mouse Model:*

Tumor-bearing mice were established by subcutaneous inoculation of A2780/CDDP cell suspension (5×10^6 cells per mouse) into the right flank region of 6-week-old athymic female nude

mice. After tumor volumes reached approximately 75 mm^3, the mice were randomly divided into 2 groups (n = 4) and given the following treatment: (1) PBS by i.p., and (2) NCP-Cis/GMP/siRNAs by i.p. at cisplatin doses of 0.5 mg/kg, GMP doses of 1.1 mg/kg, and siRNA doses of 0.25 mg/kg. The treatment groups were administered every four days, for a total of three injections. Tumor volumes and mouse body weights were monitored everyday. Tumor volumes were calculated as follows: ($width^2 \times length$)/2. All mice were sacrificed when the tumor reaches over 2500 mm^3.

5.2.16 In Vivo *Anticancer Efficacy of NCP-Cis/GMP/siRNAs in a SKOV-3 Subcutaneous Xenograft Mouse Model with Larger Tumors:*

Tumor-bearing mice were established by subcutaneous inoculation of SKOV-3 cell suspension (5 x 10^6 cells per mouse) into the right flank region of 8-week athymic female nude mice. After the tumor volume reached approximately 400 mm^3, the mice were randomly divided into two groups (n = 3) and intraperitoneally injected with PBS and NCP-Cis/GMP/siRNAs at equivalent cisplatin dose of 0.3 mg/kg, GMP dose of 0.67 mg/kg, and siRNA dose of 0.15 mg/kg once every four days for a total of three injections. Tumor volumes and body weights were monitored every day. Tumor volumes were calculated as follows: ($width^2$ x length)/2. All mice were sacrificed 6 days after the first injection.

5.2.17 Statistical Analysis:

Results were expressed as means ± standard deviation (S.D.). Two-ways ANOVA was used to determine statistical significance. A P value < 0.05 was considered statistically significant.

5.3 Results

5.3.1 Synthesis and Characterization of NCP-Cis/GMP/siRNAs:

As highlighted in the previous chapter, we developed a new DOPA-capped particle carrying cisplatin and gem, NCP-Cis/GMP. Particle synthesis was modified to incorporate gemcitabine monophosphate (GMP) into the core, followed by coating the particle with DSPC, cholesterol, and DSPE-PEG2k. This NCP showed strong synergistic effect, superior stability in blood circulation and possessed enhanced anticancer efficacy in small cell lung cancer tumor xenograft model.

We can further control the loading of cisplatin and GMP by putting different ratios of prodrugs during the synthesis of the particle. The loading ratio of the prodrugs during the synthesis is preserved in the final nanoparticle. In addition to nanoparticle formulation, we have also synthesized two other set of particles with different loadings of cisplatin and GMP (one with a loading of 24.0 wt.% cisplatin or 46.3 wt.% cisplatin prodrug and 14.8 wt.% GMP known as NCP-Cis/GMP-2, and the other with 2.2 wt.% cisplatin or 4.3 wt.% cisplatin prodrug and 33.7 wt.% GMP known as NCP-Cis/GMP-3). The three nanoparticles have comparable particle characterizations (Figure 5.1 through Figure 5.4, Table 5.2).

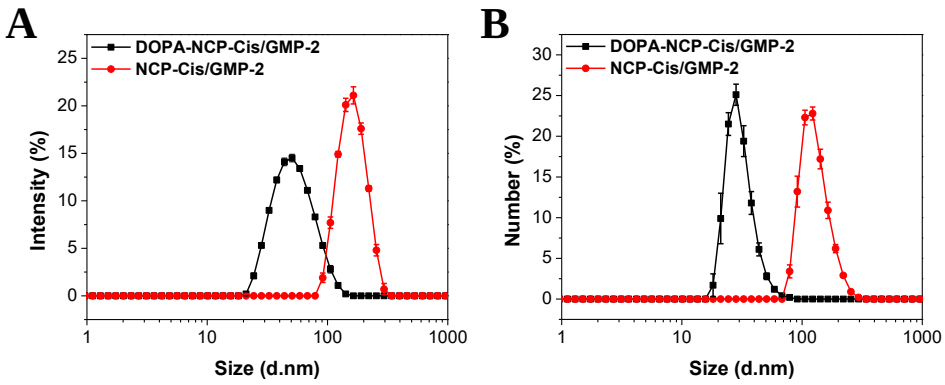

Figure 5.1. (A) Intensity-average and (B) number-average size distribution of NCP-Cis/GMP-2 particles. Bare and lipid-coated particles were measured in THF and PBS, respectively.

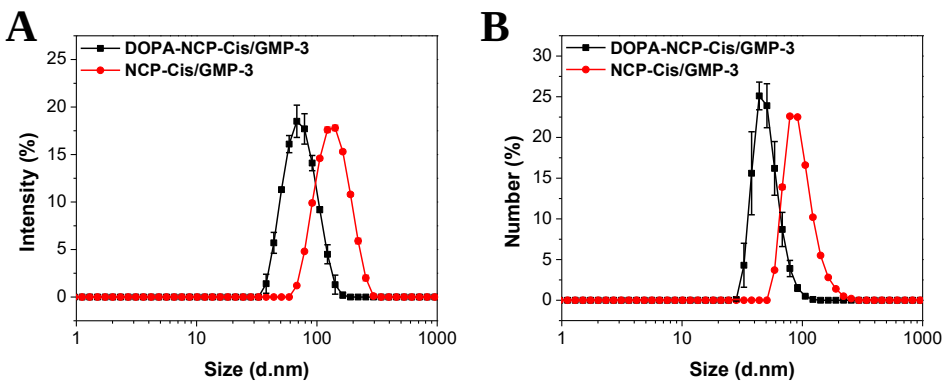

Figure 5.2. (A) Intensity-average and (B) number-average size distribution of NCP-Cis/GMP-3 particles. Bare and lipid-coated particles were measured in THF and PBS, respectively.

Table 5.2. Sizes, Polydispersities, Zeta Potentials, and Drug Loadings of NCP-Cis/GMP Particles.

NCPs	Z-Ave diameter (nm)	Number-Ave diameter (nm)	PDI	Zeta Potential (mV)	Cisplatin Loading (wt %)	GMP Loading (wt %)
DOPA-NCP-**Cis/GMP**	42.4±0.1[#]	28.0±1.0[#]	0.116±0.006	NA	12.9	26.7 (by UV-Vis)
NCP-**Cis/GMP**	83.0±1.0[$]	51.2±0.1[$]	0.143±0.011	-2.84±0.22[$]		27.1 (by TGA)
NCP-**Cis/GMP/siRNAs**	84.1±0.9[$]	48.8±3.2[$]	0.170±0.004	-3.43±0.06[$]		
DOPA-NCP-Cis/GMP-**2**	42.3±0.2[#]	22.5±0.2[#]	0.177	NA	24.0	14.8 (by UV-Vis)
NCP-Cis/GMP-**2**	163.1±0.7[$]	113.2±4.6[$]	0.132	-5.33±1.01[$]		14.5 (by TGA)
DOPA-NCP-Cis/GMP-**3**	70.0±0.4[#]	51.2±2.4[#]	0.080	NA	2.2	33.7 (by UV-Vis)
NCP-Cis/GMP-**3**	128.7±0.6[$]	96.8±0.4[$]	0.070	-4.12±1.10[$]		31.4 (by TGA)

[#]Measured in THF. [$]Measured in PBS buffer. Data are expressed as means±S.D.

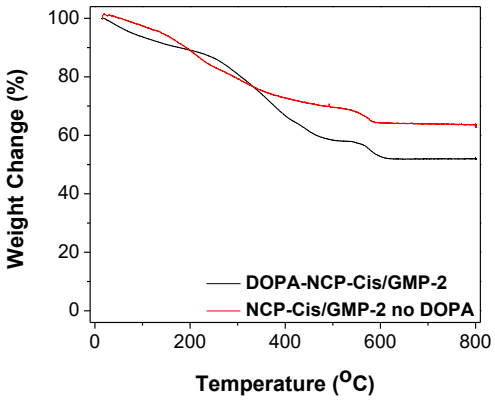

Figure 5.3. TGA analysis of DOPA-NCP-Cis/GMP-2 to determine GMP wt% loading.

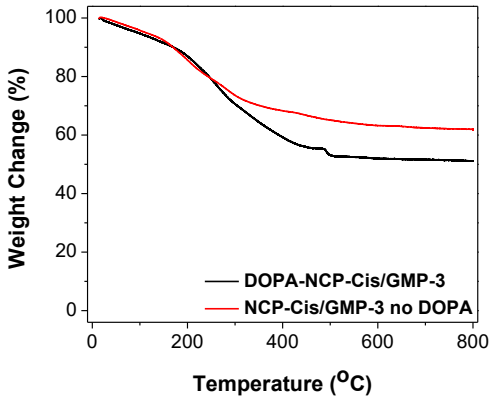

Figure 5.4. TGA analysis of DOPA-NCP-Cis/GMP-3 to determine GMP wt% loading.

We developed a strategy of incorporating siRNA in the shell while shielding it with the PEG layer to prevent nuclease degradation in physiological environments (Figure 5.5). N-succinimidyl-3-(2-pyridyldithio)propionyl-1,2-distearoyl-sn-glycero-3-phosphoethanolamine (DSPE-SPDP) was synthesized from succinimidyl 3-(2-pyridyldithio)propionate and 1,2-distearoyl-sn-glycero-3-phosphoethanolamine, and further conjugated with thiol siRNA (IDT, USA) to afford the DSPE-siRNA conjugate. The disulfide linkage is placed on the 5' end of sense strand of siRNA duplexes in order to avoid potential inhibition on the antisense strand. Mass

spectrometry analysis of the DSPE-siRNA conjugate was carried out using a MALDI-TOF (Figure 5.6). Weak peaks at 12500-14000 Da were observed for the DSPE-*sisurvivin* conjugate along with strong peaks at 6300-7200 Da for the single strand siRNA and its DSPE conjugate. NCP-Cis/GMP was encapsulated with pooled siRNAs (*siERCC-1*, *siBcl-2*, and *sisurvivin*). The addition of siRNAs did not change the particle size and surface charge (Figure 5.7, Table 5.2). The Z-average, number-average, PDI, and zeta-potential of NCP-Cis/GMP/siRNAs were determined to be 84.1±0.9 nm, 48.8±3.2 nm, 0.170±0.004, and -3.43±0.06 mV. Transmission electronic microscopy (TEM) showed monodispersed spherical nanoparticles with diameter of 30 nm (Figure 5.8). Gel retardation assays demonstrated the association of siRNAs with NCP-Cis/GMP (Figure 5.9A). The siRNAs encapsulation efficiency (EE) and loading of NCP-Cis/GMP/siRNAs were determined to be 78.4±1.6% and 4.9±0.3 wt.%, respectively, using Quant-iT RiboGreen RNA kit (Figure 5.9B).

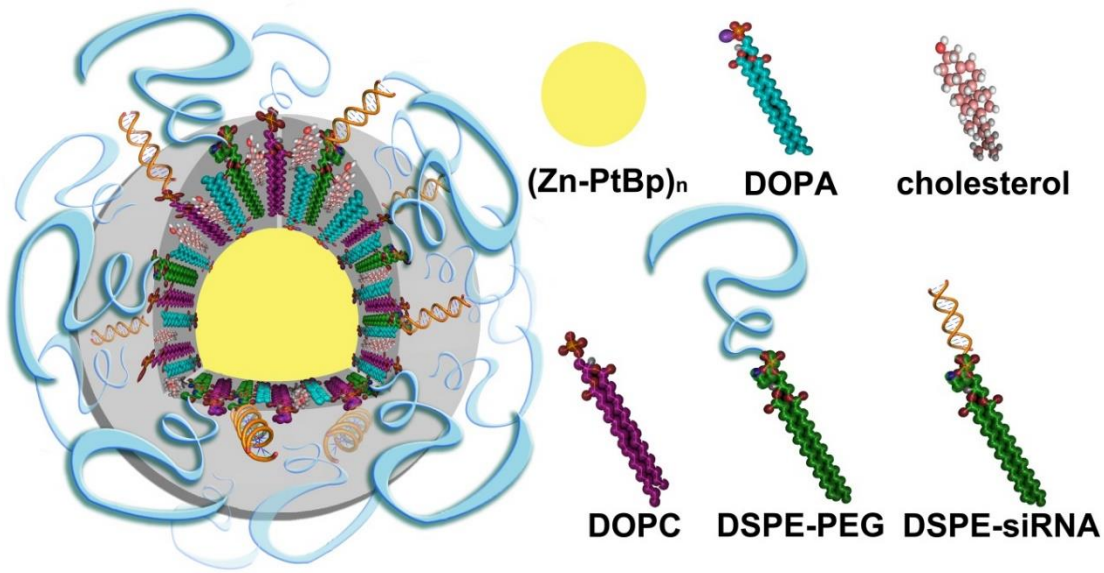

Figure 5.5. Schematic representation of NCP-Cis/GMP/siRNAs carrying cisplatin and gem in the solid core and siRNAs in the lipid shell. Reprinted with permission from Journal of the American Chemical Society, 2016, *138*, 6010-19. Copyright 2016 American Chemical Society.

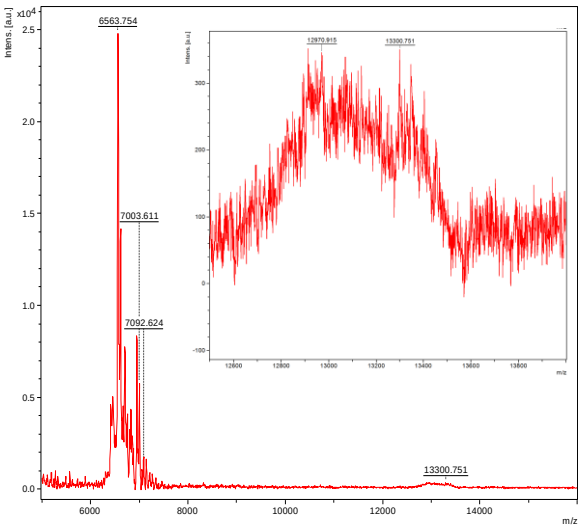

Figure 5.6. MALDI-TOF mass spectrum shows strong peaks at 6300-7200 Da for single strand siRNA and its DSPE conjugate and weak peaks at 12500-14000 Da for the DSPE conjugate of double stranded siRNA. Reprinted with permission from Journal of the American Chemical Society, 2016, *138*, 6010-19. Copyright 2016 American Chemical Society.

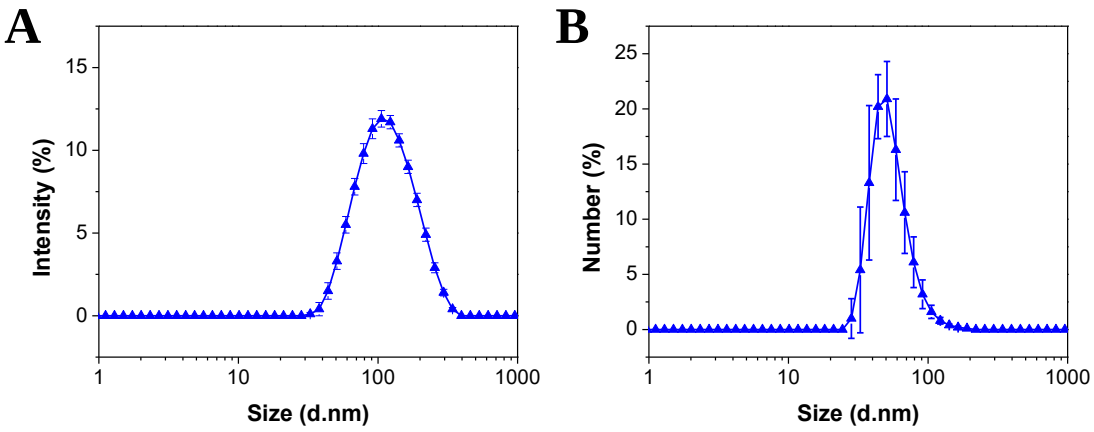

Figure 5.7. (A) Intensity-average and (B) number-average size distribution of NCP-Cis/GMP/siRNAs particles. Bare and lipid-coated particles were measured in THF and PBS, respectively. Reprinted with permission from Journal of the American Chemical Society, 2016, *138*, 6010-19. Copyright 2016 American Chemical Society.

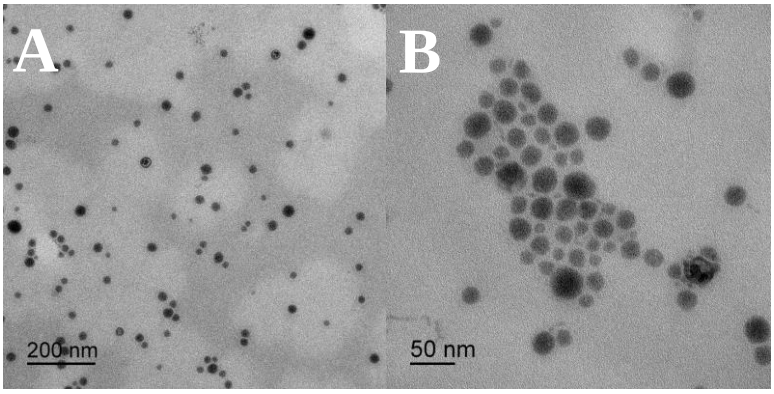

Figure 5.8. TEM micrographs of NCP-Cis/GMP/siRNAs (A, B). Reprinted with permission from Journal of the American Chemical Society, 2016, *138*, 6010-19. Copyright 2016 American Chemical Society.

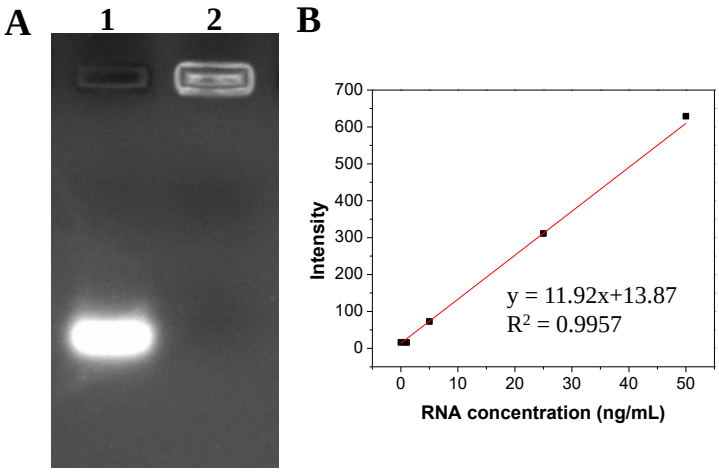

Figure 5.9. (A) Gel retardation of NCP-Cis/GMP/Alexa-siRNA (2% agarose gel, 56 V, 1 h). Lane 1-2 free siRNA, NCP-Cis/GMP/Alexa-siRNA. (B) Fluormetry analysis of siRNA concentration to determine siRNA encapsulation efficiency.

5.3.2 In Vitro *Drug Release*

In the previous chapter, I noted that NCP-Cis/GMP has minimal release after 96 h in 1x PBS buffer with or without 5 mM cysteine at 37ºC in pH 7.4. The negligible release of cisplatin and GMP from the NCP core can be attributed to the lipid layer on the particle surface, which prevents penetration of cysteine to the NCP core, thereby improving the stability of the particle in blood circulation. We also evaluate siRNA release using NCP-Cis/siRNAs in PBS supplemented

with 4.5 μM glutathione (GSH, extracellular environment) or 10 mM GSH (intracellular environment). siRNA release was slow in PBS without GSH but much faster in PBS containing 10 mM GSH (Figure 5.10). Inside cells, the disulfide bond of DSPE-siRNA was rapidly cleaved by a reducing agent, which led to enhanced siRNA release. We evaluated how NCP-Cis/siRNAs protect siRNAs from nuclease degradation by incubating NCP-Cis/siRNAs with serum and using gel electrophoresis to analyze siRNA integrity over time. As depicted in Figure 5.11, the intensity of free siRNA bands decreased rapidly with time; ~46% of the siRNA remained for DSPE-siRNA conjugate after 24h, while 92% of siRNA loaded in NCP-Cis/siRNAs maintained its integrity, suggesting that NCP-Cis/siRNAs effectively protected siRNA from degradation by nuclease in the serum.

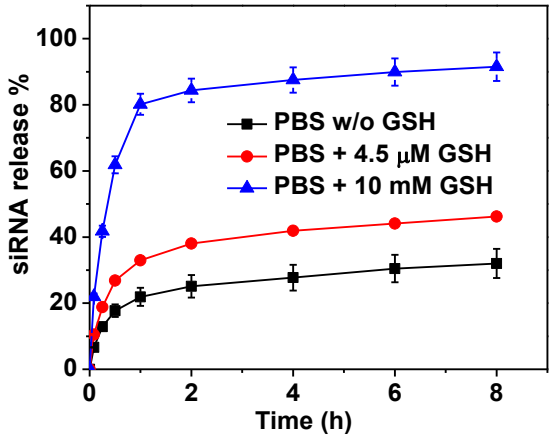

Figure 5.10. siRNA release from NCP-Cis/siRNAs in the presence or absence of reducing agents. Reprinted with permission from Journal of the American Chemical Society, 2016, *138*, 6010-19. Copyright 2016 American Chemical Society.

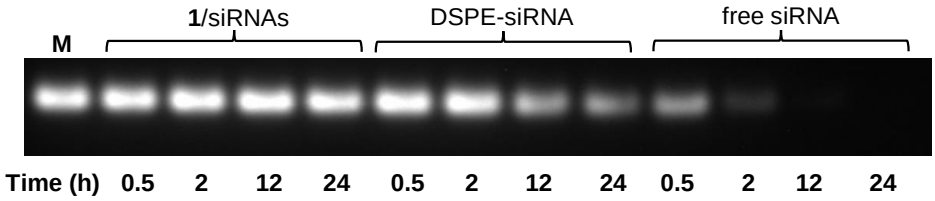

Figure 5.11. Improved siRNA stability in serum of NCP-Cis/siRNAs compared to free siRNA and DSPE-siRNA conjugate as evaluated by electrophoresis (2% agarose gel). "M" stands for untreated siRNA marker. Reprinted with permission from Journal of the American Chemical Society, 2016, *138*, 6010-19. Copyright 2016 American Chemical Society.

5.3.3 Efficient Endosomal Escape

NCP/siRNAs have a novel built-in endosomal escape mechanism that is not reliant on cationic excipients. Two carbon dioxide molecules are generated as byproducts of the intracellular release of cisplatin (Figure 5.12), which we hypothesize can change the osmotic pressure to disrupt the endosomal membrane, facilitating the escape of siRNAs from endosomal entrapment and triggering the formation of RNA-induced silencing complexes (RISCs) in the cytoplasm to mediate gene silencing (Figure 5.13).

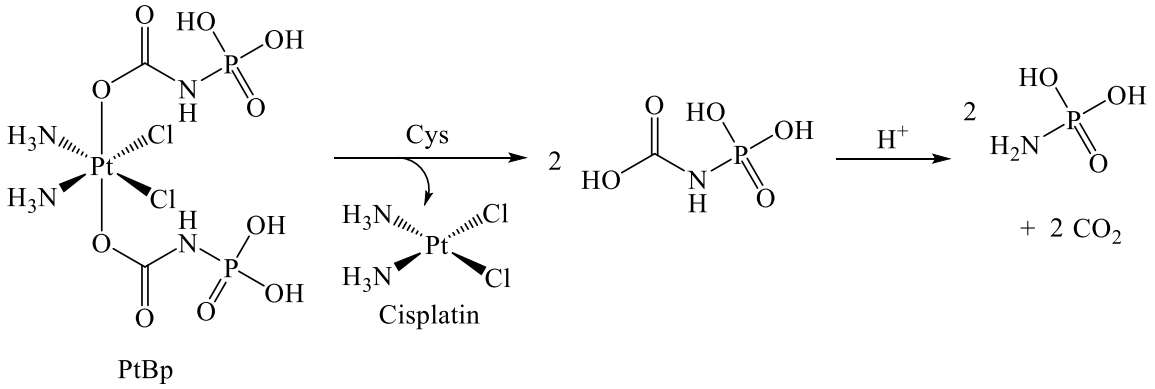

Figure 5.12. Scheme showing the CO_2 generation of PtBp in reducing environment. Reprinted with permission from Journal of the American Chemical Society, 2016, *138*, 6010-19. Copyright 2016 American Chemical Society.

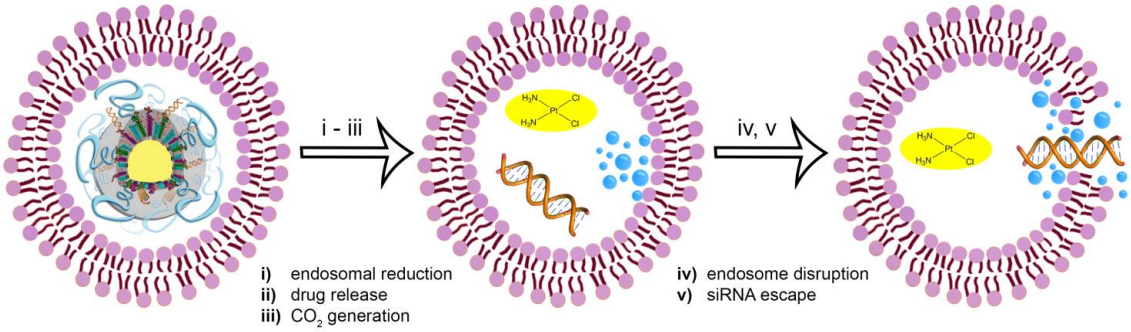

Figure 5.13. Schematic showing the endosomal escape of NCP/siRNAs. Reprinted with permission from Journal of the American Chemical Society, 2016, *138*, 6010-19. Copyright 2016 American Chemical Society.

The efficient generation of CO_2 was first confirmed in a solution, where we observed efficient CO_2 generation from PtBp in reducing environments. Vigorous gas bubbling was observed when 5 mM cysteine (Cys) was added to a solution of PtBp in PBS, but no gas generation was noted before the addition of Cys. The identity of the gas was confirmed to be CO_2 by gas chromatography, which displayed a peak with a retention time identical to that of authentic CO_2 (Figure 5.14).

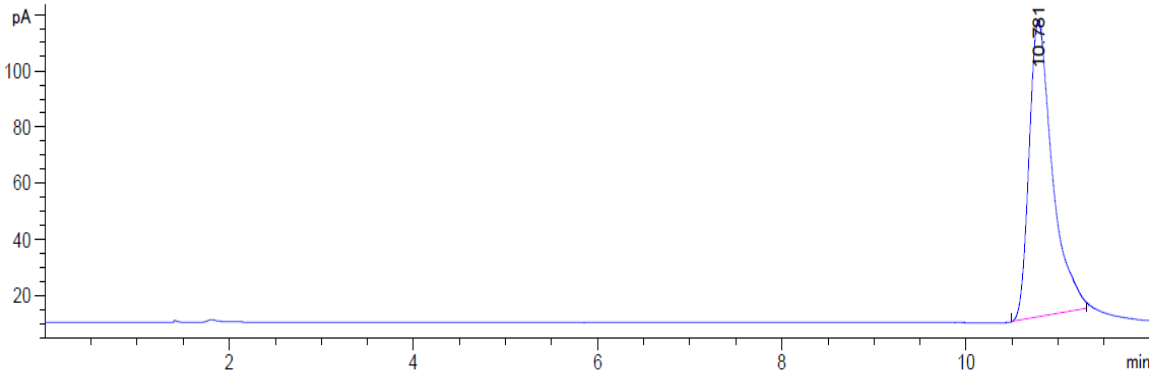

Figure 5.14. GC spectrum confirming CO_2 generation from PtBp in PBS containing 5 mM cysteine. Reprinted with permission from Journal of the American Chemical Society, 2016, *138*, 6010-19. Copyright 2016 American Chemical Society.

We used confocal laser scanning microscopy (CLSM) to evaluate endosomal escape efficiency of Alexa Fluor 647 labeled NCP-Cis/siRNAs (NCP-Cis/Alexa-siRNAs) in A2780/CDDP cells (Figure 5.15). Human OCa cells A2780/CDDP were incubated with NCP-Cis/Alexa-siRNAs for different time periods, fixed, stained with Lysotracker Green and DAPI, and observed by CLSM. The co-localization of green fluorescence (Lysotracker Green-stained endosome) and red fluorescence (Alexa Fluor 647-labeled siRNA) was calculated by Image J. NCP-Cis/Alexa-siRNAs was rapidly internalized by cells, evidenced by the co-localization of siRNA and endosome/lysosome. A linear decrease in co-localization occurred over 30 min, indicating that siRNAs can successfully escape endosomal entrapment and form RISCs in the cytoplasm (Figure 5.16).

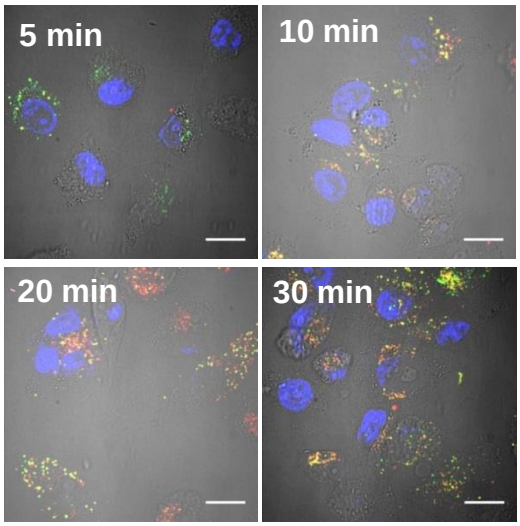

Figure 5.15. Time-dependent endosomal escape of NCP/siRNAs (Alexa Fluor 647-labeled, red fluorescence) in SKOV-3 cells. Endosomes and nuclei were stained with Lysotracker Green (green fluorescence) and DAPI (blue fluorescence), respectively. Bar = 20 μm. Reprinted with permission from Journal of the American Chemical Society, 2016, *138*, 6010-19. Copyright 2016 American Chemical Society.

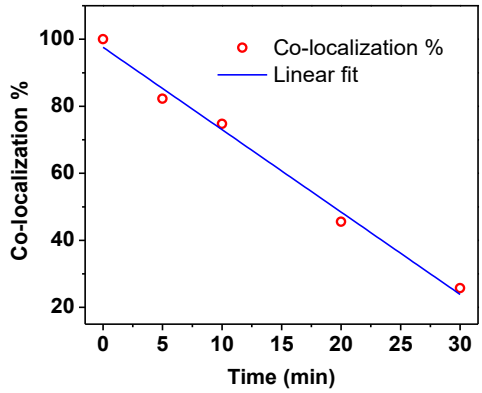

Figure 5.16. Percent co-localization of siRNA and endosome quantified by Image J from CLSM images in Figure 5.15. Reprinted with permission from Journal of the American Chemical Society, 2016, *138*, 6010-19. Copyright 2016 American Chemical Society.

5.3.4 In Vitro *Transfection Efficiency*

NCP/siRNAs successfully overcame several key barriers to gene transfection, including siRNA encapsulation, protection, release, and endosomal escape. As a result, NCP-Cis/GMP/siRNAs evoked potent gene silencing, significantly reducing mRNA expression in cisplatin-resistant SKOV-3 ovarian cancer cell lines (Figure 5.17). We compared the gene silencing efficiency of NCP-Cis/GMP/siRNAs containing three siRNAs to NCP-Cis/GMP to determine if there was siRNA downregulation of relevant proteins responsible for drug resistance. At a total siRNA dose of 15.4 nM, NCP-Cis/GMP/siRNAs efficiently downregulated ERCC-1, survivin, and Bcl-2 gene expression in SKOV-3 cells by 40-50%, as determined by Realtime-PCR. Bcl-2 knockdown efficiency of NCP-Cis/GMP/siRNAs was also compared with PBS and NCP-Cis/GMP by enzyme-linked immunosorbent assays (ELISA) in SKOV-3 cells (Figure 5.18). NCP-Cis/GMP/siRNAs demonstrates that siRNAs can effectively knockdown 42.0 ± 7.7% of its genes. Slight decreased Bcl-2 expression levels (16.8 ± 4.9%) in NCP-Cis/GMP attributed to the cytotoxicity induced by cisplatin and gem that influence expression levels of Bcl-2.

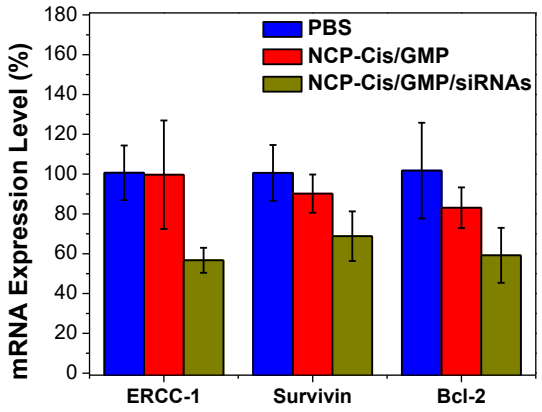

Figure 5.17. mRNA expression of ERCC-1, survivin, and Bcl-2 in cisplatin-resistant SKOV-3 OCa cells transfected with NCP-Cis/GMP/siRNAs at a total siRNA concentration of 15.4 nM (n=3).

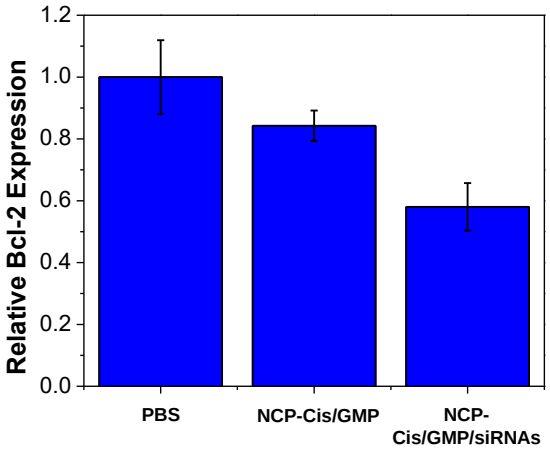

Figure 5.18. Bcl-2 relative expression levels in SKOV-3 ovarian cancer cells transfected with PBS, NCP-Cis/GMP, and NCP-Cis/GMP/siRNAs at an siRNA concentration of 15.4 nM for 4 h (n=3). Reprinted with permission from Journal of the American Chemical Society, 2016, *138*, 6010-19. Copyright 2016 American Chemical Society.

5.3.5 In Vitro *Cytotoxicity and Synergistic Effect*

Efficient gene silencing dramatically enhanced the efficacy of NCP-Cis/GMP/siRNAs compared to NCP-Cis/GMP in the cisplatin-resistant SKOV-3 ovarian cancer cells. By co-delivering cisplatin, gem, and three siRNAs, NCP-Cis/GMP/siRNAs resensitized the cells to

platinum drug treatment, drastically decreasing the dose of a drug required for 50% inhibition (IC_{50}) of cisplatin and gem relative to that of monotherapeutic treatments. *In vitro* cytotoxicity of NCP-Cis/GMP/siRNAs was tested on SKOV-3 (Figure 5.19, Table 5.3) and A2780/CDDP (Figure 5.20, Table 5.3) ovarian cancer cells. The viability of cells treated with nanoparticles or free drug at different concentrations for 72 h was measured by MTS assay. As seen in Figure 5.19, Figure 5.20, and Table 5.3, the cisplatin IC_{50} of NCP-Cis/GMP/siRNAs decreased by 3.2- and 3.4-fold decrease compared to NCP-Cis/GMP in SKOV-3 and A2780/CDDP cells, respectively. In contrast, in the cisplatin-sensitive ovarian cancer cell line A2780, we observed similar cytotoxicity between NCP-Cis/GMP and NCP-Cis/GMP/siRNAs groups (Figure 5.21). This result further confirmed our hypothesis: the efficient knockdown of MDR genes by NCP-Cis/GMP/siRNAs is vital to enhancing chemotherapeutic cytotoxicity in drug-resistant cells.

Likewise, the addition of two chemotherapeutics in a single nanocarrier showed far greater cytotoxicity over those with just one drug. The IC_{50} values of NCP-Cis and NCP-GMP against SKOV-3 cells were 8.18 ± 1.10 μM and 2.48 ± 0.31 μM, respectively, and decreased to 0.70 ± 0.18 μM and 1.43 ± 0.36 μM when combined in one carrier, which was equal to 117- and 1.7-fold decrease, respectively. The nanoparticles showed similar IC_{50} to their corresponding free drugs, with IC_{50} of 2.60 ± 0.40 μM for cisplatin and 3.44 ± 0.98 μM for GMP. Similar results were obtained with A2780/CDDP cells, the IC_{50} values of NCP-Cis/GMP were about 155-fold, 113-fold, 1.7-fold, and 2.2-fold lower than free cisplatin, NCP-Cis, free GMP, and NCP-GMP, respectively.

The combination index (CI) was between 0.4 to 1.0 for NCP-Cis/GMP against the monotherapeutic NCP and free drug over a large range of drug effect level for both SKOV-3 (Figure 5.19C) and A2780/CDDP (Figure 5.20C). The CI was further lowered to around 0.2 for

NCP-Cis/GMP/siRNAs against single drug NCP and free cisplatin and GMP. Synergy, indicated when CI was <1, was seen between cisplatin and GMP. Synergy was enhanced with the addition of siRNAs into the nanocarrier, since the siRNAs regulates anti-apoptotic genes.

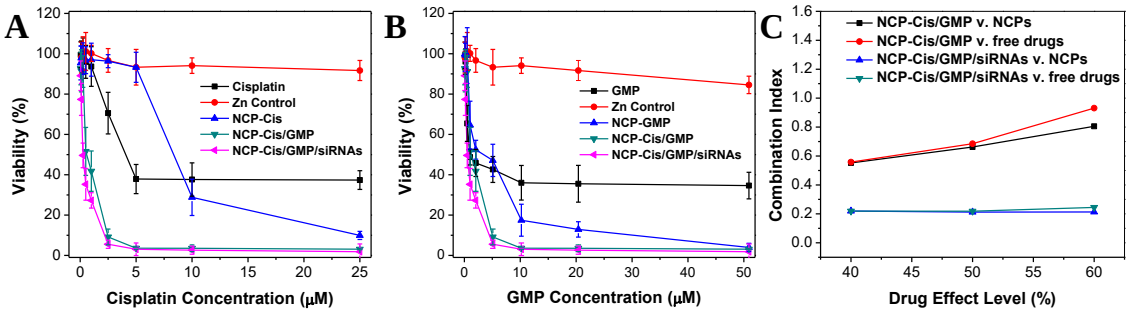

Figure 5.19. *In vitro* cytotoxicity plots (A, B) and combination index (CI) (C) of cisplatin/GMP combinations on SKOV-3 cells. The cell viabilities on SKOV-3 cells were measured after 72 h exposure to Zn Control, NCP-Cis, NCP-GMP, NCP-Cis/GMP, NCP-Cis/GMP/siRNAs, or free drugs (cisplatin, or GMP). Data are mean ± S.D. (n=6). Reprinted with permission from Journal of the American Chemical Society, 2016, *138*, 6010-19. Copyright 2016 American Chemical Society.

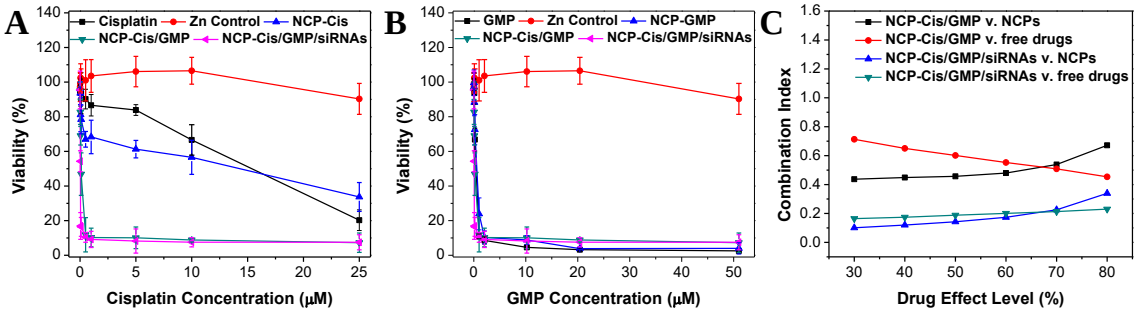

Figure 5.20. *In vitro* cytotoxicity plots (A, B) and combination index (CI) (C) of cisplatin/GMP combinations on A2780/CDDP cells. The cell viabilities on A2780/CDDP cells were measured after 72 h exposure to Zn Control, NCP-Cis, NCP-GMP, NCP-Cis/GMP, NCP-Cis/GMP/siRNAs or free drugs (cisplatin, or GMP). Data are mean ± S.D. (n=6). Reprinted with permission from Journal of the American Chemical Society, 2016, *138*, 6010-19. Copyright 2016 American Chemical Society.

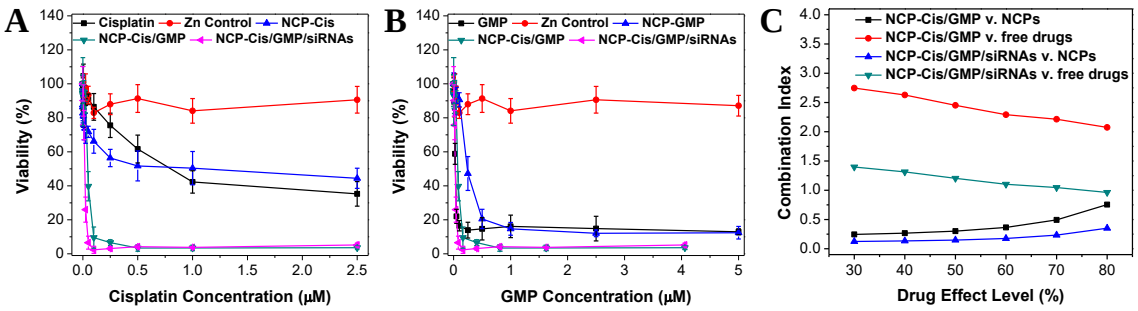

Figure 5.21. *In vitro* cytotoxicity plots (A, B) and combination index (CI) (C) of cisplatin/GMP combinations on A2780 cells. The cell viabilities on A2780 cells were measured after 72 h exposure to Zn Control, NCP-Cis, NCP-GMP, NCP-Cis/GMP, NCP-Cis/GMP/siRNAs or free drugs (cisplatin, or GMP). Data are mean ± S.D. (n=6). Reprinted with permission from Journal of the American Chemical Society, 2016, *138*, 6010-19. Copyright 2016 American Chemical Society.

Table 5.3. Cisplatin IC_{50} Values of Cisplatin, GMP, NCP-Cis, NCP-GMP, NCP-Cis/GMP, and NCP-Cis/GMP/siRNAs Against A2780/CDDP, SKOV-3, and A2780 Cells (the numbers in parenthesis refer to GMP concentrations).

	A2780/CDDP	SKOV-3	A2780
Cisplatin(μM)	12.731±1.456	2.60±0.40	0.764±0.183
GMP (μM)	(0.274±0.049)	(3.44±0.98)	(0.032±0.0.004)
Zn Control* (μM)	>25 (>50)	>50 (>50)	>50 (>50)
NCP-Cis (μM)	9.283±1.424	8.18±1.10	0.913±0.0.047
NCP-GMP (μM)	(0.364±0.096	(2.48±0.31)	(0.298±0.071)
NCP-Cis/GMP (μM)	0.082±0.017 (0.163±0.034)	0.70±0.18 (1.43±0.36)	0.040±0.015 (0.077±0.003)
NCP-Cis/GMP/siRNAs (μM)	0.024±0.002 (0.051±0.004)	0.22±0.04 (0.46±0.08)	0.032±0.009 (0.064±0.003)

*Zn Control does not contain cisplatin or GMP as they are served as a control to study the toxicity of NCP formulations. The amount of Zn Control particle was the same as NCP-Cis/GMP under the studied concentrations. Data are expressed as means±S.D.

Different formulations of NCP-Cis/GMP were also performed in three different ovarian cancer cell lines (Table 5.4). In each of the formulations, they showed enhanced synergy between cisplatin and gem over their monotherapeutic counterparts. Table 5.4 shows a clear inverse relationship between the ratios of cisplatin/GMP and IC_{50}: Nanoparticles carrying higher amounts of GMP showed significantly greater synergistic effects than nanoparticles carrying increased amounts of cisplatin. We chose the original NCP-Cis/GMP for the rest of our studies for their relative stability and optimal size. We believe that the superior physical properties of the original NCP-Cis/GMP outweigh the benefits from the *in vitro* cytotoxicity results in the *in vivo* setting.

Table 5.4. Cisplatin IC_{50} values of different formulation of NCP-Cis/GMP against A2780, A2780/CDDP, and SKOV-3 Cells (the numbers in parenthesis refer to GMP concentrations).

	NCP-Cis/GMP (μM)	NCP-Cis/GMP-2 (μM)	NCP-Cis/GMP-3 (μM)
A2780	0.040±0.015 (0.077±0.0029)	0.297±0.089 (0.184±0.062)	0.00085±0.00031 (0.011±0.004)
A2780/CDDP	0.051±0.009 (0.098±0.017)	2.3±0.2 (1.4±0.1)	0.0035±0.0002 (0.0450±0.0028)
SKOV-3	0.84±0.15 (1.8±0.4)	2.6±0.3 (1.4±0.2)	0.06±0.01 (0.57±0.25)

5.3.6 In Vitro *Cell Apoptosis*

Confocal laser scanning microscopy (CLSM) was performed on A2780/CDDP cells to determine the cellular uptake of NCP (Figure 5.22). Dyed-doped particles of NCPs were synthesized incorporating Rhodamine-B into particles for confocal imaging studies. Internalization of nanoparticles could be observed by RhB red fluorescence found in cells. Significant green FITC-Annexin V signals were found in ovarian cells incubated with cisplatin/GMP and NCP-Cis/GMP, indicating that the combination of cisplatin and GMP drugs induced substantial cell apoptosis. In contrast, weaker FITC signals were observed for A2780/CDDP incubated with monothereapeutic treatments. No cytotoxicity was observed for Zn

Control as seen by the absence of Annexin V biomarker. We also coated NCP-Cis/GMP with fluorescent siRNA (violet), and significant siRNA uptake was observed in CLSM (Figure 5.23).

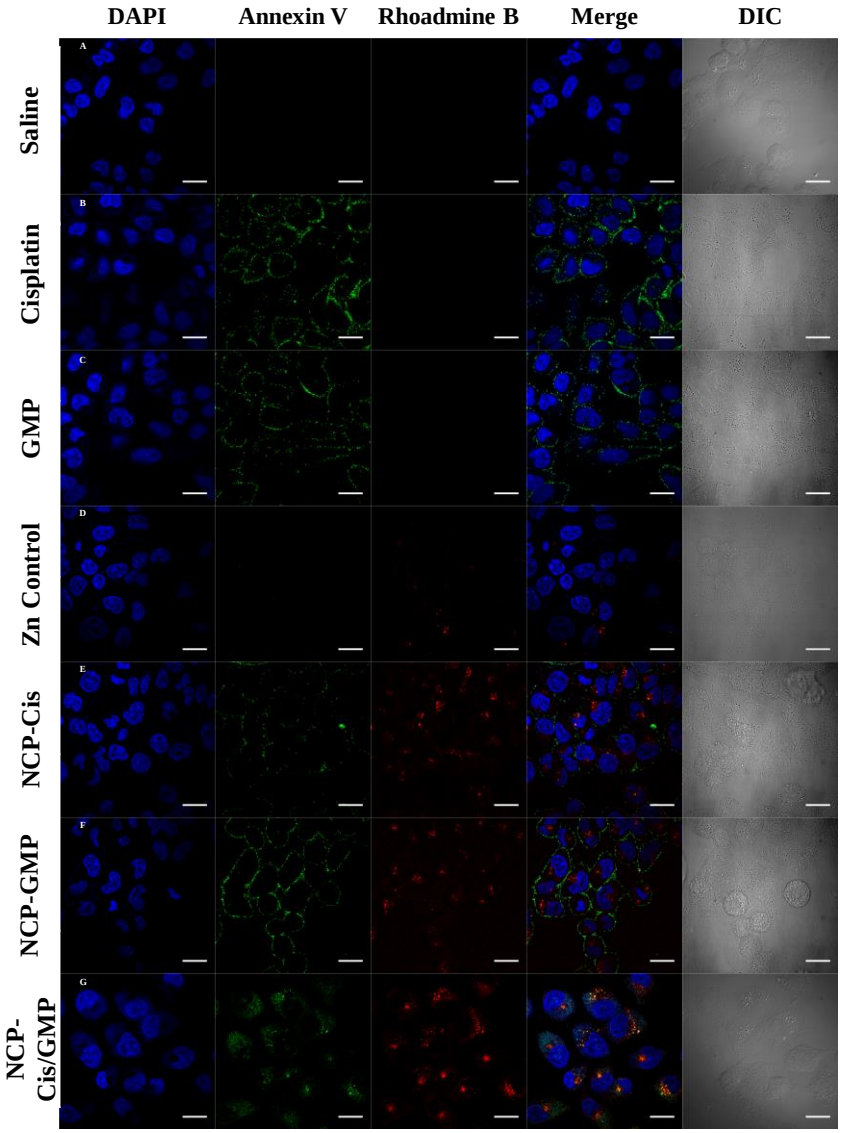

Figure 5.22. CLSM images showing cell apoptosis in A2780/CDDP cells after incubation with free drugs or particles for 24 h. Cells were stained with Alexa Fluor 488 conjugated Annexin V and the nuclei were stained with DAPI. Scale bars: 20 μm. Reprinted with permission from Journal of the American Chemical Society, 2016, *138*, 6010-19. Copyright 2016 American Chemical Society.

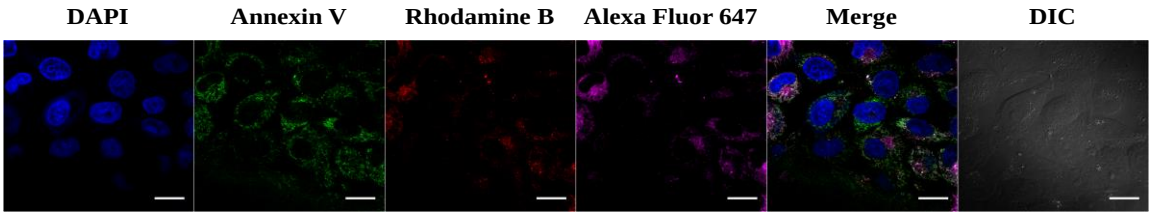

Figure 5.23. CLSM images showing the apoptosis induced by RhB-NCP-Cis/GMP/siRNAs in A2780/CDDP ovarian cancer cells. First column represents DAPI-stained nucleus. Second column represents Annenxin-V stained cells. Third column presents RhB labeled particles (only presence in NCP particles). Fourth column represents the Alexa Fluor 647-labeled siRNA. Fifth column is the merged images. Sixth column is the DIC. Bar = 20 μm. Reprinted with permission from Journal of the American Chemical Society, 2016, *138*, 6010-19. Copyright 2016 American Chemical Society.

The enhanced anticancer efficacy was further supported by the ability of NCP-Cis/GMP/siRNAs to induce cell apoptosis more efficiently than monotherapeutic nanoparticles, free drug, and NCP-Cis/GMP in SKOV-3 and A2780/CDDP cells, as confirmed by Annexin V/PI analysis. Similar to the cytotoxicity assay and CLSM analysis, the total apoptosis was observed for cisplatin, GMP, NCP-Cis, NCP-GMP, NCP-Cis/GMP, NCP-Cis/GMP/siRNAs were determined to be 1.82%, 55.50%, 1.75%, 55.02%, 85.46%, and 91.45%, respectively, for SKOV-3 cells (Figure 5.24, Table 5.5). Cisplatin, GMP, NCP-Cis, NCP-GMP, NCP-Cis/GMP, and NCP-Cis/GMP/siRNAs induced 21.32%, 24.41%, 24.48%, 21.60%, 25.79%, and 32.49% apoptosis for A2780/CDDP cell, respectively (Figure 5.25, Table 5.5). No apoptotic cells were seen in PBS and Zn Control for both ovarian cancer cell lines.

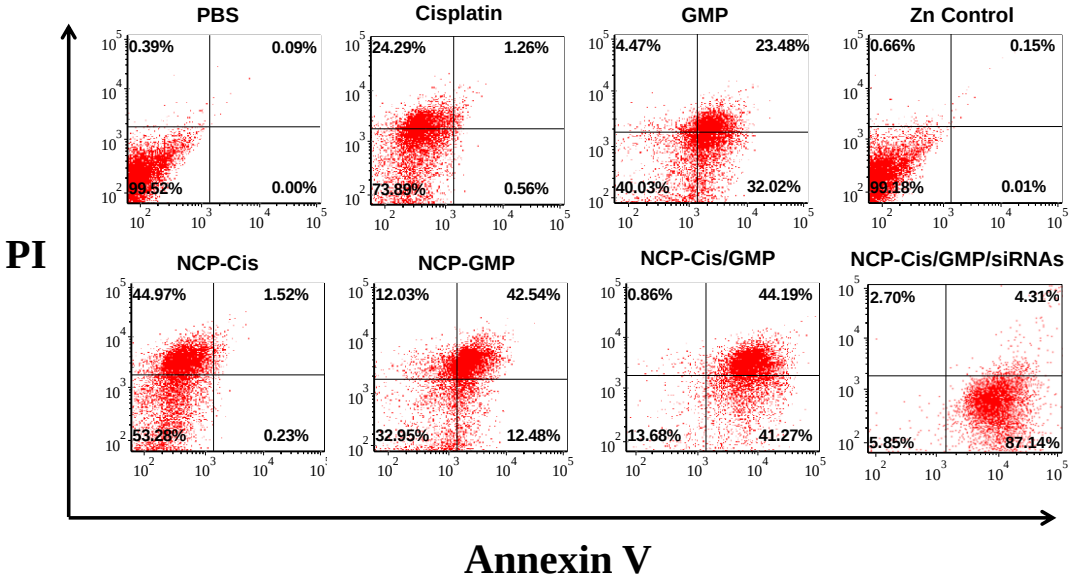

Figure 5.24. Flow cytometry analysis of PBS, cisplatin, GMP, Zn Control, NCP-Cis, NCP-GMP, and NCP-Cis/GMP, and NCP-Cis/GMP/siRNAs in SKOV-3 ovarian cancer cells. Reprinted with permission from Journal of the American Chemical Society, 2016, *138*, 6010-19. Copyright 2016 American Chemical Society.

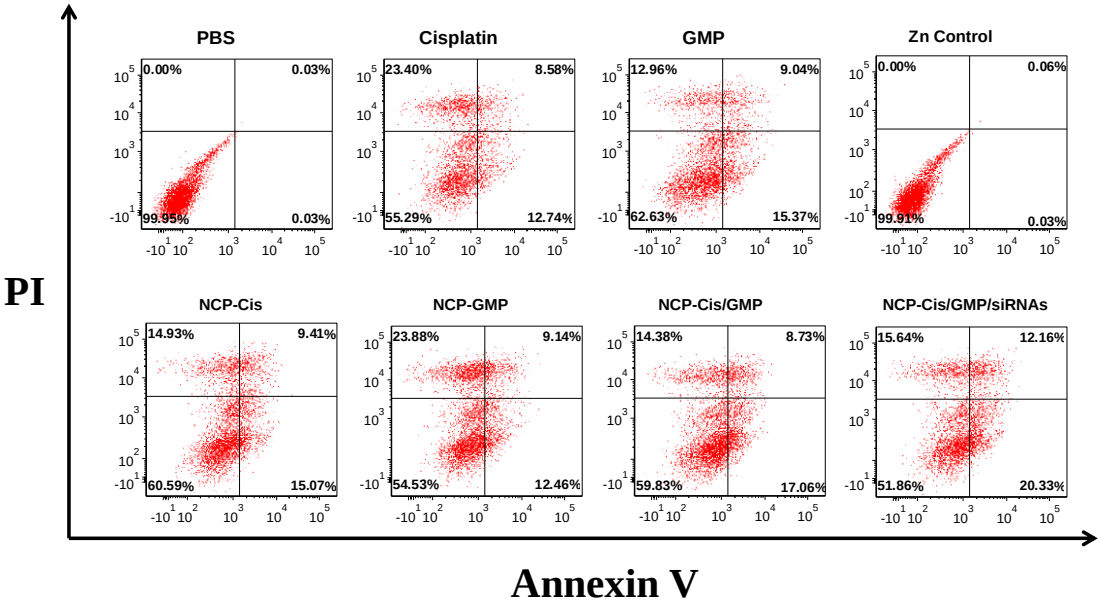

Figure 5.25. Flow cytometry analysis of PBS, cisplatin, GMP, Zn Control, NCP-Cis, NCP-GMP, and NCP-Cis/GMP, and NCP-Cis/GMP/siRNAs in A2780/CDDP ovarian cancer cells.

Table 5.5. Percentages of Healthy, Apoptotic, and Necrotic SKOV-3 and A2780/CDDP Cells After a 24-Hour Treatment of PBS, Cisplatin, GMP, Zn control, NCP-Cis, NCP-GMP, NCP-Cis/GMP, NCP-Cis/GMP/siRNAs.

	Healthy (%)	Apoptosis (%)	Necrosis (%)
SKOV-3			
PBS	99.5	1.0	0.4
Cisplatin	73.9	1.8	24.3
GMP	40.0	55.5	4.5
Zn Control	99.2	0.2	0.7
NCP-Cis	53.3	1.8	45.0
NCP-GMP	33.0	55.0	12.0
NCP-Cis/GMP	13.7	85.5	0.9
NCP-Cis/GMP/siRNAs	5.9	91.5	2.7
A2780/CDDP			
PBS	100.0	0.1	0.0
Cisplatin	55.3	21.3	23.4
GMP	62.6	24.41	13.0
Zn Control	99.9	0.1	0.0
NCP-Cis	60.6	24.5	14.9
NCP-GMP	54.5	21.5	23.9
NCP-Cis/GMP	59.8	25.8	14.4
NCP-Cis/GMP/siRNAs	51.9	32.5	15.6

5.3.7 Pharmacokinetics in Red and White Blood Cell Layer and Plasma Layer

In the previous chapter, I described the pharmacokinetics and biodistribution profiles of NCP-Cis/GMP in CT26 tumor-bearing BALB/c mice by i.v. injection. We determined that NCP-Cis/GMP exhibited half-lives ($t_{1/2\beta}$) of 18.5 ± 5.2 h and 14.7 ± 2.8 h for Pt and GMP, respectively. However, we could not quantify siRNAs concentration in red/white blood cell layer due to interference in the fluorimetry. Therefore, we evaluated the serum siRNA release of NCP-Cis/siRNAs by fluorimetry with excitation and emission wavelengths of 650 and 670 nm, respectively (Figure 5.26). By i.v. injection, the siRNA concentrations in blood were best fit by a one-compartment model with nonlinear elimination, with blood circulation half-lives of 10.7±1.2

h, which is similar to the Pt blood circulation half-life of 10.2±0.6 h. Since the majority of the particles are found in the plasma layer of the blood, in theory, the siRNAs should be intact on the particle. If the siRNAs are not intact on the particle, they would have been rapidly cleared from the bloodstream, but we were able to observe them until 48 h post injection. A gel retardation in blood serum 3 h after i.p injection of NCP-Cis/siRNAs showed that the movement of siRNA on NCP-Cis/Alexa-siRNAs was completely retarded, suggesting that siRNAs was still bound to the particle (Figure 5.27). In contrast, during gel retardation on free siRNAs, the band moved, showing that the free siRNAs are rapidly degraded by nuclease from the blood.

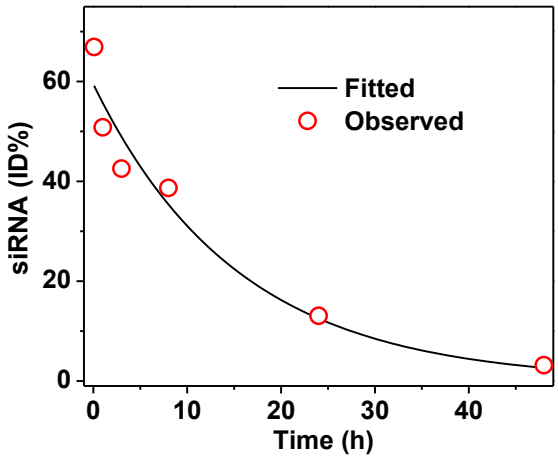

Figure 5.26. Pharmacokinetics of siRNA concentrations in blood after intravenous administration of NCP-Cis/siRNAs in CT26 tumor-bearing mice at time points 5 min, 1 h, 3h, 8 h, 24 h, and 48 h. Data are mean ± S.D. (n=3). One-compartment model was used for fitting the siRNAs distributions in serum. Reprinted with permission from Journal of the American Chemical Society, 2016, *138*, 6010-19. Copyright 2016 American Chemical Society.

Figure 5.27. Gel retardation of NCP-Cis/siRNAs in blood serum 3 h post i.p injection (4% agarose gel, 56 V, 1 h). Lane 1-2 free siRNA, NCP-Cis/siRNAs. Reprinted with permission from Journal of the American Chemical Society, 2016, *138*, 6010-19. Copyright 2016 American Chemical Society.

5.3.8 Antitumor Activity In Vivo

By combining efficient gene silencing, enhanced cytotoxicity, strong synergy among cisplatin, GMP, and siRNAs, and favorable pharmacokinetics and biodistribution, NCP-Cis/GMP/siRNAs showed unprecedented anticancer efficacy against a cisplatin-resistant SKOV-3 subcutaneous xenograft mouse model of OCa. Mice bearing SKOV-3 tumors (~150 mm^3) were treated with PBS, free cisplatin, and GMP with siRNAs, NCP-Cis/GMP, or NCP-Cis/GMP/siRNAs at 0.3 mg cisplatin/kg, 0.67 mg GMP/kg, and 0.15 mg siRNAs/kg every five days, for a total of two injections. As shown in Figure 5.28, the free drug combination failed to inhibit tumor growth, while both NCP-Cis/GMP and NCP-Cis/GMP/siRNAs treatment led to tumor regression after the first injection. NCP-Cis/GMP-treated mice showed rapid tumor regression followed by aggressive tumor regrowth 15 days later. In contrast, NCP-Cis/GMP/siRNAs completely eradicated the tumors, and the mice remained tumor-free for the 156

days until the completion of the experiment. No significant weight loss was observed in NCP-Cis/GMP/siRNAs treated group, indicating the absence of severe systemic toxicity (Figure 5.28 and Figure 5.29).

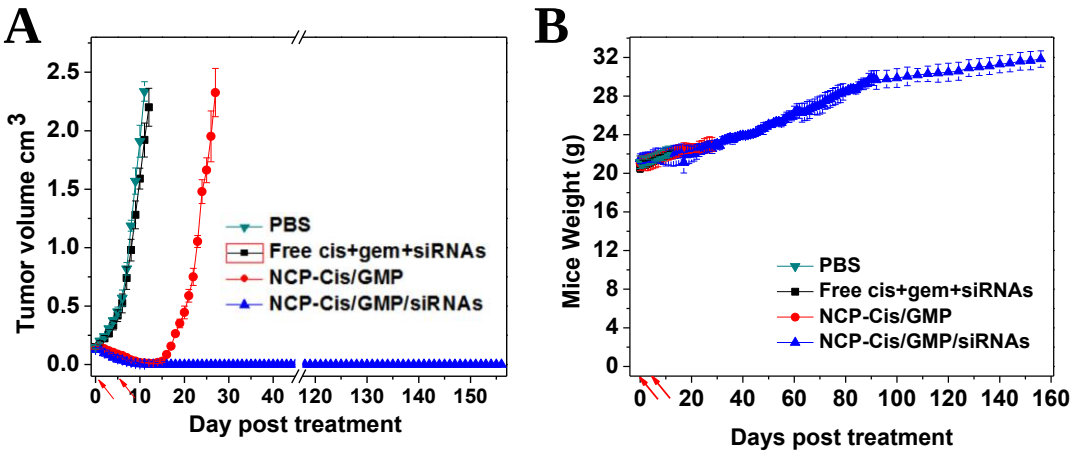

Figure 5.28. (A) Anticancer efficacy of NCP-Cis/GMP/siRNAs against SKOV-3 subcutaneous xenografts starting at tumor volume of ~150 mm^3. Free drug combination or nanoparticles were intraperitoneally injected at 0.3 mg cisplatin/kg, 0.67 mg GMP/kg, and 0.15 mg siRNAs/kg on Day 0 and Day 5 for a total of two injections. (B) Body weight evolution of SKOV-3 tumor-bearing athymic mice treated with NCP-Cis/GMP/siRNAs (0.3 mg cisplatin/kg, 0.7 GMP mg/kg, and 0.15 siRNAs mg/kg). Data are expressed as means±S.D. (n=6). Reprinted with permission from Journal of the American Chemical Society, 2016, *138*, 6010-19. Copyright 2016 American Chemical Society.

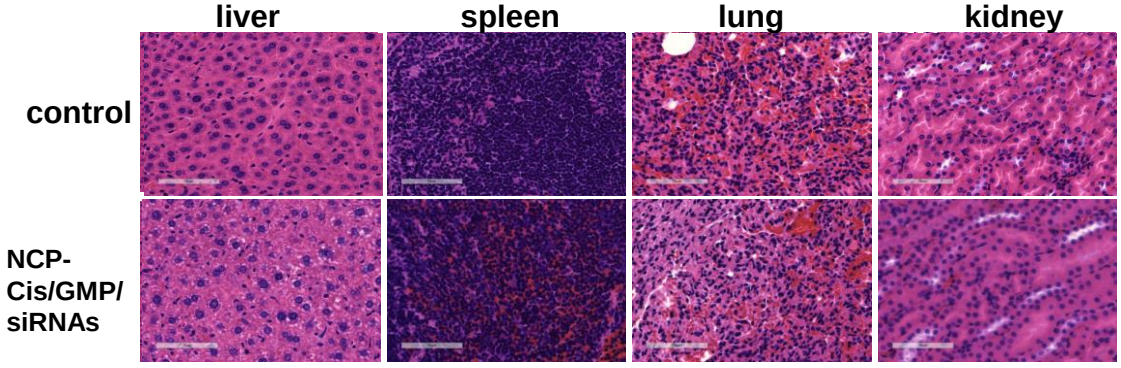

Figure 5.29. Histology images of resected organs (with H&E staining) of SKOV-3 tumor-bearing mice treated with saline or NCP-Cis/GMP/siRNAs at the efficacy endpoints. Bar = 70 μm.

In addition to SKOV-3, we also evaluated the *in vivo* antitumor effect of NCP-Cis/GMP/siRNAs on cisplatin resistant A2780/CDDP ovarian cancer at 0.5 mg cisplatin/kg, 1.1 mg GMP/kg, and 0.25 mg siRNAs/kg every four days, for a total of three injections (Figure 5.30). Due to the rapid growth nature of A2780/CDDP tumors in conjunction with the maximum tolerated dose of NCP-Cis/GMP determined from previous data, we believe that a more aggressive dosing schedule was needed for the treatment of A2780/CDDP tumors. NCP-Cis/GMP/siRNAs showed remarkable tumor inhibition, with initial rapid tumor regression of 72% after 3 days followed by a tumor size increase of 51.9% after 10 days. Two of the four mice bearing A2780/CDDP tumors exhibited complete eradiation of tumors for 94 days or until the end of the experiment (data not shown). In contrast, tumors treated with PBS control reached the threshold of 2500 mm^3 after 10 days. No significant body weight loss was observed for the control and NCP-Cis/GMP/siRNAs treatment groups.

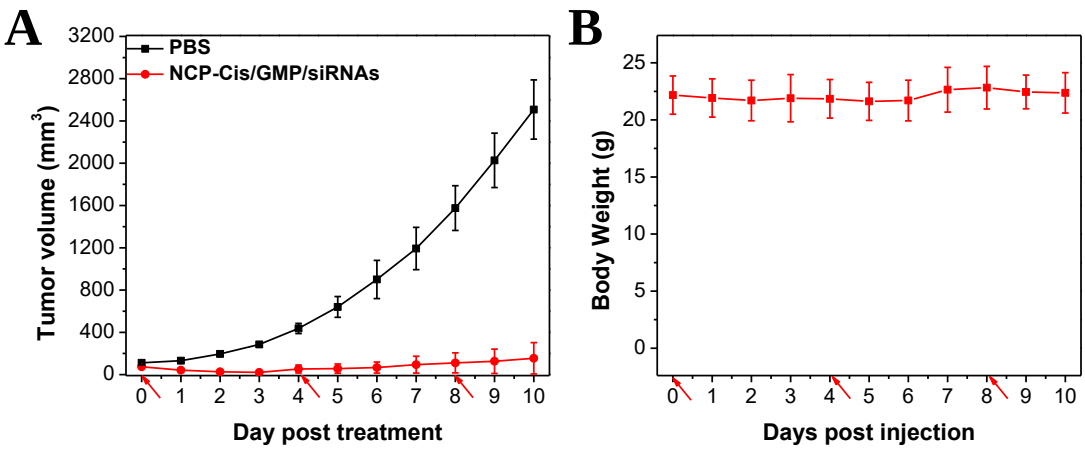

Figure 5.30. (A) Anticancer efficacy of NCP-Cis/GMP/siRNAs against A2780/CDDP subcutaneous xenografts starting at tumor volume of ~75 mm^3. Free drug combination or nanoparticles were intraperitoneally injected at 0.5 mg cisplatin/kg, 1.1 mg GMP/kg, and 0.25 mg siRNAs/kg on Day 0, Day 4, and Day 8 for a total of three injections. (B) Body weight evolution of SKOV-3 tumor-bearing athymic mice treated with NCP-Cis/GMP/siRNAs. Data are expressed as means±S.D. (n=4).

We explored the efficacy of NCP-Cis/GMP/siRNAs on tumors of different sizes by varying the tumor volume at the time of first treatment. We evaluated the *in vivo* antitumor effect of NCP-Cis/GMP/siRNAs in cisplatin-resistant SKOV-3 subcutaneous xenografts with a starting tumor volume of ~400 mm^3, administering one injection every three days for a total of two injections. As seen in Figure 5.31, no antitumor benefit was observed for NCP-Cis/GMP/siRNAs. Although we treated the tumor at same dosages we used in our efficacy studies on SKOV-3 150 mm^3 tumors and at a higher frequency, the results on the 400 mm^3 tumor strongly suggested that tumor volume plays a large role in its efficacy, perhaps because the NCP-Cis/GMP/siRNAs cannot penetrate larger tumors.

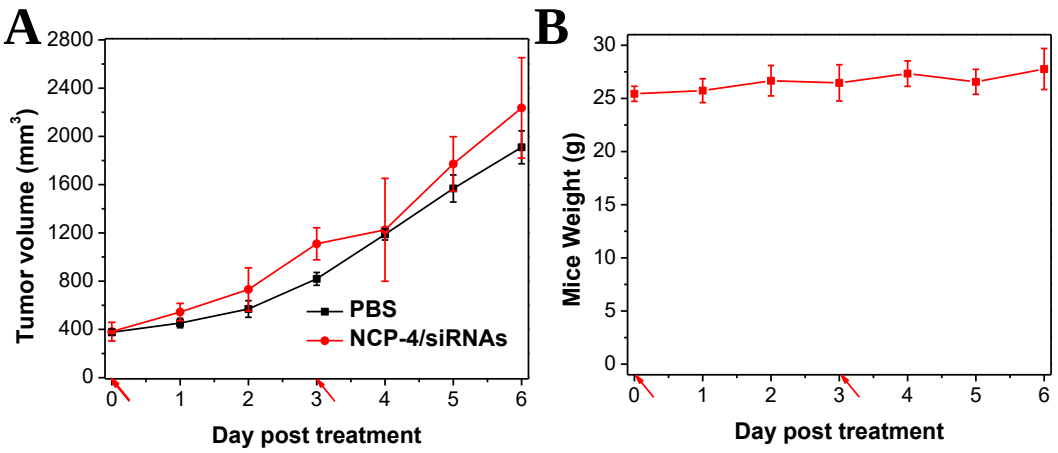

Figure 5.31. (A) Anticancer efficacy of NCP-Cis/GMP/siRNAs against SKOV-3 subcutaneous xenografts with a starting tumor volume of ~400 mm^3. NCP-Cis/GMP/siRNAs was intraperitoneally injected at 0.3 mg cisplatin/kg, 0.67 mg GMP/kg, and 0.15 mg siRNAs/kg on Day 0 and Day 3 for a total of two injections. (B) Body weight evolution of SKOV-3 tumor-bearing athymic mice treated with NCP-Cis/GMP/siRNAs. Data are expressed as means±S.D. (n=3).

5.4 Discussion

Tumors often consist of mixed populations of malignant cells with great molecular and genetic heterogeneity.[16,17] As cancers progress, they often develop mutations or acquire resistance to treatment. Combination therapy is a promising solution to significant issues of tumor

heterogeneity and drug resistance because it allows multiple therapeutics and modalities to attack multiple sites, while overcoming cross-resistance. We developed NCP-Cis/GMP/siRNAs, a single platform that combines the chemotherapeutics of cisplatin and gem with the gene therapy of RNAi. We demonstrated that delivering multiple siRNAs targeting molecular signaling pathways can effectively overcome drug resistance in OCa and resensitize OCa to cisplatin treatment. We found that it efficiently overcame drug resistance and led to complete tumor eradication over a 156-day period.

Because of their hydrophilicity and high molecular weights, free siRNAs are not readily taken up by cells. Nanoparticles, including liposomes and polymers, have thus been explored as a potential delivery platform for siRNAs, allowing them to target macrophages or liver disease in clinical trials, but these platforms have yet to show any promise in effectively treating cancer. A few examples of *in vivo* siRNA delivery using nanomaterials composed of polymers and cationic lipids or spherical nucleic acid nanoparticle conjugates have been successfully explored by others.[44] However, the development of siRNA carriers for cancer therapy has faced two main challenges: opposing surface charge requirements for efficient endosomal escape (cationic) and long blood circulation (neutral), and the delicate balance between the affinity for siRNA binding and sufficient release at the sites of action.[45-49] The proton sponge effect, a well-known endosomal escape mechanism, requires the carrier surface to be cationic in order to help siRNA escape from the endosome after endocytosis. However, nanoparticles with cationic surface charges have shown poor pharmacokinetics and biodistribution.[50-52] Furthermore, an siRNA delivery carrier needs to have a high affinity to siRNA in the extracellular environment in order to prevent nuclease degradation while achieving sufficient and rapid intracellular siRNA release in the cytoplasm to trigger prolonged gene silencing. By combining an ideal size, cationic lipid-free formulation, and

siRNA protection with a lipid shell, NCP-Cis/GMP/siRNAs maintain structural integrity in blood circulation. The prolonged blood circulation time and minimal MPS uptake allow the core-shell nanoparticles to take advantage of the EPR effect to preferentially localize in tumors.

We previously demonstrated that the lipid shell of our NCPs gradually dissociates from the solid core of core-shell particles upon entering the cells.[53] Once the particle's lipid shell is incorporated into the plasma membrane, the core is exposed to high concentrations of endogenous reducing agents, triggering cisplatin release via reductive cleavage of the metal-ligand bonds. NCP-Cis/GMP/siRNAs carrying chemotherapeutics and siRNAs can then release the drugs intracellularly. Inside the cells, the disulfide bond between DSPE and siRNAs is also cleaved by higher concentrations of cysteine and glutathione, which act as reducing agents, allowing the siRNA to be efficiently released from the lipid shell. When a cisplatin molecule is released, two CO_2 molecules are generated inside the endosomes, altering their osmotic pressure and disrupting the endosome membrane, facilitating endosomal escape of the siRNAs. Our built-in endosomal escape mechanism does not involve cationic lipids or polymers, giving NCP-Cis/GMP/siRNAs a near-neutral surface charge for prolonged systemic circulation. The efficient endosomal escape enabled by this novel mechanism potentiates gene silencing both *in vitro* and *in vivo*. We anticipate that our endosomal escape mechanism can be applied to the design of other *in vivo* delivery systems for anticancer biotherapeutics, such as microRNA, antisense oligonucleotides, etc.

5.5 Conclusion

We developed novel self-assembled core-shell nanoparticles that combine two therapies, the chemotherapy of cisplatin and gem and the gene therapy of siRNA, into a single platform for tumor eradication in cisplatin-resistant OCa mouse models. NCP-Cis/GMP/siRNAs has several

advantages over other existing nanocarriers: a) a highly modular synthesis that allows for the optimized loading of different drugs; b) the ability to carry high loadings of both chemotherapeutic and siRNAs that release at the relevant sites of action; c) a novel built-in endosomal escape mechanism that enables a cationic lipid-free siRNA delivery system; d) prolonged systemic circulation and enhanced tumor accumulation after i.v. injection; e) combination therapy that effectively treats drug-resistant cancers; f) effective tumor eradication by systemic administration in cisplatin-resistant SKOV-3 OCa cell line. We believe these nanoparticles present a promising direction for nanomedicine. Based on the numerous uses of cisplatin and gem in combination in cancer therapy, we anticipate that these core-shell nanoparticles will have broad impact on the treatment of challenging cancers.

5.6 References

(1) Menon, U.; Gentry-Maharaj, A.; Griffin, M. *Gynecol Oncol* **2014**, *132*, 490.

(2) Coleman, R. L.; Monk, B. J.; Sood, A. K.; Herzog, T. J. *Nat Rev Clin Oncol* **2013**, *10*, 211.

(3) Vaughan, S.; Coward, J. I.; Bast, R. C.; Berchuck, A.; Berek, J. S.; Brenton, J. D.; Coukos, G.; Crum, C. C.; Drapkin, R.; Etemadmoghadam, D.; Friedlander, M.; Gabra, H.; Kaye, S. B.; Lord, C. J.; Lengyel, E.; Levine, D. A.; McNeish, I. A.; Menon, U.; Mills, G. B.; Nephew, K. P.; Oza, A. M.; Sood, A. K.; Stronach, E. A.; Walczak, H.; Bowtell, D. D.; Balkwill, F. R. *Nat Rev Cancer* **2011**, *11*, 719.

(4) Roberts, D.; Schick, J.; Conway, S.; Biade, S.; Laub, P. B.; Stevenson, J. P.; Hamilton, T. C.; O'Dwyer, P. J.; Johnson, S. W. *Brit J Cancer* **2005**, *92*, 1149.

(5) Kelland, L. *Nat Rev Cancer* **2007**, *7*, 573.

(6) Ushijima, K. *Journal of oncology* **2010**, *2010*, 497429.

(7) Muggia, F. *Gynecol Oncol* **2009**, *112*, 275.

(8) Davis, A.; Tinker, A. V.; Friedlander, M. *Gynecologic Oncology* **2014**, *133*, 624.

(9) Diaz-Padilla, I.; Malpica, A. L.; Minig, L.; Chiva, L. M.; Gershenson, D. M.; Gonzalez-Martin, A. *Gynecol Oncol* **2012**, *126*, 279.

(10) Nieman, K. M.; Kenny, H. A.; Penicka, C. V.; Ladanyi, A.; Buell-Gutbrod, R.; Zillhardt, M. R.; Romero, I. L.; Carey, M. S.; Mills, G. B.; Hotamisligil, G. S.; Yamada, S. D.; Peter, M. E.; Gwin, K.; Lengyel, E. *Nat Med* **2011**, *17*, 1498.

(11) Lowery, W. J.; Lowery, A. W.; Barnett, J. C.; Lopez-Acevedo, M.; Lee, P. S.; Secord, A. A.; Havrilesky, L. *Gynecol Oncol* **2013**, *130*, 426.

(12) Yang, Y.; Hu, Y. X.; Wang, Y. H.; Li, J.; Liu, F.; Huang, L. *Mol Pharmaceut* **2012**, *9*, 2280.

(13) Agarwal, R.; Kaye, S. B. *Nat Rev Cancer* **2003**, *3*, 502.

(14) van der Zee, A. G.; Hollema, H. H.; de Bruijn, H. W.; Willemse, P. H.; Boonstra, H.; Mulder, N. H.; Aalders, J. G.; de Vries, E. G. *Gynecol Oncol* **1995**, *58*, 165.

(15) Markman, J. L.; Rekechenetskiy, A.; Holler, E.; Ljubimova, J. Y. *Adv Drug Deliver Rev* **2013**, *65*, 1866.

(16) Igney, F. H.; Krammer, P. H. *Nat Rev Cancer* **2002**, *2*, 277.

(17) Gottesman, M. M. *Annu. Rev. Med.* **2002**, *53*, 615.

(18) Van Duin, M.; De Wit, J.; Odijk, H.; Westerveld, A.; Yasui, A.; Koken, M. H. M.; Hoeijmakers, J. H. J.; Bootsma, D. *Cell (Cambridge, Mass.)* **1986**, *44*, 913.

(19) Ziegler, S.; Pries, V.; Hedberg, C.; Waldmann, H. *Angew Chem Int Edit* **2013**, *52*, 2744.

(20) Patel, N. R.; Pattni, B. S.; Abouzeid, A. H.; Torchilin, V. P. *Adv Drug Deliver Rev* **2013**, *65*, 1748.

(21) Lin, Q. Y.; Jin, C. S.; Huang, H.; Ding, L. L.; Zhang, Z. H.; Chen, J.; Zheng, G. *Small* **2014**, *10*, 3072.

(22) Zhang, J.; Li, X.; Huang, L. *J Control Release* **2014**, *190*, 440.

(23) Chen, W.; Yang, L. *Methods Mol Biol* **2016**, *1372*, 49.

(24) Cho, Y. S.; Lee, G. Y.; Sajja, H. K.; Qian, W. P.; Cao, Z. H.; He, W. L.; Karna, P.; Chen, X. Y.; Mao, H.; Wang, Y. A.; Yang, L. *Small* **2013**, *9*, 1964.

(25) Talekar, M.; Ouyang, Q.; Goldberg, M. S.; Amiji, M. M. *Mol Cancer Ther* **2015**, *14*, 1521.

(26) Yang, X. Q.; Lyer, A. K.; Singh, A.; Choy, E.; Hornicek, F. J.; Amiji, M. M.; Duan, Z. F. *Sci Rep-Uk* **2015**, *5*.

(27) Fire, A.; Xu, S. Q.; Montgomery, M. K.; Kostas, S. A.; Driver, S. E.; Mello, C. C. *Nature* **1998**, *391*, 806.

(28) Giljohann, D. A.; Seferos, D. S.; Prigodich, A. E.; Patel, P. C.; Mirkin, C. A. *J Am Chem Soc* **2009**, *131*, 2072.

(29) Tebes, S. J.; Kruk, P. A. *Gynecol Oncol* **2005**, *99*, 736.

(30) Pecot, C. V.; Calin, G. A.; Coleman, R. L.; Lopez-Berestein, G.; Sood, A. K. *Nat Rev Cancer* **2011**, *11*, 59.

(31) Ozcan, G.; Ozpolat, B.; Coleman, R. L.; Sood, A. K.; Lopez-Berestein, G. *Adv Drug Deliver Rev* **2015**, *87*, 108.

(32) Caster, J. M.; Sethi, M.; Kowalczyk, S.; Wang, E.; Tian, X.; Hyder, S. N.; Wagner, K. T.; Zhang, Y. A.; Kapadia, C.; Au, K. M.; Wang, A. Z. *Nanoscale* **2015**, *7*, 2805.

(33) Min, Y. Z.; Caster, J. M.; Eblan, M. J.; Wang, A. Z. *Chem Rev* **2015**, *115*, 11147.

(34) Huynh, E.; Zheng, G. *Nanomedicine* **2015**, *10*, 1993.

(35) Miao, L.; Wang, Y. H.; Lin, C. M.; Xiong, Y.; Chen, N. H.; Zhang, L.; Kim, W. Y.; Huang, L. *J Control Release* **2015**, *217*, 27.

(36) Ling, D.; Xia, H.; Park, W.; Hackett, M. J.; Song, C.; Na, K.; Hui, K. M.; Hyeon, T. *ACS nano* **2014**, *8*, 8027.

(37) Patil, R.; Gangalum, P. R.; Wagner, S.; Portilla-Arias, J.; Ding, H.; Rekechenetskiy, A.; Konda, B.; Inoue, S.; Black, K. L.; Ljubimova, J. Y.; Holler, E. *Macromol Biosci* **2015**, *15*, 1212.

(38) Oberoi, H. S.; Nukolova, N. V.; Kabanov, A. V.; Bronich, T. K. *Adv Drug Deliver Rev* **2013**, *65*, 1667.

(39) Davis, M. E.; Chen, Z.; Shin, D. M. *Nat Rev Drug Discov* **2008**, *7*, 771.

(40) Petros, R. A.; DeSimone, J. M. *Nat Rev Drug Discov* **2010**, *9*, 615.

(41) Ling, D.; Park, W.; Park, S. J.; Lu, Y.; Kim, K. S.; Hackett, M. J.; Kim, B. H.; Yim, H.; Jeon, Y. S.; Na, K.; Hyeon, T. *J Am Chem Soc* **2014**, *136*, 5647.

(42) Sun, T.; Wang, Y.; Xu, J.; Zhao, X.; Vangveravong, S.; Mach, R. H.; Xia, Y. *Adv Healthc Mater* **2014**, *3*, 1283.

(43) He, C.; Liu, D.; Lin, W. *Biomaterials* **2015**, *36*, 124.

(44) Jensen, S. A.; Day, E. S.; Ko, C. H.; Hurley, L. A.; Luciano, J. P.; Kouri, F. M.; Merkel, T. J.; Luthi, A. J.; Patel, P. C.; Cutler, J. I.; Daniel, W. L.; Scott, A. W.; Rotz, M. W.; Meade, T. J.; Giljohann, D. A.; Mirkin, C. A.; Stegh, A. H. *Sci Transl Med* **2013**, *5*, 209ra152.

(45) Varkouhi, A. K.; Scholte, M.; Storm, G.; Haisma, H. J. *J Control Release* **2011**, *151*, 220.

(46) Dominska, M.; Dykxhoorn, D. M. *J Cell Sci* **2010**, *123*, 1183.

(47) Gilleron, J.; Querbes, W.; Zeigerer, A.; Borodovsky, A.; Marsico, G.; Schubert, U.; Manygoats, K.; Seifert, S.; Andree, C.; Stoter, M.; Epstein-Barash, H.; Zhang, L.; Koteliansky, V.; Fitzgerald, K.; Fava, E.; Bickle, M.; Kalaidzidis, Y.; Akinc, A.; Maier, M.; Zerial, M. *Nat Biotechnol* **2013**, *31*, 638.

(48) Miele, E.; Spinelli, G. P.; Di Fabrizio, E.; Ferretti, E.; Tomao, S.; Gulino, A. *Int J Nanomedicine* **2012**, *7*, 3637.

(49) Castanotto, D.; Rossi, J. J. *Nature* **2009**, *457*, 426.

(50) Albanese, A.; Tang, P. S.; Chan, W. C. W. *Annu. Rev. Biomed. Eng.* **2012**, *14*, 1.

(51) Chou, L. Y. T.; Ming, K.; Chan, W. C. W. *Chem Soc Rev* **2011**, *40*, 233.

(52) Li, S. D.; Huang, L. *Mol Pharm* **2008**, *5*, 496.

(53) He, C.; Liu, D.; Lin, W. *ACS nano* **2015**, *9*, 991.

CHAPTER VI: Nanoscale Coordination Polymer Core-Shell Nanoparticles Combine Chemotherapy and Photodynamic Therapy to Elicit Antitumor Immunity

6.1 Introduction

Approximately 150,000 patients are diagnosed with colorectal cancer in the United States every year, with one-third dying from the metastatic disease.[1] The five year survival rate for localized colorectal cancer is ~89% while this number drops to only ~12% for cancers that have metastasized to the liver, lungs, or peritoneum.[2] Effective therapy for advanced colorectal cancer requires treatment of both primary tumors and metastatic tumors that may not be detected at the time of treatment. Numerous studies have shown that stimulation of the host immune system can lead to an immune response capable of controlling metastatic tumor growth.[3-6] Considering the highly metastatic nature of colorectal cancer and the poor five-year survival rate of patients with advanced colorectal cancer, there is a clear clinical interest in developing an effective therapeutic modality that both controls primary tumor growth and stimulate antitumor immunity to control the metastatic disease.[7]

Nanoscale coordination polymers (NCPs) are self-assembled hybrid nanomaterials constructed from metal-connecting points and organic bridging ligands.[8,9] We believe that NCPs possess several advantages over existing nanocarriers for biomedical applications, such as high tunability of composition and structure, the ability to combine multiple therapeutic agents or modalities into one platform, and intrinsic biodegradability due to the labile metal-organic ligand bonds.[10] Recently, we reported NCP-based core-shell nanoparticles carrying high payloads of cisplatin and the photosensitizer pyrolipid, NCP-Cis@pyrolipid, for combined chemotherapy and photodynamic therapy (PDT).[10] NCP-Cis@pyrolipid showed superior potency and efficacy in tumor regression in the cisplatin-resistant human head and neck cancer SQ20B xenograft mouse

model. Photodynamic therapy (PDT) is an FDA-approved anticancer modality that enhances antitumor immunity.[11] By combining nontoxic photosensitizers, light, and oxygen to produce cytotoxic reactive oxygen species (ROS), in particular singlet oxygen ($^1O_2$), PDT kills cancer cells by apoptosis and necrosis, stimulates the host immune system, and causes acute inflammation and leukocyte infiltration to the tumors which increases the presentation of tumor-derived antigens to T cells.[12-18] Kroemer and coworkers have demonstrated the oxaliplatin-induced immunogenic cell death in murine colorectal cancer models.[19] Recent studies also suggested that the immune response elicited against residual cancer cells might contribute to the complete eradication of micrometastases and cancer stem cells.[20-22] Along with effective apoptosis/necrosis caused by both PDT and oxaliplatin, we hypothesized that combination therapy using oxaliplatin and PDT would be particularly efficient, simultaneously killing tumor cells and stimulating an immune response against them. We anticipate achieving tumor inhibition not only in the primary tumor site but also in distant metastatic tumors.

This chapter focuses on NCP-based core-shell nanoparticles carrying oxaliplatin and the photosensitizer pyrolipid, NCP-Ox@pyrolipid, which can enhance antitumor immunity for superior anticancer efficacy in colorectal cancers, and their potential application in the treatment of metastatic colorectal cancer.[20-22] Inheriting all the merits of NCP-based nanoparticles, including high drug loading, prolonged systemic circulation via intravenous injection, and ideal biocompatibility, NCP-Ox@pyrolipid combines two therapeutic modalities, oxaliplatin and PDT, which not only kill cancer cells but also elicit a strong immunogenic response for controlling metastatic tumor nodules. Effective anticancer therapy of NCP-Ox@pyrolipid was demonstrated against two colorectal cancer models: syngeneic CT26 murine colorectal cancer model and HT29 human colorectal cancer xenografts. We also observed evidence for efficient antitumor immunity

evoked by NCP-Ox@pyrolipid in the form of early calreticulin (CRT) exposure on the cell surface, successful antitumor vaccination, and the abscopal effect.

6.2 Experimental Details

6.2.1 General Experimental:

All of the starting materials were purchased from Sigma-Aldrich and Fisher (USA) unless otherwise noted and used without further purification. 1,2-dioleoyl-*sn*-glycero-3-phosphate (DOPA), 1,2-distearoyl-*sn*-glycero-3-phosphocholine (DSPC), cholesterol, and 1,2-distearoyl-*sn*-glycero-3-phosphoethanolamine-N-[amino(polyethylene glycol)2000] (DSPE-PEG2k) were purchased from Avanti Polar Lipids (USA). Pyrolipid was synthesized in the lab as previously reported.[10]

Murine colon adenocarcinoma cell CT26 and human colorectal adenocarcinoma were purchased from the American Type Culture Collection (Rockville, MD, USA) and cultured in RPMI 1640 medium and Dulbecco's Modified Eagle's Medium (DMEM) (Gibco, Grand Island, NY, USA) supplemented with 10% FBS, respectively.

Athymic male nude mice (6 weeks, 24-26 g) and BALB/c male mice (6 weeks, 22-24 g) were provided by Harlan Laboratories, Inc (USA). The study protocol was reviewed and approved by the Institutional Animal Care and Use Committee (IACUC) at the University of Chicago.

6.2.2 Preparation and Characterization of NCP-Ox@pyrolipid:

DOPA-capped NCP-Ox nanoparticles were prepared according to our previous report.[23] NCP-Ox@pyrolipid was prepared by adding a THF solution (80 μL) of DSPC, cholesterol, pyrolipid, and DSPE-PEG2k (DSPC/cholesterol/pyrolipid/DSPE-PEG2k=2:1:0.8:1 in molar ratios) and DOPA-coated NCP to 500 μL of 30% (v/v) ethanol/water at 60 °C. The mixture was stirred at 1700 rpm for 1 min. THF and ethanol were completely evaporated and the NCP-

Ox@pyrolipid solution was allowed to cool down to room temperature. NCP-Ox@pyrolipid was centrifuged at 13,000 rpm for 30 min followed by the removal of the supernatant and re-suspending the particles in phosphate buffered solution (PBS). ICP-MS (Agilent 7700X, Agilent Technologies, USA) was utilized to analyze the platinum (Pt) concentration of NCP-Ox to calculate cisplatin loadings. The particle size and Zeta potential of NCP-Ox@pyrolipid in PBS were determined by Zetasizer (Nano ZS, Malvern, UK). Transmission electron microscopy (TEM, Tecnai Spirit, FEI, USA) was used to observe the morphology of NCP-Ox@pyrolipid.

6.2.3 Singlet Oxygen Generation of NCP-Ox@pyrolipid:

The singlet oxygen sensor green (SOSG) reagent (Life Technologies, USA) was employed for the detection of singlet oxygen generated by NCP-Ox@pyrolipid. After lipid coating, NCP-Ox@pyrolipid was centrifuged at 13,000 rpm for 30 min. The supernatant containing free lipid, liposome, and porphysome was discarded and the pellet was resuspended in PBS. Five μl of freshly prepared SOSG solution in methanol (5 mM) was mixed with 2 mL of NCP-Ox@pyrolipid in PBS or 0.5% Triton X-100. Porphysome with addition of 0.5% Triton X-100 at same pyrolipid concentration as NCP-Ox@pyrolipid served as a control. Samples were treated with a light-emitting diode (LED) with a wavelength of 670 nm and energy irradiance of 100 mW/cm^2 for 10 s, 20 s, 30 s, 40 s, 50 s, 100 s, and 250 s. SOSG fluorescence was measured by exciting at 504 nm and emission at 525 nm. There was no pyrolipid fluorescence contribution within this emission window.

6.2.4 Cellular Uptake of NCP-Ox@pyrolipid:

CT26 cells were seeded on 6-well plates at 5×10^5 cells/well and incubated for 24 h. NCP-Ox@pyrolipid, NCP, free cisplatin, or porphysome was added to the cells at a cisplatin dose of 5 μM or pyrolipid dose of 1.6 μM, respectively. After incubating for 1, 2, 4, and 24 h, CT26 cells

were collected, washed with PBS three times, and counted with a hemocytometer. The cells were centrifuged at 3,000 rpm for 5 min before the cell pellet was digested with 500 μL of concentrated nitric acid. After 24 h, the digestion was diluted with water and subjected to ICP-MS to determine the Pt concentration. Results were expressed as the amount of oxaliplatin (pmol) per 10^5 cells. The amount of pyrolipid taken up by the cells was quantified with a spectrofluorophotometer (RF-5301PC, Shimadzu, Japan). After incubating with NCP-Ox@pyrolipid for 1, 2, 4, and 24 h, CT26 cells were washed with PBS three times, counted with a hemocytometer, and lysed with 0.5% (w/v) SDS (pH 8.0). The fluorescence intensity of pyrolipid was determined by fluorimetry (λ_{ex}=427 nm, λ_{em}=675 nm). Results were expressed as the amount of pyrolipid (pmol) per 10^5 cells.

6.2.5 Cytotoxicity of NCP-Ox@pyrolipid in Colorectal Adenocarcinoma Cells:

The cytotoxicity of NCP-Ox@pyrolipid was tested in CT26 and HT29 cells. The cells were seeded on 96-well plates at 2500 cells/well. After incubating for 24 h, the cells were treated with NCP-Ox@pyrolipid, porphysome, NCP-Ox, and free oxaliplatin at various oxaliplatin concentrations or pyrolipid concentrations. After a 24-h incubation, the cells were irradiated with LED light (670 nm) at 60 mW/cm^2 for 15 min (equals to 54 J/cm^2). The cells without irradiation treatment served as controls. The cells were then incubated another 48 h. The cell viability was detected by (3-(4,5-dimethylthiazol-2-yl)-5-(3-carboxymethoxyphenyl)-2-(4-sulfophenyl)-2H-tetrazolium) (MTS) assay (Promega, USA) and the IC_{50} values were calculated accordingly.

6.2.6 Cell Apoptosis by Flow Cytometry:

CT26 or HT29 cells were seeded at a cell density of 5x10^5 cells per well and 2 mL total volume media containing aliquots of PBS, free oxaliplatin, NCP-Ox, NCP-Ox@pyrolipid, or porphysome at 1.00 μM oxaliplatin (or 0.22 μM pyrolipid) for CT26 and 0.33 μM oxaliplatin (or 0.09 μM pyrolipid) for HT29 and cultured for 4 h at 37^{o}C and 5% CO_2. Media were removed and

replenished with fresh media. The plates were subjected under 54 J/cm^2 light or under dark for 15 min and incubated for 20 h. The floating and adherent cells were collected by a cell scrapper and stained with Alexa Fluor 488 Annexin V and propidium iodide and analyzed on a flow cytometer.

6.2.7 In Vitro *Immunogenic Cell Death:*

The immunogenic cell death induced by NCP-Ox@pyrolipid was evaluated by immunofluorescence and flow cytometry. For immunofluorescence analysis, CT26 cells were seeded at 5×10^5 cells per well in 6-well plates and further cultured for 24 h. The culture media were replaced by 2 mL of fresh culture media containing 10% FBS. Oxaliplatin, NCP-Ox, NCP-Ox@pyrolipid, and porphysome were added to the cells, respectively, at an equivalent oxaliplatin dose of 5 μM and pyrolipid dose of 1.6 μM. Cells incubated with PBS served as control. After 24-h incubation, the cells were irradiated with LED light (670 nm) at 100 mW/cm^2 for 15 min (equals to 90 J/cm^2). Following further incubation for 4 h, the cells were washed with PBS three times, fixed with 4% paraformaldehyde, incubated with AlexaFluor 488-CRT antibody for 2 h, stained with DAPI, and observed under CLSM using 405 nm and 488 nm lasers for visualizing nuclei and CRT expression on the cell membrane, respectively. For flow cytometry analysis, CT26 cells were seeded at 1×10^6 cells per well in 6-well plates and cultured for 24 h. The culture media were replaced by 2 mL of fresh culture media containing 10% FBS. Oxaliplatin, NCP-Ox, NCP-Ox@pyrolipid, and porphysome were added to the cells, respectively, at an equivalent oxaliplatin dose of 5 μM and pyrolipid dose of 1.6 μM. Cells incubated with PBS served as a control. After a 24-h incubation, the cells were irradiated with LED light (650 nm) at 100 mW/cm^2 for 15 min (equals to 90 J/cm^2). Following another incubation of 4 h, the cells were collected, incubated with AlexaFluor 488-CRT antibody for 2 h, and stained with propidium iodide (PI). The samples were

analyzed by flow cytometer (LSRII Orange, BD, USA) to identify cell surface CRT. The fluorescence intensity of the stained cells was gated on PI-negative cells.

6.2.8 Pharmacokinetics and Tissue Distributions:

Mice were subcutaneously injected in the right flank with 1 million CT26 cells and tumors were allowed to grow until 100 mm^3 before they received intravenous administration of NCP-Ox@pyrolipid at an oxaliplatin dose of 3 mg/kg. Animals were sacrificed (3 per time-point) 5 min, 1 h, 3 h, 8 h, 24 h, and 48 h after nanoparticle administration. After collecting the blood, liver, lung, spleen, kidney, and bladder were harvested. Organs and blood were digested in concentrated nitric acid for 24 h and the Pt concentrations were analyzed by ICP-MS. The pyrolipid amounts in the blood collected at 5 min, 1 h, 3 h, 8 h, 24 h, and 48 h were determined using the same extraction and detection method as the recovery experiment as we previously reported.[10] Briefly, the blood was centrifuged at 3,000 rpm for 10 min to separate plasma. Methanol and 0.25% Triton X-100 was added to the plasma for extracting the pyrolipid and preventing aggregation, respectively. The pyrolipid concentrations were determined by UV-vis.

6.2.9 In Vivo *Anticancer Efficacy:*

The PDT efficacy of NCP-Ox@pyrolipid was investigated using the HT29 subcutaneous xenograft mouse model and CT26 flank tumor syngeneic mouse model. Tumor bearing mice were established by subcutaneous inoculation of HT29 cell suspension (2×10^6 cells per mouse) or CT26 cell suspension (1×10^6 cells per mouse) into the right flank region of 6-week athymic male nude mice or 6-week BALB/c male mice, respectively. Four groups were compared: PBS with irradiation, as a control; NCP-Ox with irradiation; NCP-Ox@pyrolipid with irradiation; and NCP-Ox@pyrolpid without irradiation. When tumors reached 100 mm^3, NCP-Ox or NCP-Ox@pyrolipid was injected intravenously into animals at an oxaliplatin dose of 2 mg/kg every

four days for a total two injections for the CT26 tumor model and four injections for the HT29 tumor model. Twenty-four hours after injection, mice were anesthetized with 2% (v/v) isoflurane, and tumors were irradiated with a 670 nm LED for 30 min. The energy irradiance was measured at 100 mW/cm^2, and the total light dose was 180 J/cm^2.

To evaluate the therapeutic efficacy, tumor growth and body weight evolution were monitored. Tumor sizes was measured with a digital caliper every day. Tumor volumes were calculated as follows: $(width^2 \times length)/2$. All mice were sacrificed when the tumor size of control group exceeded 2 cm^3, and the excised tumors were photographed and weighed. The tumors were embedded in optimal cutting temperature (OCT) medium, sectioned at 5-μm thickness, and subjected to hematoxylin and eosin (H&E) staining for histopathological analysis and TdT-mediated dUTP nick end labeling (TUNEL, Invitrogen, USA) assay for quantifying the *in vivo* apoptosis. Liver, lungs, spleen, and kidneys were also excised after the mice were sacrificed, and then embedded in OCT medium, sectioned at 5-μm thickness, stained with H&E, and observed for toxicity with light microscopy (Pannoramic Scan Whole Slide Scanner, Perkin Elmer, USA). For CT26 mouse model, blood was collected on Day 7, 8, 9, and 10, and the serum TNF-α, IFN-γ, and IL-6 production was determined by ELISA (R&D Systems, USA) to evaluate the immunogenic response evoked by the treatment.

6.2.10 Antitumor Vaccination:

A total of 5×10^5 CT26 cells, treated with PBS or NCP-Ox@pyrolipid and light irradiation, were inoculated subcutaneously into the right flank region of 6-week-old male BALB/c mice. One week later, these mice were rechallenged by injecting 1×10^5 CT26 cells into the contralateral flank. The animals were checked daily for tumor development using calipers and body weight evolution. Blood was collected one day after the first tumor injection, and the serum TNF-α, IFN-γ, and IL-

6 production was determined by ELISA (R&D Systems, USA) to evaluate the immunogenic response. All mice were sacrificed when the right tumor size of PBS group exceeded 2000 mm^3.

6.2.11 Abscopal Effect:

BALB/c mice were injected subcutaneously with 1×10^6 CT26 cells into the right flank (primary tumor) and 2×10^5 CT26 cells into the left flank (secondary tumor). When the primary tumors reached ~100 mm^3, mice were i.p. injected with NCP-Ox@pyrolipid at an oxaliplatin dose of 2 mg/kg every two days for a total of two injections. Twenty-four hours after injection, mice were anesthetized with 2% (v/v) isoflurane, and primary tumors were irradiated with a 670 nm LED at a light dose of 180 J/cm^2 given at 100 mW/cm^2. The primary and secondary tumor sizes and mouse body weights were monitored every day. The tumor size was measured with a digital caliper and calculated as follows: $(width^2 \times length)/2$. All mice were sacrificed when the primary tumor size of the control group exceeded 2000 mm^3.

6.2.12 Statistical Analysis:

Results were expressed as means ± standard deviation (S.D.). Two-ways ANOVA was used to determine statistical significance. A P value < 0.05 was considered statistically significant.

6.3 Results and Discussion

6.3.1 Self-Assembly and Characterization of NCP-Ox@pyrolipid

NCP-Ox particles carrying an oxaliplatin prodrug were prepared as previously reported by us.[23] Briefly, a mixture of $Zn(NO_3)_2$ and an oxaliplatin prodrug, $Pt(dach)Cl_2(OH)_2$ (dach=*R*, *R*-diaminocyclohexane), with 1,2-dioleoyl-sn-glycero-3-phosphate sodium salt (DOPA) in the Triton X-100/1-hexanol/cyclohexane/water reverse microemulsion was vigorously stirred at room temperature for 30 min to afford spherical DOPA-coated NCP-Ox particles of 55.3±0.2 nm in Z-average by dynamic light scattering (DLS). NCP-Ox has an oxaliplatin loading of 27.6 wt% as determined by inductively coupled plasma-mass spectrometry (ICP-MS). NCP-Ox@pyrolipid nanoparticles were prepared by coating NCP-Ox core with an asymmetric lipid bilayer containing pyrolipid and PEG. A tetrahydrofuran (THF) solution (80 μL) of pyrolipid, cholesterol, 1,2-distearoyl-*sn*-glycero-3-phosphocholine (DSPC), 1,2-distearoyl-sn-glycero-3-phosphoethanolamine-N-[methoxy(polyethylene glycol)-2000] (DSPE-PEG2k) (DSPC/cholesterol/pyrolipid/DSPE-PEG2k=2:1:0.8:1 in molar ratios), and DOPA-capped NCP-Ox were added to 500 μL of 30% (v/v) ethanol/water and kept stirring at 1700 rpm at 60 °C for 1 min. The THF and ethanol in the nanoparticle suspension was completely evaporated before subsequent use in *in vitro* and *in vivo* experiments. NCP-Ox@pyrolipid is a core-shell nanostructure with DOPA-capped coordination polymer NCP-Ox carrying oxaliplatin as a solid core and a self-assembled and asymmetric lipid bilayer as a shell (Figure 6.1). The NCP-Ox cores were constructed from the coordination between Zn^{2+} and phosphate groups of the oxaliplatin prodrug, which were then capped with a monolayer of DOPA *via* Zn-phosphate interactions between NCPs and DOPA molecules and hydrophobic-hydrophobic interactions among DOPA molecules (Figure 6.2). The lipid shell contains pyrolipid as photosensitizer for PDT and 20 mol%

of PEG-coating to minimize mononuclear phagocyte system (MPS) uptake and prolong blood circulation after systemic injection. The pyrolipid encapsulation efficiency and loading were determined to be 45.0% and 17.8 wt.%, respectively. We hypothesized that this core-shell structured NCP-Ox@pyrolipid would efficiently kill cancer cells with chemotherapy and PDT, as well as stimulate an immunogenic response, enabling the effective treatment of both primary and metastatic colorectal cancers.

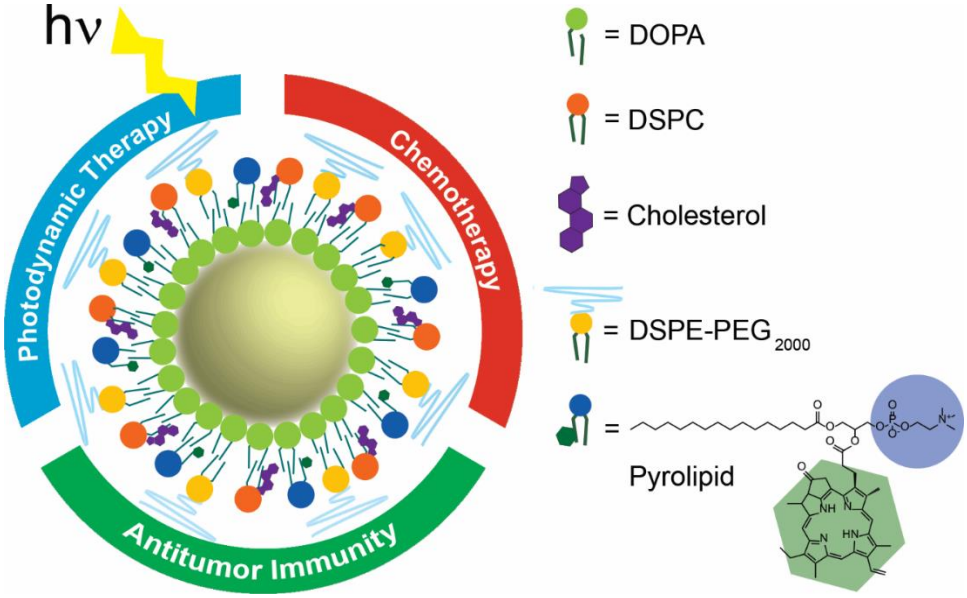

Figure 6.1 Schematic showing the core-shell NCP-Ox@pyrolipid nanoparticles that elicit antitumor immunity by a combination of oxaliplatin and PDT

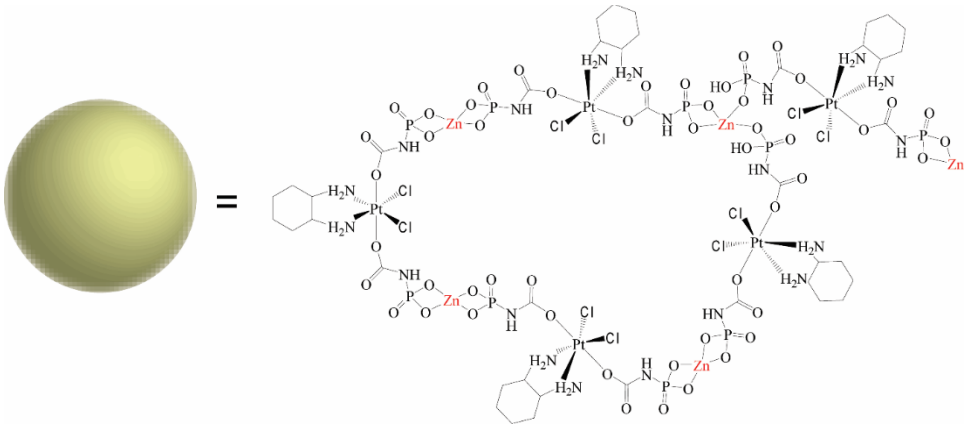

Figure 6.2 Schematic representation showing the core of NCP-Ox nanoparticles.

TEM images of NCP-Ox@pyrolipid demonstrated the formation of uniform and spherical nanoparticles (Figure 6.3). DLS measurements gave a Z-average diameter, number-average diameter, polydispersity index (PDI), and zeta potential of 83.0±1.0 nm, 51.2±0.1 nm, 0.143±0.011, and -3.67±0.85 mV, respectively (Figure 6.3), of NCP-Ox@pyrolipid dispersed in phosphate buffered saline (PBS). The small sizes and near neutral surface charge of NCP-Ox@pyrolipid suggested their potential in *in vivo* applications. The pyrolipid encapsulation efficiency and loading were determined to be 45.0% and 8.6 wt.%, respectively.

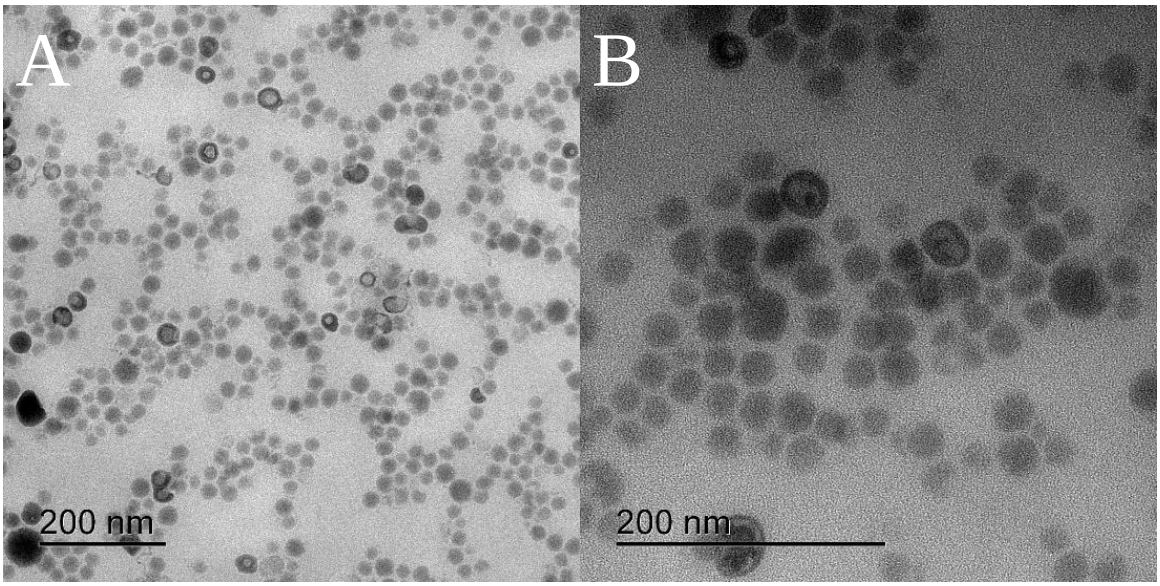

Figure 6.3 TEM images of NCP-Ox@pyrolipid (drop cast from a PBS dispersion). Bar=200 nm

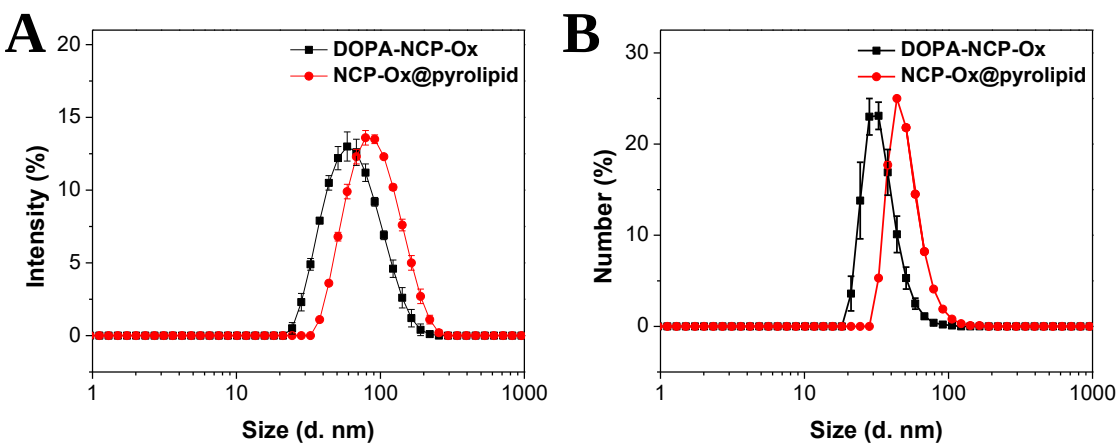

Figure 6.4 Intensity-average (A) and Number-average (B) size distribution of DOPA-NCP-Ox and NCP-Ox@pyrolipid. DOPA-NCP-Ox and NCP-Ox@pyrolipid particles were measured in THF and PBS buffer, respectively.

When dispersed in THF, the lipid bilayer of NCP-Ox@pyrolipid dissolved, and pyrolipid showed a broad Soret band around 400 nm and a distinct Q-band at 669 nm (Figure 6.5). Porphysome was prepared by following the procedure reported by Zheng and coworkers.[23] As we reported previously, pyrolipid was incorporated into the highly oriented and asymmetric lipid bilayer with a high loading. When the lipid bilayer is intact, the pyrolipid excited states are highly quenched, and therefore no energy transfer to triplet oxygen was observed as evidenced by the low amount of $^1O_2$ generated determined by the singlet oxygen sensor green (SOSG) reagent (Figure 6.6). After addition of Triton X-100 to NCP-Ox@pyrolipid and porphysome to disrupt the lipid bilayer, pyrolipid regained its fluorescence and efficiently generated similar amount of $^1O_2$ by SOSG.[24-27]

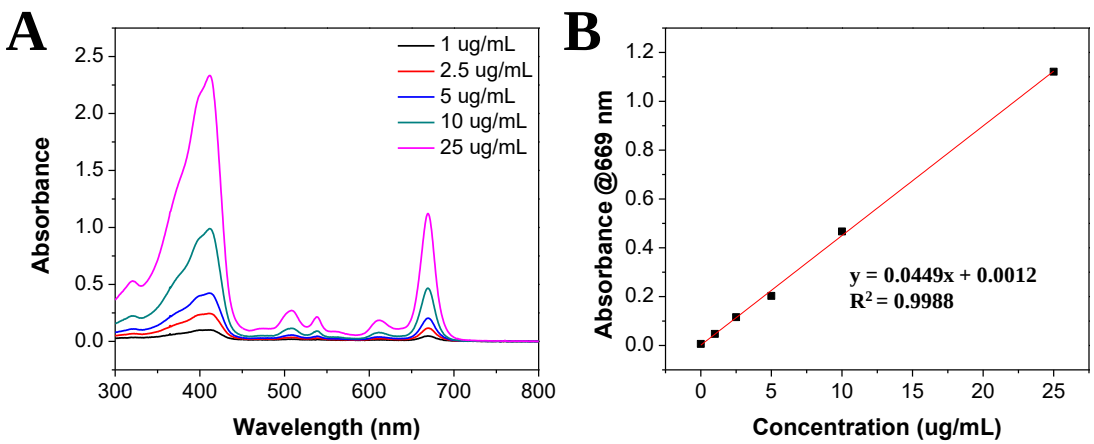

Figure 6.5 UV-Vis absorption spectra of NCP-Ox@pyrolipid in THF

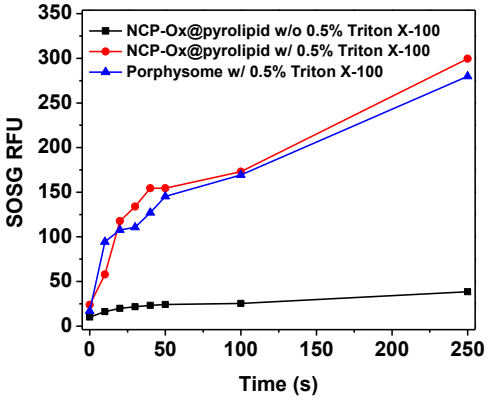

Figure 6.6 Time-dependent $^1O_2$ generation by NCP-Ox@pyrolipid and porphysome in PBS upon LED light irradiation (670 nm, 120 mW/cm^2) reported by the SOSG fluorescence intensity for intact particles versus particles with disrupted lipid bilayer.

6.3.2 Cellular Uptake and Cytotoxicity

The time-dependent cellular uptake of NCP-Ox@pyrolipid was evaluated in CT26 cells with an incubation time ranging from 1 h to 24 h. Free oxaliplatin, porphysome, and the original NCP-Ox [carrying a cisplatin prodrug and coated with 1,2-dioleoyl-*sn*-glycero-3-phosphocholine (DOPC), cholesterol, and DSPE-PEG$_{2k}$] served as comparisons. The Pt and pyrolipid concentrations in the cells after incubating with NCP particles, oxaliplatin, or porphysome were

determined by ICP-MS and fluoremitry, respectively. As depicted in Figure 6.7, the cellular uptake of NCP-Ox@pyrolipid in terms of both oxaliplatin and pyrolipid was rapid and mostly completed within 1 h, as evidenced by the stable uptake amounts of both oxaliplatin and pyrolipid over time up to 24 h. Except for free oxaliplatin of which the cellular uptake amount dropped significantly with time, cellular uptake of oxaliplatin and pyrolipid remained stable throughout the 24-h experiment, suggesting the internalization of NCP-Ox@pyrolipid might lead to the reduced efflux of oxaliplatin by changing the dynamics, porosity, and permeability of the cell membrane.[10,28]

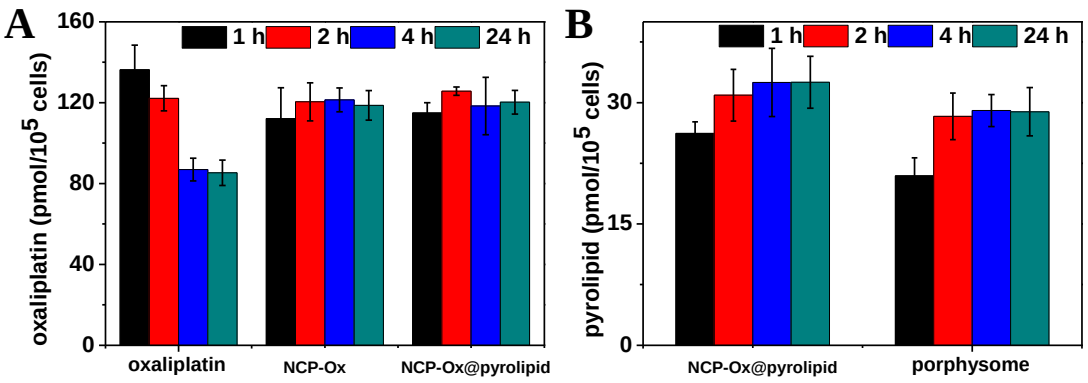

Figure 6.7 Cellular uptake of NCP-Ox@pyrolipid, NCP-Ox, free oxaliplatin, and porphysome in CT26 cells determined by ICP-MS (oxaliplatin uptake) and fluorimetry (pyrolipid uptake). Data expressed as means±S.D. (n=3).

The cytotoxicity of NCP-Ox@pyrolipid was evaluated against two colorectal cancer cells including murine colorectal adenocarcinoma CT26 and human colorectal adenocarcinoma HT29 cells. By combining chemotherapy of oxaliplatin and PDT modalities into one single nanoparticle, NCP-Ox@pyrolipid is expected to induce apoptosis/necrosis as well as elicit immunogenic cell death upon LED light irradiation. As shown in Table 6.1 and Figure 6.8 and Figure 6.9, the oxaliplatin IC_{50} of free oxaliplatin, NCP-Ox, and NCP-Ox@pyrolipid in the dark showed no significant difference in both cell lines, suggesting pyrolipid does not cause cytotoxicity without light activation. However, upon irradiation at 54 J/cm^2 light irradiation (670 nm), the oxaliplatin

IC_{50} of NCP-Ox@pyrolipid was decreased by ~4-fold and ~5-fold in CT26 and HT29 cells, respectively. The pyrolipid IC_{50} values also significantly dropped for NCP-Ox@pyrolipid with irradiation accordingly. No toxicity was observed for porphysome under light and dark in both cell lines within the tested pyrolipid concentration range.

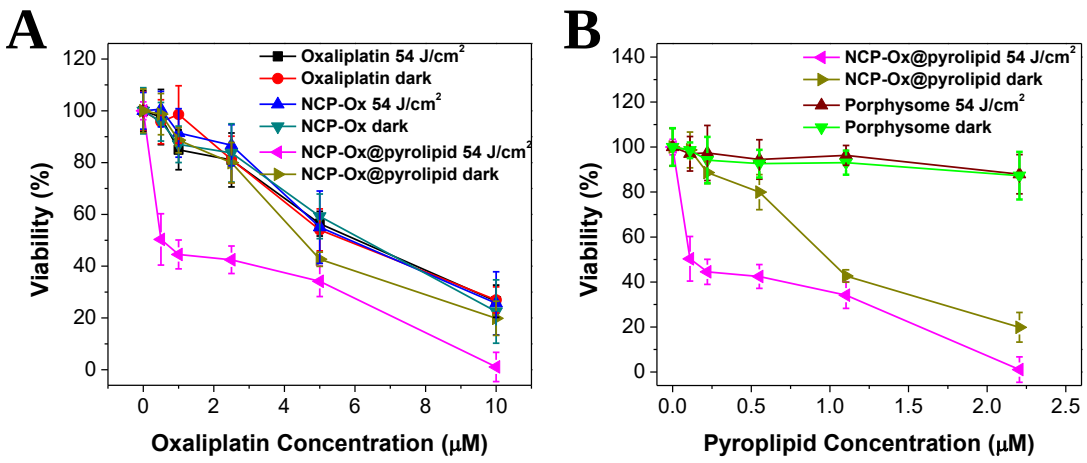

Figure 6.8. *In vitro* cell viability of CT26 cells treated with NCP-Ox@pyrolipid and porphysome at different oxaliplatin or pyroplipid doses. Data are mean ± S.D. (n=6).

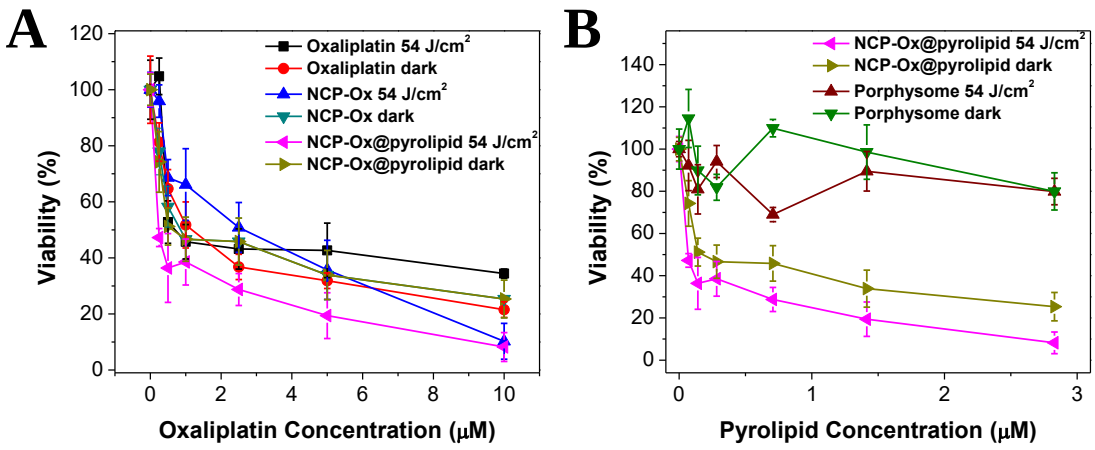

Figure 6.9. *In vitro* cell viability of HT29 cells treated with NCP-Ox@pyrolipid and porphysome at different oxaliplatin or pyroplipid doses. Data are mean ± S.D. (n=6).

Table 6.1 Oxaliplatin and pyrolipid IC_{50} values (μM) in CT26 and HT29 cells treated with various formulations. The numbers in parentheses refer to pyrolipid concentrations.

	Irradiation[a]	NCP-Ox@pyrolipid	NCP	Oxaliplatin	Porphysome[b]
CT26	√	1.00±0.30 (0.22±0.09)	5.07±1.02	4.97±0.49	>2.21
	×	3.97±0.60 (0.88±0.21)[c]	4.74±0.67	5.05±0.95	N/A
HT29	√	0.32±0.15 (0.09±0.04)	1.96±0.47	1.87±0.31	>2.83
	×	1.27±0.44 (0.36±0.12)[c]	1.42±0.49	1.44±0.32	N/A

[a]Cells were irradiated with LED light (670 nm) at 60 mW/cm^2 for 15 min (equals to 54 J/cm^2).

Direct treatment of cancer cells by NCP-Ox@pyrolipid with or without light irradiation that resulted in apoptosis/necrosis was evaluated by flow cytometry of cells stained with Alexa Fluor 488 Annexin V/dead cell apoptosis kit. As shown in Figure 6.10, Figure 6.11 and Table 6.2, NCP-Ox@pyrolipid under light significantly increased cell apoptosis in both colon cancer cell lines with 35.8% and 43.1% of cells undergoing apoptosis in CT26 and HT29, respectively. Free oxaliplatin and NCP-Ox in light or darkness and NCP-Ox@pyrolipid in darkness showed similar apoptotic cells, ranging from 21-26% in CT26 and 17-28% in HT29. Both PBS and porphysome treated cells showed no neurosis or apoptosis.

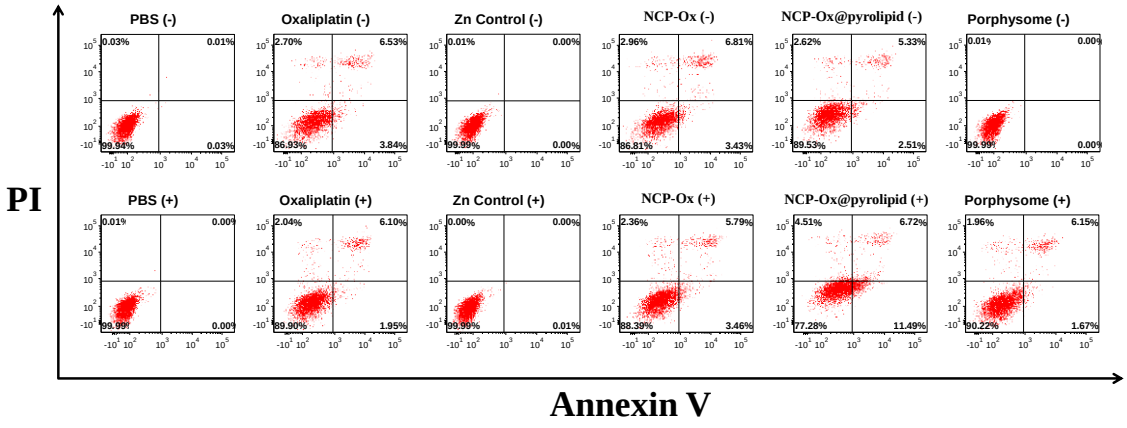

Figure 6.10 Flow cytometry analysis of saline, oxaliplatin, NCP-Ox, NCP-Ox@pyrolipid, and porphysome under light or dark in CT26 colon cancer cells. "+" and "-" in the figure legends refer to with and without irradiation, respectively.

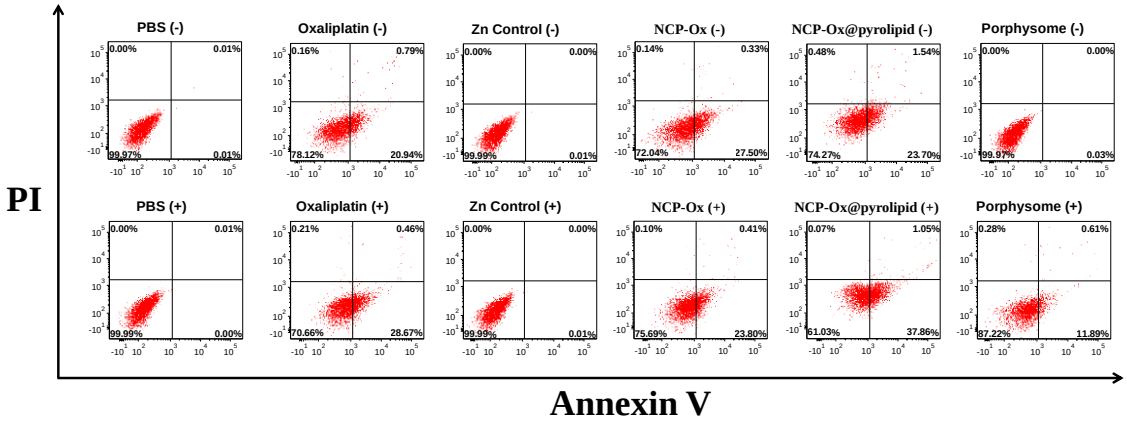

Figure 6.11 Flow cytometry analysis of saline, oxaliplatin, NCP-Ox, NCP-Ox@pyrolipid, and porphysome under light or dark in HT29 colon cancer cells. "+" and "-" in the figure legends refer to with and without irradiation, respectively.

Table 6.2 Apoptotic percentage of CT26 and HT29 cells treated with PBS, free oxaliplatin, NCP-Ox, NCP-Ox@pyrolipid, and porphysome under light and dark after 24 h incubation

	CT26		**HT29**	
	irradiation	dark	irradiation	dark
PBS	0.00%	0.04%	0.01%	0.02%
Oxaliplatin	8.05%	10.37%	29.13%	21.73%
Zn Control	0.01%	0.00%	0.01%	0.01%
NCP-Ox	9.25%	10.24%	24.21%	27.83%
NCP-Ox@pyrolipid	18.21%	7.84%	38.91%	25.24%
Porphysome	7.82%	0.00%	12.50%	0.03%

6.3.3 Immunogenic Cell Death Response

CRT is a distinct biomarker exposed on the surface of cells undergoing immunogenic cell death (ICD).[30,31] After the demonstration of efficient cellular uptake and negligible efflux of NCP-Ox@pyrolipid in CT26 cells, the CRT expression on cells treated with NCP-Ox@pyrolipid was determined by immunofluorescence (Figure 6.12) and flow cytometry (Figure 6.13) and compared to PBS-, oxaliplatin-, NCP-, and porphysome-treated cells. Cells were collected and stained with Alexa Fluor 488-CRT antibody and propidium iodide (PI) for flow cytometry analysis, where the fluorescence intensity of CRT-stained cells was gated on PI-negative cells. For immunostaining analysis, the cells were stained with Alexa Fluor 488-CRT and DAPI and observed under confocal laser scanning microscopy (CLSM). Significant amounts of CRT were detected on the surface of cells treated with free oxaliplatin, NCP, and NCP-Ox@pyrolipid, whether in light or darkness, due to oxaliplatin's ability to induce ICD. Porphysome only induced CRT expression upon light irradiation, suggesting that PDT, but not pyrolipid, is an inducer of ICD. The CRT exposure demonstrated by flow cytometry and CLSM by PDT of NCP-Ox@pyrolipid proved the effective ICD induced by the treatment.

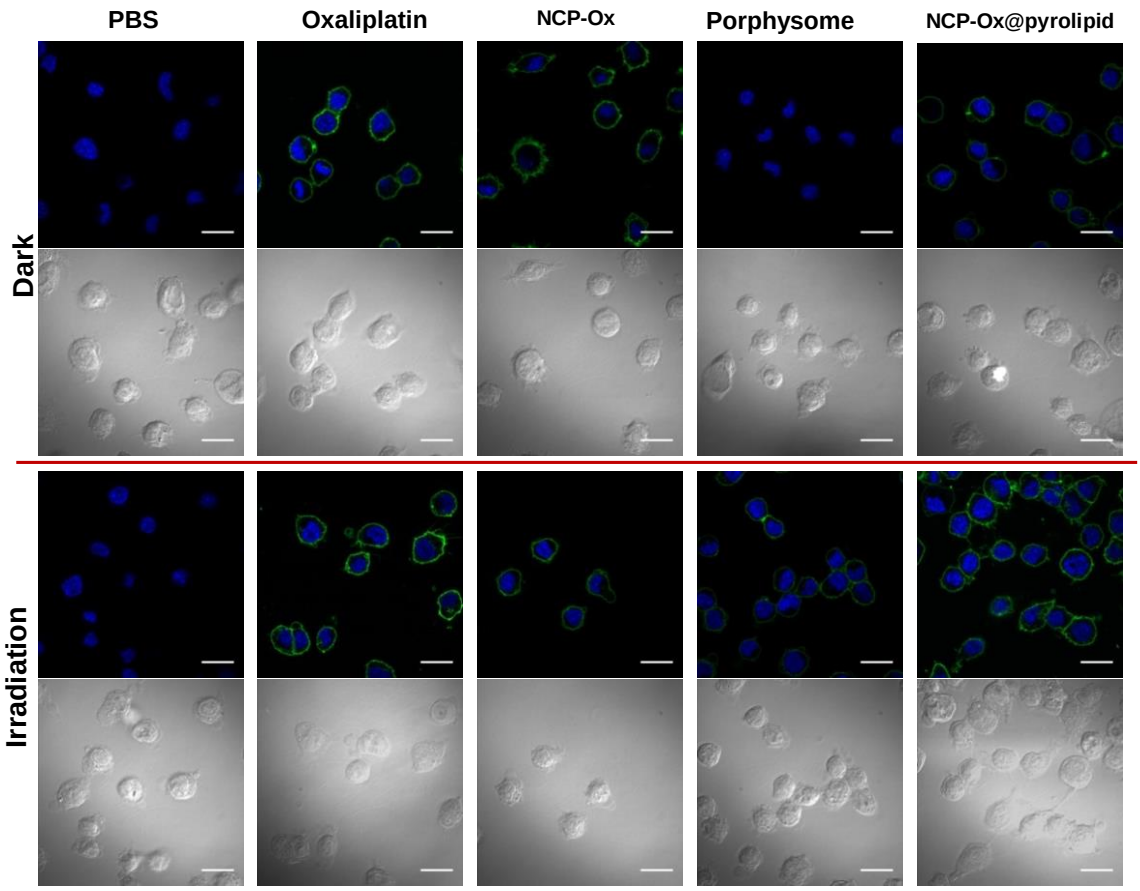

Figure 6.12 Immunofluorescence microscopy of CRT expression on the cell surface of CT26 cells treated with PBS, free oxaliplatin, NCP-Ox, porphysome, and NCP-Ox@pyrolipid in the absence or presence of light irradiation (90 J/cm^2). Blue: DAPI stained nuclei; Green: Alexa Fluor 488-CRT antibody. Bar=20 μm.

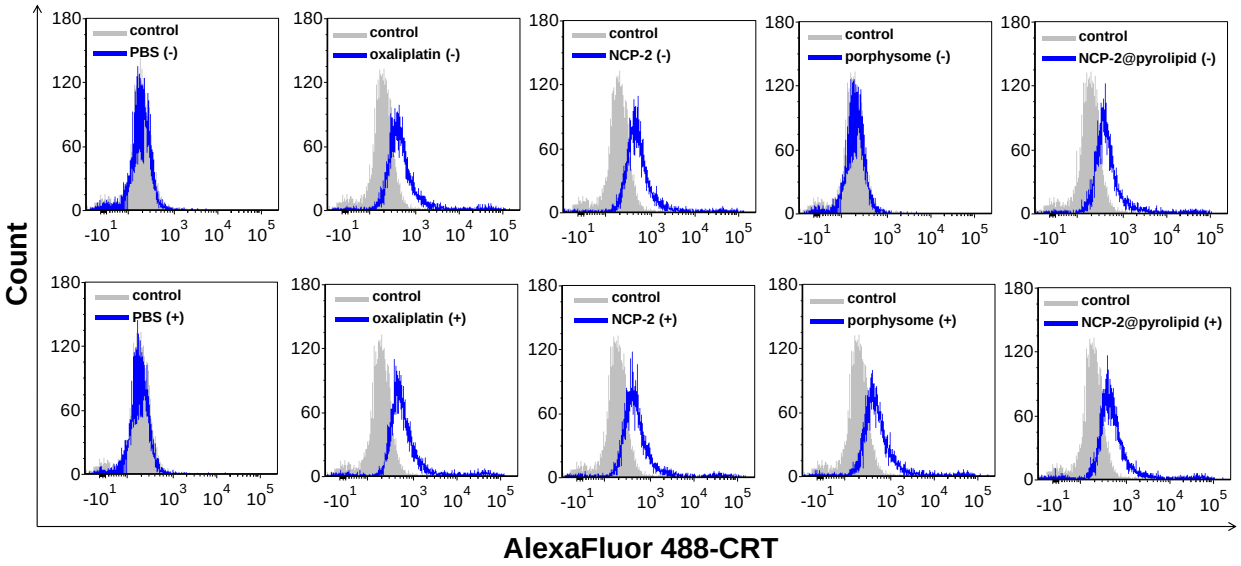

Figure 6.13 CRT exposure determines the immunogenicity of NCP-Ox@pyrolipid induced cell death. CRT exposure on the cell surface of CT26 cells was assessed after incubation with oxaliplatin, NCP-Ox, NCP-Ox@pyrolipid, or porphysome with or without light irradiation (90 J/cm^2) by immunofluorescence staining followed by flow cytometry analysis. The fluorescence intensity was gated on PI-negative cells. "+" and "-" in the figure legends refer to with and without irradiation, respectively.

6.3.4 In Vivo *Pharmacokinetic and Biodistribution Studies*

A pharmacokinetic and biodistribution study of NCP-Ox@pyrolipid was carried out on CT26 tumor-bearing BALB/c mice (Figure 6.14). The oxaliplatin distribution was quantified by ICP-MS and the pyrolipid concentration in the blood was quantified by UV-vis spectroscopy after extraction by methanol as we previously reported.[10] Both oxaliplatin and pyrolipid concentrations in blood versus time were fitted by a one-compartment model (Figure 6.14C and Figure 6.14D). Blood circulation half-lives of oxaliplatin and pyrolipid were determined to be 11.8±1.9 and 8.4±2.6 h, respectively, and did not exhibit statistically significant differences. Besides the prolonged blood circulation, NCP-Ox@pyrolipid exhibited low uptake by the MPS, as shown by the low % ID/g (percent injected dose per gram tissue) in the liver (< 7.1±2.5%), spleen (<10.4±4.3%), and kidney (<9.1±2.5%). The peak tumor uptake reached 6.8±1.7 % ID/g 24 h post

injection. With optimal particle size, surface properties, and stability, NCP-Ox@pyrolipid exhibited long blood circulation half-lives for both oxaliplatin and pyrolipid and high tumor uptake with low MPS clearance after i.p. injections.

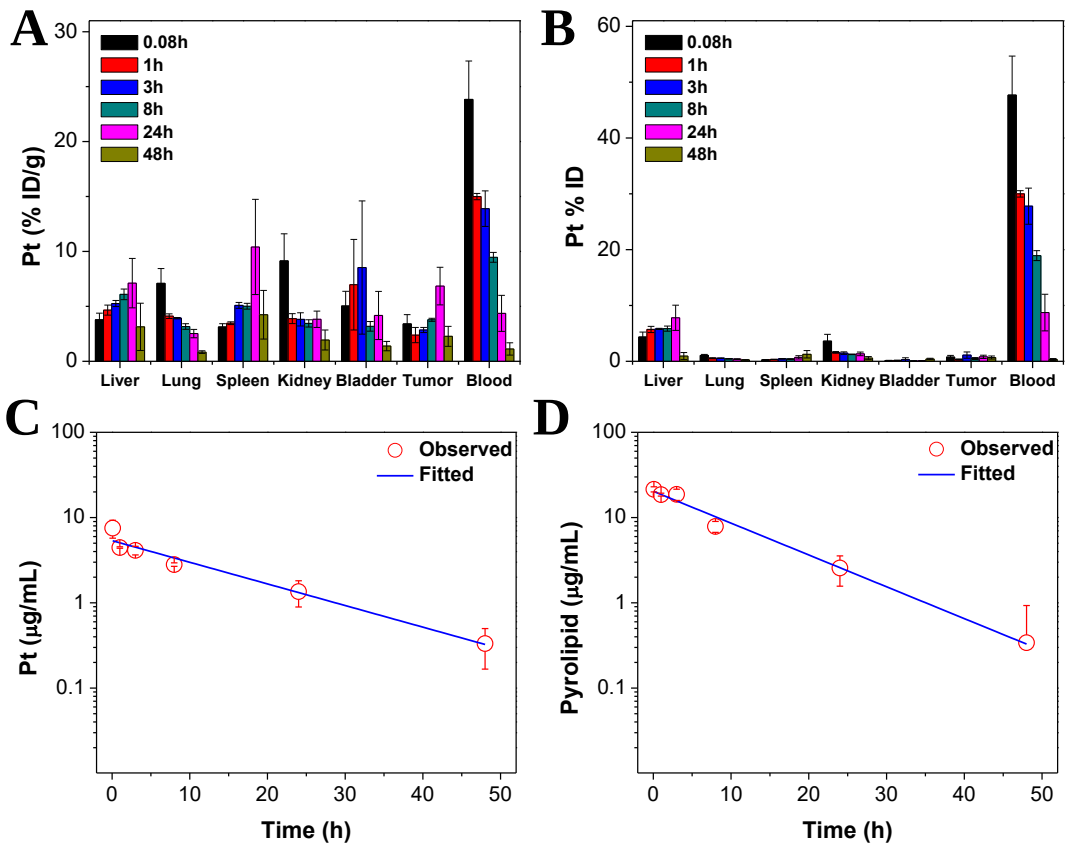

Figure 6.14 (A) Percentage injected dose per gram (% ID/g) and (B) percentage injected dose (% ID) of Pt in tissues and blood after intravenous administration of NCP-Ox@pyrolipid in CT26 tumor-bearing mice at time points 5 min, 1 h, 3 h, 8 h, 24 h, and 48 h. Data are mean ± S.D. (n=3). (C) Average observed and predicted time-dependent Pt distributions in blood after administration of NCP-Ox@pyrolipid (n=3). (D) Average observed and predicted time-dependent pyrolipid distributions in blood after administration of NCP-Ox@pyrolipid (n=3). One-compartment model was used for fitting the Pt and pyrolipid distributions in blood.

6.3.5 Anticancer Activity in Colorectal Adenocarcinoma Mouse Models

Two colorectal adenocarcinoma mouse models including BALB/c mice bearing murine colorectal cancer CT26 and nude mice with subcutaneous xenografts of human colorectal cancer

HT29 were employed to assess the *in vivo* anticancer activity of NCP-Ox@pyrolipid (Figure 6.15 and Figure 6.16). All doses were based on free oxaliplatin or pyrolipid equivalents. CT26 or HT29 tumor bearing mice were treated by intravenous injection of (1) PBS, (2) NCP-Ox at an oxaliplatin dose of 2 mg/kg, (3) and (4) NCP-Ox@pyrolipid at an oxaliplatin dose of 2 mg/kg every four days for a total of two treatments for CT26 model and four treatments for HT29 model. Twenty four hours post injection, mice in group (1)-(3) were anesthetized with 2% (v/v) isoflurane and tumors were irradiated with a 670 nm LED at an irradiance of 100 mW/cm^2 for 30 min. Tumor volumes (Figure 6.15A and Figure 6.16A) were measured daily. The mice were sacrificed when tumor volumes reached 2000 mm^3. NCP-Ox@pyrolipid (+) significantly suppressed tumor growth compared with PBS (+) (P=0.0003), NCP-Ox (+) (P=0.014), and NCP-Ox@pyrolipid (-) (P=0.044) in CT26 bearing mice. NCP-Ox@pyrolipid (+) produced a 2.6-fold decrease in tumor weight compared to PBS and a 1.8-fold decrease compared to NCP-Ox and NCP-Ox@pyrolipid (-). Likewise, in the HT29 model, NCP-Ox@pyrolipid (+) potently arrested tumor growth compared to PBS and NCP-Ox@pyrolipid (-) (P=0.002). Weights of tumors treated with NCP-Ox@pyrolipid were four times less than those treated with PBS and 2.4 times less than those treated with NCP-Ox@pyrolipid. In both tumor models, there was no significant decrease in the body weight of the treated mice (data not shown). In both CT26 and HT29 models, mice receiving PBS, NCP-Ox, or NCP-Ox@pyrolipid in darkness had tumors with large areas of viable cancer cells (Figure 6.17 and Figure 6.18). Tumors from mice receiving NCP-Ox@pyrolipid with irradiation, however, showed significant amounts of apoptotic cells, as confirmed by TUNEL assay (Figures 6.19 through 6.22**)**.

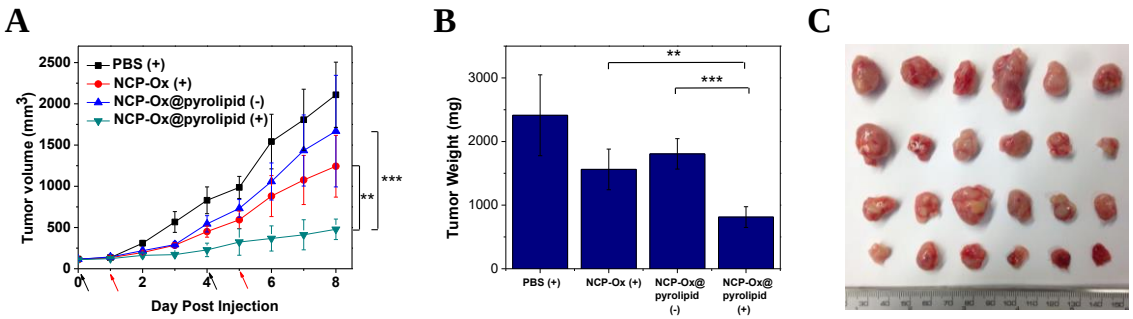

Figure 6.15 Anticancer efficacy of PBS, NCP-Ox (+) (2 mg/kg oxaliplatin), NCP-Ox@pyrolipid (-), (2 mg/kg oxaliplatin or 1.4 mg/kg pyrolipid) and NCP-Ox@pyrolipid (+) (2 mg/kg oxaliplatin or 1.4 mg/kg pyrolipid) in BALB/c mice bearing CT26 xenografts. Mice were intravenous injected with the treatments on days 0 and 4. Mice were irradiated with 100 mW/cm^2 on days 1 and 5 for CT26 mice. Tumor growth curve was observed (A). Each point was the mean ± S.D. (n = 3; ** p<0.01, ***p<0.001). The tumor weight (B) and visualization (C) were compared between groups. "+" and "-" in the figure legends refer to with and without irradiation, respectively.

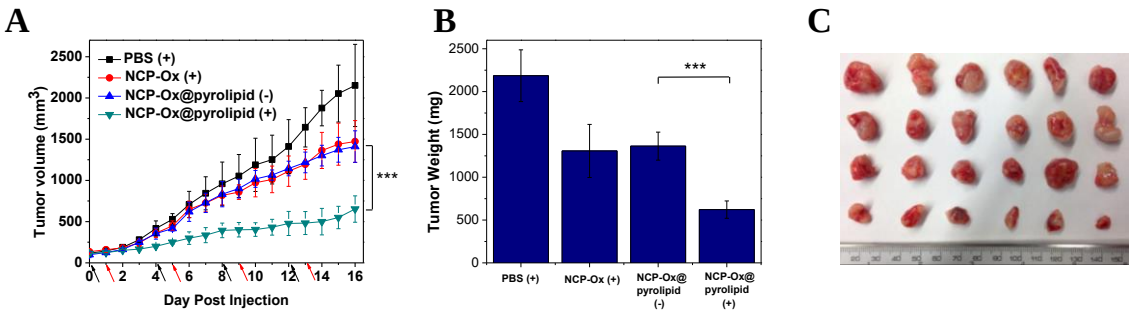

Figure 6.16 Anticancer efficacy of PBS, NCP-Ox (+) (2 mg/kg oxaliplatin), NCP-Ox@pyrolipid (-), (2 mg/kg oxaliplatin or 1.4 mg/kg pyrolipid) and NCP-Ox@pyrolipid (+) (2 mg/kg oxaliplatin or 1.4 mg/kg pyrolipid) in nude mice bearing HT29 xenografts. Mice were intravenous injected with the treatments on days 0, 4, 8, and 12. Mice were irradiated with 100 mW/cm^2 on days 1, 5, 9, and 13. Tumor growth curve was observed (A). Each point was the mean ± S.D. (n = 3; ***p<0.001). The tumor weight (B) and visualization (C) were compared between groups.

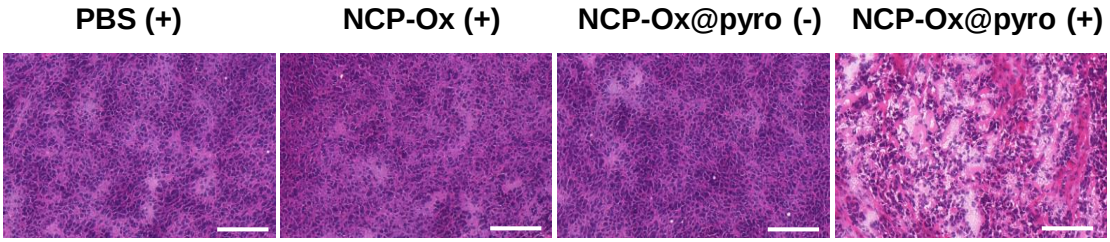

Figure 6.17 H&E staining of tumor sections harvested from CT26 tumor-bearing mice receiving PBS w/ irradiation, NCP-Ox w/ irradiation, NCP-Ox@pyrolipid w/o irradiation, and

Figure 6.17, continued NCP-Ox@pyrolipid w/ irradiation. "+" and "-" in the figure legends refer to with and without irradiation, respectively. Bar=50 μm.

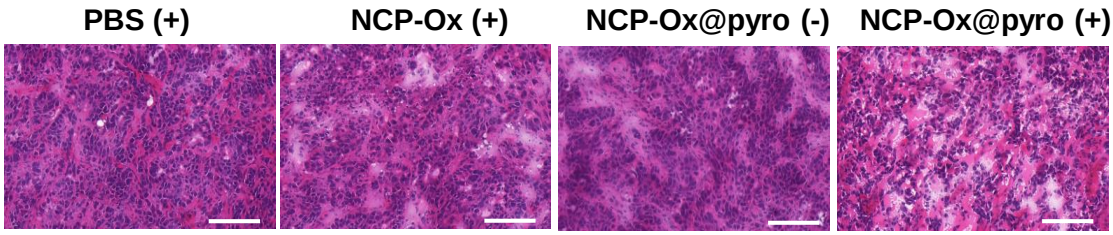

Figure 6.18 H&E staining of tumor sections harvested from HT29 tumor-bearing mice receiving PBS w/ irradiation, NCP-Ox w/ irradiation, NCP-Ox@pyrolipid w/o irradiation, and NCP-Ox@pyrolipid w/ irradiation. "+" and "-" in the figure legends refer to with and without irradiation, respectively. Bar=50 μm.

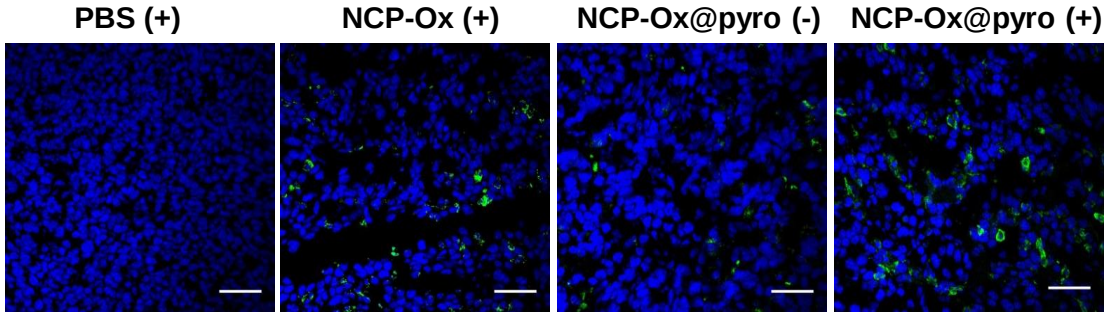

Figure 6.19 Representative CLSM images of TUNEL assays of tumor tissues. DNA fragments in apoptotic CT26 cells were stained with fluorescein-conjugated deoxynucleotides (green), and the nuclei were stained with DAPI (blue). "+" and "-" in the figure legends refer to with and without irradiation, respectively. Bar represents 50 μm.

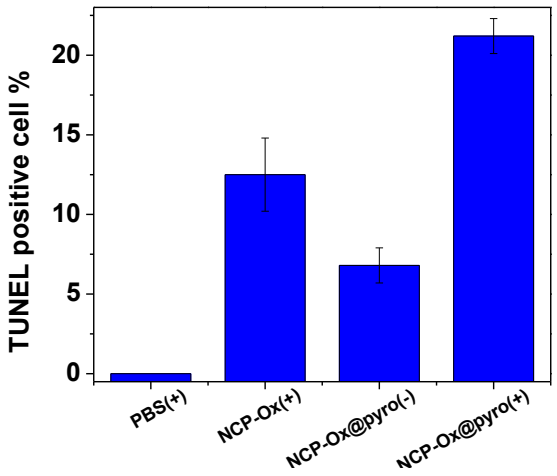

Figure 6.20 Percentages of TUNEL-positive cells in CT26 tumor tissues. "+" and "-" in the figure legends refer to with and without irradiation, respectively. Each point was the mean ± S.D. (n = 3)

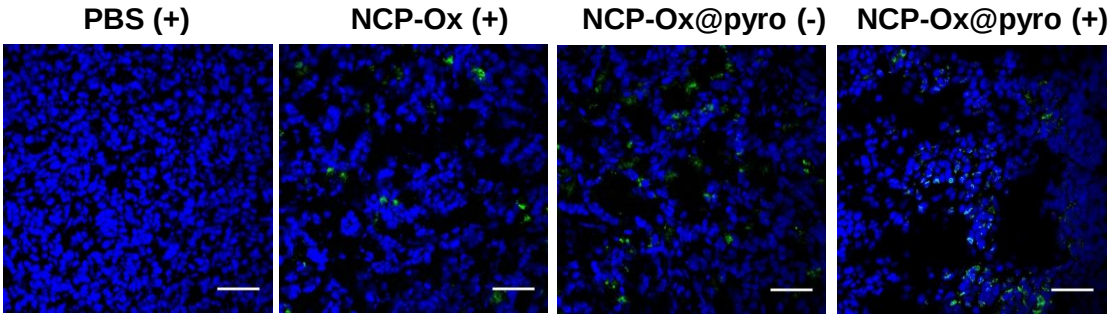

Figure 6.21 Representative CLSM images of TUNEL assays of tumor tissues. DNA fragments in apoptotic HT29 cells were stained with fluorescein-conjugated deoxynucleotides (green), and the nuclei were stained with DAPI (blue). "+" and "-" in the figure legends refer to with and without irradiation, respectively. Bar represents 50 μm.

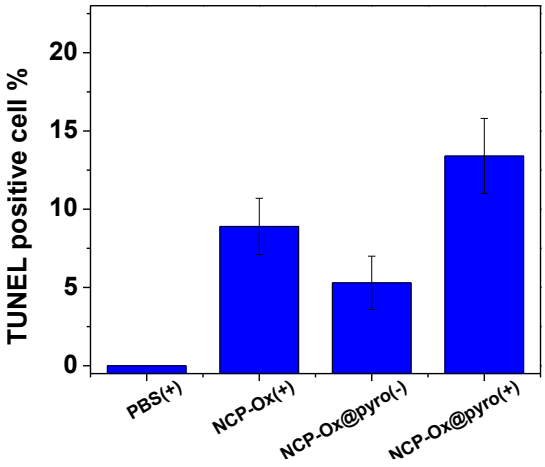

Figure 6.22 Percentages of TUNEL-positive cells in HT29 tumor tissues. "+" and "-" in the figure legends refer to with and without irradiation, respectively. Each point was the mean ± S.D. (n = 3)

6.3.6 In Vivo *Antitumor Immunity*

In order to evaluate the immune response evoked by PDT of NCP-Ox@pyrolipid, blood was collected from the CT26 mouse model from the seventh day after tumor inoculation, and TNF-α, IFN-γ, and IL-6 production (all three are proinflammatory cytokines) were evaluated in the serum by enzyme-linked immunosorbent assay (ELISA), which showed an acute immunoresponse a day after PDT treatment (Figure 6.23). Release of such cytokines indicates acute inflammation, an important mechanism of inducing antitumor immunity by PDT.[32] No significant differences were observed in the three proinflammatory cytokine levels among control and monotherapy groups during the testing period. However, significantly higher TNF-α ($P = 7.9\times10^{-4}$ vs. control), IL-6 ($P = 2.4\times10^{-5}$ vs. control), and IFN-γ ($P = 3.89\times10^{-7}$ vs. control) levels were noted in mice treated by NCP-Ox@pyrolipid with irradiation on Day 9, suggesting that PDT causes inflammation and successfully activates the innate immune response (Figure 6.23). However, two days after PDT treatment, all three proinflammatory cytokine levels rapidly dropped to baseline levels in mice receiving PDT of NCP-Ox@pyrolipid, suggesting that the inflammation was only

an acute response.[32] No significant difference was observed in the three proinflammatory cytokine levels among control and monotherapy groups during the testing period.

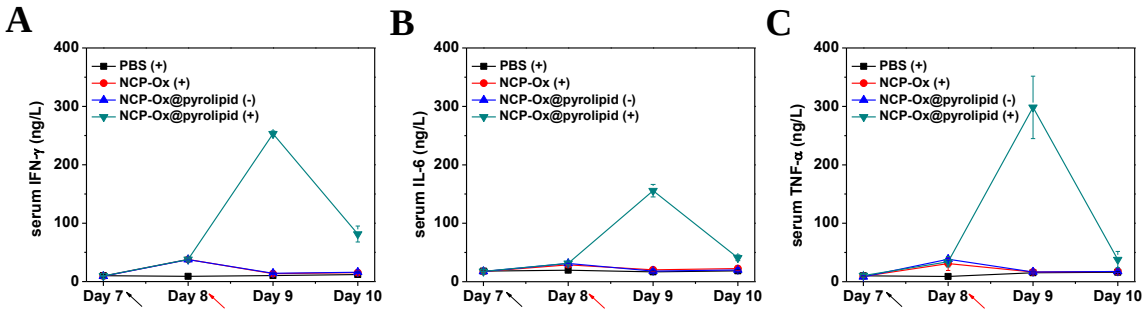

Figure 6.23 *In vivo* immunogenic responses induced by NCP-Ox@pyrolipid in CT26 tumor bearing BALB/c mice. (A)-(C) Serum concentrations of IFN-γ, IL-6, and TNF-α on Day 7, 8, 9, 10 post tumor inoculation (Day 0, 1, 2, and 3 post first treatment). NCP-Ox@pyrolipid with irradiation treated CT26 cells vaccinated efficiently against live tumor cells. CT26 cells treated *in vitro* with NCP-Ox@pyrolipid and light irradiation were inoculated subcutaneously in BALB/c mice. After 7 days, mice were rechallenged with live CT26 cells. "+" and "-" in the figure legends refer to with and without irradiation, respectively. Each point was the mean ± S.D. (n = 3)

In ICD, dying cancer cells operate as a vaccine to stimulate a tumor-specific immune response. A common practice is to inject tumor cells pretreated with ICD inducer into one flank of a mouse and untreated tumor cells into the other and then observe the growth of the tumors. If there is no tumor growth in the flank with untreated cells, it means that the drugs are able to induce immunogenic cell death. An antitumor vaccination experiment was performed to confirm ICD induced by PDT of NCP-Ox@pyrolipid in an *in vivo* setting. PDT was applied to CT26 cells incubated with NCP-Ox@pyrolipid *in vitro* to induce ICD, serving as a tumor vaccine upon inoculation into BALB/c mice. As shown in Figure 6.24, mice receiving the NCP-Ox@pyrolipid-treated and light-irradiated vaccine were protected against a subsequent challenge with live CT26 cells and remained tumor-free in contrast to mice in the control group, which all developed tumors upon the second challenge. Cytokines level observed one day after first tumor inoculation were

much higher for NCP-Ox@pyrolipid treated mice (Figure 6.24C). This result indicated that PDT of NCP-Ox@pyrolipid induced strong ICD in CT26 cells, which acted as an effective vaccine against live tumor cells in immunocompetent mice.

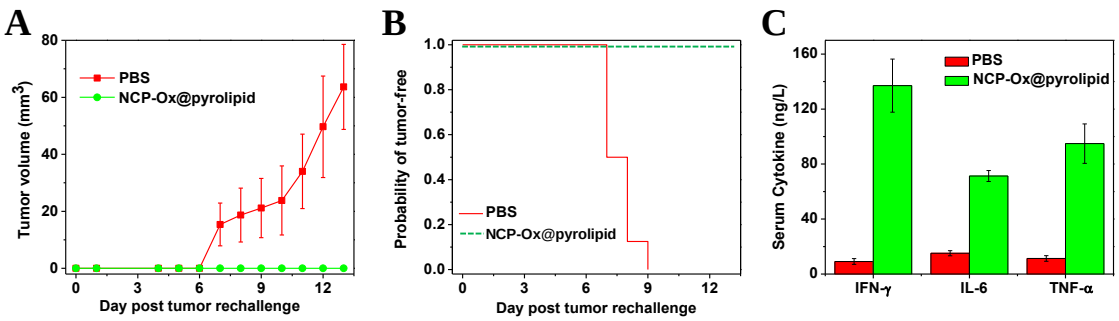

Figure 6.24 NCP-Ox@pyrolipid with irradiation-treated CT26 cells were vaccinated against live tumor cells. CT26 cells treated *in vitro* with NCP-Ox@pyrolipid and light irradiation were inoculated subcutaneously in BALB/c mice. After 7 days, mice were rechallenged with live CT26 cells. (A) Tumor growth curve of the left tumors (rechallenged tumors). (B) Probability of tumor-free mice after tumor rechallenge. (C) Serum concentrations of IFN-γ, IL-6, and TNF-α one day after the first tumor inoculation. "+" and "-" in the figure legends refer to with and without irradiation, respectively. Data expressed as means±S.D. (n=6).

6.3.7 Abscopal Effect

We next examined if chemotherapy and PDT of NCP-Ox@pyrolipid enhanced the anticancer efficacy and antitumor immunity. The abscopal effect is observed when localized treatment of a tumor causes inhibition of tumors distant from the treated tissue. A bilateral mouse tumor model of colorectal cancer CT26 was developed by subcutaneously injecting cancer cells into both the left and right flank regions of nude mice. The right tumors were designated primary tumors for local light irradiation, and the left tumors were designated distant (abscopal) tumors with no direct treatment. When the primary tumors reached ~100 mm^3, mice were randomly divided into five groups (n=6): (1) PBS with irradiation and NCP-Ox@pyrolipid (2) without or (3) with irradiation. NCP-Ox@pyrolipid was i.p. injected into animals at an oxaliplatin dose of 2 mg/kg every three day for a total of two injections, followed by light irradiation of the primary

tumors every day for six days at a light dose of 180 J/cm^2 (670 nm, 100 mW/cm^2). Without light irradiation, NCP-Ox@pyrolipid caused significant growth delay in primary tumors but showed no improvement in the control of the distant tumor growth (Figure 6.25). In comparison NCP-Ox@pyrolipid with local light irradiation led to efficient tumor regression of the primary tumor with tumors only 1.4 % the size of PBS treated tumors at the endpoint. More importantly, distant tumors that did not receive local light irradiation were also inhibited. These results indicated that the combination of PDT and oxaliplatin synergize in a tumor-specific immune response to inhibit distant tumors that were not treated. NCP-Ox@pyrolipid thus demonstrates great potential for treating metastatic cancers.

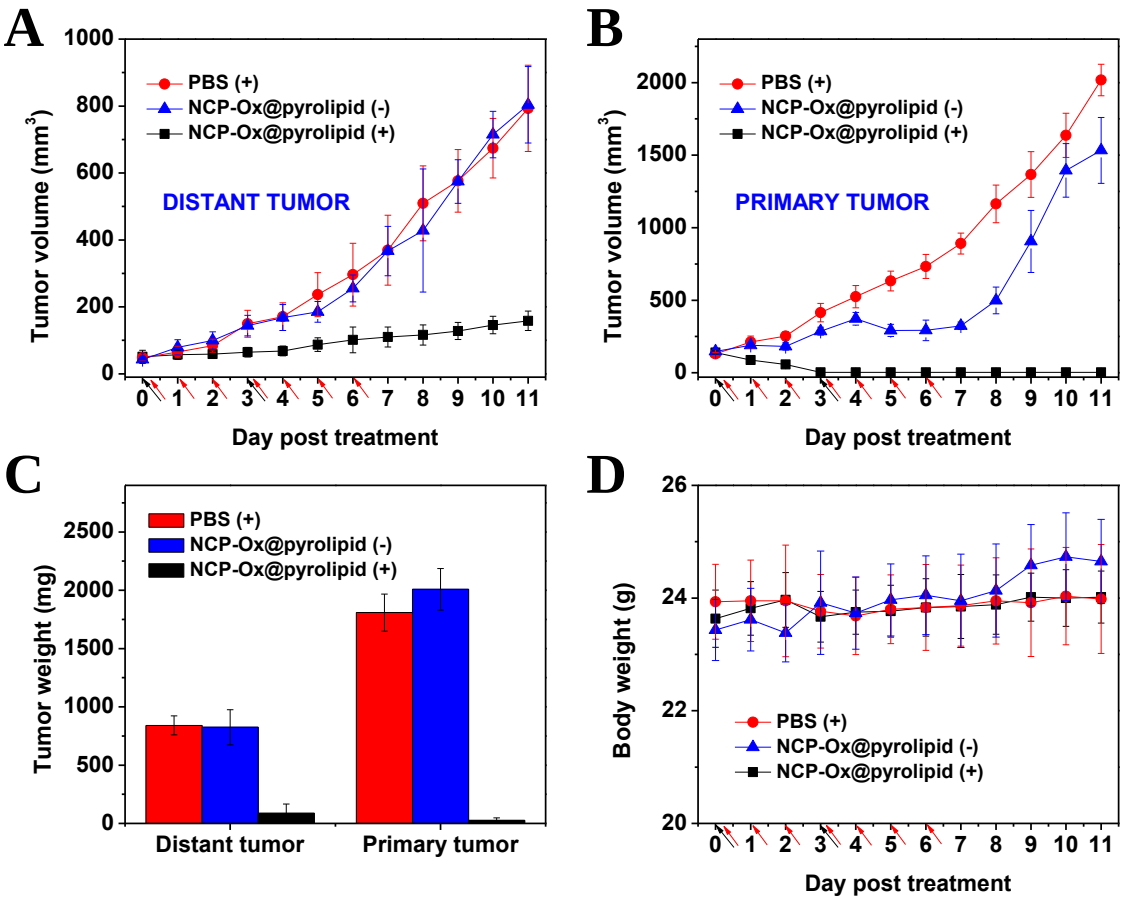

Figure 6.25 Abscopal effect of NCP-Ox@pyrolipid observed in bilateral tumor model of CT26, in which cancer cells were subcutaneously injected into both the right and left flank regions of

Figure 6.25, continued each animal. The right tumors were designated primary tumors for light irradiation, and the left tumors were designated the distant tumors and did not receive light irradiation. For the CT26 model, PBS or NCP-Ox@pyrolipid was i.p. injected into mice, followed by light irradiation at a dose of 180 J/cm^2 (670 nm, 100 mW/cm^2). NCP-Ox@pyrolipid was carried out every three day for a total of two treatments, while PDT was carried out every day for a total of seven treatments. Tumor growth inhibition curves were observed (A, B). Tumor weights (C) were compared between groups. The average body weight of mice remained constant (D). The arrows in (A), (B), and (D) represent the times of drug administration (black) and irradiation (red). "+" and "-" in the figure legends refer to with and without irradiation, respectively. Each point was the mean ± S.D. (n = 6).

6.4 Conclusions

We have developed an effective NCP-enabled combination therapy for metastatic colorectal cancer that combines oxaliplatin chemotherapy and pyrolipid-based PDT. NCP-Ox@pyrolipid carries high loadings of oxaliplatin and pyrolipid that leads to long circulation times and enhanced tumor accumulation after systemic administration. The combination of oxaliplatin and PDT along with their systemic antitumor immunity was not only significantly more effective in regressing the growth of not only primary tumors but also inhibited the growth of distant tumors in bilateral syngeneic mouse model of colorectal cancer. NCP-Ox@pyrolipid combines chemotherapy and PDT, as well as the antitumor immunogenic response induced by oxaliplatin and PDT, to offer a new strategy for treating both primary and metastatic cancers.

6.5 References

(1) Siegel, R. L.; Miller, K. D.; Jemal, A. *Ca-Cancer J Clin* **2015**, *65*, 5.

(2) Ciombor, K. K.; Wu, C.; Goldberg, R. M. *Annu Rev Med* **2015**, *66*, 83.

(3) Rosenberg, S. A.; Yang, J. C.; Restifo, N. P. *Nat Med* **2004**, *10*, 909.

(4) Grivennikov, S. I.; Greten, F. R.; Karin, M. *Cell* **2010**, *140*, 883.

(5) Whiteside, T. L. *Oncogene* **2008**, *27*, 5904.

(6) de Visser, K. E.; Eichten, A.; Coussens, L. M. *Nat Rev Cancer* **2006**, *6*, 24.

(7) Kindler, H. L.; Shulman, K. L. *Current treatment options in oncology* **2001**, *2*, 459.

(8) Liu, D.; Poon, C.; Lu, K.; He, C.; Lin, W. *Nature communications* **2014**, *5*, 4182.

(9) He, C. B.; Liu, D. M.; Lin, W. B. *Chem Rev* **2015**, *115*, 11079.

(10) He, C.; Liu, D.; Lin, W. *ACS nano* **2015**, *9*, 991.

(11) Shams, M.; Owczarczak, B.; Manderscheid-Kern, P.; Bellnier, D. A.; Gollnick, S. O. *Cancer Immunol. Immunother.* **2015**, *64*, 287.

(12) Mroz, P.; Hashmi, J. T.; Huang, Y. Y.; Lang, N.; Hamblin, M. R. *Expert Rev Clin Immu* **2011**, *7*, 75.

(13) Garg, A. D.; Nowis, D.; Golab, J.; Agostinis, P. *Apoptosis* **2010**, *15*, 1050.

(14) Krosl, G.; Korbelik, M.; Dougherty, G. J. *Brit J Cancer* **1995**, *71*, 549.

(15) Korbelik, M.; Dougherty, G. J. *Cancer Res* **1999**, *59*, 1941.

(16) Hendrzak-Henion, J. A.; Knisely, T. L.; Cincotta, L.; Cincotta, E.; Cincotta, A. H. *Photochem Photobiol* **1999**, *69*, 575.

(17) Celli, J. P.; Spring, B. Q.; Rizvi, I.; Evans, C. L.; Samkoe, K. S.; Verma, S.; Pogue, B. W.; Hasan, T. *Chem Rev* **2010**, *110*, 2795.

(18) Agostinis, P.; Berg, K.; Cengel, K. A.; Foster, T. H.; Girotti, A. W.; Gollnick, S. O.; Hahn, S. M.; Hamblin, M. R.; Juzeniene, A.; Kessel, D.; Korbelik, M.; Moan, J.; Mroz, P.; Nowis, D.; Piette, J.; Wilson, B. C.; Golab, J. *Ca-Cancer J Clin* **2011**, *61*, 250.

(19) Tesniere, A.; Schlemmer, F.; Boige, V.; Kepp, O.; Martins, I.; Ghiringhelli, F.; Aymeric, L.; Michaud, M.; Apetoh, L.; Barault, L.; Mendiboure, J.; Pignon, J. P.; Jooste, V.; van Endert, P.; Ducreux, M.; Zitvogel, L.; Piard, F.; Kroemer, G. *Oncogene* **2010**, *29*, 482.

(20) Zitvogel, L.; Apetoh, L.; Ghiringhelli, F.; Andre, F.; Tesniere, A.; Kroemer, G. *J Clin Invest* **2008**, *118*, 1991.

(21) Zitvogel, L.; Apetoh, L.; Ghiringhelli, F.; Kroemer, G. *Nat Rev Immunol* **2008**, *8*, 59.

(22) Obeid, M.; Panaretakis, T.; Tesniere, A.; Joza, N.; Tufi, R.; Apetoh, L.; Ghiringhelli, F.; Zitvogel, L.; Kroemer, G. *Cancer Res* **2007**, *67*, 7941.

(23) Liu, D.; Poon, C.; Lu, K.; He, C.; Lin, W. *Nat Commun* **2014**, *5*.

(24) Lovell, J. F.; Jin, C. S.; Huynh, E.; Jin, H.; Kim, C.; Rubinstein, J. L.; Chan, W. C. W.; Cao, W.; Wang, L. V.; Zheng, G. *Nature Materials* **2011**, *10*, 324.

(25) Jin, C. S.; Cui, L.; Wang, F.; Chen, J.; Zheng, G. *Adv Healthc Mater* **2014**, *3*, 1240.

(26) Lovell, J. F.; Jin, C. S.; Huynh, E.; MacDonald, T. D.; Cao, W. G.; Zheng, G. *Angew Chem Int Edit* **2012**, *51*, 2429.

(27) Lovell, J. F.; Jin, C. S.; Huynh, E.; Jin, H. L.; Kim, C.; Rubinstein, J. L.; Chan, W. C. W.; Cao, W. G.; Wang, L. V.; Zheng, G. *Nat Mater* **2011**, *10*, 324.

(28) Carter, K. A.; Shao, S.; Hoopes, M. I.; Luo, D.; Ahsan, B.; Grigoryants, V. M.; Song, W. T.; Huang, H. Y.; Zhang, G. J.; Pandey, R. K.; Geng, J.; Pfeifer, B. A.; Scholes, C. P.; Ortega, J.; Karttunen, M.; Lovell, J. F. *Nature communications* **2014**, *5*.

(29) Yang, A. D.; Fan, F.; Camp, E. R.; van Buren, G.; Liu, W.; Somcio, R.; Gray, M. J.; Cheng, H.; Hoff, P. M.; Ellis, L. M. *Clin. Cancer Res.* **2006**, *12*, 4147.

(30) Green, D. R.; Ferguson, T.; Zitvogel, L.; Kroemer, G. *Nat Rev Immunol* **2009**, *9*, 353.

(31) Kroemer, G.; Galluzzi, L.; Kepp, O.; Zitvogel, L. *Annu Rev Immunol* **2013**, *31*, 51.

(32) Castano, A. P.; Mroz, P.; Hamblin, M. R. *Nat Rev Cancer* **2006**, *6*, 535.